

University of Windsor

Scholarship at UWindor

Electronic Theses and Dissertations

Theses, Dissertations, and Major Papers

2009

Geochemistry of the Neoproterozoic Wadi Ghadir and Fawakhir ophiolites and associated rocks, Central Eastern Desert, Egypt: Implication for geodynamic setting

Yasser Medhat Hassan Abd El-Rahman
University of Windsor

Follow this and additional works at: <https://scholar.uwindsor.ca/etd>

Recommended Citation

Abd El-Rahman, Yasser Medhat Hassan, "Geochemistry of the Neoproterozoic Wadi Ghadir and Fawakhir ophiolites and associated rocks, Central Eastern Desert, Egypt: Implication for geodynamic setting" (2009). *Electronic Theses and Dissertations*. 7905.
<https://scholar.uwindsor.ca/etd/7905>

This online database contains the full-text of PhD dissertations and Masters' theses of University of Windsor students from 1954 forward. These documents are made available for personal study and research purposes only, in accordance with the Canadian Copyright Act and the Creative Commons license—CC BY-NC-ND (Attribution, Non-Commercial, No Derivative Works). Under this license, works must always be attributed to the copyright holder (original author), cannot be used for any commercial purposes, and may not be altered. Any other use would require the permission of the copyright holder. Students may inquire about withdrawing their dissertation and/or thesis from this database. For additional inquiries, please contact the repository administrator via email (scholarship@uwindsor.ca) or by telephone at 519-253-3000ext. 3208.

**GEOCHEMISTRY OF THE
NEOPROTEROZOIC WADI GHADIR AND
FAWAKHIR OPHIOLITES AND
ASSOCIATED ROCKS, CENTRAL EASTERN
DESERT, EGYPT: IMPLICATION FOR
GEODYNAMIC SETTING**

By

Yasser Medhat Hassan Abd El-Rahman

A Dissertation

Submitted to the Faculty of Graduate Studies
through Earth and Environmental Sciences
in Partial Fulfillment of the Requirements for
the Degree of Doctor of Philosophy at the

University of Windsor

Windsor, Ontario, Canada

2009

© 2009 Yasser Abd El-Rahman



Library and Archives
Canada

Published Heritage
Branch

395 Wellington Street
Ottawa ON K1A 0N4
Canada

Bibliothèque et
Archives Canada

Direction du
Patrimoine de l'édition

395, rue Wellington
Ottawa ON K1A 0N4
Canada

Your file *Votre référence*
ISBN: 978-0-494-57651-9
Our file *Notre référence*
ISBN: 978-0-494-57651-9

NOTICE:

The author has granted a non-exclusive license allowing Library and Archives Canada to reproduce, publish, archive, preserve, conserve, communicate to the public by telecommunication or on the Internet, loan, distribute and sell theses worldwide, for commercial or non-commercial purposes, in microform, paper, electronic and/or any other formats.

The author retains copyright ownership and moral rights in this thesis. Neither the thesis nor substantial extracts from it may be printed or otherwise reproduced without the author's permission.

AVIS:

L'auteur a accordé une licence non exclusive permettant à la Bibliothèque et Archives Canada de reproduire, publier, archiver, sauvegarder, conserver, transmettre au public par télécommunication ou par l'Internet, prêter, distribuer et vendre des thèses partout dans le monde, à des fins commerciales ou autres, sur support microforme, papier, électronique et/ou autres formats.

L'auteur conserve la propriété du droit d'auteur et des droits moraux qui protègent cette thèse. Ni la thèse ni des extraits substantiels de celle-ci ne doivent être imprimés ou autrement reproduits sans son autorisation.

In compliance with the Canadian Privacy Act some supporting forms may have been removed from this thesis.

While these forms may be included in the document page count, their removal does not represent any loss of content from the thesis.

Conformément à la loi canadienne sur la protection de la vie privée, quelques formulaires secondaires ont été enlevés de cette thèse.

Bien que ces formulaires aient inclus dans la pagination, il n'y aura aucun contenu manquant.


Canada

Declaration of Co-authorship/Previous Publication

I. Co-authorship declaration

This is a clarification that this thesis is a product of my own work. Field work was carried out with the co-operation of Ali Polat and Yildirim Dilek and with help from Mohamed El-Sharkawy and Shawki Sakran. Ali Polat, Yildirim Dilek and Brian J. Fryer contributed to the thesis through criticism and revision of the original versions of the manuscripts. Field observations, laboratory analyses, data interpretation, key ideas and manuscript preparation were performed by the author.

II. Declaration of publication

This thesis includes three original papers that are in press, in revision and submitted for publication in peer-viewed international journals. The approximate contributions of the authors for each manuscript are given in percentages in the table below:

Chapter 2	Yasser Abd El-Rahman (65%) , Ali Polat (15%), Yildirim Dilek (10%), Brian J. Fryer (6%), Mohamed El-Sharkawy (3%), Shawki Sakran (1%), Geochemistry and tectonic evolution of the Neoproterozoic Wadi Ghadir ophiolite, Eastern Desert, Egypt.	In press (Lithos)
Chapter 3	Yasser Abd El-Rahman (65%) , Ali Polat (15%), Yildirim Dilek (9%), Brian J. Fryer (9%), Mohamed El-Sharkawy (1%), Shawki Sakran (1%), Formation of Neoproterozoic proto-arc oceanic crust in the Nubian Shield: Geochemical evidence from the Fawakhir Ophiolite, Eastern Desert, Egypt.	In Revision (Precambrian Research)
Chapter 4	Yasser Abd El-Rahman (70%) , Ali Polat (15%), Brian J. Fryer (10%), Yildirim Dilek (3%), Mohamed El-Sharkawy (1%), Shawki Sakran (1%), The provenance and tectonic setting of the Neoproterozoic Um Hassa Greywacke Member, Wadi Hammamat area, Egypt: Evidence from petrography and geochemistry.	Submitted in May 2009 (Journal of African Earth Sciences)

I certify that the above material describes work completed during my registration as graduate student at the University of Windsor.

I declare that, to the best of my knowledge, my thesis does not infringe upon anyone's copyright nor violate any proprietary rights and that any ideas, techniques, quotations, or any other material from the work of other people included in my thesis, published or otherwise, are fully acknowledged in accordance with the standard referencing practices.

I declare that this is a true copy of my thesis, including any final revisions, as approved by my thesis committee and the Graduate Studies office, and that this thesis has not been submitted for a higher degree to any other University or Institution.

Abstract

The geochemistry of the ophiolitic complexes and younger late orogenic sedimentary rocks in the Wadi Ghadir and Fawakhir areas has been studied to constrain the tectonic evolution of the Central Eastern Desert. The Wadi Ghadir ophiolite is composed of gabbros and pillow lavas that are intruded by many dike swarms and all of them display subduction zone chemical signatures. The ophiolitic rocks and the surrounding *mélange* were intruded by younger dikes with Andean-type geochemical signature. The Wadi Ghadir ophiolite has chemical similarities to the oceanic crust formed in back-arc basins. The location of the Wadi Ghadir ophiolite to the northeast of the Nugrus volcanic arc and the appearance of forearc amphibolites to the southwest of the Nugrus arc rocks indicates a NE-dipping subduction zone. The accretion of this arc-back-arc system onto the passive margin to the west resulted in the reversal in the subduction direction and the establishment of a new Andean-type continental margin.

The Fawakhir ophiolite comprises serpentinized ultramafic rocks, gabbros, sheeted dike complexes, and pillow lavas. The geochemical characteristics of the Fawakhir ophiolite are comparable to the forearc oceanic crust developed in the Izu-Bonin-Mariana arc system. However, pillow lavas preserved in the *mélange* to the west have a geochemical signature similar to that of a modern back-arc oceanic crust which suggests formation of an intra-oceanic arc system above an east-dipping subduction zone. As in Wadi Ghadir, the Fawakhir ophiolite is intruded by later calc-alkaline dikes possessing geochemical signatures similar to rocks that occur at modern active continental margins. The initiation of the Andean-type calc-alkaline magmatism may indicate a reversal in

subduction polarity from east-dipping during arc accretion to west-dipping and formation of an active continental margin.

The Umm Hassa Greywacke member is the top unit of the Hammamat Group which is late orogenic molasse-type sedimentary rocks. Continental arc volcanic rocks and oceanic island arc-ophiolitic sources are the main contributors to the sediments of the Um Hassa greywackes. Considering the geodynamic evolution of the Central Eastern Desert, the Um Hassa greywackes were deposited in retroarc foreland basin behind the continental arcs developed over a west-dipping subduction zone.

Acknowledgements

I would like to thank my dissertation advisors Dr. Ali Polat and Dr. Brian J. Fryer, especially Dr. Polat, for supporting this work and for providing the opportunity for me to independently pursue the study. This study was supported by PREA and NSERC (250926 and 250978) grants to Dr. Polat and NSERC (83117) grant to Dr. B. J. Fryer.

Special thanks for Dr. Yildirim Dilek for his discussion on the ophiolites and providing excellent critiques and constructive comments on the first manuscript. My deepest gratitude to Dr. Mohamed El-Sharkawy and Dr. Shawki Sakran for organizing and guidance of the first field trip

Thanks to Dr. Zhaoping Yang, Mr. J.C. Barrett and Dr. Juan Carlos Ordóñez Calderón for their help during ICP-MS analyses. I am grateful to Mr. Michael Murphy at UCD for his cyber help regarding some chemical analyses.

I would also like to thank all the faculty, staff members and graduate students, especially Mr. Ahmed Sajid, in the Department of Earth and Environmental Sciences for their support. I am highly grateful to the Geology Department at Cairo University for support.

I am deeply grateful to my mother and my brother Assem for making Doa'a for me all the time. I highly appreciate the company of many Egyptian friends here in Windsor which minimized my homesickness feelings.

Table of Contents

Declaration of Co-authorship/Previous Publication.....	iii
Abstract.....	v
Acknowledgements.....	vii
List of Tables.....	xi
List of Figures.....	xiii
Chapter 1: Introduction.....	1
1.1.The ophiolite controversy.....	2
1.2.Background on the Arabian-Nubian Shield.....	6
1.3.Neoproterozoic Egyptian ophiolites.....	9
1.4.Late-orogenic Neoproterozoic sedimentary rocks.....	11
1.5.Objectives.....	14
1.6.Framework of the thesis.....	17
References.....	18
Chapter 2: Geochemistry and tectonic evolution of the Neoproterozoic Wadi Ghadir ophiolite, Eastern Desert, Egypt.....	27
2.1. Introduction.....	27
2.2. Geology of the WGO.....	29
2.3. Petrography.....	32
2.4. Analytical methods.....	34
2.5. Geochemical results.....	35
2.5.1. Gabbros.....	35
2.5.2. Pillow lavas.....	36
2.5.3. Dikes.....	37

2.5.4. <i>Ophiolitic mélange</i>	38
2.6. Discussion.....	39
2.6.1. <i>Alteration process and element mobility</i>	39
2.6.2. <i>Mantle source characteristics</i>	41
2.6.3. <i>Tectonic setting and geodynamic evolution</i>	44
2.7. Conclusions.....	48
References.....	49

Chapter 3: Formation of Neoproterozoic proto-arc oceanic crust in the Nubian Shield: Geochemical evidence from the Fawakhir Ophiolite, Eastern Desert, Egypt.....85

3.1. Introduction.....	85
3.2. Regional geology and field characteristics.....	88
3.3. Petrography.....	90
3.4. Analytical methods.....	92
3.5. Geochemical results.....	93
3.5.1. <i>Pyroxenites and gabbros</i>	93
3.5.2. <i>Ophiolitic volcanic rocks</i>	94
3.5.3. <i>Mélange blocks</i>	95
3.5.4. <i>Calc-alkaline dikes</i>	95
3.6. Discussion.....	96
3.6.1. <i>Alteration</i>	96
3.6.2. <i>Fractional crystallization</i>	98
3.6.3. <i>Mantle source characteristics</i>	99
3.6.4. <i>Pyroxenite genesis</i>	102
3.6.5. <i>Geodynamic setting</i>	103
3.7. Conclusion and implications.....	108
References.....	110

Chapter 4: The provenance and tectonic setting of the Neoproterozoic Um Hassa Greywacke Member, Wadi Hammamat area, Egypt:

Evidence from petrography and geochemistry.....143

4.1. Introduction.....143
4.2. Field relations and characteristics.....145
4.3. Petrography.....146
4.4. Analytical Methods.....148
4.5. Geochemical results.....148
4.6. Discussion.....149
 4.6.1. *Effects of sedimentary processes on geochemistry*.....149
 4.6.2. *Provenance*.....152
 4.6.3. *Tectonic setting*.....155
4.7. Conclusion.....158
References.....159

Chapter 5: Summary and implications.....179

5.1. Formation of Neoproterozoic ophiolites in Egypt.....179
5.2. Assessing the subduction polarity.....180
5.3. From island arc(s) to active continental margin.....181
5.4. Emplacement of the ophiolite complexes.....183
5.5. Late orogenic sedimentary rocks.....183
5.6. Ophiolite-induced evolutionary model for the Central Eastern Desert.....184
5.7. Implication for crust growth.....186
References.....199

Vita Auctoris.....195

List of Tables

Table 2.1. Measured and recommended major element values for USGS standards DNC-1 and BIR-1.....	72
Table 2.2. Measured and recommended values for USGS standards BHVO-1 and BHVO-2.....	73
Table 2.3. Major (wt%) and trace element (ppm) concentrations and significant element ratios for ophiolitic rocks and associated dikes.....	74
Table 2.4. Summary of major (wt.%) and trace (ppm) element concentrations and significant element ratios for the Wadi Ghadir ophiolitic complex and associated dikes.....	81
Table 2.5. Major (wt%) and trace element (ppm) concentrations and significant element ratios for ophiolitic mélange fragments and associated fragmented dikes.....	82
Table 3.1. Mineralogical composition of Qift-Qusier ophiolitic rocks.....	135
Table 3.2. Measured and recommended major element values for USGS standards DNC-1 and BIR-1.....	135
Table 3.3. Measured and recommended values for USGS standards BHVO-1 and BHVO-2.....	136
Table 3.4. Major (wt%) and trace element (ppm) concentrations and significant element ratios for ophiolitic gabbro and pyroxenite.....	137
Table 3.5. Major (wt%) and trace element (ppm) concentrations and significant element ratios for metavolcanics.....	138
Table 3.6. Major (wt%) and trace elements (ppm) concentrations and significant element ratios for calc-alkaline dikes and mélange volcanics.....	141
Table 3.7. Summary of major (wt.%) and trace (ppm) element concentrations and significant element ratios for the Wadi Ghadir ophiolitic complex and associated dikes.....	142
Table 4.1. Modal composition of Um Hassa greywackes.....	175
Table 4.2. Measured and recommended major element values for DNC-1 (recommended by USGS) and BIR-1 (recommended by Max-Planck-Institute) standards.....	176

Table 4.3. Measured and recommended values for USGS standards BHVO-1 and BHVO-2 (recommended by Max-Planck-Institute).....	177
Table 4.4. Chemical composition of Um Hassa greywackes.....	178

List of Figures

Fig. 1.1. Location map of the study area (green stars), one along the Qift-Qusier Road and the other at Wadi Ghadir area to the south.....	1
Fig. 1.2. (a) Arabian-Nubian Shield (ANS) as the northern extension of the East-Africa-Antarctic collisional orogen (EAAO) at Neoproterozoic time.....	7
Fig. 1.3. The common model proposed for the evolution of the ophiolitic rocks of the Eastern Desert of Egypt.....	12
Fig. 1.4. Hieroglyphic inscription engraved on the Um Hassa greywacke “Bekhen-stone” of Wadi Hammamat area.....	13
Fig. 1.5. Distribution of the molasse basins in the Eastern Desert with associated tectonic features.....	16
Fig. 2.1. (a) Schematic map showing major rock types exposed to the west of Marsa Alam, (b) Simplified geological map of the area extending from Wadi Ghadir in the northeast to Hafafit area in the southwest. (c) Geological map of the main ophiolitic complex of the Wadi Ghadir mélangé.....	57
Fig. 2.2. Field photographs of ophiolitic block at Wadi Ghadir.....	58
Fig. 2.3. Photomicrographs of the Wadi Ghadir ophiolitic rocks.....	59
Fig. 2.4. Zr/TiO ₂ versus SiO ₂ diagram (a) Wadi Ghadir ophiolite complex and for (b) Wadi Ghadir ophiolitic mélangé and island arc fragments. Zr versus Y diagram (c) the Wadi Ghadir ophiolite complex and of (d) the Wadi Ghadir ophiolitic mélangé and island arc fragments.....	60
Fig. 2.5. Variation diagrams of Zr versus (a) La, (b) Sm, (c) Nb, (d) Yb, (e) TiO ₂ , (f) Rb for the Wadi Ghadir ophiolite complex and associated dikes.....	61
Fig. 2.6. Chondrite-normalized REE patterns for, (a) Gabbros, (b) Pillow lavas; solid yellow symbols for porphyritic pillows, (c) D3 dikes, (d) D1 dikes, (e) D2 dikes, and (f) D4 dikes.	62
Fig. 2.7. MORB-normalized trace element patterns for, (a) Gabbros, (b) Pillow lavas; solid yellow symbols for porphyritic pillows, (c) D3 dikes, (d) D1 dikes, (e) D2 dikes, and (f) D4 dikes.	63

Fig. 2.8. (a) Chondrite-normalized REE patterns for the Wadi Ghadir mélangé blocks, (b) MORB-normalized trace element patterns for the Wadi Ghadir mélangé blocks, (c) Chondrite-normalized REE patterns for fragmented dikes in the Wadi Ghadir ophiolitic mélangé, (d) MORB-normalized trace element patterns for fragmented dikes in the Wadi Ghadir ophiolitic mélangé, (e) Chondrite-normalized REE patterns for arc rocks north of Hafafi and northwest of the Wadi Ghadir ophiolitic mélangé, (f) MORB-normalized trace element patterns for arc rocks north of Hafafi and northwest of the Wadi Ghadir ophiolitic mélangé.....	64
Fig. 2.9. (a-e) Plot of M/Yb versus Nb/Yb for the ophiolitic rocks and associated dikes in the Wadi Ghadir area where M is (a) Zr, (b) Y, (c) La, (d) Sm, (e) U. MORB and OIB represent the position of the mid-ocean ridge and oceanic island mantle source respectively. (f) Th/Yb versus Ta/Yb diagram.....	65
Fig. 2.10. Variation of Ce and Yb contents in the ophiolitic rocks of Wadi Ghadir and associated dikes. Island arc (Low Ce/Yb) and continental margin (High Ce/Yb) trends.....	66
Fig. 2.11. Variation of La/Sm_{cn} versus Sm in the ophiolitic and associated rocks of the Wadi Ghadir area.....	67
Fig. 2.12. Variation of La/Yb versus Yb for ophiolitic rocks and associated dikes of the Wadi Ghadir area.....	68
Fig. 2.13. Ti-V discrimination diagram for Wadi Ghadir ophiolitic rocks and Hafafit amphibolites.....	69
Fig. 2.14. Comparison of the Wadi Ghadir ophiolitic rocks with back-arc basins and different ophiolites.....	70
Fig. 2.15. Tectonic model for evolution of the Wadi Ghadir area relative to the Nugrus unit and Hafafit from oceanic crust to active continental margin.....	71
Fig. 3.1. (a) Overview map of the Arabian-Nubian Shield rocks along the Red Sea. (b) The distribution of ophiolitic fragments in the Eastern Desert of Egypt.....	119
Fig. 3.2. A simplified geological map of the Qift-Quseir road.....	120
Fig. 3.3. (a) The geological map of the Fawakhir area. (b) Symbolic stratigraphic section showing the main rocks units of the Fawakhir ophiolite.....	121

Fig. 3.4. Field photographs of the ophiolitic mantle and plutonic section of Fawakhir area.....	122
Fig. 3.5. Field photographs of the volcanic rocks and associated metasediments.....	123
Fig. 3. 6. Photomicrograph of the Fawakhir ophiolite and the mélange fragments.....	124
Fig. 3.7. (a) Zr/TiO ₂ versus SiO ₂ diagram for the ophiolitic rocks and cutting dikes and the eastern mélange rocks. (b) Zr versus Y diagram.....	125
Fig. 3.8. Variation diagrams of Zr versus major and minor elements.....	126
Fig. 3.9. Variation diagrams of Zr versus trace elements.....	127
Fig. 3.10. Chondrite-normalized REE patterns for, (a) Ophiolitic pyroxenite and gabbros, (b) Ophiolitic pillow lavas (c) Eastern mélange volcanic blocks, (d) Calc-alkaline dikes.....	128
Fig. 3.11. Primitive mantle-normalized trace element patterns for, (a) Ophiolitic pyroxenite and gabbros, (b) Ophiolitic pillow lavas (c) Eastern mélange volcanic blocks, (d) Calc-alkaline dikes.....	129
Fig. 3.12. (a-e) Plot of M/Yb versus Nb/Yb for the ophiolitic rocks and associated dikes at the Wadi Ghadir area where M is, (a) Zr, (b) Y, (c) La, (d) Sm, (e) U. MORB and OIB represent the position of the mid-ocean ridge and oceanic island mantle source respectively. (f) Th/Yb versus Ta/Yb diagrams.....	130
Fig. 3.13. Variation in Th/Yb versus Sr/Nd.....	131
Fig. 3.14. Variation of Ce and Yb contents of the ophiolitic rocks of Wadi Ghadir and associated dikes. Island arc (Low Ce/Yb) and Continental margin (High Ce/Yb) trends.....	132
Fig. 3.15. Cr-Y discrimination diagram for the Fawakhir ophiolite, calc-alkaline dikes and eastern mélange blocks.....	133
Fig. 3.16. Schematic model for the tectonic evolution of the Fawakhir ophiolite and central Eastern Desert along the Qift-Qusier Road.....	134
Fig. 4.1. (a) Overview map of the Arabian-Nubian Shield rocks along the Red Sea. (b) Simplified geological map of the Hammamat-Meatiq region (c) Geological map of the Hammamat area.....	165
Fig. 4.2. (a) Precambrian Hammamat Group (HG) overlain unconformably by Phanerozoic Nubian Sandstone (NS). (b) Polymictic Conglomerate of Um Had Member,	

notice the purple Dokhan-type volcanics, epidosite (solid ellipse) and plagigranite (dashed ellipse) fragments. (c) Bedded (upper) and cleaved (lower) greywacke of Um Hassa Member.....	166
Fig. 4.3. Photomicrographs of Um Hassa greywackes showing different kinds of framework components.....	167
Fig. 4.4. Log (Na ₂ O/K ₂ O) versus Log (SiO ₂ /Al ₂ O ₃) for chemical classification of sandstones.....	168
Fig. 4.5. Variation diagrams of SiO ₂ against, (a) MgO. (b) Fe ₂ O ₃ *. (c) Al ₂ O ₃ . (d) K ₂ O.....	169
Fig. 4.6. (a) Chondrite-normalized REE patterns for Um Hassa greywackes. (b) Upper Continental crust-normalized spider diagram for Um Hassa greywackes.....	170
Fig. 4.7. (a) A-CN-K ternary diagram of molecular proportions of Al ₂ O ₃ -(CaO+Na ₂ O)-K ₂ O for Um Hassa greywackes with chemical index of alteration scale (CIA). (b) Provenance discrimination diagrams of Roser and Korsch (1988).....	171
Fig. 4.8. Modal sandstone ternary plots for Um Hassa greywackes.....	172
Fig. 4.9. Tectonic setting discrimination diagrams for Um Hassa greywackes.....	173
Fig. 4.10. Tectonic model for the formation of Hammamat Group at Wadi Hammamat area inferred from the petrography and geochemistry of the Um Hassa Greywacke Member.....	174
Fig. 5.1. Simplified diagrams showing the geodynamic evolution of the Central Eastern Desert.....	189

Chapter 1

Introduction

This study presents new field and petrographical observations, and high-precision whole-rock major and trace element data for the Neoproterozoic ophiolitic rocks and associated sedimentary rocks from the Central Eastern Desert of Egypt. One of the study areas is located along Qift-Qusier Road and the second is in the Wadi Ghadir area (Fig. 1.1). Given that the Eastern Desert of Egypt constitutes the northwest extension of the Arabian-Nubian Shield, this chapter starts with presenting a brief introduction to the Arabian Nubian Shield. This introduction is followed by succinct information concerning the controversies over the origin of the ophiolitic rocks and the late-orogenic sedimentary rocks of Egypt and other areas in the Arabian-Nubian Shield. The objectives and achievements of the study are presented at the end of the chapter.

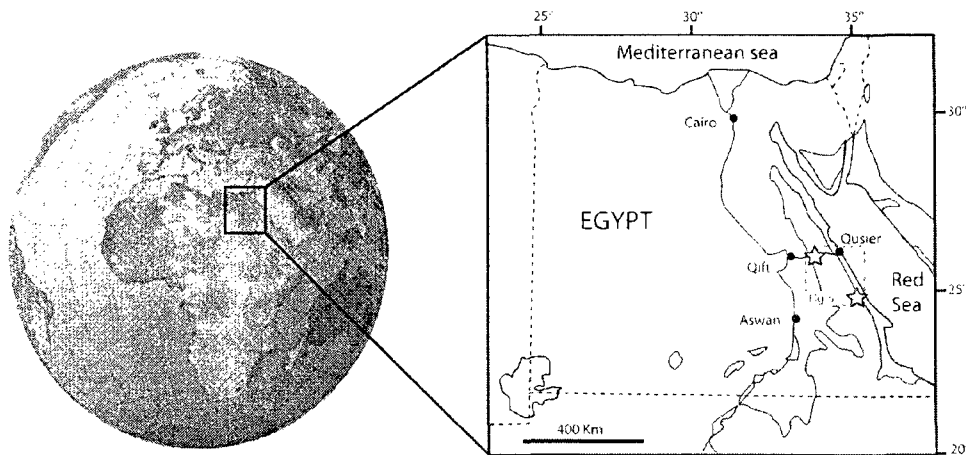


Fig. 1.1. Location map of the the study areas (the stars), one along the Qift-Qusier Road and the other one at Wadi Ghadir area to the south. The orange area represents the Precambrian rocks of Egypt (The dashed red inset enlarged at Fig. 1.5).

1.1. The ophiolite controversy

The term “ophiolite” was first introduced in the early nineteenth century by Bongniart (1813; cited in Hébert, 2007) to describe the serpentinites in the mélange in Europe (Amstutz, 1980). In the early twentieth century, Steinmann (1927, 2003) applied the “ophiolite” term to the spatially-associated suboceanic assemblage of the serpentinized peridotite, diabase-spilite, and chert (Steinmann Trinity) (Bernoulli and Jenkyns, 2009; and reference therein). In the mid-twentieth century, the analogy between the ophiolitic rocks and the oceanic crust was inferred within the blooming plate tectonic theory (Hébert, 2007). The ideal classic ophiolite sequence, described at Penrose Conference in 1972, starts from tectonized ultramafic rocks at the bottom, the mantle portion of the sequence, which is overlain by the crustal cumulate unit, including ultramafic cumulates and layered gabbro which is succeeded by the isotropic gabbro (Anonymous, 1972). The next unit contains diabasic sheeted dikes of which fed the overlying, typically pillowed, basaltic flows. Such a sequence is interpreted to be formed by sea-floor spreading at ancient mid-ocean ridges and then incorporated into orogenic systems (Moore, 2003 and reference therein). Since that time many debates have taken place over ophiolites concerning mainly their tectonic setting of origin, classification, and their occurrences especially in Precambrian times (Kusky, 2004).

Miyashiro (1973) raised the debate over the tectonic setting of formation of ophiolites. Depending only on geochemistry, Miyashiro (1973) proposed an island arc setting for the Troodos ophiolite. This led to the development of the supra-subduction zone (SSZ) ophiolite concept (Alabaster et al., 1982; Casey and Dewey, 1984; Pearce et al., 1984; 2003; Hawkins, 2003). The SSZ-ophiolites can be formed mainly by

subduction initiation and slab retreat in the forearc of the infant or reconfigured island arc (Casey and Dewey, 1984; Stern and Bloomer, 1992; Shervais, 2001; Flower and Dilek, 2003). Moores et al. (2000) considered that the combination of the extensional structural evidence, sheeted dike complexes, formed at mid-ocean ridge spreading centers and the subduction zone geochemical signature of most ophiolites a conundrum. Instead of being developed above a subduction zone, Moores et al. (2000) proposed the historical contingency model, which proposed that most ophiolites formed at mid-ocean spreading centers that tapped a mantle which was affected previously by subduction. Metcalf and Shervais (2008) used the similarity between most Mesozoic and Cenozoic ophiolites and present-day island arc magmas rather than to any mid-ocean ridge magmas to refute the historical contingency model of Moores et al. (2000). The evidence for the hydrous magma through the crystallization sequence and the enrichment of SSZ-ophiolites in low field-strength elements confirm the formation of such ophiolites above a subduction zone rather than incorporation of the residue of slab melting into the mid-ocean ridge spreading center magma (Metcalf and Shervais, 2008).

Following the debate over the tectonic setting at which the ophiolites formed, the diversity of ophiolites became remarkable. This diversity led to many attempts to classify ophiolites depending on different perspectives. Miyashiro (1975) classified ophiolites on the basis of the magmatic affinities of the volcanic rocks, into tholeiitic-calc-alkaline series, tholeiitic series, and tholeiitic-alkaline series. Serri (1982) divided ophiolites into low Ti-type and high-Ti type based on the geochemistry of the ophiolitic crustal rocks. In terms of incorporation of ophiolites into orogenic belts, Moores (1982) classified ophiolites into two types, Tethyan-type which rest tectonically on passive continental

margins, and Cordilleran-type which are associated with island arc rocks and accretionary mélanges. The differences between these two types were emphasized by Beccaluva et al. (2004) in terms of structure, tectonics and magmatic features. Nicolas (1989) classified ophiolites based on the tectonic settings of their emplacement which is a close approach to what Moores (1982) proposed. Boudier and Nicolas (1985) classified ophiolites according to their mantle composition, which reflects the degree of partial melting. Nicolas and Boudier (2003) attributed such diversity in ophiolites to the spreading rate of the oceanic crust. Thus, they classified ophiolites into harzburgite-type, harzburgite-lherzolite-type, and lherzolite-type in order of decreasing spreading rate. Dilek (2003) introduced a more comprehensive classification of ophiolites considering their lithological assemblages, chemical composition, internal structure, regional geological characteristics, tectonic setting of ophiolite generation, and the amalgamation into orogenic belts. Recently, Pearce (2008) adopted two geochemical proxies, Th-Nb and Ti-Yb, to classify ophiolites and to identify Archean oceanic crusts.

Ophiolites played a major role in formulating the plate tectonic paradigm. These rocks demonstrate two modes of lithospheric motion, sea-floor spreading at divergent margins and obduction-accretion at convergent margins. There is a debate over the first appearance of ophiolites in Earth history (Kusky, 2004; Furnes et al., 2007). Being the hallmark of the plate tectonic paradigm, ophiolites define when the modern-style plate tectonic regime started. Ophiolites with Phanerozoic-style crustal architecture began to be a dominant rock unit in Neoproterozoic time (Dilek, 2003). In addition to the ophiolite predominance in the Neoproterozoic era, the presence of blueschists and ultra-high pressure terranes at that time may indicate present-day style subduction tectonics (Stern,

2005). Neoproterozoic ophiolites are especially common in the Arabian-Nubian Shield (Stem et al., 2004) and in the Central Asian Orogenic Belt (Şengör et al., 1996; Kröner, et al., 2007).

The identification of complete Phanerozoic-like ophiolites older than the Neoproterozoic, especially in the Archean, is difficult. The difficulty behind the identification of older ophiolites can be attributed to structural complexity and intense tectonism (Sylvester et al., 1997; Kerrich and Polat, 2006). The term “inferred ophiolite” was used to describe fragmentally preserved ophiolitic-like Archean mafic-ultramafic rock assemblages (Corcoran et al., 2004). Although some Archean greenstone belts are intensely deformed, Furnes et al. (2007) was able to describe the Paleoarchean Isua ophiolite, the oldest known complete ophiolitic sequence, including the sheeted dike complex, from within the ~3.8 Ga Isua supracrustal belt. Their identification of the sheeted dikes and the cogenetic relationship between the dikes and the pillow lava were challenged by Nutman and Friend (2007) and Hamilton (2007). Robinson et al. (2008) suggested that the sheeted dike complexes in ophiolites are an unusual feature rather than being a key element in identifying ophiolites. In addition to deformation, the difficulty in identifying a complete Penrose-type ophiolite section in Archean rocks can be attributed to the different nature between the pre-1 Ga oceanic crust and its counterparts in Neoproterozoic and Phanerozoic times (Moorea, 2002; and references therein). Archean ophiolites were thick and resemble modern oceanic plateaux which resulted in the accretion of only the upper volcanic section of the oceanic crust (Kusky, 2004; and references therein). Dilek and Polat (2008) demonstrated the comparative anatomical

differences between the thick Archean and thin Phanerozoic oceanic crusts evolved in supra-subduction zone environments.

1.2. Background on the Arabian-Nubian Shield

The Arabian-Nubian Shield (ANS) is an exposure of Precambrian, mostly Neoproterozoic, crystalline rocks in northeast Africa (Nubian part) and eastern Arabia (Arabian part) separated by the Red Sea. It represents the northern extent of the East African Orogen (EAO), also known as the East-Africa-Antarctic Orogen (EAAO) by Jacobs and Thomas (2004), which is a major collision zone formed near the end of the Proterozoic by the collision between east and west Gondwana (Stern, 1994). This collision marks the disappearance of the major Mozambique Ocean basin and the formation of juvenile Neoproterozoic continental crust as a part of the Pan-African orogenic cycle (Fig. 1.2a). Kröner (1984) proposed a 950-450 Ma age range for the Pan-African Orogeny. The ANS is predominantly more juvenile than the southern Mozambique belt which is composed of a mobilized older crust that underwent intense deformation during the Pan-African Orogeny (Stern, 1994). The ANS formed through initial juvenile arc formation in intra-oceanic arc settings followed by amalgamation of arc rocks and suturing of the oceanic crusts. The accretion and suturing processes culminated in a final continental collision displaying escape tectonic structures.

The collision of the island arcs during ANS evolution resulted in the formation of major linear suture zones of deformed ophiolitic rocks separating less deformed terranes (Fig. 1.2b). Many of these terranes are composite where they contain smaller crustal units that have their own accretion history (Johnson and Kattan, 2008). The major suture zones

of the ANS can be classified into two types, arc-arc and arc-continent sutures (Abdelsalam and Stern, 1996). The arc-arc sutures trend mostly NE-SW representing the zones of closure of the oceanic basins between juvenile arc terranes at ~800-700 Ma

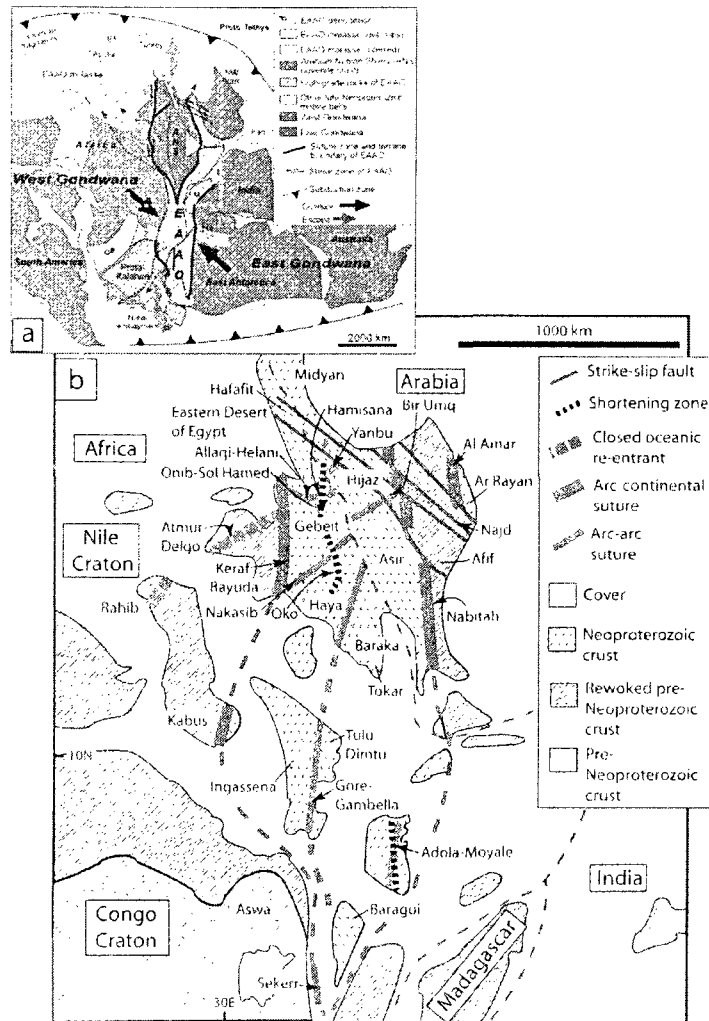


Fig. 1.2. (a) Arabian-Nubian Shield (ANS) as the northern extension of East-Africa-Antarctic collisional orogen (EAAO) at Neoproterozoic time (after Jacobs and Thomas, 2004). Abbreviations: Da-Damara belt; EF-European fragments; LH-Lützow Bay; M-Madagascar; Z-Zambesi belt, (b) Sketch tectonic map of the ANS (after Adelsalam and Stern, 1996).

(Stoeser and Camp, 1985; Pallister et al., 1988, Kröner et al., 1992; Johnson et al., 2002). The Allaqi-Heiani-Onib-Sol Hamed-Yanbu and Nakasib- Bir Umq sutures are good examples of this type. Following arc-arc collision, the ANS collided with pre-Neoproterozoic continental blocks, east and west Gondwana, at ~750-630 Ma, postdating the suturing events within the ANS terranes (Stoeser and Stacey, 1988; Stern, 1994; Johnson et al., 2001). Abdelsalam and Stern (1996) referred to these boundaries as arc-continent sutures as they juxtapose arc terranes with continental blocks after consumption of marginal oceanic basins. These sutures trend north-south and their best examples are the Nabitah suture in the east and the Keraf suture in the west (Fig. 1.2b). Shackleton (1996) considered the Nabitah suture a northern manifestation of the final collision event between east and west Gondwana. The final collision of west and east Gondwana deformed the ANS along north trending shortening zones developed between ~650-550 Ma (Stern et al., 1990; Abdelsalam, 1994; Abdelsalam and Stern, 1996). The well-known example of these zones is the Hamisana shear zone (Fig. 1.2b). The shortening deformation culminated with the development of northwest trending sinistral strike-slip faults of the Najd fault system, at ~640-540 Ma (Abdelsalam et al, 1998). The Najd fault system is considered the most prominent of the northwest trending strike-slip fault zones crosscutting the NE-SW and N-S trending structure in the ANS. Stern (1994) interpreted these strike-slip shear zones and associated extension features as escape tectonic features associated with the collision between East and West Gondwana along the Mozambique Belt.

In addition to the ophiolitic- and arc-related metasedimentary and tholeiitic and calc-alkaline (CA) magmatic rocks, other younger rocks including dikes, molasse-type

sedimentary rocks, high-K volcanic rocks and alkaline granites, were formed during the last stages of Neoproterozoic development of the ANS. These late-tectonic features are related to the extensional stage of the tectonic development of the ANS (Blasband et al., 2000; Johnson and Woldehaimanot, 2003).

The gneisses crop out in the Arabian-Nubian Shield as domes and their origin are not well-constrained. These domal structures have two crustal units, a highly metamorphosed lower one comprising deformed granitoids and a volcano-sedimentary sequence, and a weakly metamorphosed upper crustal unit of island-arc related metavolcanic and metasedimentary rocks in association with the ophiolitic rocks. The controversy over these rocks stems from whether they are pre-Neoproterozoic remnants of a pre-Pan African continental basement overthrust by oceanic arcs and oceanic sequences (Al Filali et al., 1993) or they represent juvenile Neoproterozoic crust formed during island arc accretion and orogen-parallel extension in the late Proterozoic (Bregar et al., 2002).

1.3. Neoproterozoic Egyptian ophiolites

Neoproterozoic rocks in Egypt constitute the northern exposure of the Nubian part of the ANS and are localized in the Eastern Desert (ED) and Sinai. The Neoproterozoic rocks form mountainous terrains with modern elevations of up to 2500 m, known as Red Sea Hills, running parallel to the Red Sea. The major ophiolites are exposed in the central and southern Eastern Desert of Egypt. The ophiolitic rocks in the southern Eastern Desert (SED) are well exposed in the Allaqi-Heiani-Gerf belt which is a part of an arc-arc suture zone, the Allaqi-Heiani-Onib-Sol Hamid-Yanbu suture (Stern et al., 1990;

Abdelsalam and Stern, 1996). The belt is dextrally offset by the N-trending Hamisana shear zone (Fig. 1.2b). In the Central Eastern Desert (CED), the ophiolitic rocks are abundant but they don't form a well-defined elongate suture zone. Rather, they are scattered over a wide area. The ophiolite of the CED occurs in tectonic mélanges or as olistromal debris (Shackleton et al., 1980; Ries et al., 1983; Church, 1988; El Gaby et al., 1988). Generally, the CED is highly affected by the NW-trending strike-slip movement of the Najd Fault System. Sultan et al. (1992) attributed the formation of the ophiolitic mélange in the CED to deformation accompanied by the post- accretionary Najd fault system rather than suturing. The Najd deformation stage is so pronounced that it is difficult to find any preserved fabric related to the suturing event predating the Najd deformation (Abdelsalam and Stern, 1996).

Although the term "ophiolite" was introduced in the context of the geosynclinal evolution theory of the Eastern Desert by Bittmann (1958), El-Bayoumi (1980) was a pioneer in identifying and describing a complete ophiolitic sequence from the Eastern Desert. Since the discovery of the complete ophiolitic sequence at Wadi Ghadir (El Sharkawy and El Bayoumi, 1979; El Bayoumi, 1980), the tectonic setting of the ophiolitic rocks in the Eastern Desert became a matter of debate. El-Bayoumi (1980; 1983) interpreted the Wadi Ghadir ophiolitic rocks to be an assemblage of oceanic crust formed above a plume head.

Later, the suprasubduction zone setting started to dominate the interpretation of the tectonic origin of the ophiolitic rocks in the CED. The most preferred model (Kröner et al., 1987; El-Sayed et al., 1999; Abd El-Naby and Frisch, 2006) is the one proposed by El Ramly et al. (1984) (cited in Kröner, 1985) and El Bayoumi and Greiling (1984). They

interpreted the ophiolitic rocks in the CED as remnants of marginal back-arc oceanic crust formed above a west-dipping subducted oceanic slab and separating island arcs from the continental crust (Andean-margin?) to the west which is preserved as gneissic domes (Fig. 1.3). Ries et al. (1983) proposed a southeast-dipping subduction zone for the evolution of the Neoproterozoic rocks along the Central Eastern Desert. However as noticed by Kröner et al. (1987), Ries et al. (1983)'s model would not be able to reconcile either the proposed suprasubduction-origin of ophiolitic rocks nor the mantle melting beneath the passive continental margin to the west. Shackleton (1994) argued that the direction of subduction polarity is not clear due to the scarcity of geochemical evidence. Farahat et al. (2004) studied the pillowed lavas in the CED and attributed their origin to rifting of continental crust in an ensialic back-arc basin. Recently, forearc geochemical signatures of the mantle ophiolitic rocks of the ED were recognized by Azer and Stern (2007) and Khalil and Azer (2007). A forearc setting was proposed for many areas in the ANS (Stern et al., 2004 and references therein). On the other hand, Zimmer et al. (1995) reported trace element geochemical and isotopic data for the Gerf ophiolite which show strong affinities for a true N-MORB setting. On the basis of the Nd and Sr isotopes, Stein and Goldstein (1996) and Stein (2003) proposed the involvement of a plume-type source and incorporation of oceanic plateaus in the juvenile crust formation process of the Neoproterozoic ANS.

1.4. Late-orogenic Neoproterozoic sedimentary rocks

Following the accretion of the arcs and fragments of oceanic crust, late-orogenic sedimentary and volcanic rocks were formed at the terminal stage of the evolution of the ANS. In Egypt, the late orogenic volcanic rocks were named the Dokhan Volcanic Series

and the late-orogenic sedimentary rocks were named the Hammamat Series by Hume (1934). The Hammamat area is famous for the quarrying of these renowned greywacke-siltstone “Bekhen-stone” and conglomerate “Breccia Vede d’Egitto” during the Pharaonic and Greco-Roman ages, respectively (Klemm and Klemm, 2001) (Fig. 1.4). Akaad and Nowier (1969) classified the 4 km thick sequences of the Hammamat Series in the Wadi Hammamat area into two formations, the lower Iгла Formation and the upper Shihimiya Formation. The Iгла Formation is composed of purple hematitic siltstones, greywackes and conglomerates. They divided the Shihimiya Formation into three members, the lower green-grey Rasafa Siltstone Member, followed by the polymictic Um Had Conglomerate Member and the upper Um Hassa Greywacke Member. The age of the Hammamat Group at Wadi Hammamat is between 616 and 519 Ma which are the ages of underlying Dokhan Volcanics and of the granites intruding the sedimentary rocks, respectively (Ries and Darbyshire, cited in Ries et al., 1983).

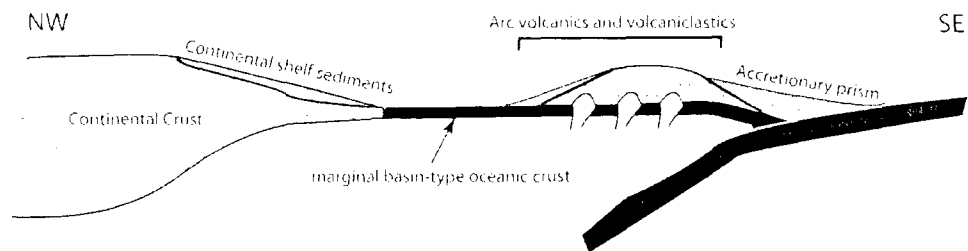


Fig. 1.3. The common model proposed for the evolution of the ophiolitic rocks of the Eastern Desert of Egypt (after Kröner 1985).

Although there is agreement that the Hammamat Group in the ED contains immature and molasse-type sedimentary rocks, there are many debates on their stratigraphic position, grade of metamorphism, and tectonic significance (Ries et al., 1993; Wilde and Youssef, 2002, and references therein). Regarding their relation with the Dokhan Volcanics, the Hammamat Group either underlies (Stern and Hedge, 1985),



Fig. 1.4 Hieroglyphic inscription engraved on the Um Hassa greywacke "Bekhen-stone" of Wadi Hammamat area.

overlies (Ries et al., 1983) or is interlayered (El-Gaby 1994) with Dokhan Volcanics. In terms of metamorphism, Hassan and Hashad (1990) proposed that the Hammamat Group was affected only by contact metamorphism, but Ahmed et al. (1988, cited in Wilde and Youssef, 2002) and Willis et al. (1988) mentioned that the Hammamat Group was

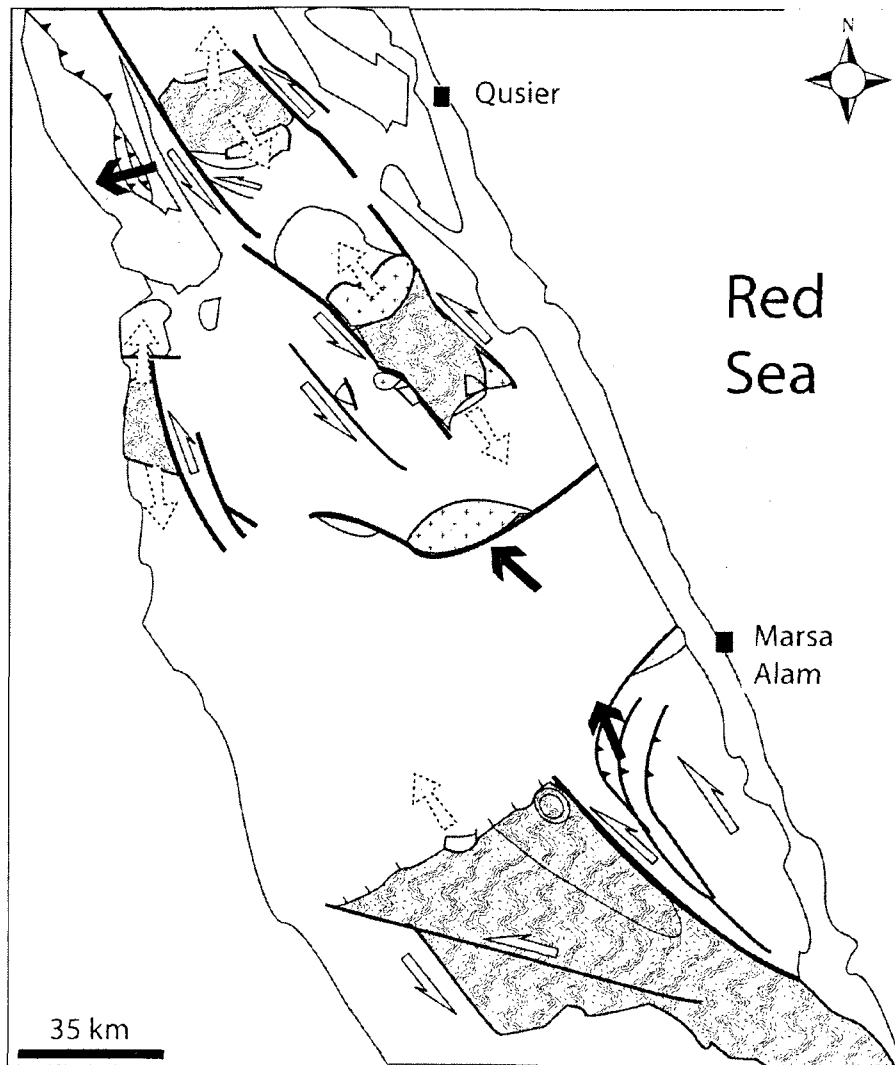
affected by low grade regional metamorphism as well. Various tectonic settings have been proposed for the Hammamat Group. Fritz et al. (1996) and Fritz and Messner (1999) considered these molasse-type basins as intramontane basins and classified them into two types on the basis of their spatial distribution within the orogen (Fig. 1.5). The first type is the external foreland basins located along the western part of the orogen. The second intramontane type is related to extensional collapses associated with the Najd strike slip fault system in agreement with Ries et al. (1993). Holail and Moghazi (1998) proposed an origin as intra-arc tectonic sediments for the Hammamat Group in the Eastern Desert of Egypt. However, Anderson et al. (2009) suggested the possibility that the Hammamat Group at Wadi Hammamat was deposited in piggy-back basins. The Hammamat sedimentary rocks being deposited in an intramontane region were suspected by Wilde and Youssef (2001, 2002). They suggested that the Hammamat Group was deposited in a major continental-scale fluvial system rather than being deposited in isolated basins. The same model was proposed by Ries et al. (1983) for the upper part of the Hammamat Group at Wadi Hammamat.

1.5. Objectives

The main objectives of this study stem mainly from the exuberant debates over the origin of the Neoproterozoic ophiolitic rocks and associated late orogenic sedimentary rocks in Egypt. This study uses new field and petrographical observations, and major and trace element geochemical data from the Neoproterozoic ophiolitic rocks and associated molasse-type sedimentary rocks of the Central Eastern Desert of Egypt to better constrain:

- 1) Tectonic settings in which the ophiolitic rocks formed in the Central Eastern Desert.
- 2) The nature of the mantle sources from which these oceanic rocks were derived.
- 3) The role and extent of contribution of the subduction- and/or plume-related processes in the formation of these ophiolitic rocks,
- 4) The direction of subduction during Neoproterozoic times above which these ophiolitic rocks had been formed and accreted,
- 5) The nature of contribution of the ophiolitic-derived material to the late orogenic sedimentary rocks,
- 6) The nature and provenance of the late orogenic molasse-type sedimentary rocks of the Central Eastern Desert.
- 7) The tectonic setting of the depositional basins of such sediments,
- 8) The geodynamic evolution of the Central Eastern Desert of Egypt during the Neoproterozoic.

A better understanding of these points, especially point 8, is important for further understanding of the crustal evolution of the ANS during Neoproterozoic times when continental growth rates reached up to $1 \text{ km}^3 \cdot \text{year}^{-1}$ (Reymer and Schubert, 1986). Although the field observations and petrography of the ophiolitic rocks will be described, whole-rock geochemistry will be the main tool to be used to address the objectives listed above. A total of 117 samples were analyzed for major elements and 135 samples were analyzed for their trace element composition. However, both petrography and geochemistry will be used for the sedimentary rocks. The samples were collected during two field trips in 2004 and 2006 to the Wadi Ghadir area and Qift-Qusier road.



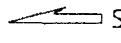
- | | | | |
|---|-----------------------|--|----------------------|
|  | Phanerozoic sediments |  | Normal faults |
|  | Pan-African nappes |  | Thrust faults |
|  | Molasse sediments |  | Normal Faulting |
|  | Syntectonic pluton |  | Strike-slip faulting |
|  | Basement domes |  | Thrusting |

Fig. 1.5. Distribution of the molasse basins in the Eastern Desert with the associated tectonic features.
(after Fritz et al., 1996)

1.6. Framework of the thesis

The thesis consists of three core chapters (2, 3, 4) preceded by an Introduction (chapter 1) followed by Conclusions (chapter 5). Each of the core chapters is presented in paper format which results in some repetition in the analytical procedure, geological background and references.

Chapter 2 presents a study of the Wadi Ghadir ophiolite in the Central Eastern Desert. The Wadi Ghadir ophiolite is the first-recorded most complete ophiolitic complex preserved within the *mélange* of the Eastern Desert. The chapter deals mainly with the whole-rock geochemistry of the crustal units of the Wadi Ghadir ophiolite and the different dike phases intruding them. This chapter also tries to draw attention to the evolution of the area through inferring the tectonic setting of the Wadi Ghadir ophiolite and the spatially associated rock units. This chapter was accepted for publication in *Lithos* and is in press now (published online).

Chapter 3 presents a study on another occurrence of the ophiolitic rocks in the Central Eastern Desert, the Fawakhir ophiolite. As in the previous chapter, this study uses the whole rock chemistry of the different ophiolitic crustal rock units and the dissected dikes to understand the tectonic setting in which the Fawakhir ophiolite formed. In addition, the study introduces geochemical results from another occurrence of the pillow lavas along Qift-Qusier Road, which transects the whole *mélange* of the Central Eastern Desert. The variation between the *mélange* blocks and the Fawakhir ophiolite will be studied trying to understand the geodynamic evolution of this transect along the Central Eastern Desert. This Chapter has been submitted to *Precambrian Research*.

Chapter 4 contains new petrographic and geochemical data on the late-orogenic molasse-type sedimentary rocks in the Wadi Hammamat area. This study can be considered a complementary practice to understand the evolution of the Neoproterozoic rocks along the Qift-Qusier transect. As these sedimentary rocks are younger than the ophiolitic rocks, the inference of their provenance and their tectonic setting leads to a better understanding of the temporal evolution of the Neoproterozoic rocks of the CED along the Qift-Qusier transect. This chapter will be submitted to the *Journal of African Earth Sciences*.

References

- Abd El-Naby, H., Frisch, W., 2006. Geochemical constraints from the Hafafit Metamorphic Complex (HMC): Evidence of Neoproterozoic back-arc basin development in the Central Eastern Desert of Egypt. *Journal of African Earth Sciences* 45, 173-186.
- Abdelsalam, M.G. 1994. The Oko Shear Zone, Sudan: post-accretionary deformation in the Arabian-Nubian Shield. *Journal of the Geological Society, London* 151, 767-776.
- Abdelsalam, M.G., Stern, R.J. 1996. Sutures and shear zones in the Arabian Nubian Shield. *Journal of African Earth Sciences*, 23, 289-310.
- Abdelsalam, M.G., Stern, R.J., Copeland, P., Elfaki, E.M., Elhur, B., Ibrahim, F.M., 1998. The Neoproterozoic Keraf suture in NE Sudan: Sinistral transpression along the eastern margin of West Gondwana. *Journal of Geology* 106, 133-147.
- Ahmed, A.E.A., Habesh, M.L., Mawas, S.G., 1988. Dokhan Volcanics of Abu Gawa area and their epiclastic derivatives, Central Eastern Desert, Egypt. *Bulletin of the Faculty of Science, Assiut University* 17, 195-222.
- Al Filali, I.Y., Hassan, M.A., Hashad, A.H., 1993. Significance of some mantled gneiss domes in the Arabian-Nubian Shield. *Annual Geological Survey, Egypt*, xix, 33-46.
- Alabaster, T., Pearce, J. Malpas, J., 1982. Volcanic stratigraphy and petrogenesis of the Oman ophiolitic complex. *Contributions to Mineralogy and Petrology* 81, p. 168-183.
- Amstutz, G.C., 1980. The early history of term Ophiolites and its evolution until 1945. In Panayiotou, A., (ed) *Ophiolites-Proceedings of the International Ophiolite symposium, Cyprus, 1979*, 149-152.

- Andresen, A., Abu El-Rus, M.A., Myhre, P.I., Boghdady, G.Y., Corfu, F., 2009. U-Pb TIMS age constraints on the evolution of the Neoproterozoic Meatiq Gneiss Dome, Eastern Desert, Egypt. *International Journal of Earth Sciences*, 98, 481-497.
- Anonymous, 1972. Penrose Field Conference on ophiolites. *Geotimes* 17, 24-25.
- Azer, M.K., Stern, R.J., 2007. Neoproterozoic (835-720 Ma) serpentinites in the Eastern Desert, Egypt: Fragments of forearc mantle. *The Journal of Geology* 115, 457-472.
- Beccaluva, L., Coltorti, M., Giunta, G., Siena, F., 2004. Tethyan vs. Cordilleran ophiolites: a reappraisal of distinctive tectono-magmatic features of supra-subduction complexes in relation to the subduction mode. *Tectonophysics* 393, 163-174.
- Bernoulli, D., Jenkyns, H.C., 2009. Ophiolites in ocean–continent transitions: From the Steinmann Trinity to sea-floor spreading. *Comptes Rendus Geoscience*, doi:10.1016/j.crte.2008.09.009
- Bittmann, A., 1958. Geosynclinal volcanism, ophiolites and Barramiya rocks. *The Egyptian Journal of Geology* II, 61-65.
- Blasband, B., White, P., Brooijmans, H., de Boorder, H. Visser, W., 2000. Late Proterozoic extensional collapse in the Arabian-Nubian Shield. *Journal of the Geological Society, London*, 157, 615–628.
- Boudier, F., Nicolas, A., 1985. Harzburgite and lherzolite subtypes in ophiolitic and oceanic environments. *Earth and Planetary Science Letters* 76, 84-92.
- Bregar, M., Bauernhofer, A., Pelz, K., Kloetzli, U., Fritz, H. and Neumayr, P., 2002. A late Neoproterozoic magmatic core complex in the Eastern Desert: emplacement of granitoids in a wrench-tectonic setting. *Precambrian Research* 118, 59-82.
- Brongniart, A., 1813. Essai de classification minéralogique des roches mélanges. *Journal des Mines* XXXIV, 190-199.
- Casey, J.F., Dewey, J.F., 1984. Initiation of subduction zones along transform and accreting plate boundaries, triple-junction evolution, and forearc spreading centres-implications for ophiolitic geology and obduction. In Gass, I.G., Lippard, S.J., Shelton, A.W., (eds) *Ophiolites and oceanic lithosphere*, Geological Society of London Special Publications 13, 269-290.
- Church, W.R., 1988. Ophiolites, sutures, and microplates of the Arabian-Nubian Shield: A critical comment. In: El-Gaby, S., Greiling, R.O. (Eds.), *The Pan-African Belt of Northeast Africa and Adjacent Areas: Tectonic Evolution and Economic Aspects of a Late Proterozoic Orogen*, Friedrich, Vieweg, Sohn Verlagsgesellschaft mbH, 289-316.

- Corcoran, P.L., Mueller, W.U., Kusky, T.M., 2004. Inferred ophiolites in the Archean Slave Craton. In: Kusky T.M., ed. *Precambrian Ophiolites and Related Rocks*. *Developments in Precambrian Geology* 13, 363-404.
- Dilek, Y., 2003. Ophiolite pulses, mantle plumes and orogeny. In Dilek, Y., Robinson, R.T., (eds) *Ophiolites in Earth History*. Geological Society of London Special Publications 218, 9-19.
- Dilek, Y., 2003. Ophiolite concept and its evolution. In Dilek, Y. and Newcomb, S., (eds.) *Ophiolite Concept and the Evolution of Geological Thoughts*: Boulder, Colorado, Geological Society of America Special Paper 373, 1-16.
- Dilek, Y., Polat, A., 2008. Suprasubduction zone ophiolites and Archean tectonics. *Geology* 36, 431-432.
- El Bayoumi, R.M., 1980. Ophiolites and associated rocks of Wadi Ghadir, east of Gabal Zabara, Eastern Desert, Egypt. Ph.D. Thesis, Cairo University, Egypt, 171 pp.
- El Bayoumi, R.M., 1983. Ophiolites and mélange complex of Wadi Ghadir area, Eastern Desert, Egypt. *Bulletin of King Abdelaziz University* 6, 329-342.
- El Bayoumi, R.M.A., Greiling, R.O., 1984. Tectonic evolution of a Pan-African plate margin in southeastern Egypt – a suture zone overprinted by low angle thrusting? In: Klerkx, J., Michot, J. (Eds.), *Géologie Africaine-African Geology*. Musee royal de l'Africaine Centrale, Tervuren, Belg, 47-56.
- El Gaby, S., List, F.K., Tehrani, R., 1988. Geology, evolution and metallogensis of the Pan-African belt in Egypt. In: El-Gaby, S., Greiling, R.O. (Eds.), *The Pan-African Belt of Northeast Africa and Adjacent Areas: Tectonic Evolution and Economic Aspects of a Late Proterozoic Orogen*. Friedrich. Vieweg, Sohn Verlagsgesellschaft mbH, 17-68.
- El Ramly, M.F., Greiling, R., Kröner, A., Rashwan, A.A., 1984. On the tectonic evolution of the Wadi Hafafit area and environs, Eastern Desert of Egypt. *Bulletin of King Abdelaziz University* 6, 113-126.
- El Sayed M.M., Furnes H., Mohamed F.H., 1999. Geochemical constraints on the tectonomagmatic evolution of the late Precambrian Fawakhir ophiolite, Central Eastern Desert, Egypt. *Journal of African Earth Science* 29, 515-533.
- El Sharkawy, M.A., El Bayoumi, R.M., 1979. The ophiolites of Wadi Ghadir area Eastern Desert, Egypt. *Annual Geological Survey, Egypt* 9, 125-135.
- Farahat E.S., El Mahalawi M.M., Hoinkes G., Abdel Aal A.Y., 2004. Continental back-arc basin origin of some ophiolites from the Eastern Desert of Egypt. *Mineralogy and Petrology* 82, 81-104.

- Flower, M.F.J., Dilek, Y., 2003. Arc-trench rollback and forearc accretion: 1.A collision-induced flow model for Tethyan ophiolites. In Dilek, Y., Robinson, R.T., (eds) *Ophiolites in Earth History*. Geological Society of London Special Publications 218, 21-41.
- Fritz, H., Messner, M., 1999. Intramontane basin formation during oblique convergence in the Eastern Desert of Egypt: magmatically versus tectonically induced subsidence. *Tectonophysics* 315, 145–162.
- Fritz, H., Wallbrecher, E., Khudeir, A.A., Abu El Ela, F., and Dallmeyer, D.R., 1996. Formation of Neoproterozoic metamorphic core complexes during oblique convergence (Eastern Desert, Egypt). *Journal of African Earth Sciences* 23, 311-329.
- Furnes, H., de Wit, M., Staudigel, H., Rosing, M., Muehlenbachs, K., 2007. A vestige of Earth's oldest ophiolite. *Science* 315, 1704-1707.
- Furnes, H., de Wit, M., Staudigel, H., Rosing, M., Muehlenbachs, K., 2007. Response to comments on "A vestige of Earth's oldest ophiolite". *Science* 318, 746e.
- Hamilton, W.B., Comment on "A vestige of Earth's oldest ophiolite". *Science* 318, 746d.
- Hassan, M.A., Hashad A.H., 1990. Precambrian of Egypt. In: R. Said, (ed) *The Geology of Egypt*, A.A. Balkema, Rotterdam, Netherlands, 201–245.
- Hawkins, J.W., 2003. Geology of suprasubduction zones-Implications for the origin of ophiolites. In Dilek, Y. and Newcomb, S., (eds.) *Ophiolite Concept and the Evolution of Geological Thoughts: Boulder, Colorado*, Geological Society of America Special Paper 373, 17-29.
- Hébert, R., 2007. Ophiolite: From the beginning to the modern times. *Geoscience Canada* 34, 135-150.
- Holail, H.M., Moghazi, A.M., 1998. Provenance, tectonic setting and geochemistry of greywackes and siltstones of the Late Precambrian Hammamat Group, Egypt. *Sedimentary Geology* 116, 227-250.
- Hume, W.E., 1934. *Geology of Egypt. Volume 2: The fundamental Pre-Cambrian rocks of Egypt and the Sudan: Their distribution, age and character.* Government Press, Cairo.
- Jacobs, J., Thomas, R.J., 2004. Himalayan-type indenter-escape tectonics model for the southern part of the late Neoproterozoic-early Paleozoic East African-Antarctic orogen. *Geology* 32, 721-724.
- Johnson, P.R., Abdelsalam, M., Stern, R.J., 2002. The Bir Umq-Nakasib fault zone: Geology and structure of a Neoproterozoic suture. Kingdom of Saudi Arabia and Sudan. Saudi Geological Survey Open-File Report SG-OF-2002-1.

- Johnson, P.R., Kattan, F.H., 2008. Lithostratigraphic revision in the Arabian Shield: the impacts of geochronology and tectonic analysis. *The Arabian Journal for Science and Engineering* 33, 3-16.
- Johnson, P.R., Kattan, F.H., Wooden, J.L., 2001. Implications of SHRIMP and Microstructural Data on the Age and Kinematics of Shearing in the Asir Terrane, Southern Arabian Shield, Saudi Arabia. *Gondwana Research* 4, 172-173.
- Johnson, P.R., Woldehaimanot, B., 2003. Development of the Arabian-Nubian Shield: perspective on accretion and deformation in the northern East African Orogen and the assembly of Gondwana. In, Yoshida, M., Windley., B.F., and Dasgupta, S., (eds) *Proterozoic East Gondwana: Supercontinent assembly*. Geological Society, London, Special Publication 206, 289-325.
- Kerrick, R., Polat, A., 2006. Archean greenstone-tonalite duality: Thermochemical mantle convection models or plate tectonics in the early Earth global dynamics. *Tectonophysics* 415, 141-165.
- Khalil, A.E.S., Azer, M.K., 2007. Supra-subduction affinity in the Neoproterozoic serpentinites in the Eastern Desert, Egypt: Evidence from mineral composition. *Journal of African Earth Sciences* 49, 136-152.
- Klemm, D.D., Klemm, R., 2001. The building stones of ancient Egypt-a gift of its geology. *Journal of African Earth Sciences* 33, 631-642.
- Kröner, A., 1984. Late Precambrian plate tectonics and orogeny: a need to redefine the term Pan-African, in Klerkx, J., and Michot, J., (eds.) *African Geology*. Tervuent Musee, R. L'Afrique Centrale, 23-28.
- Kröner, A., 1985. Ophiolites and the evolution of tectonic boundaries in the late Proterozoic Arabian-Nubian Shield of northeast Africa and Arabia. *Precambrian Research* 27, 277-300.
- Kröner, A., Greiling, R.O., Reischmann, T., Hussein, I.M., Stern, R.J., Durr, S., Kruger, J., Zimmer, M., 1987. Pan-African crustal evolution in the Nubian segment of northeast Africa. In: Kröner, A., (Ed.) *Proterozoic lithospheric evolution*. American Geophysical Union, *Geodynamics Series* 17, 237-257.
- Kröner, A., Todt, W., Hussein, I.M., Mansour, M., Rashwan, A.A., 1992. Dating of late Proterozoic ophiolites in Egypt and the Sudan using the single grain zircon evaporation technique. *Precambrian Research* 59, 15-32.
- Kröner, A., Windley, B.F., Badarch, G., Tomurtogoo, O., Hegner, E., Jahn, B.M., Gruschka, S., Khain, E.V., Demoux, A., Wingate, M.T.D., 2007. Accretionary growth and crustal

formation in the Central Asian Orogenic Belt and comparison with the Arabian-Nubian Shield. In Hatcher, R.D., Carlson, Jr.M.B., MacBride, J.H., and Catalan, J.M. (Eds.) 4-D framework of the continental crust-In targeting crustal processes through time. Geological society of America, Memoir 200, 181-209.

- Kusky, T.M., 2004. Precambrian ophiolites and related rocks. Amsterdam, Netherland, Elsevier.
- Metcalfe, R.V., Shervais, J.W., 2008. Suprasubduction-zone ophiolites: Is there really an ophiolite conundrum? In Wright, J.E., Shervais, J.W., (eds) Ophiolites, arcs, and batholiths: A tribute to Cliff Hopson. . Geological Society of America Special Paper 438, 191-222.
- Miyashiro, A., 1973. The Troodos complex was probably formed in an island arc. Earth and Planetary Science Letters 19, 218-224.
- Miyashiro, A., 1975. Classification, characteristics, and origin of ophiolites. Journal of Geology 83, 249-281.
- Moores, E.M., 1982. Origin and emplacement of ophiolites. Reviews of Geophysics and Space Physics 20, 735-760.
- Moores, E.M., 2002. Pre-1 Ga (pre-Rodinian) ophiolites: Their tectonic and environmental implication. Geological Society of American Bulletin 114, 80-95.
- Moores, E.M., 2003. A personal history of the ophiolite concept. In Dilek, Y. and Newcomb, S., (eds.) Ophiolite Concept and the Evolution of Geological Thoughts: Boulder, Colorado, Geological Society of America Special Paper 373, 17-29.
- Moores, E.M., Kellogg, L.H., Dilek, Y., 2000. Tethyan ophiolites, mantle convection, and tectonic "historical contingency": a resolution of the "ophiolite conundrum". In Dilek, Y., Moores, E.M., Elthon, D., Nicolas, A., (eds) Ophiolites and oceanic crust: New insights from field studies and the Ocean Drilling Program. Geological Society of America Special Paper 349, 3-12.
- Nicolas, A., 1989. Structures of ophiolites and dynamics of oceanic lithosphere. Dordrecht, Netherlands, Kluwer Academic Publishers.
- Nicolas, A., Boudier, F., 2003. Where ophiolites come from and what they tell us. In Dilek, Y. and Newcomb, S., (eds.) Ophiolite Concept and the Evolution of Geological Thoughts: Boulder, Colorado, Geological Society of America Special Paper 373, 137-152.
- Nutman, A.P., Friend, C.R.L., 2007. Comment on "'A vestige of Earth's oldest ophiolite'". Science 318, 746c.
- Pallister, J.S., Stacey, J.S., Fischer, L.B., Premo, W.R., 1988. Precambrian ophiolites of Arabia: geologic settings, U-Pb geochronology, Pb-isotope characteristics, and implications for continental accretion. Precambrian Research, 38: 1-54.

- Pearce, J.A., 2003. Supra-subduction zone ophiolites: The search for modern analogues. In Dilek, Y. and Newcomb, S., (eds.) *Ophiolite Concept and the Evolution of Geological Thoughts*: Boulder, Colorado, Geological Society of America Special Paper 373, 269-293.
- Pearce, J.A., 2008. Geochemical fingerprinting of oceanic basalts with applications to ophiolite classification and the search for Archean oceanic crust. *Lithos* 100, 14-48.
- Pearce, J.A., Lippard, S.J., Roberts, S., 1984. Characteristics and tectonic significance of supra-subduction zone ophiolites. In Kokelaar, B.P. and Howells, M.F., (eds) *Marginal Basin Geology: Volcanic and Associated Sediments and Tectonic Processes in Modern and Ancient Marginal Basins*. Geological Society of London Special Publications 16, 77-94.
- Reymer, A., Schubert, G., 1986. Rapid growth of major segments of continental crust. *Geology* 14, 299-302.
- Ries, A.C., Osman, A.F., Sadek, M.F., Ragab, A.I., Abdeen, M.M., 1993. Preliminary comparison of six late- to post-Pan-African molasse basins, E. Desert, Egypt. In Thorweihe, U., Schandelmeier, H., (eds) *Geoscientific research in Northeast Africa*. Balkema, Rotterdam.
- Ries, A.C., Shackleton R.M., Graham R.H., Fitches W.R., 1983. Pan-African structures, ophiolites and mélanges in the Eastern Desert of Egypt: a traverse at 26° N. *Journal of Geological Society* 140, 75-95.
- Robinson, P.T., Malpas, J., Dilek, Y., Zhou, M., 2008. The significance of sheeted dike complexes in ophiolites. *GSA Today* 18, 4-10.
- Şengör, A.M.C., Natal'in B.A., 1996. Turcic-type orogeny and its role in the making of the continental crust. *Annual Review of Earth Planet Science* 24, 263-337.
- Serri, G., 1981. The petrochemistry of ophiolite gabbroic complexes: a key for the classification of ophiolites into low-Ti and high-Ti types. *Earth and Planetary Science Letters* 52, 203-212.
- Shackleton, R.M., 1994. Review of late Proterozoic sutures, ophiolitic mélanges and tectonics of eastern Egypt and north-east Sudan. *Geologische Rundschau* 83, 537-546.
- Shackleton, R. M., 1996. The final collision zone between East and West Gondwana: where is it? *Journal of African Earth Sciences* 23, 271-287.
- Shackleton, R.M., Ries A.C., Graham R.H., Fitches W.R., 1980. Late Precambrian ophiolite mélange in the eastern desert of Egypt. *Nature* 285, 472-474.
- Shervais, J.W., 2001. Birth, death, and resurrection: The life cycle of supra-subduction zone ophiolites. *Geochemistry, Geophysics, Geosystems*, 2, doi: 10.1029/2000GC000080.

- Stein, M., 2003. Tracing the plume material in the Arabian-Nubian Shield. *Precambrian Research* 123, 223-234.
- Stein, M., Goldstein, S.L., 1996. From plume head to continental lithosphere in the Arabian-Nubian Shield. *Nature* 382, 773-778.
- Steinmann, G., 1927. Der ophiolitischen Zonen in der Mediterranean Kettengebirgen. 14th International Geological Congress in Madrid 2, 638-667.
- Steinmann, G., 2003. Die ophiolitischen Zonen in den mediterranen Kettengebirgen (The ophiolitic zones in the Mediterranean mountain chains). Bernouilli, D. and Friedman, G.M., translators. in Dilek, Y. and Newcomb, S., (eds.) *Ophiolite Concept and the Evolution of Geological Thoughts: Boulder, Colorado, Geological Society of America Special Paper* 373, 77-91.
- Stern, R.J., 1994. Arc assembly and continental collision in the Neoproterozoic East African Orogen: implications for the consolidation of Gondwanaland. *Annual Review of Earth and Planet Sciences* 22, 319–351.
- Stern, R.J., 2005. Evidence from ophiolites, blueschists, and ultrahigh-pressure metamorphic terranes that modern episodes of subduction tectonics began in Neoproterozoic time. *Geology* 33, 557-560.
- Stern, R.J., Bloomer, S.H., 1992. Subduction zone infancy: Examples from the Eocene Izu-Bonin-Mariana and Jurassic California arcs. *Geological Society of American Bulletin* 104, 1621-1636.
- Stern, R.J., Hedge, C.E., 1985. Geochronologic and isotropic constraints on Late Precambrian crustal evolution in the Eastern Desert of Egypt. *American Journal of Science* 285, 97-127.
- Stern, R.J., Johanson, P.R., Kroner, A., Yibas, B., 2004. Neoproterozoic ophiolites of the Arabian-Nubian Shield. In: Kusky TM, ed. *Precambrian Ophiolites and Related Rocks. Developments in Precambrian Geology*, vol. 13, Amsterdam: Elsevier. 95-128.
- Stern, R.J., Nielsen, K.C., Best, E., Sultan, M., Arvidson, R.E. and Kröner, A., 1990. Orientation of late Precambrian sutures in the Arabian-Shield shield. *Geology* 18, 1103-1106.
- Stoeser, D.B., Camp, V.E., 1985. Pan African microplate accretion of the Arabian Shield. *Geological Society of American Bulletin* 96, 817-26.
- Stoeser, D.B., Stacey, J.S., 1988. Evolution, U-Pb geochronology, and isotope geology of the Pan-African Nabitah orogenic belt of the Saudi Arabian Shield. in S. El-Gaby and R.O. Greiling, eds., *The Pan-African belt of Northeast Africa and adjacent areas: Braunschweig Wiesbaden, Vieweg and Shn*, 227-288.

- Sultan, M., Bickford, M.E., El Kaliouby, B., and Arvidson, R.E., 1992. Common Pb systematics of Precambrian granitic rocks of the Nubian Shield (Egypt) and tectonic implications. *Geological Society of American Bulletin* 104, 456-70.
- Sylvester, P.J., Haper, G.D., Byerly, G.R., Thurston, P.C., 1997. Volcanic aspects. In de Wit, M., Ashwal, L.D., (eds) *Greenstone belts*. Oxford Monograph on Geology and Geophysics 35, 55-90.
- Wilde, S.A., Youssef, K., 2001. SHRIMP U-Pb dating of detrital zircons from Hammamat Group at Gebel Um Tawat, Northern-Eastern Desert, Egypt. *Gondwana Research* 4, 202-206.
- Wilde, S.A., Youssef, K., 2002. A re-evaluation of the origin and setting of the late Precambrian Hammamat Group based on SHRIMP-U-Pb dating of detrital zircons from Gebel Umm Tawat, North Eastern Desert, Egypt. *Journal of Geological Society London* 159, 595-604.
- Willis, K.M., Stern, R.J., Clauer, 1988. Age and geochemistry of Late Precambrian sediments of the Hammamat Series from the Northeastern Desert of Egypt. *Precambrian Research* 42, 173-187.
- Zimmer, M., Kröner, A., Jochum, K.P., Reischmann, T., Todt, W., 1995. The Gabal Gerf complex: a Precambrian N-MORB ophiolite in the Nubian Shield, NE Africa. *Chemical Geology* 123, 29-51.

Chapter 2

Geochemistry and tectonic evolution of the Neoproterozoic Wadi Ghadir ophiolite, Eastern Desert, Egypt

2.1. Introduction

Preservation of ophiolitic rocks in the geological record has important implications for understanding the evolution of ancient orogenic belts (Dilek, 2003). Given that ophiolites are fragments of ancient oceanic lithosphere that were tectonically accreted to continental margins, they provide evidence for seafloor spreading and closure of ocean basins along convergent plate margins (Stern, 2004). The Neoproterozoic Era is unique in Earth history because it marks the widespread formation of ophiolites (Stern, 2005). Neoproterozoic ophiolites are especially common in the Arabian-Nubian Shield (ANS) and in the Central Asian Orogenic Belt (CAOB) (Şengör and Natal'n, 2004; Stern, 2005, 2007). Ages of the ANS ophiolites are tightly clustered around 870 to 690 Ma (Dilek and Ahmed, 2003; Stern et al., 2004), in comparison to ages of CAOB ophiolites which range from ~ 1000 Ma to Permian (Kröner et al., 2007).

The Eastern Desert of Egypt is part of the Neoproterozoic ANS. The ANS is separated by the Red Sea into the Nubian Shield in northeast Africa and the Arabian Shield in western Arabia. The ANS represents the northern part of the East African Orogen (EAO), a large orogenic system formed near the end of the Proterozoic by collision between East and West Gondwana during the Pan-African Orogeny (Stern, 1994).

Deciphering the tectonic settings of the ophiolites in the ANS is an important step for understanding the evolution of the Pan-African orogeny. The tectonic setting and evolution of Proterozoic ophiolites in the ANS remain controversial (Zimmer et al., 1995; El-Sayed et al., 1999; Reischmann, 2000; Dilek and Ahmed, 2003; Farahat et al., 2004; Şengör and Natal'in, 1996; Stern et al., 2004). Ophiolites of the Central Eastern Desert (CED) of Egypt occur as dismembered blocks in a tectonic *mélange* (Shackleton et al., 1980; Ries et al., 1983; Church, 1988; El-Gaby et al., 1988). According to Sultan et al. (1992) and Abdelsalam and Stern (1996), the ophiolitic *mélange* in the CED is a result of deformation by the post-accretionary Najd fault system and therefore does not represent a suture zone. El-Sharkawy and El-Bayoumi (1979) and El-Bayoumi (1980) were pioneers in identifying the Neoproterozoic oceanic crust in the Wadi Ghadir. On the basis of the geochemistry of the ophiolitic rocks, El-Bayoumi (1980) proposed a similarity to mid-ocean ridge basalt (MORB) affected by plume-related magma. Kröner (1985) suggested a marginal basin tectonic setting for the origin of these Neoproterozoic oceanic rocks. Using the geochemistry of the pillow lavas, Farahat et al. (2004) proposed an ensialic back-arc basin setting for ophiolitic rocks in the CED, including the Wadi Ghadir ophiolite (WGO).

The ANS ophiolitic mantle is composed mainly of tectonized harzburgite with lherzolite and is extensively serpentinitized (Stern et al., 2004). On the basis of spinel compositions, two different tectonic settings have been inferred for the peridotites in the Eastern Desert ophiolites. Ahmed et al. (2001) proposed that the ophiolitic harzburgite is either a fragment of oceanic lithosphere modified by arc-related magmas or a fragment of back-arc basin lithosphere. Azer and Stern (2007) suggested that the serpentinitized

peridotites of the Eastern Desert ophiolites resemble peridotites from modern oceanic forearcs. The serpentinites of the WGO are interpreted to be derived from harzburgite-dunite parental rocks formed at a mid-ocean ridge and subsequently emplaced in a subduction zone setting (Khalil, 2007). The petrogenesis and mantle source composition of the crustal rocks of the WGO are therefore poorly understood.

We present new geochemical data for forty six samples from the WGO units (gabbros, pillow lavas and cutting dikes) and twenty two samples from the surrounding ophiolitic mélangé. The objectives of this study are: (1) to document the geochemistry and petrogenesis of the WGO and cross-cutting dikes; (2) to evaluate the composition of the mantle source of the ophiolitic magmas; and (3) to present a geodynamic model for the evolution of the WGO.

2.2. Geology of the WGO

The Wadi Ghadir area is located in the central part of the Eastern Desert of Egypt and is occupied by a Neoproterozoic ophiolitic mélangé composed mainly of ophiolitic fragments embedded in a sheared serpentinite and pelitic matrix (Fig. 2.1a,b). The ophiolitic rocks were described in detail by El-Bayoumi (1980). He reported the best exposure of ophiolitic rocks which occurs along Wadi El Beda and Wadi Saudi, the southwestern and western extensions of Wadi Dob Nia, which is a tributary of Wadi Ghadir (Fig. 2.1b). The ophiolite in Wadi El Beda is composed of tectonically imbricated blocks of gabbroic and volcanic rocks dipping to the southwest. Ultramafic mantle rocks are lacking in the ophiolite, but are widespread in the mélangé as highly serpentinized blocks ranging from centimeters to kilometers in size, reaching up to mountain size as in

Gebel Lawi and Gebel El Lewiwi. The Wadi Ghadir mélange is intruded by leucogabbros at Wadi El Beda and by different types of calc-alkaline granitoid plutons exposed in the eastern part of the Wadi Ghadir area (Fig. 2.2a; El-Bayoumi, 1983).

Plutonic rocks of the WGO are composed of layered, coarse-grained massive and hypabyssal gabbros. Although they are structurally imbricated units, dipping moderately to the southwest, the layered gabbro is considered as the basal unit, transitional upward into the massive coarse-grained gabbro and the hypabyssal gabbro at the top. The basal gabbro is rhythmically layered with plagioclase-rich leuco-layers alternating with dark layers rich in altered pyroxene (Fig. 2.2b), both showing cumulate textures. The coarse-grained massive gabbro has a mottled appearance of rosette structure (Fig. 2.2c), which resulted from the irregular concentrations of dark altered pyroxene and light plagioclase crystals in adjacent spots. The massive gabbro displays horizontal shear zones with mylonitic and foliated fabrics. Hypabyssal gabbro has the same mineralogy but finer grain size than the other two types of gabbros. Some of these gabbro exposures show relict pyroxene and plagioclase phenocrysts. The gabbroic complex encloses large pods of pegmatitic gabbro and less common anorthosite, trondhjemite, and plagiogranite. The gabbroic complex is intruded by many diabasic dikes and sills. Their attitudes vary from sub-horizontal at the base, parallel to the layered gabbro, to sub-vertical near the top. Zircon dating of a plagiogranite revealed an age of 746 ± 19 Ma for the WGO (Kröner et al., 1992).

Pillow lavas are exposed at the northeastern end of Wadi El Beda and the eastern end of Wadi Saudi (Fig. 2.1c). The pillow lava flows of Wadi El Beda extend for 400 m in length. Pillows vary in shape, from circular to oval and in size from 20 cm to 1.5 m in

diameter. Pillows, especially the larger ones, have massive green cores and vesicular margins (Fig. 2.2d). Pillow lavas are aphanitic, but plagioclase microphenocrysts are locally visible. In Wadi Saudi pillow lavas extend laterally for about 70 m. In contrast to the vesicular pillow lavas of Wadi El Beda, pillow lavas in Wadi Saudi are plagiophyric and less vesicular (Fig. 2.2e).

The mafic dikes are abundant in the area, cross-cutting the plutonic complex and the pillow lavas as individual dike swarms. The dikes intruding the gabbros vary in orientation, mainly striking NW-SE and NE-SW. In pillow lavas of Wadi El Beda, the dikes strike mostly NW-SE and dip SW. Some dikes cross-cutting the pillow lavas are folded, with fold axes plunging $\sim 25^\circ$ NW.

The rest of the Wadi Ghadir mélangé is heterogeneous. Although the predominant blocks in the mélangé are ophiolitic, blocks of talc-carbonate rocks, serpentinites, volcano-sedimentary and plutonic rocks are also common. The mélangé also encloses highly disrupted dike swarms forming coherent massive blocks within the sheared mélangé matrix (Fig. 2.2f). The block-to-matrix ratio of the Wadi Ghadir mélangé (WGM) decreases towards the east. Farther to the west mafic and intermediate volcanic rocks occur as large blocks within a finer sedimentary matrix. To the north of the Hafafit gneissic dome, intermediate and felsic volcanic rocks crop out in a tuffaceous matrix, extending to Marsa Alam in the east. All volcanic rocks have been defined as a part of an island arc-back-arc complex in the Central Eastern Desert (Takla et al., 1990; Ramly et al., 1998; Hassanien, 2001).

2.3. Petrography

Different types of gabbros in the WGO share many petrographical features. They are composed generally of plagioclase and altered pyroxene. Gabbros have subophitic to ophitic texture (Fig. 2.3a). The crystallization sequence varies from olivine-plagioclase-clinopyroxene, which is the dominant order, to less common olivine-clinopyroxene-plagioclase. In cumulate gabbros, plagioclase and pyroxene represent the cumulus and intercumulus phases, respectively. Plagioclase laths are altered to epidote, albite, sericite and chlorite in order of decreasing abundance. The degree of albitization varies from intense pseudomorphic replacement to the development of chess-board albite rims around plagioclase laths. Augite is variably altered to hornblende (Fig. 2.3b). Some pyroxene crystals form coarse oikocrysts enclosing many plagioclase laths. Hornblende is altered further to fine aggregates of actinolite and chlorite. The space between plagioclase cumulate crystals is locally occupied by secondary minerals such as actinolite, chlorite, epidote and calcite, and accessory minerals, such as opaque minerals, apatite and quartz. Plagioclase ranges from ~90% in leucoeratic layers to ~20% in the melanocratic layers. Plagioclase laths, especially in the leucoeratic layers, exhibit local alignment parallel to layer boundaries.

Pillow lavas in the WGO are divided into aphyric and porphyritic lavas, both of which are composed of altered plagioclase and ferromagnesian minerals. The ferromagnesian minerals are completely altered to hornblende, actinolite, and chlorite. The aphyric pillow lavas are rich in vesicles and amygdales (20-30%) (Fig. 2.3c). The amygdales are filled with calcite, chlorite, quartz, actinolite, epidote, and/or biotite. Porphyritic pillow lavas have large plagioclase phenocrysts, up to 4 mm long (Fig. 2.3d).

some of which display a glomeroporphyritic texture. Plagioclase phenocrysts are embedded in a microlitic groundmass composed of plagioclase, actinolite, chlorite, epidote, and titanite. The plagioclase phenocrysts are corroded and slightly altered to epidote, chlorite, carbonate, silica, and sericite. Vesicles and amygdales are less common in the porphyritic pillows (< 10%). The amygdales are filled with silica, carbonate, chlorite and epidote. Actinolite in the groundmass of both types of pillow lavas is altered to chlorite and epidote.

Dikes intruding the WGO are mainly basaltic and less commonly diabasic (Fig. 2.3e, f), and have a similar mineral assemblage of plagioclase, actinolite after pyroxene, epidote, chlorite and opaque minerals as in the pillow lavas. Basaltic dikes are aphyric to slightly porphyritic with coarser varieties showing subophitic textures. Plagioclase is zoned and is extensively epidotized, particularly in its core. Actinolite, chlorite, epidote and titanite are the main secondary minerals.

The diabasic and basaltic dikes in the WGM have almost the same petrography as the dikes in the WGO. Dioritic blocks are composed mainly of plagioclase and neomorphic biotite and accessory quartz. Chlorite, epidote and sericite are the main alteration minerals. To the north of Hafafit, the volcanic blocks range in composition from basalt to rhyolite. These volcanic rocks resemble the other are metavolcanics of the Idfu-Marsa Alam Road described by Hassanien (2001). They are commonly porphyritic where the mafic and intermediate varieties have plagioclase and chloritized pyroxene and/or hornblende phenocrysts (Fig. 2.3g), and the felsic varieties have quartz and plagioclase phenocrysts (Fig. 2.3h).

2.4. Analytical methods

Rock samples were crushed, and then pulverized using an agate mill at University of Windsor. Major elements and Se were analyzed by Thermo Jarrell-Ash Enviro II ICP at ACTLABS in Ancaster, Canada. Samples were fused with a flux of lithium metaborate and lithium tetraborate in an induction furnace and then dissolved in 5% nitric acid containing an internal standard. Totals of major element oxides are 100 ± 1 wt% and the analytical precisions for major elements are 1-2% and better than 5% for Se. United States Geological Survey's geochemical references, dolerite (DNC-1) and Icelandic basalt (BIR-1), were used as international reference standards to estimate accuracy of the major elements (Table 2.1).

Samples were analyzed for rare earth elements (REE), high field strength elements (HFSE), large ion lithophile elements (LILE) and transition metals (Ni, Co, Cr and V) by a high-sensitivity Thermo Elemental X7 ICP-MS in the Great Lakes Institute for Environmental Research (GLIER), University of Windsor, Canada, using the protocol of Jenner et al. (1990). Samples were dissolved in concentrated HF-HNO₃ mixture in screw-top Teflon (Savillex®) bombs for three days and further attacked with concentrated HNO₃-H₃BO₃-H₂C₂O₄ and then twice with 50% HNO₃. United States Geological Survey's geochemical references, Hawaiian basalts (BHVO-1 and BHVO-2), were used as international reference standards to estimate accuracy of the measured trace elements (Table 2.2). Analytical precision is estimated as follows: 1-10 % for REE, Rb, Sr, Ba, Y, Nb, Co, Cu, Zr, and U; 10-20% for V, Ni, Zn, Cs, Mo, and Ga; and 20-30% for Ta, Th, Cr, and Pb.

Major element analyses are calculated to 100 wt% anhydrous basis. Mg-numbers were calculated as molar ratios of $[\text{Mg}^{2+}/(\text{Mg}^{2+}+\text{Fe}^{2+})]*100$ after Ragland (1989). Chondrite (cn) and MORB compositions are derived from Sun and McDonough (1989), and Pearce (1982) respectively. Europium (Eu/Eu^*) anomalies were calculated with respect to neighboring REE (Rollinson, 1993).

2.5. Geochemical results

Whole-rock major and trace element data for the WGO are presented in Tables 2.3 and 2.4. The data for various *mélange* rocks are presented in Table 5. Sample “EGY-06-61” from the calc-alkaline leucogabbro, which crosscuts the *mélange* (Fig. 2.1b), is added to the D4 dikes columns of Table 2.3 for comparison. All rocks from the WGO and the *mélange* display basaltic to andesitic compositions (Fig. 2.4a). Blocks from the WGM are basaltic to andesitic, but blocks in the Hafafit *mélange* have a wider compositional range from basaltic to rhyolitic (Fig. 2.4c).

2.5.1. Gabbros

Gabbros of the WGO are tholeiitic (Fig. 2.4b). They have Mg-numbers between 43 and 71, and their SiO_2 content ranges from 46 to 51 wt%. They have the lowest incompatible trace element (REE, Zr, Nb) contents of cogenetic rocks (Fig. 2.5). TiO_2 , Fe_2O_3 , and MgO display a large variation, but Al_2O_3 , CaO and Na_2O are moderately variable (Table 2.3).

Chondrite-normalized REE patterns of the gabbros are variable (Fig. 2.6a). The samples with the highest Mg-number show convex upward, light rare earth element-(LREE-) depleted patterns with $\text{La}/\text{Yb}_{\text{cn}}=0.63$ and $\text{La}/\text{Sm}_{\text{cn}}=0.49$ (Table 2.3). With decreasing Mg-number, REE patterns become flat and then slightly enriched in LREE.

The sample with the lowest Mg-number has $La/Yb_{cn}=1.69$ and $La/Sm_{cn}=1.03$. The less evolved sample has a positive Eu anomaly which decreases with an increase in the overall abundance of REE. The absolute abundances of REE in the gabbroic rocks vary as samples with low Mg-numbers have higher total REE contents than samples with higher Mg-numbers.

MORB-normalized trace element patterns of the gabbroic rocks are enriched in LILE (Sr, K, Rb, Ba, Th) relative to HFSE (Nb, Ta, Zr, Ti, Y) and HREE and show negative Nb and Ta anomalies (Fig. 2.7a). The gabbroic rocks are slightly enriched in LILE, up to 10 x MORB values, and the less evolved samples are slightly depleted in HFSE and REE compared to MORB (Fig. 2.7a). Values of the transition metals, Sc and Cr are close to MORB values.

2.5.2. Pillow lavas

Pillow lava samples are composed predominantly of basaltic andesites and andesites (Fig. 2.4a). They have the lowest Mg-numbers (29-38) of all rock types in the WGO. Pillow lavas of Wadi El Beda (amygdaloidal pillows) plot in the tholeiitic field, whereas the pillow lavas of Wadi Saudi (porphyritic pillows) plot in the calc-alkaline field (Fig. 2.4b). Porphyritic pillows have higher Al_2O_3 , CaO, and Na_2O but lower Fe_2O_3 , MgO, and TiO_2 than amygdaloidal pillows. Porphyritic pillows are more enriched in Zr (349-441 ppm) and other incompatible elements relative to amygdaloidal pillows (Fig. 2.5).

Both porphyritic and amygdaloidal pillow lavas have similar chondrite-normalized REE patterns (Fig. 2.6b). They are both enriched in LREE, but the porphyritic pillows are more fractionated ($La/Yb_{cn}=4.1-5.4$ and $La/Sm_{cn}=1.8-1.9$) than the amygdaloidal pillows

($La/Yb_{cn}=2.2-2.7$ and $La/Sm_{cn}=1.2-1.3$). The porphyritic pillows show negative Eu anomalies ($Eu/Eu^*=0.61-0.65$). Both pillow lava types are enriched in LILE, HFSE and REE relative to MORB (Fig. 2.7b).

2.5.3. Dikes

Although dikes cutting the WGO are similar petrographically, their chemical compositions display a large variation. They plot in tholeiitic (D1 dikes, D3 dikes), transitional (D2 dikes) and calc-alkaline (D4 dikes) fields (Fig. 2.4b). Their Mg-numbers range from 31 to 70 and greatly overlap with, but are generally higher than, those of the pillow lavas.

Chondrite-normalized REE patterns of different generations of dikes show some variations. Tholeiitic dikes have both LREE-depleted chondrite-normalized patterns (D3 dikes) and slightly LREE-enriched patterns (D1 dikes) (Fig. 2.6c,d). LREE-depleted samples have La/Yb_{cn} ranging between 0.8 and 1.5 and La/Sm_{cn} between 0.5 and 0.9 with convex-upward patterns, similar to the less fractionated gabbros. The other tholeiitic series is LREE-enriched ($La/Yb_{cn}=1.9-2.6$ and $La/Sm_{cn}=1.2-1.7$). Rare earth element patterns of D1 dikes are similar to those of the amygdaloidal pillow lavas.

Dikes of the transitional series (D2) have Mg-numbers ranging between 43 and 59, and Zr contents in the range of 90 to 160 ppm. Chondrite-normalized REE patterns of D2 dikes are enriched in LREE with $La/Yb_{cn}=3.0-3.4$ and $La/Sm_{cn}=1.8-2.0$ (Fig. 2.6e). Their patterns are similar to those of the porphyritic pillow lavas, and they also exhibit negative Eu anomalies ($Eu/Eu^*=0.73-0.96$). Calc-alkaline dikes (D4) have Mg-numbers ranging between 50 and 61 and Zr contents between 122 and 204 ppm. The chondrite-normalized

REE patterns of D4 dikes show strong LREE enrichment with La/Yb_{cn} between 5.5 and 13.2 (Fig. 2.6f).

The tholeiitic dikes show minor variations in their trace-element patterns. D3 dikes are slightly depleted in HFSE and REE relative to MORB (Fig. 2.7c), but D1 dikes have HFSE contents close to MORB values (Fig. 2.7d). Transition metal contents of both groups are variable relative to MORB. The patterns of D2 dikes are characterized by a Th peak similar to the porphyritic pillow lavas (Fig. 2.7e).

MORB-normalized trace element patterns of D4 dikes are characterized by enrichment in highly incompatible elements LILE, LREE and HFSE over HREE (Fig. 2.7f). These rocks are highly enriched in LILE in comparison to MORB ($\geq 10 \times$ MORB) but are depleted in HREE relative to MORB. Compared to the other types of rocks in the study area, D4 dikes have the highest contents of the most incompatible trace elements and the most fractionated REE patterns.

2.5.4. Ophiolitic mélange

The blocks in the ophiolitic mélange along Wadi El Beda show much variation in lithology and chemistry. Their chemical affinities range from tholeiitic to calc-alkaline (Fig. 2.4d). The diorite sample (EGY6-06-63) has the highest SiO_2 and Na_2O but the lowest MgO and CaO contents compared to other basaltic and diabasic rocks in the mélange. The basaltic fragments have near-flat chondrite-normalized REE patterns, $La/Yb_{cn}=1.2-1.8$ and $La/Sm_{cn}=0.9-1.3$, whereas the intermediate igneous rocks have LREE-enriched patterns, $La/Yb_{cn}=6.2-23.2$ and $La/Sm_{cn}=2.3-2.6$ (Fig. 2.8a). All mélange units are characterized by negative Nb and Ta anomalies and enrichment in LILE over

HFSE (Fig. 2.8b,d,f). Blocks of dikes within the Wadi El Beda ophiolitic mélange are made of tholeiitic basalt (Fig. 2.4c, d) which show consistent chondrite-normalized REE patterns that are flat to slightly LREE-enriched, $La/Yb_{cn}=1.6-5.7$ and $La/Sm_{cn}=0.9-2.3$ (Fig. 2.8c). As are other blocks in the mélange, the dikes are characterized by enrichment in LILE over HFSE and have negative Nb and Ta anomalies (Fig. 2.8d).

To the north of the Hafafit gneissic dome, the volcanic blocks in the mélange range in composition from basalt to rhyolite with transitional to calc-alkaline affinity (Fig. 2.4c, d). These rocks are enriched in LREE and LILE over HFSE where their degree of enrichment is higher than the rest of the blocks in the Wadi Ghadir ophiolitic mélange (Fig. 2.8). The ratios of La/Yb_{cn} and La/Sm_{cn} range from 2.1 to 22.8 and from 1.2 to 3.8, respectively. These rocks are also characterized by negative Nb, Ti and Eu anomalies (Fig. 2.8f).

2.6. Discussion

2.6.1. Alteration process and element mobility

Although the WGO rocks preserve their original igneous textures, they show textural evidence for extensive alteration and metamorphic overprint. Metamorphism and alteration of ophiolitic rocks resulted mainly from oceanic hydrothermal processes (Gillis and Banerjee, 2000). Static, in terms of texture, alteration is common in the gabbroic rocks during the first phase of ocean-floor metamorphism as evidenced by the replacement of primary pyroxene, (augite) by hornblende. Subsequently, the gabbros and the volcanic rocks were altered hydrothermally to an assemblage of actinolite, albite, chlorite, epidote, and titanite which are greenschist-like mineral assemblage. Honnorez (2003) considered ocean-floor metamorphism and hydrothermal alteration as two end

members of a wide range of water-rock interaction. The volcanic rocks of the WO are more affected by the hydrothermal alteration phase than the gabbroic rocks. Accretion-related dynamic metamorphism mainly affected the mélangé matrix, reaching greenschist facies conditions.

To assess the alteration effect on the original chemistry of the WGO, we adopted the alteration criteria of Polat et al. (2002) and Polat and Hofmann (2003). All samples have loss on ignition (LOI) values less than 6 wt%, suggesting that the rocks have not been highly altered. The consistency of REE patterns of the Wadi Ghadir rocks and lack of Ce anomalies suggest that the concentrations of these elements were not modified significantly, and that they reflect their magmatic concentrations (Fig. 2.6). The LILE segments of MORB-normalized trace element pattern for the gabbroic rock are consistent relative to the rest of the rock units. This consistency may indicate the less mobility of the LILE in the gabbros relative to the other rock units. The mobility of the LILE can be attributed to the hydrothermal alteration phase rather than the ocean-floor metamorphism.

Large ion lithophile elements (LILE) are expected to be mobile under most alteration conditions, but most major elements, high field strength elements (HFSE), REE) and transitional metals are expected to be immobile under most metamorphic conditions (Winchester and Floyd, 1976; Dostal et al., 1980; Humphries, 1984; Polat and Hofmann, 2003). Due to this differential mobility, HFSE and REE (but not LILE) show a good correlation with the least mobile element, Zr, on binary diagrams for the WGO (Fig. 2.5).

Blocks in the ophiolitic mélangé are expected to be more altered than the main WGO due to the intensive deformation which they experienced. The degree of alteration

in the mélangé is difficult to evaluate because of the heterogeneous nature of various rocks making up the blocks. The LILE segments of the MORB-normalized patterns for the arc rocks exposed north of the Hafafit gneissic dome are more dispersed than the HFSE segments (Fig. 2.8f). This dispersion indicates the high mobility of the LILE relative to the HFSE. The same conclusion can be reached through the MORB-normalized trace element patterns of the blocks of dikes within the WGM (Fig. 2.8b, e).

2.6.2. Mantle source characteristics

All samples analyzed for this study have consistent MORB-normalized trace element patterns characterized by enrichment of Th, and the LILE for the gabbroic rocks, relative to rest of the HFSE thus creating negative Nb and Ta anomalies. Such geochemical characteristics are consistent with magma compositions generated in supra-subduction zone settings and are attributed to mantle wedge melting affected by fluid released from a subducted slab (Pearce, 1982; Tatsumi and Kogiso, 2003). Enrichment in LILE stems from the mobility of these elements during slab dehydration (Pearce and Peate, 1995). High-field strength elements behave in a conservative way during subduction, and so their concentration in the rocks reflects their concentration in the mantle wedge (Pearce, 2008). To discriminate between the relative contribution of a mantle source and a subduction component, Pearce (1983) and Pearce and Peate (1995) developed plots using M/Yb versus $Nb(Ta)/Yb$, where M is the incompatible element of interest (Fig. 2.9). On these diagrams, subduction-related enrichment of element (M) results in displacement from the mantle array, which is defined by mantle-derived oceanic basalts.

For Zr and Y, all rock types of the Wadi Ghadir area form linear trends overlapping with the mantle array (Fig. 2.9a, b). These values pass through the values of MORB and below OIB, indicating that HFSE and HREE were not important components in the subduction flux. Light REE (La) and MREE (Sm) plots are still confined to the mantle array but slightly moved towards the upper boundary (Fig. 2.9c, d). D4 dikes plot above the upper boundary of the mantle array. These features collectively suggest that LREE and, to some extent MREE, were added to the mantle wedge from the subducted slab but not in significant amounts except for D4 dikes that were highly affected by fluxes from the subducted slab and/or the sub-continental lithospheric mantle. Large ion lithophile elements (U and Th) form linear trends that are sub-parallel to, but are displaced above, the mantle array towards higher U/Yb and Th/Yb ratios (Fig. 2.9e, f). These higher ratios indicate high contributions of these elements from a subduction component.

The behavior of some elements, conservative or non-conservative, is dependent on the nature of contributions from the subducted slab to the mantle wedge, either in fluid or in melt. Zirconium is one of these elements (Pearce and Peate, 1995). Zirconium plots in the mantle array thus indicating a minor role of sediments or sediment melting during the petrogenesis of these rocks. The limited contribution from subducted sediments to the mantle wedge is detected also through the tendency of the samples towards higher Ba/La ratios rather than higher Th/Yb (Class et al., 2000; Woodhead et al., 2001) and the relatively low Th/Ce ratios (<0.1) (Hawkesworth et al., 1997) (Table 2.3). As the sediment input to the mantle wedge is limited, all samples, except D4 dikes, follow the low Ce/Yb trend of Hawkesworth et al. (1993) (Fig. 2.10). The blocks in the Wadi

Ghadir ophiolitic mélange have low Th/Ce ratios and relatively higher Ba/La ratios than Th/Yb (Table 2.3).

As they are less affected by the subduction-related fluxes, conservative elements can be used to evaluate the composition of the mantle wedge, and their ratios are useful in assessing the mantle wedge composition without being affected by pooled and fractional partial melting or fractional crystallization (Pearce and Peate, 1995). On M/Yb versus Nb/Yb diagrams (Fig. 2.9), where M is a conservative element, our data plot along the mantle array where D3 dikes and gabbroic rocks extend to the depleted MORB end whereas the rest cluster around average MORB. Melting of a slightly depleted mantle source is consistent with high Zr/Nb in the gabbroic rocks (31-62) and D3 dikes (48-118) compared to an average N-MORB ratio (~32). D4 dikes extend to the enriched end of the mantle array but not to OIB values, and this is consistent with their lower Zr/Nb (23-29) than average MORB. Other dike groups, D1 and D2, along with porphyritic and amygdaloidal pillow lavas, have Zr/Nb ratios ranging from 22 to 52 with values closer to average MORB on the mantle array. Blocks of dikes in the WGM have Zr/Nb ratios (25-64) close to the range of D1 and D2 dikes and pillow lavas. We infer that magmas of both WGO and the disrupted dikes in the mélange may have been derived from the same mantle source.

Variations in trace element patterns and in Zr/Nb ratios of the analyzed samples indicate either mantle heterogeneity and/or selective tapping of the mantle column in a dynamic melting model (Pearce et al. 1995). Variations in La/Sm_{cn} relative to Sm suggest that the gabbroic rocks and D1, D2, D3, and D4 dikes may be the products of heterogeneous mantle and/or dynamic melting. Porphyritic lavas and D2 dikes and

amygdaloidal lavas and D1 dikes may be genetically related, however, through fractional crystallization processes (Fig. 2.11).

The elevated Gd/Yb_{cn} ratio (>1) of the WGO indicates that the mantle source was at a depth of garnet stability. The garnet signature in these rocks may have resulted from melting of garnet peridotite, which is stable at a depth >90 km (OIB source), melting of a garnet pyroxenite/spinel peridotite source (N-MORB source) (cf. Hirschmann and Stöpler, 1996), or addition of subduction-related melts in equilibrium with garnet eclogite (cf. Kessel et al., 2005). Calc-alkaline dikes (D4) have the highest Gd/Yb_{cn} ratio (2.2-3.7). On the La/Yb versus Yb diagram of Baker et al. (1997), the analyzed samples plot close to the spinel lherzolite trend except for D4 dikes that extend along the garnet lherzolite melting curve (Fig. 2.12). This may indicate derivation of the magmas of D4 dikes from a deeper source or at least mixing of their magmas with melt from a garnet lherzolite source. However, the other samples have higher Yb contents at the same MgO contents indicating the generation of their melts from a shallower spinel lherzolite mantle, which may have been veined by garnet pyroxenite.

2.6.3. Tectonic setting and geodynamic evolution

Although a complete Penrose-type sequence is absent in the WGO, its gabbroic rocks and pillow lavas are interpreted as remnants of Neoproterozoic oceanic crust (El-Sharkawy and El-Bayoumi, 1979; El-Bayoumi, 1980, 1983; Kröner et al., 1992; Farahat et al., 2004). Normal-MORB-normalized patterns of these ophiolitic rocks along with D1, D2, and D3 dikes are consistent with the evolution of the WGO in a supra-subduction zone geodynamic setting (cf. Pearce, 1982, 2003; Pearce et al., 1984).

The ophiolitic rocks and associated D1, D2, and D3 dikes of the Wadi Ghadir area have high average abundances of incompatible HFSE and Y and low ratios of Ti/Zr, V/Ti, and Sc/Yb (Table 2.3). These features characterize melting of a normal MORB mantle source beneath back-arc basin spreading centres (Woodhead et al., 1993). The systematic compositional variations in the WGO rocks are analogous to the compositional variations observed from in-situ oceanic crust of modern back-arc basins such as the Manus Basin (Sinton et al., 2003). The compositional variations of back-arc-related rocks can be attributed to source heterogeneity beneath back-arc basins that resulted from variable mixing of fertile mantle, melt-depleted mantle and slab-derived components (Martinez and Taylor, 2003). The chemistry of the mantle wedge is affected by fluids derived from the subducted slab; it is also influenced by subduction-induced corner flow (Ewart and Hawkesworth 1987). This counter flow mantle convection provides a continuous supply of fertile mantle, but due to back-arc extension and melt extraction, the mantle advected into the wedge beneath the arc undergoes depletion (McCulloch and Gamble 1991; Hawkins 2003). The nature of back-arc magmatism is a result of mixing of a MORB-like source and limited enrichment in LILE relative to arc magmatism (Taylor and Martinez, 2003). The degree of mixing of these components is controlled by the distance to the island arc (Sinton et al., 2003). The inferred back-arc basin origin of the WGO is consistent with previous studies (El-Bayoumi and Greiling, 1984; Kröner, 1985; Kröner et al., 1987; Farahat et al., 2004).

Because all analyzed samples have TiO₂ contents more than 1 wt%, the WGO can be classified, following Serri (1981), as a high-Ti ophiolite. In this sense, the WGO compares well with some other Tethyan ophiolites such as, Troodos in Cyprus and

Semail in Oman and the Proterozoic ophiolites in the ANS such as Jabal Al Wask in Saudi Arabia and Onib in Sudan (Zimmer et al., 1995; Hussein et al., 2004 and references therein). Using the criteria in Pearce et al. (1984) and Pearce (2008), we infer that the chemical signature, the crystallization sequence, mantle residue and Y proxy of the WGO are similar to most supra-subduction zone ophiolites formed in back-arc basins. On the Ti-V variation diagram, the WGO samples overlap with recent back-arc basins fields such as the Lau and Manus Basins (Fig. 2.13a). The WGO have higher La/Sm_{cn} values than the Lau Basin samples, but are within the range of the Manus Basin samples and their Nb/La_{pm} ratios is similar to that of both the Lau and Manus Basins (Fig. 2.14a, b, c). The Lau Basin has higher Nb/Th_{pm} ratio than the WGO, but the latter still has a Nb/Th_{pm} ratio within the range of the Manus Basin, confirming its back-arc tectonic setting (Fig. 2.14d). Regarding its La/Sm_{cn} ratio, the WGO overlaps with the Betts Cove (Bédard, 1999), Oman (Godard et al., 2006) and the Dagzhuka-Tibet (Xia et al., 2003) ophiolites. It also overlaps with the Oman ophiolites in terms of its TiO_2 and Zr contents and Nb/Th_{pm} ratios and with the Betts Cove and Tibet fore-arc ophiolites, in terms of its Nb/Th_{pm} ratios (Fig. 2.14). The high TiO_2 and Zr values of the WGO were also reported by El-Bayoumi (1980). His TiO_2 and Zr values range from 0.74 to 3.64 wt% and from 27 to 448 ppm, respectively.

The Wadi Ghadir area is a part of a mélangé separated from the Hafafit gneissic dome by the volcanic and volcanoclastic rocks of the Nugrus volcanic arc complex (Abd El-Naby and Frisch, 2006). We infer that the Nugrus arc developed as a SW-facing intra-oceanic arc system above a NE-dipping (in present coordinate system) subduction zone,

and that the WGO was situated in a back-arc setting behind that Nugrus volcanic arc, tapping into a fertile MORB mantle source (Fig. 2.15a).

The late-stage D4 dikes have unique characteristics relative to the other rocks in the study area. These dikes are calc-alkaline in composition, and although their MORB-normalized patterns are similar to the other subduction-related rocks (i.e. enriched in LILE relative to HFSE and negative Nb and Ta anomalies), they have stronger enrichment in LILE than the WGO and its associated dikes. They also differ from the other rocks by higher concentrations of Nb and Ta relative to Zr and of Zr relative to Y and Yb (Table 2.3). These features indicate contributions from a mantle source enriched in incompatible elements, such as sub-continental lithospheric mantle (Pearce, 1983). These geochemical characteristics and also the similarity between chondrite-normalized REE patterns of D4 dikes and the calc-alkaline volcanic rocks of an Andean magmatic arc (Thorpe et al., 1984; D’Orazio et al., 2003) suggest their generation in an active continental margin setting.

D4 dikes may mark the onset of calc-alkaline volcanism in the area characterizing the transformation of the passive continental margin into an active margin after the accretion of Nugrus volcanic arc and its WGO back-arc crust. This is in accordance with Kröner’s (1985) model for the evolution of the Nubian part of the ANS. The conversion from a passive continental margin into an active margin was accompanied by a change in subduction polarity following ophiolite emplacement (Fig. 2.15b). The newly established SW-dipping subduction produced calc-alkaline magmatism in the form of early basaltic dikes (D4 dikes) and leucogabbro intruding the mélangé, WGO and Hafafit gneissic dome. The mantle source of D4 dikes included melt-depleted mantle that was previously

beneath the Nugrus island arc and enriched sub-continental lithospheric mantle beneath the Hafafit dome. This is shown by the enrichment in highly incompatible elements (e.g. La and Ce) relative to Y and Yb (Fig. 2.7). With the establishment of a SW-dipping subduction zone, the granitic calc-alkaline plutons and the leucogabbro of the new Andean-type continental margin formed (El-Bayoumi, 1980, 1983; Takla et al., 1992). These plutonic rocks include mafic xenoliths derived from the WGO and the ophiolitic mélange.

2.7. Conclusions

The geochemical characteristics of the gabbros and pillow lavas of the WGO are consistent with their origin in a back-arc basin tectonic setting. The ophiolitic rocks and D1, D3 dikes intruding into them were derived from melting of slightly depleted to fertile N-MORB mantle. The garnet signature can be attributed to melting of a spinel peridotite mantle, veined or layered, with garnet pyroxenite. On the other hand, the geochemistry of calc-alkaline D4 dikes and granitoid plutons intruding the WGO and the ophiolitic mélange represent active continental margin products that formed after ophiolite emplacement via an arc-passive margin collision. Magmas of D4 dikes likely originated from melting of fertile N-MORB mantle that had been affected by contributions from sub-continental lithosphere mantle and/or garnet-peridotite mantle. The porphyritic pillow lavas and D2 dikes have intermediate geochemical characteristics between the two groups, and we attribute their origin to a transitional tectonic setting between the back-arc setting and the onset of active continental margin magmatism, following a subduction polarity change after the emplacement of the WGO and the Nugrus volcanic arc onto Hafafit passive margin.

Acknowledgements

We thank J.C. Barrette, J.C. Ordóñez-Calderón and Zhaoping Yang for their help during geochemical analyses. Reviewers A. Kröner and J. Dostal are acknowledged for their comprehensive and incisive critiques on the manuscript, which have resulted in significant improvements to the paper. We thank N. Eby for his constructive editorial comments. PREA and NSERC grants (250926) of A. Polat and NSERC grant (83117) of B. J. Fryer are greatly acknowledged.

References

- Abd El-Naby, H., Frisch, W., 2006. Geochemical constraints from the Hafafit Metamorphic Complex (HMC): Evidence of Neoproterozoic back-arc basin development in the central Eastern Desert of Egypt. *Journal of African Earth Sciences* 45, 173-186.
- Abdelsalam, M.G., Stern, R.J., 1996. Sutures and shear zones in the Arabian-Nubian Shield. *Journal of African Earth Sciences* 23, 289-310.
- Ahmed, A.H., Arai, S., Attaia, A.K., 2001. Petrological characteristics of the Pan African podiform chromitite and associated peridotites of the Proterozoic ophiolite complexes, Egypt. *Mineralium Deposita* 36, 72-84.
- Azer, M.K., Stern, R.J., 2007. Neoproterozoic (835-720) serpentinites in the Eastern Desert, Egypt: Fragments of forearc mantle. *The Journal of Geology* 115, 457-472.
- Baker, J.A., Menzies, M.A., Thirlwall, M.F., Macpherson, C.G., 1997. Petrogenesis of Quaternary intraplate volcanism, Sana'a, Yemen: implications for plume–lithosphere interaction and polybaric melt hybridization. *Journal of Petrology* 38, 1359–1390.
- Barrett, T.J., MacLean, W.H., 1994. Chemostratigraphy and hydrothermal alteration in exploration for VHMS deposits in greenstone and younger volcanic rocks. In: Lentz, D.R. (Ed.), *Alteration and Alteration Processes Associated with Ore-Forming Systems*. Geological Association of Canada, Short Course Notes 11, 433-467.
- Bédard, J.H., 1999. Petrogenesis of boninites from the Betts Cove ophiolite, Newfoundland, Canada: Identification of subducted source component. *Journal of Petrology* 40, 1853-1889.

- Church, W.R., 1988. Ophiolites, sutures, and micro-plates of the Arabian–Nubian Shield: A critical comment. In: El-Gaby, S., Greiling, R.O. (Eds.), *The Pan-African Belt of Northeast Africa and Adjacent Areas: Tectonic Evolution and Economic Aspects of a Late Proterozoic Orogen*. Friedrich. Vieweg, Sohn Verlagsgesellschaft mbH, 289-316.
- Class, C.D., Miller, D.M., Goldstein, S.L., Langmuir, C.H., 2000. Distinguishing melt and fluid subduction components in Umnak volcanics, Aleutian arc. *Geochemistry, Geophysics, and Geosystems* 1, paper number 1999GC000010.
- D'Orazio, M., Innocenti, F., Manetti, P., Tamponi, M., Tonarini, S., González-Ferrán, O., Lahsen, A., Omarini, R., 2003. The Quaternary calc-alkaline volcanism of the Patagonian Andes close to the triple junction: geochemistry and petrogenesis of volcanic rocks from the Cay and Maca volcanoes ($\approx 45^{\circ}\text{S}$, Chile). *Journal of South America Earth Sciences* 16, 219–242.
- Dilek, Y., 2003. Ophiolite pulses, mantle plumes and orogeny. In: Dilek, Y., Robinson, P.T. (Eds.) *Ophiolite in Earth History*. Geological Society, London, Special Publication 218, 9-19.
- Dilek, Y., Ahmed, Z., 2003. Proterozoic ophiolites of the Arabian Shield and their significance in Precambrian tectonics. In: Dilek, Y., Robinson, P.T. (Eds.) *Ophiolite in Earth History*. Geological Society, London, Special Publication 218, 685-700.
- Dostal, J., Strong, D.F., Jamieson, R.A., 1980. Trace element mobility in the mylonite zone within the ophiolite aureole, St. Anthony Complex, Newfoundland. *Earth and Planetary Science Letters* 49, 188-192.
- El Bayoumi, R.M., 1980. Ophiolites and associated rocks of Wadi Ghadir, east of Gabal Zabara, Eastern Desert, Egypt. Ph.D. Thesis, Cairo University, Egypt, 171 pp.
- El Bayoumi, R.M., 1983. Ophiolites and mélange complex of Wadi Ghadir area, Eastern Desert, Egypt. *Bulletin of King Abdelaziz University* 6, 329–342.
- El Bayoumi, R.M.A., Greiling, R.O., 1984. Tectonic evolution of a Pan-African plate margin in southeastern Egypt – a suture zone overprinted by low angle thrusting? In: Klerkx, J., Michot, J. (Eds.), *Géologie Africaine-African Geology*. Musée royal de l'Afrique Centrale, Tervuren, Belg. 47–56.
- El Gaby, S., List, F.K., Tehrani, R., 1988. Geology, evolution and metallogenesis of the Pan-African belt in Egypt. In: El Gaby, S., Greiling, R.O. (Eds.), *The Pan-African Belt of Northeast Africa and Adjacent Areas: Tectonic Evolution and Economic Aspects of a Late Proterozoic Orogen*. Friedrich. Vieweg, Sohn Verlagsgesellschaft mbH, 17–68.

- El Sayed, M.M., Furnes H., Mohamed F.H., 1999. Geochemical constraints on the tectonomagmatic evolution of the late Precambrian Fawakhir ophiolite, central Eastern Desert, Egypt. *Journal of African Earth Sciences* 29, 515–533.
- El Sharkawy, M.A., El Bayoumi, R.M., 1979. The ophiolites of Wadi Ghadir area Eastern Desert, Egypt. *Annals of the Geological Survey of Egypt* IX, 125–135.
- Ewart, A., Hawkesworth C.J., 1987. The Pleistocene-Recent Tonga-Kermadec arc lavas: Interpretation to new isotopic and rare earth data in terms of a depleted mantle source model. *Journal of Petrology* 28, 495-530.
- Farahat, E.S., El Mahalawi, M.M., Hoinkes, G., Abdel Aal, A.Y., 2004. Continental back-arc basin origin of some ophiolites from the Eastern Desert of Egypt. *Mineralogy and Petrology* 82, 81-104.
- Flower, M.F.J., and Levine, H.M., 1987. Petrogenesis of a tholeiite-boninite sequence from Ayios Mamas, Troodos ophiolite: evidence for splitting of a volcanic arc? *Contribution to Mineralogy and Petrology* 97, 509-524.
- Gillis, K.M., Banerjee, N.R., 2000. Hydrothermal alteration patterns in supra-subduction zone ophiolites. In: Dilek, Y., Moores, E.M., Elthon, D., Nicolas, A. (Eds.), *Ophiolites and Oceanic Crust: New Insights from Field Studies and the Ocean Drilling Program*. Boulder, Colorado, Geological Society of America Special Paper 349, 283–297.
- Godard, M., Bosch, D., Einaudi, F., 2006. A MORB source for low-Ti magmatism in the Semail ophiolite. *Chemical Geology* 234, 58-78.
- Green, N. L., 2006. Influence of slab thermal structure on basalt source regions and melting conditions: REE and HFSE constraints from the Garibaldi volcanic belt, northern Cascadia subduction system. *Lithos* 87, 23-49.
- Hassanien, S.M., 2001. Volcano-sedimentary sequence of Gabal Um Khariga, Central Eastern Desert, Egypt. *Egyptian Journal of Geology* 45, 65-88.
- Hawkesworth, C. J., Gallagher, K., Hergt, J. M., McDermott, F., 1993. Mantle and slab contributions in arc magmas. *Annual Review of Earth and Planetary Sciences* 21, 175–204.
- Hawkesworth, C.J., Turner, S.P., McDermott, F., Peate, D.W., and van Calsteren, P., 1997. U-Th isotopes in arc magmas: implications for element transfer from the subducted crust. *Science* 276, 551–555.
- Hawkins, J.W., 2003. Geology of supra-subduction zones-Implications for the origin of ophiolites. In: Dilek, Y., Newcomb, S., (Eds.) *Ophiolite Concept and the Evolution of*

Geological Thought. Boulder, Colorado. Geological Society of America Special Paper 373, 227–268

- Hirschmann, M.M., Stolper, E.M., 1996. A possible role for garnet pyroxenite in the origin of the “garnet signature” in MORB. *Contribution to Mineralogy and Petrology* 124, 185–208.
- Honnorez, J., 2003. Hydrothermal alteration vs. ocean-floor metamorphism. A comparison between two case histories: the TAG hydrothermal mound (Mid-Atlantic Ridge) vs. DSDP-ODP Hole 504B (Equatorial East Pacific). *Comptes Rendus Geoscience* 335, 781–824.
- Humphries, S.E., 1984. The mobility of the rare earth elements in the crust. In: Henderson, P. (Ed.) *Rare Earth Element Geochemistry*. Elsevier, Amsterdam, 317–342.
- Hussein, I.M., Kröner, A., Reischmann, T., 2004. The Wadi Onib mafic-ultramafic complex: A Neoproterozoic supra-subduction zone ophiolite in the northern Red Sea Hills of the Sudan. In: Kusky, T.M. (Ed.) *Precambrian Ophiolites and Related Rocks*. Developments in Precambrian Geology 13, Amsterdam: Elsevier. 163–206.
- Jenner, G. A., Longrich, H. P., Jackson, S. E., and Fryer, B. J., 1990. ICP-MS - a powerful tool for high-precision trace-element analysis in earth sciences: evidence from analysis of selected U.S.G.S. reference samples. *Chemical Geology* 83, 133–148.
- Kessel, R., Schmidt, M.W., Ulmer, P., Pettke, T., 2005. Trace element signature of subduction-zone fluids, melts and supercritical fluids at 120–180 km depths. *Nature* 437, 724–727.
- Khalil, K.I., 2007. Chromite mineralization in ultramafic rocks of the Wadi Ghadir area, Eastern Desert, Egypt: mineralogical, microchemical and genetic study. *Neues Jahrbuch für Mineralogie - Abhandlungen* 183, 283–296.
- Kröner, A., 1985. Ophiolites and the evolution of tectonic boundaries in the late Proterozoic Arabian-Nubian Shield of northeast Africa and Arabia. *Precambrian Research* 27, 277–300.
- Kröner, A., Greiling, R.O., Reischmann, T., Hussein, I.M., Stern, R.J., Durr, S., Kruger, J., Zimmer, M., 1987. Pan-African crustal evolution in the Nubian segment of northeast Africa. In: Kröner, A. (Ed.) *Proterozoic Lithospheric Evolution*. American Geophysical Union, Geodynamics Series 17, 237–257.
- Kröner, A., Todt, W., Hussein, I.M., Mansour, M., Rashwan, A.A., 1992. Dating of late Proterozoic ophiolites in Egypt and the Sudan using the single grain zircon evaporation technique. *Precambrian Research* 59, 15–32.
- Kröner, A., Windley, B.F., Badarch, G., Tomurtogoo, O., Hegner, E., Jahn, B.M., Gruschka, S., Khain, E.V., Demoux, A., Wingate, M.T.D., 2007. Accretionary growth and crustal

- formation in the Central Asian Orogenic Belt and comparison with the Arabian-Nubian Shield. In Hatcher, R.D., Carlson, Jr.M.B., MacBride, J.H., and Catalan, J.M. (Eds.) 4-D framework of the continental crust-In targeting crustal processes through time. Geological society of America, Memoir 200, 181-209.
- Martinez, F., Taylor, B., 2003. Controls on back-arc crustal accretion: insights from the Lau, Manus and Mariana basins. In: Larter, R.D., and Leat, E.T. (Eds.) Intra-oceanic subduction systems: Tectonic and magmatic processes. Geological Society, London, Special Publication 219, 19-54.
- McCulloch, M.T., Gamble, J.A., 1991. Geochemical and geodynamical constraints on subduction zone magmatism. *Earth Planet Science Letters* 102, 358–374.
- Pearce, J.A., 1982. Trace element characteristics of lavas from destructive plate boundaries. In: Thorpe R.S. (Ed.) *Andesites: Orogenic Andesites and Related Rocks*. Chichester: John Wiley. 525–547.
- Pearce, J.A., 1983. Role of sub-continental lithosphere in magma genesis at active continental margins. In: Hawkesworth, C. J., Norry, M. J. (Eds.) *Continental Basalts and Mantle Xenoliths*. Nantwich, UK: Shiva, 230–249.
- Pearce, J.A., 2003. Supra-subduction zone ophiolites: the search for modern analogues. In: Dilek, Y., Newcomb, S., (Eds.) *Ophiolite Concept and the Evolution of Geological Thought*. Boulder, Colorado. Geological Society of America Special Paper 373, 269-295.
- Pearce, J.A., 2008. Geochemical fingerprinting of oceanic basalts with applications to ophiolite classification and the search for Archean oceanic crust. *Lithos* 100, 14-48.
- Pearce, J.A., Baker, P.E., Harvey, P.K., and Luff, I.W., 1995. Geochemical evidence for subduction fluxes, mantle melting and fractional crystallization beneath the South Sandwich island arc. *Journal of Petrology* 36, 1073–1109.
- Pearce, J.A., Ernewein, M., Bloomer, S.H., Parson, L.M., Murton, B.J., Johnson, L., 1994. Geochemistry of Lau Basin volcanic rocks: influence of ridge segmentation and arc proximity. In: Smellie, J.L. (Ed.) *Volcanism Associated with Extension at Consuming Plate Margins*. Geological Society, London, Special Publication, 81, 53-75.
- Pearce, J.A., Lippard, S.J., Roberts, S., 1984. Characteristics and tectonic significance of supra-subduction zone ophiolites. In: Kokelaar, P.B., Howells, M.F. (Eds.), *Marginal Basin Geology*. Geological Society, London, Special Publication, 16, 77–94.
- Pearce, J.A., Peate, D.W., 1995. Tectonic implications of the composition of volcanic arc lavas. *Annual Review of Earth and Planetary Sciences* 23, 251–285.

- Polat, A., Hofmann, A.W., 2003. Alteration and geochemical patterns in the 3.7–3.8 Ga Isua greenstone belt, West Greenland. *Precambrian Research* 126, 197–218.
- Polat, A., Hofmann, A.W., Rosing, M.T., 2002. Boninite-like volcanic rocks in the 3.7–3.8 Ga Isua greenstone belt, West Greenland: Geochemical evidence for intra-oceanic subduction zone processes in the early Earth. *Chemical Geology* 184, 231–254.
- Ragland, P.C., 1989. *Basic Analytical Petrology*. Oxford University Press, New York.
- Ramly, M.F., Soliman, F.A., Rasmy, A.H., Abu El Farh, M.H., 1998. Petrographic and geochemical characteristics of the island arc rocks in the area between Wadi Garf and Wadi Um Khariga, Central Eastern Desert of Egypt. *Annals of the Geological Survey of Egypt* V.XXI, 1-22.
- Reischmann, T., 2000. Ophiolites and island arcs in the late Proterozoic Nubian Shield. *Ophioliti* 25, 1-13.
- Ries, A.C., Shackleton, R.M., Graham, R.H., Fitches, W.R., 1983. Pan-African structures, ophiolites and mélanges in the Eastern Desert of Egypt: a traverse at 26° N. *Journal of Geological Society, London* 140, 75–95.
- Rollinson, H.R., 1993. *Using Geochemical Data: Evaluation, Presentation and Interpretation*. Longman/Wylyie, Harlow/New York.
- Rotolo, S.G., Castorina, F., Cellura, D., Pompilio, M., 2006. Petrology and geochemistry of submarine volcanism in the Sicily channel rift. *The Journal of Geology* 114, 355-365.
- Sengor, A.M.C., Natal'in B.A., 1996. Turkeic-type orogeny and its role in the making of the continental crust. *Annual Review of Earth Planet Science* 24, 263-337.
- Serri, G., 1981. The petrochemistry of ophiolite gabbroic complexes: a key for the classification of ophiolites into low-Ti and high-Ti types. *Earth and Planetary Science Letters* 52, 203-212.
- Shackleton, R.M., Ries, A.C., Graham, R.H., Fitches, W.R., 1980. Late Precambrian ophiolite mélange in the eastern desert of Egypt. *Nature* 285, 472–474.
- Shervais, J.W., 1982. Ti-V plots and the petrogenesis of modern and ophiolitic lavas. *Earth Planetary Science Letters* 59, 101-118.
- Sinton, J.M., Ford, L.L., Chappell, B., McCulloch, M.T., 2003. Magma genesis and mantle heterogeneity in the Manus back-arc basin, Papua New Guinea. *Journal of Petrology* 44, 159-195.
- Stern, R.J., 1994. Arc assembly and continental collision in the Neoproterozoic East African Orogen: implications for the consolidation of Gondwanaland. *Annual Review of Earth and Planet Sciences* 22, 319–351.

- Stern, R.J., 2004. Subduction initiation: spontaneous and induced. *Earth Planetary Science Letters* 266, 275-292.
- Stern, R.J., 2005. Evidence from ophiolites, blueschists, and ultrahigh-pressure metamorphic terranes that modern episodes of subduction tectonics began in Neoproterozoic time. *Geology* 33, 557-560.
- Stern, R.J., 2007. Neoproterozoic crustal growth: The solid Earth system during a critical episode of Earth history. *Gondwana Research* 14, 33-50.
- Stern, R.J., Johanson, P.R., Kröner, A., Yibas, B., 2004. Neoproterozoic ophiolites of the Arabian-Nubian Shield. In: Kusky, T.M. (Ed.) *Precambrian Ophiolites and Related Rocks. Developments in Precambrian Geology* 13, Amsterdam: Elsevier. 95-128.
- Sultan, M., Bickford, M.E., El Kaliouby, B., Arvidson, R.E., 1992. Common Pb systematics of Precambrian granitic rocks of the Nubian shield (Egypt) and tectonic implications. *Geological Society of American Bulletin* 104, 456-470.
- Sun, S.-S., McDonough, W.F., 1989. Chemical and systematic of oceanic basalts: implications for mantle composition and processes. In: Saunders, A.D., Norry, M.J. (Eds.) *Magmatism in Ocean Basins. Geological Society, London. Special Publication* 42, 313-345.
- Takla, M.A., Basta, F.F., Shenouda, H.H., El-Maghraby, A.M., 1992. Geochemistry of gneisses and granitoids of Wadi Ghadir area, Eastern Desert, Egypt. *Geology of the Arab World* 1st, 477-506.
- Takla, M.A., Hassanien, S., Sakran, S., 1990. Geochemistry of the ophiolitic mélange between Idfu-Marsa Alam Road and Wadi Shait, Eastern Desert, Egypt. *Egyptian Mineralogist* 2, 31-50.
- Tatsumi, Y., Kogiso, T., 2003. The subduction factory: its role in the evolution of the Earth's crust and mantle. In: Larter, R.D., and Leat, E.T., (Eds.) *Intra-oceanic Subduction Systems: Tectonic and Magmatic Processes. Geological Society, London, Special Publication* 219, 55-80.
- Taylor, B., Martinez, F., 2003. Back-arc basin basalt systematic. *Earth and Planetary Science Letters* 210, 481-497.
- Thorpe, R.S., Francis, P.W., O'Callaghan, L., 1984. Relative roles of source composition, fractional crystallization and crustal contamination in the petrogenesis of Andean volcanic rocks. *Philosophical Transactions of the Royal Society of London (A)* 310, 675-692.
- Winchester, J.A., Floyd, P.A., 1976. Geochemical magma type discrimination: application to altered and metamorphosed basic igneous rocks. *Earth and Planetary Science Letters* 28, 459-469.

- Winchester, J.A., Floyd, P.A., 1977. Geochemical discrimination of different magma series and their differentiation products using immobile elements. *Chemical Geology* 20, 325–343.
- Woodhead, J., Eggins, S., Gamble, J., 1993. High-field-strength and transition element systematics in island-arc and back-arc basin basalts-evidence for multiphase melt extraction and a depleted mantle wedge. *Earth and Planet Science Letters* 114, 491-504.
- Woodhead, J.D., Hergt, J.M., Davidson, J.P., Eggins, S.M., 2001. Hafnium isotope evidence for 'conservative' element mobility during subduction processes. *Earth and Planetary Science Letters* 192, 331–346.
- Xia, B., Yu, H., Chen, G., Qi, L., Zhao, T., Zhou, M., 2003. Geochemistry and tectonic environment of the Dagzhuk ophiolite in the Yarlung-Zangbo suture zone, Tibet. *Geochemical Journal* 37, 311-324.
- Zimmer, M., Kröner, A., Joehum, K.P., Reischmann, T., Todt, W., 1995. The Gabal Gerf complex: a Precambrian N-MORB ophiolite in the Nubian Shield, NE Africa. *Chemical Geology* 123, 29–51.

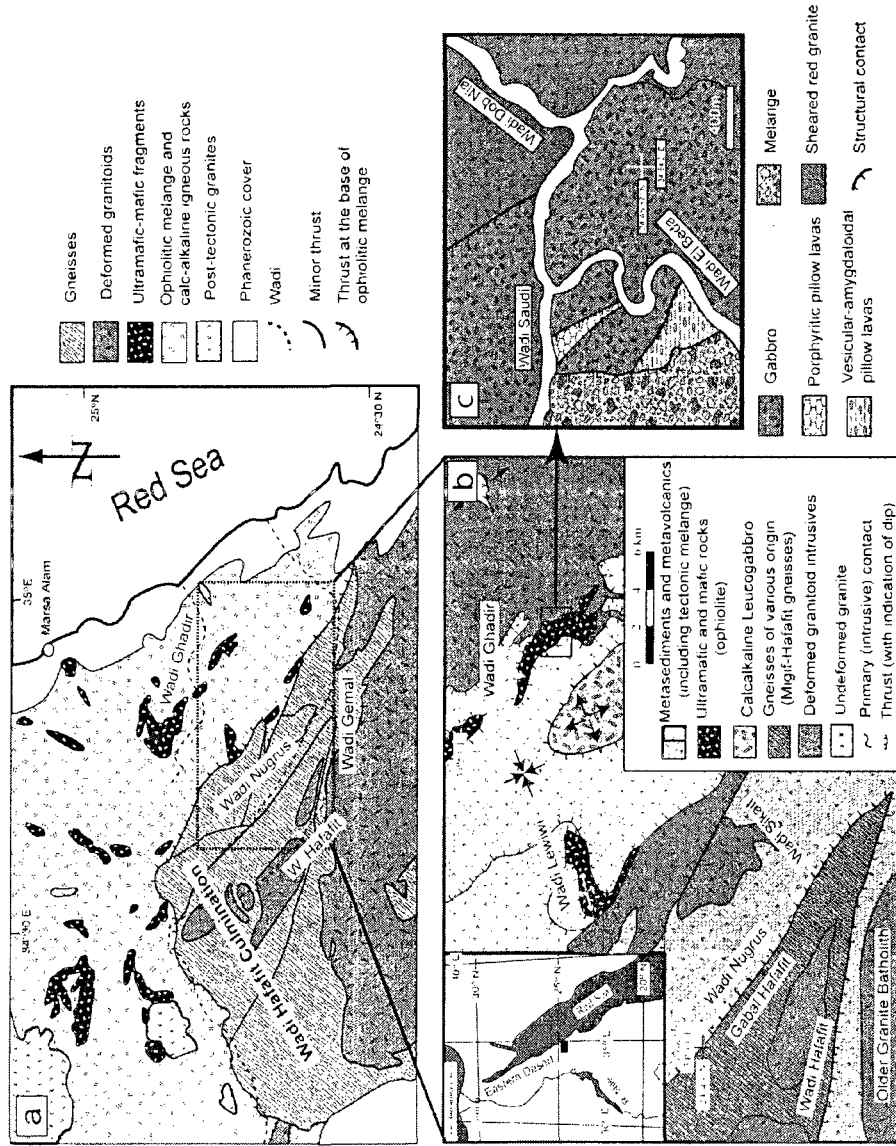


Fig. 2.1. (a) Schematic map showing major rock types exposed to the west of Marsa Alam (Kröner et al., 1987). (b) Simplified geological map for the area extending from Wadi Ghadir in the northeast to Hafafit area in the southwest. Converging and diverging arrows define interference structure of basin and dome respectively. (El-Bayoumi and Greiling, 1984). (c) Geological map of the main ophiolitic complex of the Wadi Ghadir mélangé. (inset map in 1b shows the location of the study area in the Eastern Desert of Egypt)

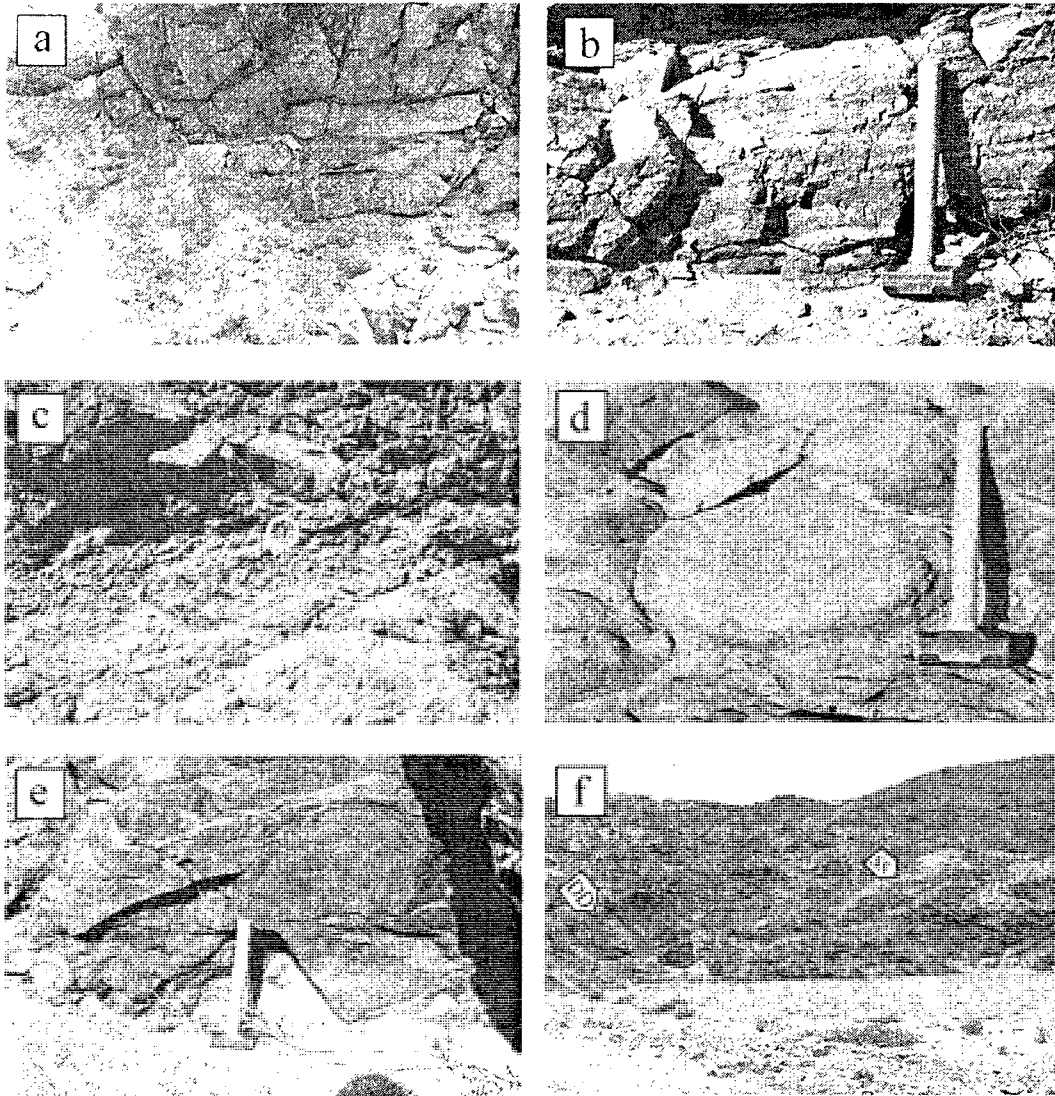


Fig. 2.2. Field photographs of ophiolitic block at Wadi Ghadir. (a) Offset granitic dike intruding ophiolitic gabbros at Wadi Saudi. (b) Sub-horizontal layering of alternating plagioclase-rich light bands and pyroxene-rich dark bands, layered gabbro unit at Wadi Saudi. (c) Isotropic gabbro unit at Wadi Saudi enclosing pocket of pegmatitic gabbro. (d) Oval pillow lavas of Wadi El Beda with concentric and radial fractures. (e) Porphyritic pillow lavas of Wadi Saudi rich in white patches of plagioclase phenocrysts. (f) Disrupted dike (DD) fragments within sheared serpentinite (SS) matrix of the Wadi Ghadir ophiolitic mélangé in Wadi Beda.

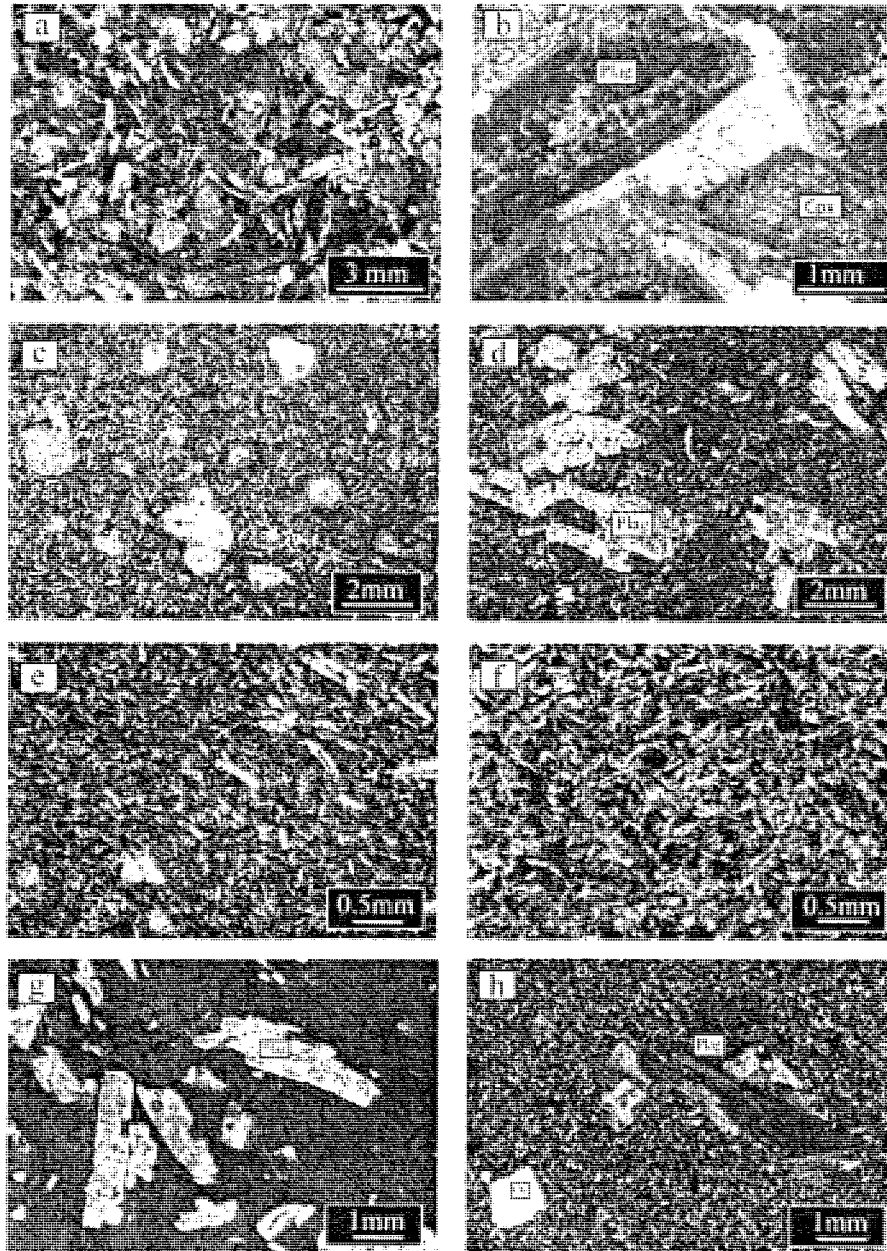


Fig. 2.3. Photomicrographs of the Wadi Ghaidr ophiolitic rocks. (a) Ophitic and subophitic texture in gabbroic rocks. (XPL) (b) Rim alteration of pyroxene (Cpx) into green hornblende and fibrous actinolite and plagioclase (Plag) to albite, sericite and chlorite. (PPL) (c) Amygdaloidal pillow lavas, amygdales are filled with carbonate, actinolite and chlorite. (PPL) (d) Porphyritic texture and glomeroporphyritic texture formed by plagioclase phenocrysts. (PPL). (e) Basaltic dike with plagioclase microphenocryst. (PPL). (f) Diabasic dike with randomly oriented plagioclase laths and secondary amphiboles. (XPL). (g) Plagioclase phenocrysts in basaltic andesite (PPL). (h) Quartz (Qz) and plagioclase phenocrysts in dacite (XPL). XPL, crossed polarized light. PPL, plane polarized light.

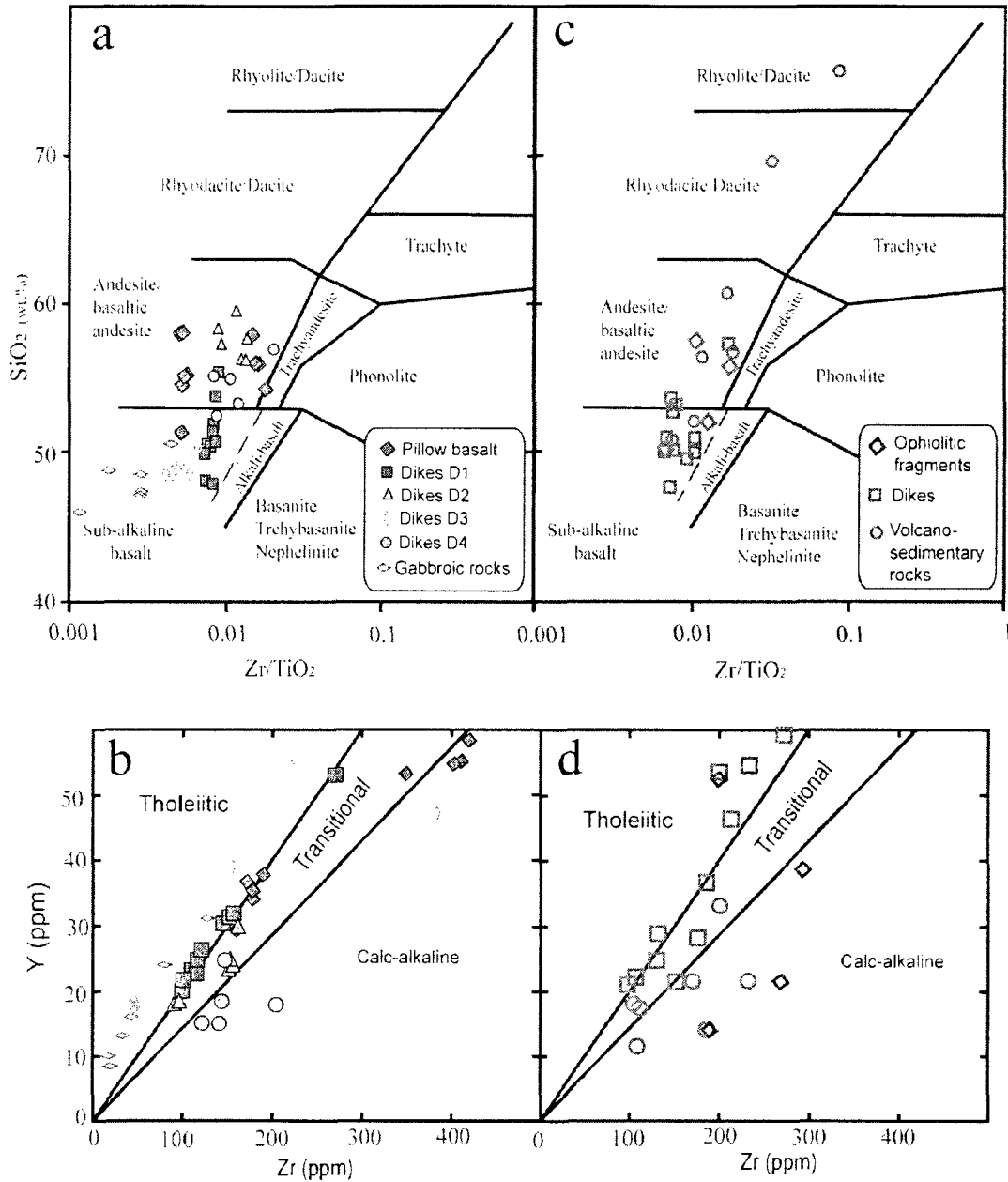


Fig. 2.4. (a) Zr/TiO_2 versus SiO_2 diagram of Winchester and Floyd (1977); and (b) Zr versus Y diagram of Barrett and Maclean (1994) for Wadi Ghadir ophiolite complex. (c) Zr/TiO_2 versus SiO_2 diagram and (d) Zr versus Y diagram for Wadi Ghadir ophiolitic mélangé and island arc fragments.

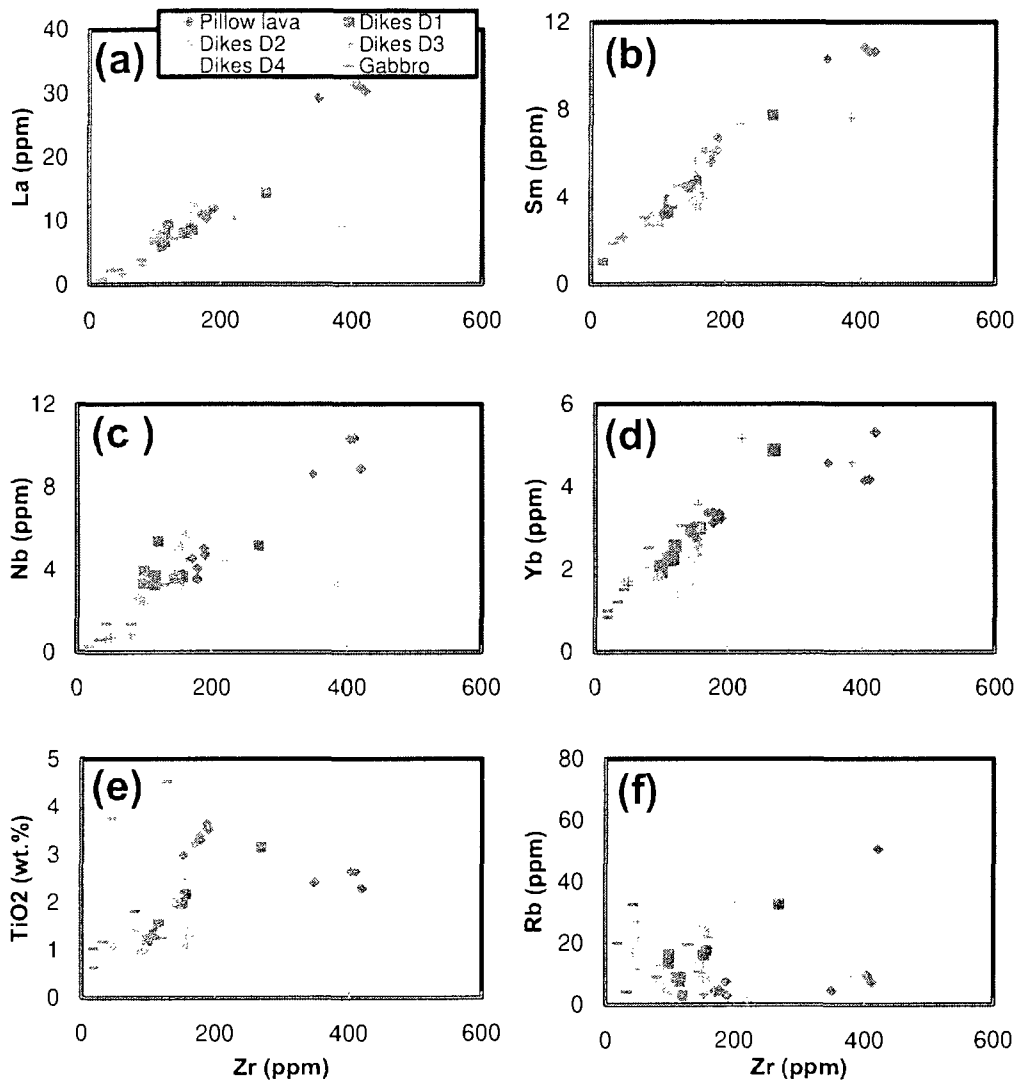


Fig. 2.5. Variation diagrams of Zr versus (a) La, (b) Sm, (c) Nb, (d) Yb, (e) TiO₂, (f) Rb for the Wadi Ghadir ophiolitic complex and associated dikes.

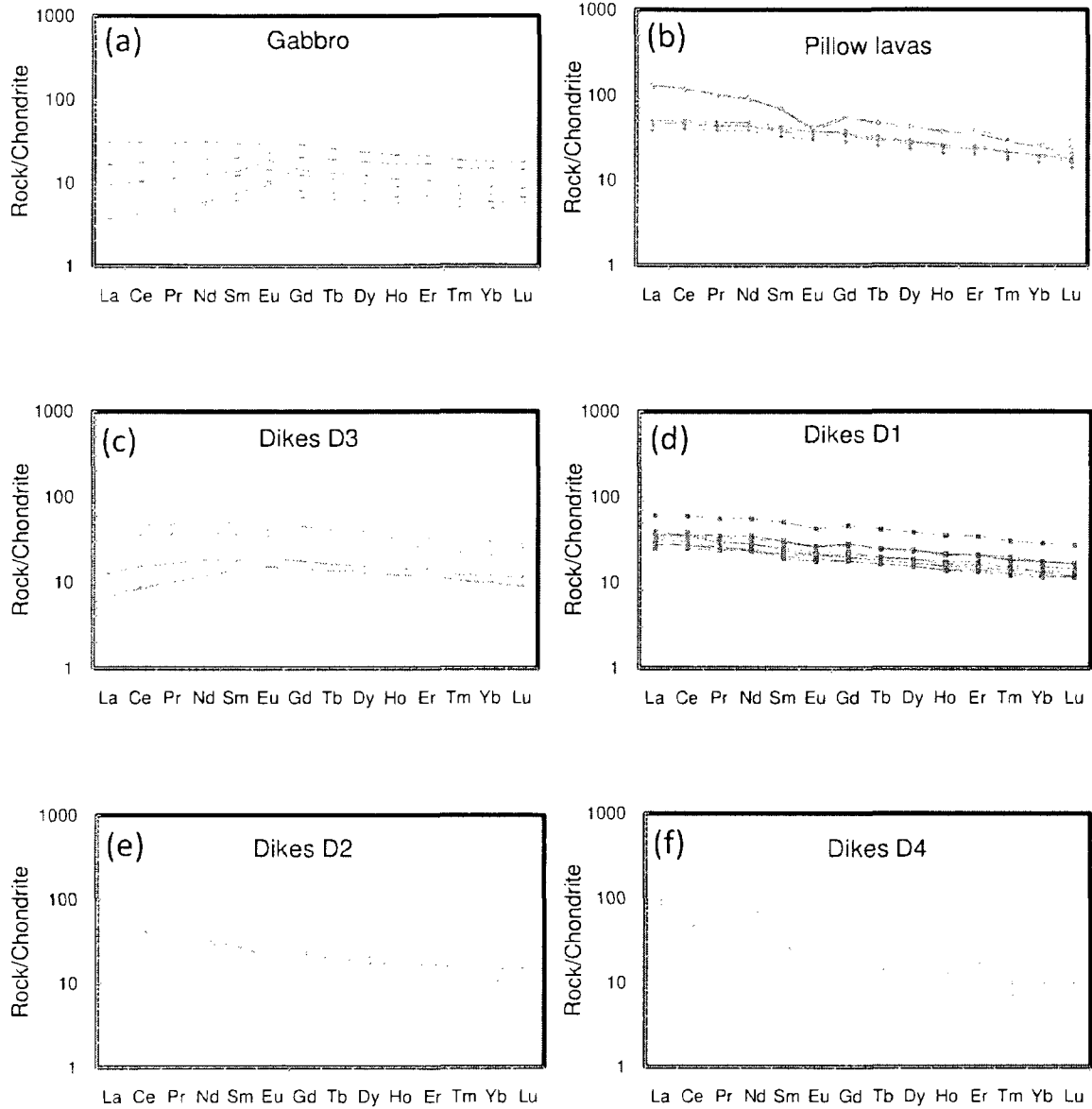


Fig. 2.6. Chondrite-normalized REE patterns for, (a) Gabbros, (b) Pillow lavas; solid yellow symbols for porphyritic pillows, (c) D3 dikes, (d) D1 dikes, (e) D2 dikes, and (f) D4 dikes. (normalizing chondrite values from Sun and McDonough, 1989).

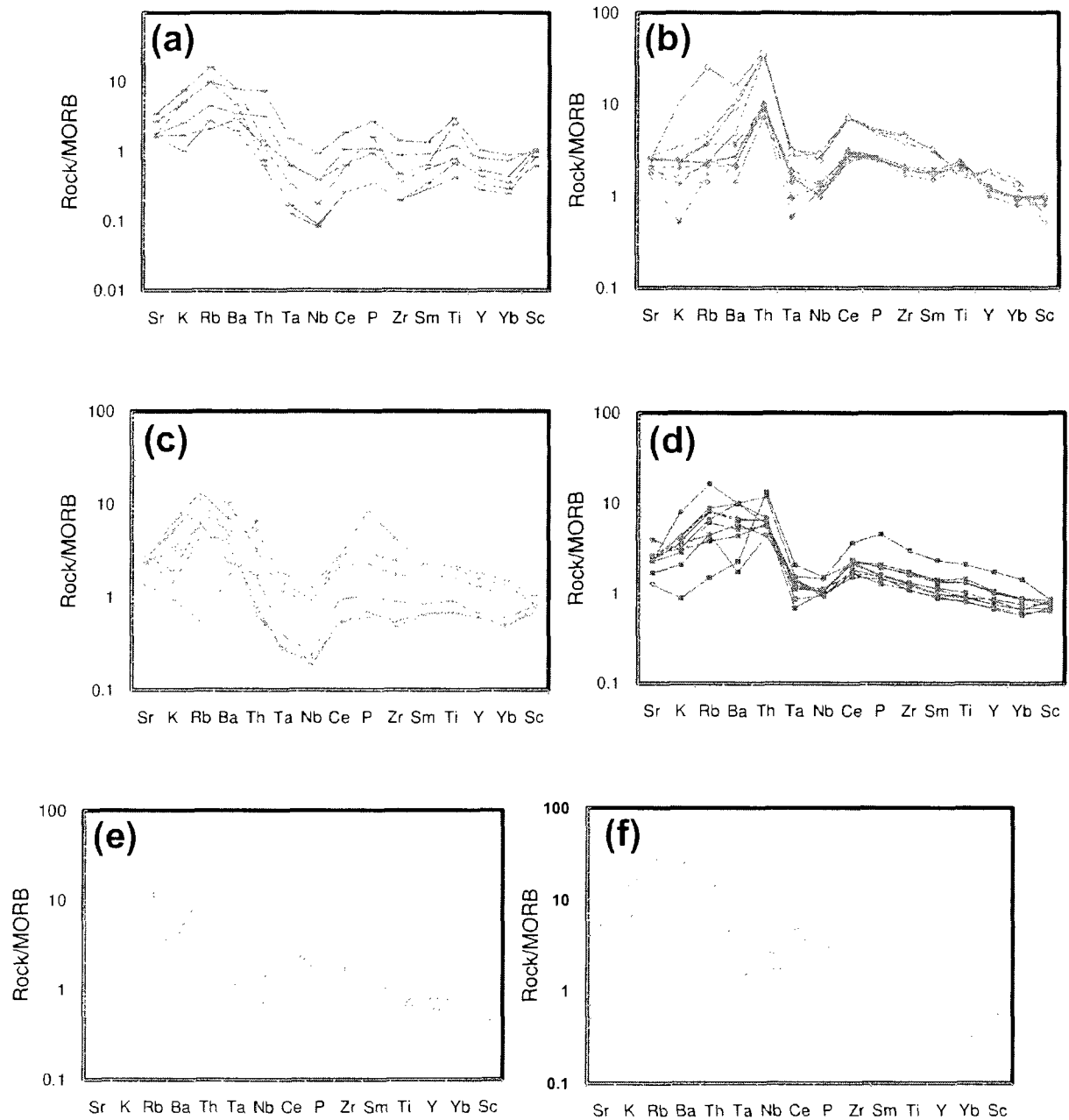


Fig. 2.7. MORB-normalized trace elements patterns for, (a) Gabbros, (b) Pillow lavas; solid yellow symbols for porphyritic pillows, (c) D3 dikes, (d) D1 dikes, (e) D2 dikes, and (f) D4 dikes. Symbols as in Figure (2.6). (normalizing MORB-values after Pearce, 1982).

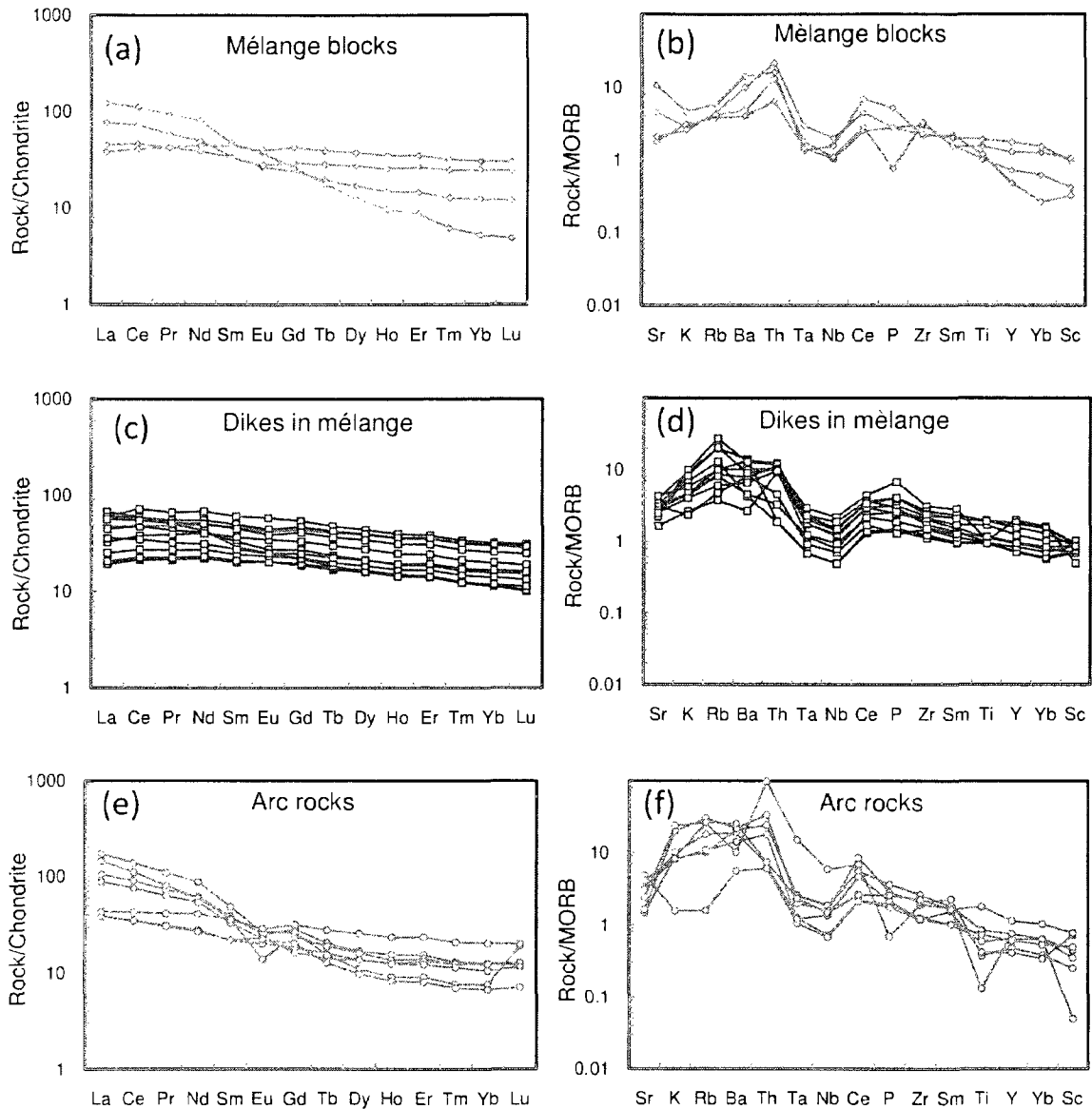


Fig. 2.8. (a) Chondrite-normalized REE patterns for the Wadi Ghadir mélangé blocks, (b) MORB-normalized trace element patterns for the Wadi Ghadir mélangé blocks, (c) Chondrite-normalized REE patterns for fragmented dikes in the Wadi Ghadir ophiolitic mélangé, (d) MORB-normalized trace element patterns for fragmented dikes in the Wadi Ghadir ophiolitic mélangé, (e) Chondrite-normalized REE patterns for arc rocks north of Hafafi and northwest of the Wadi Ghadir ophiolitic mélangé, (f) MORB-normalized trace element patterns for arc rocks north of Hafafi and northwest of the Wadi Ghadir ophiolitic mélangé. (chondrite and MORB values after Sun and McDonough (1989) and Pearce (1982) respectively)

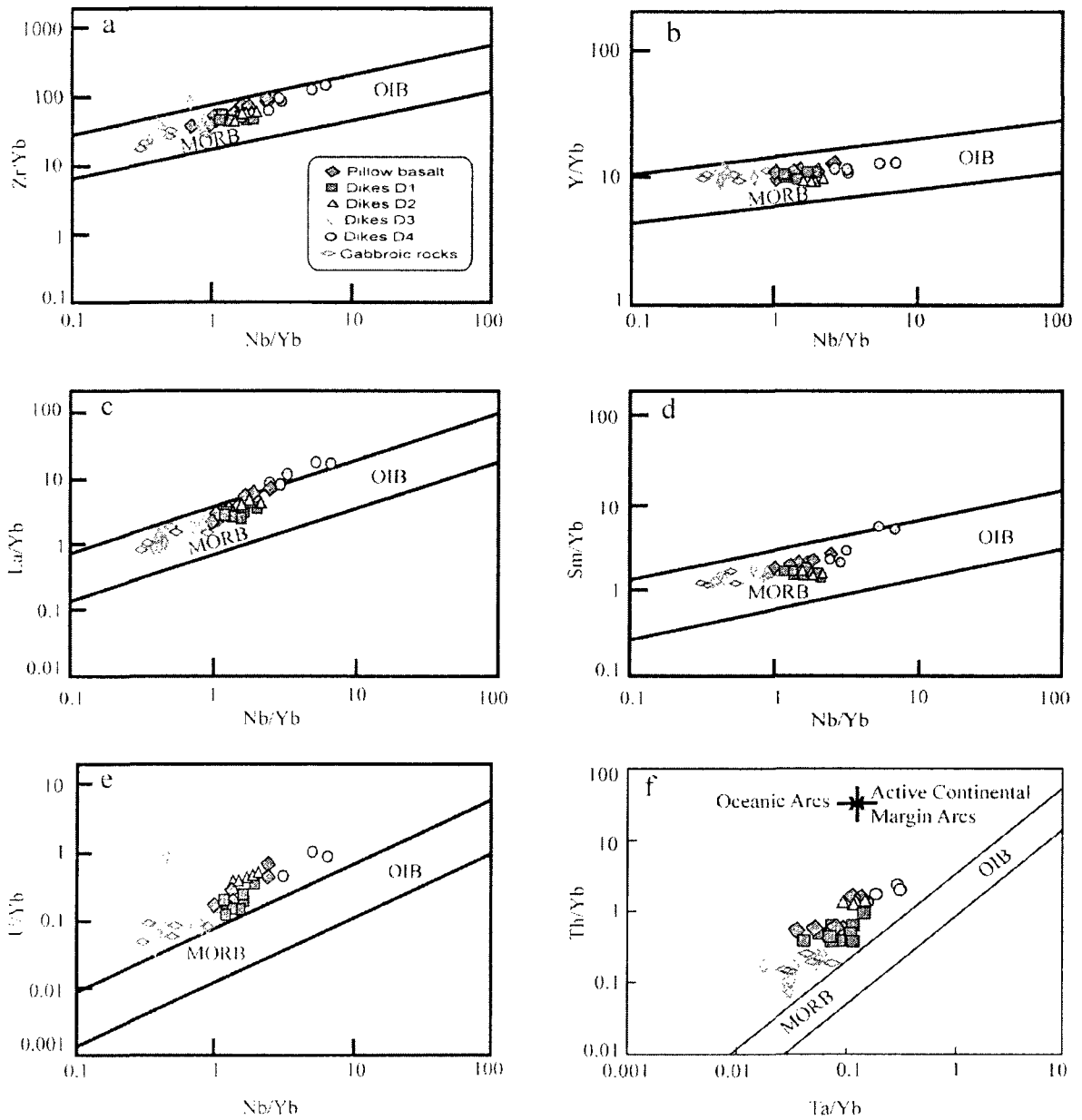


Fig. 2.9. (a-e) Plot of M/Yb versus Nb/Yb for the ophiolitic rocks and associated dikes in the Wadi Ghadir area where M is (a) Zr, (b) Y, (c) La, (d) Sm, (e) U. MORB and OIB represent the position of the mid-ocean ridge and oceanic island mantle source respectively. Mantle array (MORB-OIB array) after Green (2006). (f) Th/Yb versus Ta/Yb diagram with mantle array after Pearce (1983).

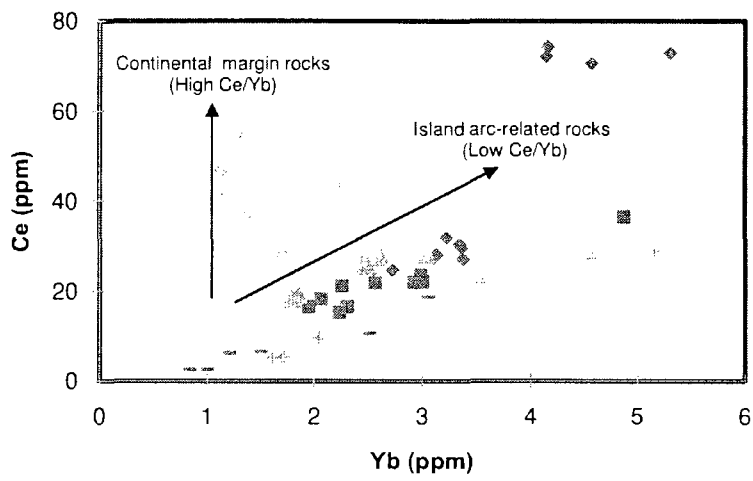


Fig. 2.10. Variation of Ce and Yb contents in the ophiolitic rocks of Wadi Ghadir and associated dikes. Island arc (Low Ce/Yb) and continental margin (High Ce/Yb) trends after Hawkesworth et al. (1993). Symbols as in figure (2.5).

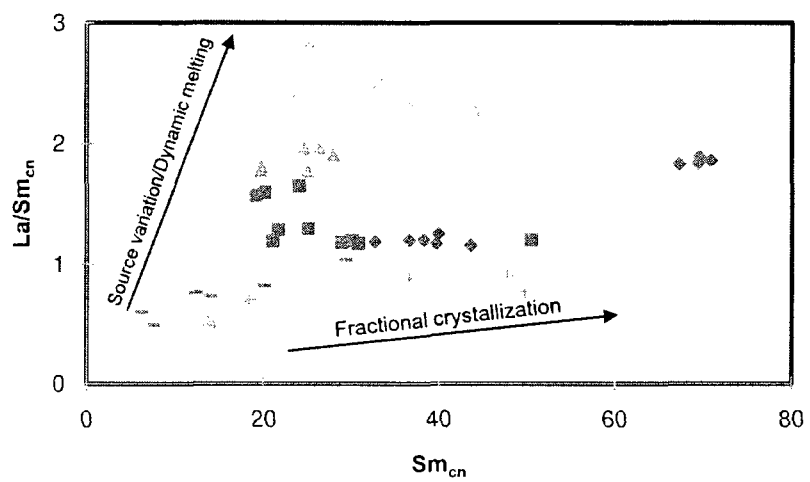


Fig. 2.11. Variation of $\text{La}/\text{Sm}_{\text{cn}}$ and Sm in the ophiolitic and associated rocks of the Wadi Ghadir area. Source variation and/or dynamic melting trend and fractional crystallization trend after Pearce et al. (1995). Symbols as in figure (2.5).

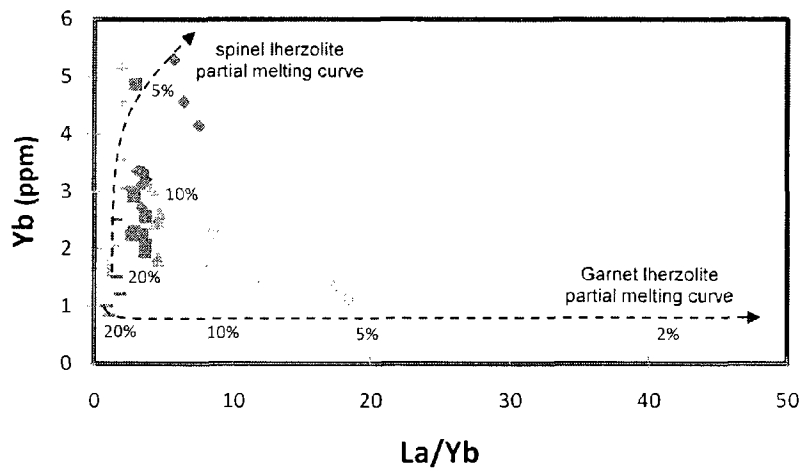


Fig. 2.12. Variation of La/Yb versus Yb for ophiolitic rocks and associated dikes of the Wadi Ghadir area. Modal melting curves of garnet-lherzolite and spinel-lherzolite sources derived from Baker et al., (1997) but scale for percentage of melting of mantle after Rotolo et al. (2005). Symbols as in figure (2.5).

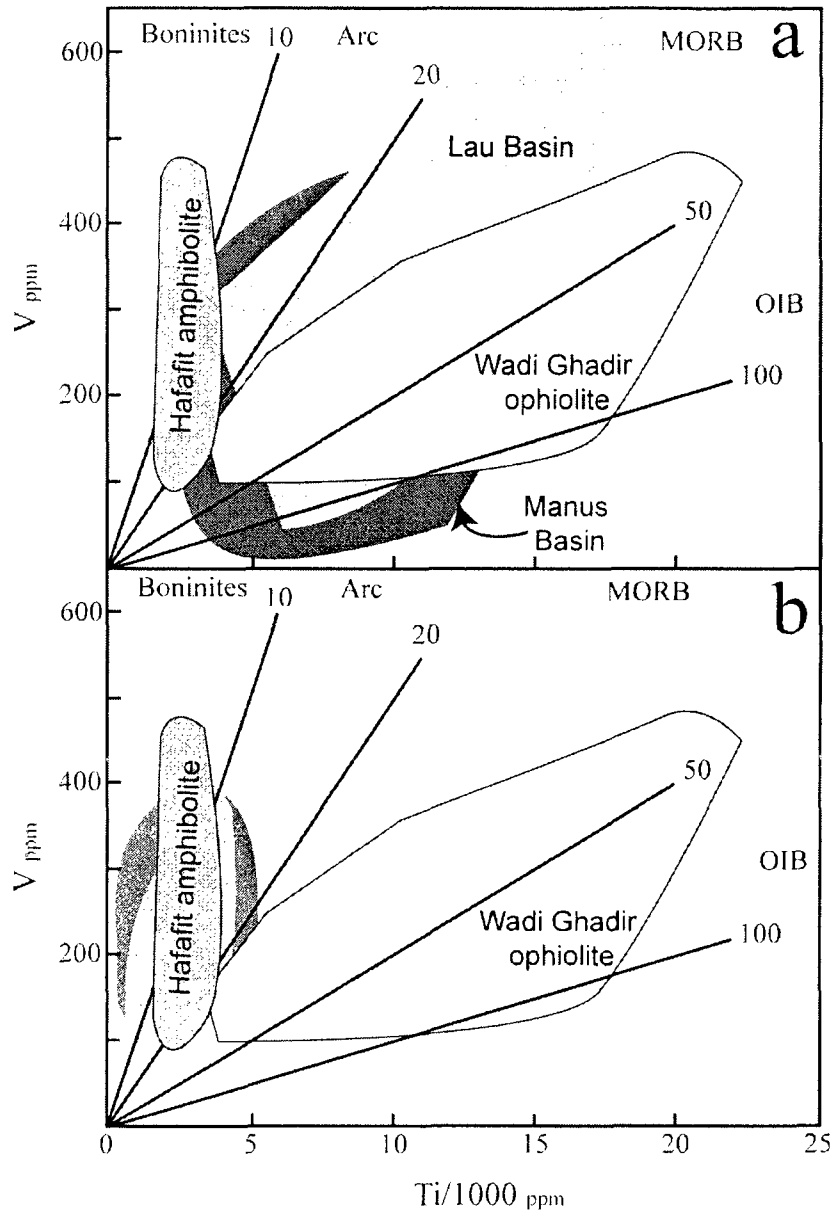


Fig. 2.13. Ti-V discrimination diagram (Shervais, 1982) for Wadi Ghadir ophiolitic rocks (light gray field) and Hafafit amphibolites (dark gray field) to compare with (a) back-arc basins, Lau Basin (light blue) and Manus Basin (Dark blue); and (b) forearc/arc ophiolites, Betts Cove (Red) and Troodos (Pink). Data for Lau Basin from Pearce et al. (1994); for Manus Basin from Sinton et al. (2003); for Betts Cove ophiolite from Bédard (1999); and for Troodos ophiolite from Flower and Levine (1987).

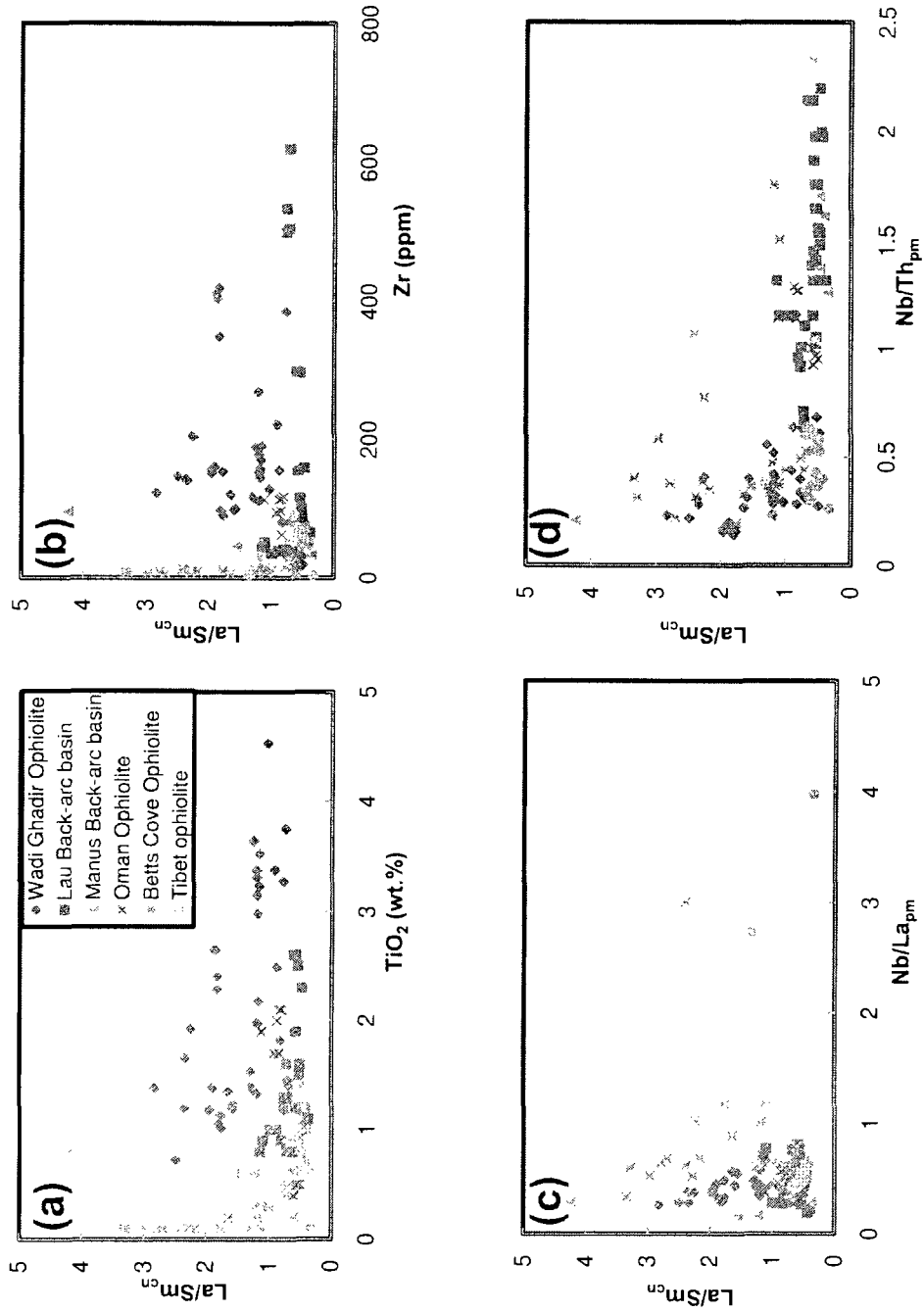


Fig. 2.14. Comparison of the Wadi Ghadir ophiolite rocks with back-arc basins and different ophiolites through (a) TiO_2 versus La/Sm_{en} ; (b) Zr versus La/Sm_{en} ; (c) Nb/La_{pm} versus La/Sm_{en} ; and (d) Nb/Th_{pm} versus La/Sm_{en} . Data for Lau Basin from Pearce et al. (1994); for Manus Basin from Sinton et al. (2003); for Betts Cove ophiolite from Bédard (1999); for Dagzhuka (Tibet) from Xia et al. (2003); and for Oman ophiolite from Godard et al. (2006).

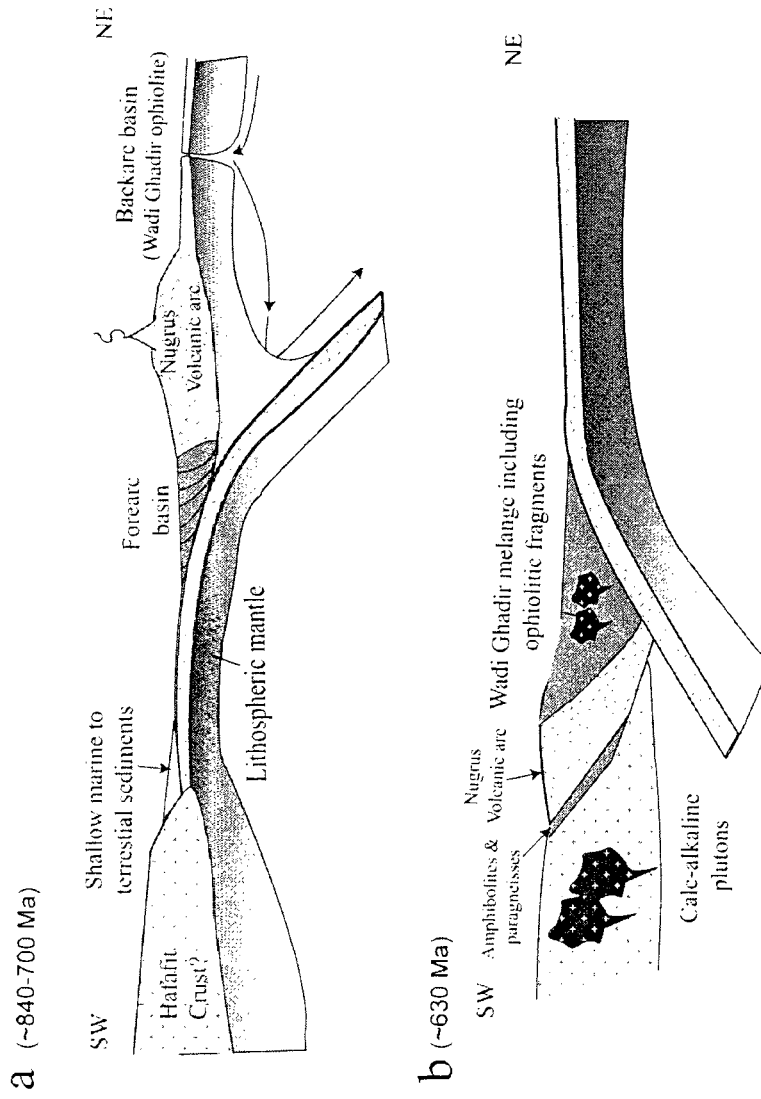


Fig. 2.15. Tectonic model for evolution of the Wadi Ghadir area relative to the Nugrus unit and Hafafit crust to active continental margin. (a) Partial melting of mantle beneath back-arc during formation of the Wadi Ghadir ophiolitic rocks. Arrows show approximate direction of flow and how the mantle beneath Nugrus arc becomes isolated relative to fertile mantle and recipient only to depleted flow from back-arc rift/spreading area. (b) Collision of Nugrus arc system with Hafafit block (old mature arc or crust) resulted in a reversal of subduction polarity from east to west. The reversal of subduction polarity led to formation of accretion area behind the collision zone and the beginning of calc-alkaline magmatism (D4 dikes and probably leucogabbro) and to transformation of the Wadi Ghadir area from oceanic crust to active continental margin. At the collision zone the sediments of Hafafit and forearc of Nugrus arc are squeezed and transformed into amphibolite, mylonite and paragneisses. Northeast and southwest directions are present-day directions. Locations arc in present coordinate system, ages are approximate after Stern (2007).

Element	DNC-1		BIR-1	
	Measured	Recommended	Measured	Recommended
SiO ₂	48.08	47	48.99	47.8
Al ₂ O ₃	18.73	18.3	15.84	15.4
Fe ₂ O ₃ ^(T)	9.76	9.93	11.26	11.3
MnO	0.147	0.149	0.176	0.171
MgO	10.15	10.1	9.68	9.68
CaO	11.62	11.3	13.74	13.2
Na ₂ O	1.67	1.87	1.6	1.75
K ₂ O	0.27	0.234	0.09	0.03
TiO ₂	0.49	0.48	0.992	0.96
P ₂ O ₅	0.08	0.09	0.03	0.05

Table 2.1. Measured and recommended major elements values for USGS standards DNC-1 and BIR-1.

Element	BHVO-2 (n=21)		BHVO-1 (n=11)	
	Measured	Recommended	Measured	Recommended
Li	4.2	5.0	4.69	
V	313	317	321	
Cr	258	280	247	
Co	44	45	45	
Ni	155	119	150	
Cu	133	127	144	
Zn	110	103		
Rb	8.9	9.8	9.2	
Sr	382	389	390	
Y	22.8	26.0	23.3	28
Zr	156	172	165	179
Nb	14.32	18.00	14.9	19
Cs	0.10		0.11	0.13
Ba	128	130	128	139
La	14.70	15	14.78	16
Ce	36.69	38	37.01	39
Pr	5.18		5.13	5.4
Nd	23.76	25.0	23.40	25
Sm	5.90	6.20	5.83	6.4
Eu	1.98		1.97	2.06
Gd	6.23	6.30	6.20	6.4
Tb	0.89	0.90	0.91	0.96
Dy	5.1		5.10	5.2
Ho	0.94	1.04	0.95	0.99
Er	2.5		2.47	
Tm	0.32		0.31	0.33
Yb	1.92	2.00	1.88	2
Lu	0.26	0.28	0.26	0.29
Hf	4.23	4.10	4.52	4.4
Ta	0.9	1.04	0.86	1.2
Pb	2.58		4.18	2.6
Th	1.6	1.20	1.40	1.1
U	0.43		0.44	

Table 2.2. Measured and recommended values for USGS standards BHVO-1 and BHVO-2.

Porphyritic Pillows				
	EGY-06-78	EGY-06-88	EGY-04-75	EGY-04-76
SiO ₂ (wt%)	54.26	57.86	56.03	55.96
Al ₂ O ₃	17.30	16.12	16.24	16.76
Fe ₂ O ₃ ¹	10.95	7.74	10.08	9.98
MnO	0.13	0.11	0.14	0.13
MgO	2.31	2.36	2.13	2.10
CaO	6.61	5.70	7.29	6.58
Na ₂ O	3.95	6.90	4.50	4.75
K ₂ O	1.56	0.24	0.35	0.51
TiO ₂	2.29	2.40	2.64	2.65
P ₂ O ₅	0.64	0.58	0.59	0.60
LOI	1.05	1.89	4.3	3.72
Mg-number	29.4	37.6	29.5	29.4
Cr (ppm)	25	n.d.	33	33
Sc	26	21	26	26
V	158	137	164	160
Co	27	25	25	27
Ni	106	125	50	53
Rb	50.6	4.6	7.3	9.4
Cs	2.3	0.2	0.2	0.2
Ba	316	97	186	216
Sr	299	236	318	334
Pb	11.6	12.0	11.0	10.5
U	1.97	1.85	2.92	1.91
Th	7.48	6.80	7.00	6.77
Y	58.2	53.3	55.3	54.8
Zr	420	349	411	404
Ta	0.59	0.51	0.48	0.57
Nb	8.85	8.60	10.32	10.28
La	30.18	29.17	31.09	31.21
Ce	72.87	70.58	74.32	72.11
Pr	9.59	9.31	9.80	9.86
Nd	42.47	41.35	42.85	43.82
Sm	10.63	10.30	10.65	10.84
Eu	2.20	2.21	2.39	2.39
Gd	11.28	10.91	11.74	11.84
Tb	1.77	1.73	1.80	1.78
Dy	10.85	10.32	10.82	10.90
Ho	2.16	2.04	2.10	2.08
Er	6.28	5.77	5.73	5.79
Tm	0.85	0.75	0.73	0.71
Yb	5.31	4.57	4.16	4.14
Lu	0.75	0.61	0.55	0.51
Mo	0.4	0.3	1.4	1.4
Cu	19.5	76.6	32.6	175.3
Zn	114.2	129.5	109.8	105.6
Ga	95.0	60.9	57.0	60.7
Al ₂ O ₃ TiO ₂	7.6	6.7	6.1	6.3
Nb:Y	0.15	0.16	0.19	0.19
La:Yb _{cn}	4.08	4.58	5.36	5.40
La:Sm _{cn}	1.83	1.83	1.88	1.86
Gd:Yb _{cn}	1.76	1.98	2.34	2.36
Eu:Eu*	0.61	0.64	0.63	0.65
Th:Yb	1.41	1.49	1.68	1.63
Th:Ce	0.103	0.096	0.094	0.094
Ce:Yb	14	15	18	17
Zr:Nb	47	41	40	39
Ti:Zr	33	41	39	39
Ba:La	10	3	6	7
V:Ti	0.012	0.010	0.010	0.010
Sc:Y	0.45	0.39	0.47	0.47
Latitude (N)	24° 46' 0.3"	24° 46' 17.2"	24° 46' 38.93"	24° 46' 38.90"
Longitude (E)	34° 53' 29.9"	34° 53' 12.3"	34° 53' 10.54"	34° 53' 10.52"

* n.d. abbreviation for not detected

Table 2.3. Major (wt%) and trace element (ppm) concentrations and significant element ratios for ophiolitic rocks and associated dikes.

Amygdaloidal Pillows

	<i>EGY-06-74</i>	<i>EGY-04-58</i>	<i>EGY-04-63</i>	<i>EGY-04-67</i>	<i>EGY-04-68</i>	<i>EGY-04-72</i>
SiO ₂	58.09	54.49	55.01	58.16	51.25	54.96
Al ₂ O ₃	11.45	13.37	13.53	12.88	14.57	13.84
Fe ₂ O ₃ [†]	8.60	11.60	12.28	10.80	14.15	11.72
MnO	0.21	0.19	0.22	0.18	0.21	0.18
MgO	1.89	2.57	2.73	2.24	3.08	3.63
CaO	12.65	8.75	8.19	7.59	8.50	7.03
Na ₂ O	3.76	5.21	4.02	4.32	3.91	4.55
K ₂ O	0.08	0.31	0.36	0.21	0.38	0.20
TiO ₂	2.98	3.23	3.37	3.31	3.64	3.52
P ₂ O ₅	0.31	0.32	0.30	0.31	0.33	0.33
LOI	9.06	2.74	1.6	3.43	5.4	2.62
Mg-number	30.3	30.5	30.6	29.2	30.1	38.0
Cr	14	59	n.d.	30	30	26
Sc	33	38	40	39	42	41
V	337	431	430	415	459	452
Co	30	37	34	35	41	38
Ni	112	49	91	47	50	51
Rb	3.4	4.3	4.6	4.7	7.4	2.8
Cs	0.3	0.2	0.2	0.2	0.4	0.1
Ba	29	42	54	43	74	42
Sr	194	254	304	241	314	210
Pb	3.4	5.7	4.0	4.3	4.5	5.2
U	0.42	1.01	0.62	0.63	0.68	0.67
Th	1.42	2.02	1.99	1.76	1.90	1.92
Y	30.2	36.7	34.1	35.2	37.8	38.7
Zr	153	170	178	178	188	190
Ta	0.26	0.17	0.29	0.11	0.34	0.29
Nb	3.44	4.54	3.53	4.05	5.01	4.70
La	9.19	11.00	10.38	10.89	11.82	11.93
Ce	24.70	29.55	27.15	28.17	30.32	31.92
Pr	3.65	4.26	4.10	4.15	4.58	4.58
Nd	17.72	20.57	20.09	19.96	22.18	22.78
Sm	5.00	6.07	5.60	5.86	6.11	6.67
Eu	1.72	2.19	1.98	1.86	2.21	2.16
Gd	5.88	7.19	6.83	6.96	7.36	7.73
Tb	0.95	1.14	1.06	1.10	1.16	1.21
Dy	5.91	7.07	6.77	6.65	7.23	7.45
Ho	1.17	1.42	1.35	1.36	1.44	1.48
Er	3.34	4.01	3.91	3.76	3.98	4.25
Tm	0.44	0.54	0.54	0.49	0.55	0.56
Yb	2.72	3.35	3.37	3.12	3.34	3.22
Lu	0.36	0.46	0.49	0.41	0.44	0.42
Mo	0.1	1.1	0.5	0.8	0.4	0.3
Cu	15.4	14.1	20.4	10.4	28.5	12.5
Zn	59.9	105.1	108.8	82.5	104.8	112.3
Ga	27.1	35.7	41.7	32.5	41.8	38.9
Al ₂ O ₃ ·TiO ₂	3.8	4.1	4.0	3.9	4.0	3.9
Nb Y	0.11	0.12	0.10	0.12	0.13	0.12
La Yb _n	2.42	2.35	2.21	2.50	2.54	2.66
La Sm _n	1.19	1.17	1.20	1.20	1.25	1.15
Gd Yb _n	1.79	1.77	1.67	1.84	1.82	1.99
Eu Eu*	0.97	0.99	0.98	0.89	1.00	0.92
Th Yb	0.52	0.60	0.59	0.56	0.57	0.60
Th Ce	0.057	0.068	0.073	0.062	0.063	0.060
Ce Yb	9	9	8	9	9	10
Zr Nb	44	37	50	44	38	40
Ti Zr	117	114	114	112	116	111
Ba La	3	4	5	4	6	4
V Ti	0.019	0.022	0.021	0.021	0.021	0.021
Sc Y	1.09	1.03	1.17	1.11	1.11	1.06
Latitude (N)	24° 45' 44.5"	24° 45' 46.84"	24° 45' 54.94"	24° 45' 44.82"	24° 45' 44.39"	24° 45' 46.76"
Longitude (E)	34° 53' 22.1"	34° 53' 32.24"	34° 53' 29.65"	34° 53' 29.11"	34° 53' 28.10"	34° 53' 26.27"

Table 2.3. (continued)

Dikes D1										
	<i>EGY-06-82</i>	<i>EGY-06-83</i>	<i>EGY-06-89</i>	<i>EGY-04-44</i>	<i>EGY-04-47</i>	<i>EGY-04-48</i>	<i>EGY-04-50</i>	<i>EGY-04-52</i>	<i>EGY-04-59</i>	<i>EGY-04-66</i>
SiO ₂	51.77	55.36	53.84	50.57	50.32	51.50	49.95	50.28	47.95	48.05
Al ₂ O ₃	18.08	15.20	13.46	16.16	16.78	17.84	16.91	16.22	18.93	17.07
Fe ₂ O ₃	8.28	9.06	14.74	9.52	11.99	8.64	12.20	12.73	10.33	10.99
MnO	0.14	0.17	0.22	0.14	0.18	0.14	0.18	0.19	0.15	0.14
MgO	7.03	7.11	3.44	8.32	6.30	6.95	6.38	6.42	7.77	9.06
CaO	9.93	6.86	6.62	10.01	8.45	9.61	8.58	7.85	9.62	10.04
Na ₂ O	2.93	4.61	2.77	3.20	3.21	3.34	3.09	3.22	3.20	2.63
K ₂ O	0.47	0.13	1.21	0.54	0.56	0.64	0.43	0.66	0.46	0.31
TiO ₂	1.20	1.35	3.15	1.33	1.97	1.23	1.98	2.17	1.39	1.53
P ₂ O ₅	0.18	0.19	0.55	0.17	0.23	0.15	0.24	0.25	0.19	0.19
LOI	1.81	2.74	2.61	2.5	4.43	2.87	4.67	4.5	4.78	4.2
Mg-number	62.7	60.9	31.6	63.4	51.0	61.4	50.9	50.0	59.9	62.0
Cr	60	78	n.d.	306	60	243	63	56	69	558
Sc	26	31	35	34	31	28	32	34	28	33
V	186	207	327	211	155	184	163	179	177	213
Co	38	38	34	41	42	35	41	40	39	49
Ni	125	146	153	123	38	79	38	37	102	197
Rb	13.3	3.0	32.7	8.9	16.1	16.4	12.2	17.6	7.6	9.0
Cs	0.7	0.2	1.4	0.7	0.5	1.7	0.4	0.4	0.1	0.2
Ba	199	45	202	117	129	136	104	200	87	35
Sr	315	152	281	283	287	311	274	277	474	203
Pb	13.7	8.8	8.8	2.0	5.2	2.6	3.2	2.3	5.0	3.2
U	0.49	1.17	0.84	0.34	0.45	0.70	0.36	0.57	0.35	0.44
Th	1.40	2.66	2.37	0.87	1.31	1.29	1.12	1.18	1.19	0.88
Y	20.8	25.8	52.4	22.7	31.3	20.1	30.2	31.7	22.6	24.8
Zr	98	120	269	110	152	99	145	157	115	116
Ta	0.16	0.38	0.28	0.26	0.21	0.22	0.22	0.12	0.25	0.20
Nb	3.31	5.34	5.13	3.45	3.75	3.93	3.56	3.64	3.25	3.73
La	7.55	9.37	14.36	5.92	8.50	7.06	8.08	8.54	6.59	7.67
Ce	18.37	21.89	36.48	15.27	23.60	16.60	22.01	22.19	16.63	21.20
Pr	2.46	2.91	5.28	2.25	3.30	2.35	3.13	3.34	2.44	2.76
Nd	11.15	13.12	25.99	11.08	16.17	10.80	15.27	16.37	11.53	13.33
Sm	3.06	3.67	7.72	3.21	4.60	2.91	4.42	4.71	3.31	3.83
Eu	1.10	1.20	2.47	1.25	1.33	1.11	1.54	1.53	1.26	1.28
Gd	3.68	4.39	9.45	3.98	5.78	3.65	5.51	5.85	4.11	4.67
Tb	0.61	0.74	1.56	0.68	0.94	0.61	0.91	0.94	0.67	0.72
Dy	3.91	4.75	9.78	4.21	5.99	3.87	5.75	6.06	4.24	4.66
Ho	0.79	0.98	1.98	0.86	1.20	0.77	1.17	1.23	0.90	0.94
Er	2.33	2.88	5.69	2.48	3.49	2.20	3.35	3.48	2.60	2.68
Tm	0.32	0.40	0.77	0.34	0.51	0.30	0.46	0.47	0.36	0.39
Yb	2.06	2.56	4.87	2.23	2.98	1.95	2.92	3.00	2.31	2.25
Lu	0.30	0.37	0.69	0.30	0.43	0.29	0.41	0.42	0.33	0.30
Mo	0.3	3.4	0.4	0.3	0.4	0.2	0.4	0.3	0.5	0.5
Cu	64.5	51.7	41.8	61.0	28.9	38.2	31.9	33.1	8.0	15.9
Zn	91.4	2919.8	179.2	61.5	98.2	60.4	98.6	90.0	79.6	105.2
Ga	71.7	39.1	86.6	35.1	45.0	38.9	42.4	50.2	44.6	33.9
Al ₂ O ₃ , TiO ₂	15.1	11.3	4.3	12.1	8.5	14.5	8.6	7.5	13.6	11.1
Nb-Y	0.16	0.21	0.10	0.15	0.12	0.20	0.12	0.11	0.14	0.15
La-Yb _{cn}	2.62	2.62	2.11	1.90	2.04	2.60	1.99	2.04	2.05	2.44
La-Sm _{cn}	1.59	1.65	1.20	1.19	1.19	1.57	1.18	1.17	1.29	1.29
Gd-Yb _{cn}	1.47	1.42	1.60	1.48	1.60	1.55	1.56	1.62	1.47	1.71
Eu-Eu*	1.00	0.91	0.89	1.03	0.91	0.97	0.94	0.90	1.06	0.95
Th-Yb	0.68	1.04	0.49	0.39	0.44	0.66	0.38	0.39	0.52	0.39
Th-Ce	0.076	0.122	0.065	0.057	0.056	0.078	0.051	0.053	0.072	0.042
Ce-Yb	9	9	7	7	8	9	8	7	7	9
Zr-Nb	30	22	52	32	40	25	41	43	35	31
Ti-Zr	73	67	70	72	78	75	82	83	72	79
Ba-La	26	5	14	20	15	19	13	23	13	5
V-Ti	0.026	0.026	0.017	0.026	0.013	0.025	0.014	0.014	0.021	0.023
Sc-Y	1.25	1.20	0.67	1.50	0.99	1.40	1.06	1.07	1.24	1.33
Latitude (N)	24° 36'	24° 46'	24° 46'	24° 46'	24° 46'	24° 46'	24° 46'	24° 46'	24° 45'	24° 45'
Longitude (E)	17.3"	16.3"	16.6"	19.24"	06.56"	18.48"	03.50"	03.43"	46.84"	48.53"
	34° 53'	34° 53'	34° 53'	34° 53'	34° 53'	34° 53'	34° 53'	34° 53'	34° 53'	34° 53'
	44.4"	25.4"	8.6"	43.80"	42.83"	38.08"	45.92"	43.30"	32.24"	37.32"

Table 2.3. (continued)

Dikes D2

	<i>EGY-06-73</i>	<i>EGY-04-45</i>	<i>EGY-04-54</i>	<i>EGY-04-55</i>	<i>EGY-04-69</i>	<i>EGY-04-70</i>
SiO ₂	57.27	57.63	56.13	56.14	58.27	59.57
Al ₂ O ₃	16.83	16.22	16.99	16.93	16.13	16.52
Fe ₂ O ₃ [†]	6.89	6.91	7.90	7.83	6.75	7.56
MnO	0.11	0.10	0.12	0.12	0.11	0.10
MgO	4.94	4.56	4.93	5.04	4.69	2.85
CaO	8.20	6.82	8.28	8.15	7.24	4.47
Na ₂ O	4.29	6.05	3.88	3.99	5.29	6.09
K ₂ O	0.26	0.38	0.42	0.43	0.31	1.27
TiO ₂	1.05	1.13	1.18	1.19	1.02	1.38
P ₂ O ₅	0.15	0.18	0.19	0.17	0.14	0.21
LOI	1.58	1.28	2.91	3.1	2.01	2.73
Mg-number	58.7	56.7	55.3	56.1	57.9	42.8
Cr	42	118	35	44	126	22
Sc	24	22	23	24	22	19
V	153	140	158	161	138	123
Co	27	24	24	24	25	18
Ni	63	50	56	56	37	20
Rb	4.7	5.6	9.2	10.4	5.6	23.3
Cs	0.2	0.2	0.3	0.4	0.2	0.7
Ba	112	115	91	77	95	263
Sr	318	346	208	209	409	386
Pb	3.4	8.7	5.2	8.9	4.5	7.9
U	0.76	1.24	1.16	1.10	0.72	1.32
Th	2.38	3.75	3.89	3.65	2.32	4.19
Y	18.9	25.0	24.2	23.4	18.0	29.7
Zr	97	153	156	151	90	160
Ta	0.20	0.27	0.31	0.37	0.21	0.28
Nb	2.52	5.17	4.57	4.63	2.74	5.73
La	8.42	10.50	12.25	11.41	8.23	12.60
Ce	19.31	25.85	27.43	25.58	18.20	28.03
Pr	2.54	3.26	3.53	3.34	2.39	3.75
Nd	11.36	13.81	15.37	14.39	10.97	15.99
Sm	3.01	3.83	4.03	3.77	3.01	4.28
Eu	1.02	1.02	1.15	1.09	0.91	1.11
Gd	3.49	4.43	4.52	4.35	3.51	4.99
Tb	0.57	0.71	0.72	0.70	0.54	0.84
Dy	3.53	4.42	4.62	4.44	3.35	5.30
Ho	0.71	0.92	0.94	0.90	0.70	1.10
Er	2.10	2.74	2.86	2.73	1.94	3.30
Tm	0.28	0.39	0.39	0.39	0.27	0.46
Yb	1.85	2.44	2.62	2.50	1.79	3.04
Lu	0.26	0.38	0.38	0.37	0.26	0.44
Mo	0.1	0.4	0.4	0.5	0.4	0.4
Cu	40.7	20.2	34.7	30.4	4.1	5.7
Zn	62.4	113.1	69.1	68.4	52.6	68.1
Ga	50.0	38.3	40.2	39.0	35.0	55.6
Al ₂ O ₃ TiO ₂	16.0	14.3	14.4	14.2	15.9	11.9
Nb/Y	0.13	0.21	0.19	0.20	0.15	0.19
La/Yb _n	3.26	3.09	3.36	3.28	3.29	2.97
La/Sm _n	1.80	1.77	1.96	1.95	1.77	1.90
Gd/Yb _n	1.56	1.50	1.42	1.44	1.62	1.35
Eu/Eu*	0.96	0.77	0.81	0.83	0.85	0.73
Th/Yb	1.29	1.54	1.48	1.46	1.29	1.38
Th/Ce	0.123	0.145	0.142	0.143	0.128	0.149
Ce/Yb	10	11	10	10	10	9
Zr/Nb	38	30	34	33	33	28
Ti/Zr	65	44	45	47	68	52
Ba/La	13	11	7	7	12	21
V/Ti	0.024	0.021	0.022	0.023	0.023	0.015
Sc/Y	1.27	0.88	0.95	1.03	1.22	0.64
Latitude (N)	24° 45' 39.1"	24° 46' 19.24"	24° 46' 00.77"	24° 46' 00.41"	24° 45' 43.42"	24° 45' 43.42"
Longitude (E)	34° 53' 26.3"	34° 53' 43.80"	34° 53' 41.46"	34° 53' 40.67"	34° 53' 26.77"	34° 53' 26.77"

Table 2.3. (continued)

Dikes D3

	<i>EGY-06-86a</i>	<i>EGY-06-86b</i>	<i>EGY-06-84</i>	<i>EGY-06-87</i>	<i>EGY-04-62</i>	<i>EGY-04-61</i>	<i>EGY-04-65</i>	<i>EGY-04-77</i>	<i>EGY-04-78</i>
SiO ₂	48.53	48.89	50.30	49.87	48.51	48.82	48.82	48.68	48.91
Al ₂ O ₃	17.33	18.01	13.86	15.43	17.71	17.50	14.56	17.56	17.71
Fe ₂ O ₃ ¹	8.61	8.23	15.51	12.80	9.65	9.65	15.79	8.90	8.96
MnO	0.14	0.14	0.25	0.20	0.15	0.15	0.23	0.14	0.13
MgO	10.07	9.92	4.37	5.76	8.90	8.45	4.39	9.87	9.82
CaO	11.28	10.78	8.24	9.51	10.45	10.94	7.69	11.00	9.93
Na ₂ O	2.15	1.90	3.63	2.73	2.63	2.61	4.02	2.19	2.56
K ₂ O	0.76	0.99	0.14	0.94	0.47	0.29	0.22	0.53	0.79
TiO ₂	1.05	1.06	3.38	2.49	1.40	1.45	3.27	1.07	1.05
P ₂ O ₅	0.07	0.08	0.37	0.28	0.13	0.13	1.00	0.08	0.08
LOI	4.04	4.11	2.5	2.39	3.49	3.84	2.58	4	4.82
Mg-number	69.9	70.5	35.8	47.1	64.7	63.4	35.5	68.7	68.5
Cr	68	75	n.d.	25	105	108	n.d.	324	328
Sc	27	29	41	42	33	32	34	31	29
V	188	191	470	346	212	205	277	188	184
Co	54	43	42	43	37	40	27	40	44
Ni	266	267	171	158	123	145	83	218	227
Rb	17.0	27.0	1.1	25.1	7.5	12.8	9.3	11.6	22.1
Cs	0.7	0.7	0.2	0.4	0.2	0.2	0.2	0.7	0.5
Ba	100	140	33	208	47	48	83	76	99
Sr	321	268	166	316	281	332	299	288	337
Pb	18.5	17.4	6.4	21.7	3.8	36.9	3.6	2.4	2.2
U	0.13	0.06	0.44	0.25	0.12	0.13	0.39	1.48	0.12
Th	0.14	0.13	1.33	0.67	0.36	0.35	1.09	0.16	0.17
Y	17.7	17.8	54.2	39.1	20.3	20.3	47.4	18.3	17.8
Zr	43	50	221	155	81	80	385	48	50
Ta	0.05	0.05	0.32	0.20	0.04	0.07	0.26	0.05	0.05
Nb	0.64	0.66	4.41	3.22	0.83	0.86	3.27	0.74	0.73
La	1.59	1.67	10.23	7.62	3.03	2.99	9.10	1.62	1.71
Ce	5.26	5.39	28.92	21.92	9.68	9.37	27.24	5.09	5.31
Pr	0.95	0.97	4.50	3.47	1.59	1.58	4.61	0.97	0.97
Nd	5.55	5.58	23.25	17.99	8.67	8.51	24.75	5.61	5.64
Sm	2.09	2.10	7.31	5.61	2.79	2.81	7.61	2.20	2.12
Eu	0.89	0.87	2.35	2.04	1.12	1.09	2.69	0.95	0.87
Gd	2.93	2.95	9.25	7.00	3.63	3.71	9.58	3.08	2.92
Tb	0.51	0.51	1.56	1.17	0.60	0.62	1.52	0.51	0.50
Dy	3.34	3.32	10.02	7.46	3.92	3.94	9.36	3.50	3.34
Ho	0.70	0.70	2.07	1.52	0.83	0.82	1.88	0.70	0.68
Er	1.99	1.98	5.97	4.30	2.41	2.39	5.46	1.98	1.98
Tm	0.27	0.27	0.81	0.58	0.32	0.32	0.73	0.27	0.27
Yb	1.70	1.72	5.15	3.55	2.05	2.04	4.58	1.61	1.62
Lu	0.23	0.24	0.71	0.48	0.29	0.28	0.64	0.24	0.23
Mo	0.3	0.2	0.3	0.5	0.5	0.5	0.4	0.2	0.5
Cu	87.7	71.9	54.3	62.0	57.5	68.0	27.8	58.3	73.2
Zn	283.1	77.0	179.1	164.2	66.1	118.9	106.3	50.8	51.9
Ga	51.9	59.8	59.0	85.3	34.9	34.7	48.8	32.0	34.3
Al ₂ O ₃ /TiO ₂	16.6	17.0	4.1	6.2	12.0	12.6	4.5	16.4	16.8
Nb/Y	0.04	0.04	0.08	0.08	0.04	0.04	0.07	0.04	0.04
La/Yb _{cn}	0.67	0.70	1.42	1.54	1.05	1.06	1.43	0.72	0.76
La/Sm _{cn}	0.49	0.51	0.90	0.88	0.70	0.7	0.77	0.48	0.52
Gd/Yb _{cn}	1.43	1.42	1.48	1.63	1.50	1.46	1.73	1.59	1.49
Eu/Eu*	1.10	1.07	0.87	1.00	1.06	1.08	0.97	1.06	1.06
Th/Yb	0.08	0.07	0.26	0.19	0.17	0.17	0.24	0.10	0.10
Th/Ce	0.026	0.024	0.046	0.030	0.037	0.037	0.040	0.031	0.031
Ce/Yb	3	3	6	6	5	5	6	3	3
Zr/Nb	67	76	50	48	97	93	118	65	69
Ti/Zr	146	127	92	96	104	109	51	134	126
Ba/La	63	84	3	27	16	16	9	47	58
V/Ti	0.030	0.030	0.023	0.023	0.025	0.024	0.014	0.029	0.029
Sc/Y	1.52	1.63	0.76	1.07	1.63	1.58	0.72	1.69	1.63
Latitude (N)	24° 46' 17.2"	24° 46' 17.2"	24° 46' 16"	24° 46' 17.2"	24° 45' 54.94"	24° 45' 54.94"	24° 45' 48.53"	24° 46' 17.11"	24° 46' 17.11"
Longitude (E)	34° 53' 12.3"	34° 53' 12.3"	34° 53' 6.2"	34° 53' 12.3"	34° 53' 29.65"	34° 53' 29.65"	34° 53' 37.32"	34° 53' 12.41"	34° 53' 12.41"

Table 2.3. (continued)

Dikes D4					
	<i>EGY-06-61</i>	<i>EGY-06-79</i>	<i>EGY-04-46</i>	<i>EGY-04-49</i>	<i>EGY-04-74</i>
SiO ₂	56.97	53.29	54.92	55.12	52.54
Al ₂ O ₃	17.50	19.34	15.44	16.51	17.62
Fe ₂ O ₃ [†]	6.70	6.88	9.67	9.23	7.93
MnO	0.12	0.11	0.13	0.12	0.12
MgO	5.20	5.00	4.86	4.65	5.73
CaO	6.54	9.98	6.77	6.61	9.66
Na ₂ O	3.96	3.50	3.98	4.66	3.33
K ₂ O	2.07	0.47	1.67	1.03	1.28
TiO ₂	0.73	1.20	1.92	1.66	1.38
P ₂ O ₅	0.22	0.25	0.62	0.43	0.38
LOI	2.35	2.6	3.22	5.8	5.08
Mg-number	60.6	59.0	49.9	49.9	58.9
Cr	28	44	141	100	42
Sc	21	22	15	15	26
V	116	143	188	199	183
Co	23	28	30	27	23
Ni	44	79	56	52	61
Rb	58.1	12.7	32.2	24.8	20.7
Cs	0.5	0.3	0.5	0.7	0.7
Ba	274	134	522	350	332
Sr	383	462	685	666	621
Pb	4.5	4.6	5.4	7.1	12.1
U	1.09	0.75	1.12	1.17	0.68
Th	3.41	2.10	2.88	2.73	2.55
Y	24.6	18.2	17.9	14.9	15.0
Zr	146	143	204	141	122
Ta	0.35	0.27	0.41	0.33	0.27
Nb	5.65	4.89	8.91	5.81	4.44
La	19.54	12.84	23.45	20.59	16.82
Ce	43.43	28.46	54.84	46.76	37.12
Pr	5.31	3.54	7.44	6.32	4.73
Nd	22.01	15.07	32.29	27.76	19.32
Sm	5.06	3.51	6.72	5.67	3.83
Eu	1.34	1.23	1.89	1.65	1.23
Gd	5.06	3.70	6.03	4.78	3.74
Tb	0.78	0.58	0.76	0.59	0.52
Dy	4.68	3.47	3.94	3.33	3.06
Ho	0.92	0.69	0.69	0.57	0.60
Er	2.66	1.99	1.73	1.48	1.70
Tm	0.36	0.27	0.23	0.19	0.23
Yb	2.28	1.68	1.35	1.12	1.41
Lu	0.32	0.24	0.20	0.16	0.19
Mo	0.1	0.4	1.2	0.4	0.4
Cu	43.6	24.4	26.3	32.2	18.7
Zn	70.4	67.9	103.6	143.5	72.4
Ga	72.8	54.6	81.8	65.1	55.8
Al ₂ O ₃ /TiO ₂	24.1	16.1	8.0	10.0	12.7
Nb/Y	0.23	0.27	0.50	0.39	0.30
La/Yb _n	6.14	5.48	12.50	13.15	8.56
La/Sm _n	2.50	2.36	2.25	2.34	2.83
Gd/Yb _n	1.83	1.82	3.71	3.52	2.19
Eu/Eu*	0.81	1.05	0.93	0.93	1.01
Tb/Yb	1.49	1.25	2.14	2.43	1.81
Th/Ce	0.078	0.074	0.053	0.058	0.069
Ce/Yb	19	17	41	42	26
Zr/Nb	26	29	23	24	27
Ti/Zr	30	50	57	71	68
Ba/La	14	10	22	17	20
V/Ti	0.027	0.020	0.016	0.020	0.022
Sc/Y	0.85	1.21	0.84	1.01	1.73
Latitude (N)	24° 43' 36.3"	24° 46' 0.6"	24° 46' 19.49"	24° 46' 11.50"	24° 45' 36.11"
Longitude (E)	34° 52' 45.8"	34° 53' 30"	34° 53' 41.93"	34° 53' 36.10"	34° 53' 24.40"

Table 2.3. (continued)

Gabbros						
	<i>EGY-04-42</i>	<i>EGY-04-43</i>	<i>EGY-04-51</i>	<i>EGY-04-57</i>	<i>EGY-06-80</i>	<i>EGY-06-81</i>
SiO ₂	48.78	47.14	48.55	50.58	46.07	47.38
Al ₂ O ₃	16.90	18.68	14.45	15.62	16.50	17.13
Fe ₂ O ₃	9.72	10.00	14.30	11.64	13.43	9.35
MnO	0.15	0.14	0.24	0.17	0.18	0.15
MgO	9.42	8.69	5.35	6.31	5.86	11.61
CaO	10.59	11.50	8.39	9.79	10.35	11.71
Na ₂ O	2.61	2.18	3.04	3.51	2.62	1.85
K ₂ O	0.76	0.26	0.78	0.39	1.14	0.16
TiO ₂	1.03	1.18	4.53	1.82	3.75	0.63
P ₂ O ₅	0.04	0.20	0.33	0.13	0.11	0.04
LOI	4.75	3.31	2.51	2.5	2.61	2.89
Mg-number	65.8	63.3	42.6	51.8	46.4	71.1
Cr	86	133	n.d.	n.d.	n.d.	125
Sc	42	25	40	43	45	34
V	251	188	312	353	824	157
Co	44	38	32	34	40	53
Ni	116	156	124	66	166	215
Rb	20.1	4.2	19.6	9.1	32.6	5.5
Cs	0.5	0.5	0.2	0.6	1.2	0.5
Ba	94	59	157	71	157	39
Sr	326	205	215	220	419	195
Pb	2.4	2.0	3.6	2.4	8.4	10.8
U	0.05	0.07	0.45	0.21	0.12	0.07
Tb	0.15	0.24	1.48	0.64	0.29	0.12
Y	10.0	13.1	31.1	23.9	16.0	8.3
Zr	18	33	128	80	43	18
Ta	0.03	0.06	0.27	0.11	0.11	0.02
Nb	0.31	0.61	3.26	1.37	1.38	0.29
La	0.88	2.24	7.20	3.90	2.43	0.88
Ce	2.63	6.25	18.81	10.69	6.58	2.62
Pr	0.47	1.03	2.88	1.72	1.09	0.43
Nd	2.79	5.58	14.65	9.01	5.97	2.51
Sm	1.15	1.89	4.49	3.06	2.13	0.95
Eu	0.61	0.84	1.71	1.33	1.09	0.57
Gd	1.68	2.54	5.91	4.16	2.94	1.37
Tb	0.28	0.41	0.95	0.71	0.49	0.24
Dy	1.92	2.53	6.00	4.59	3.16	1.57
Ho	0.39	0.52	1.23	0.96	0.64	0.33
Er	1.16	1.47	3.49	2.79	1.78	0.94
Tm	0.17	0.19	0.49	0.39	0.23	0.13
Yb	1.01	1.21	3.05	2.51	1.51	0.84
Lu	0.14	0.17	0.44	0.36	0.22	0.12
Mo	0.4	0.4	0.6	0.3	0.2	0.1
Cu	80.5	36.7	45.2	10.4	44.5	96.1
Zn	63.3	65.9	113.0	85.3	109.3	86.4
Ga	33.8	33.9	47.2	41.1	69.5	37.9
Al ₂ O ₃ /TiO ₂	16.4	15.8	3.2	8.6	4.4	27.0
Nb:Y	0.03	0.05	0.10	0.06	0.09	0.03
La:Yb _{cn}	0.63	1.32	1.69	1.11	1.16	0.75
La:Sm _{cn}	0.49	0.77	1.03	0.82	0.74	0.60
Gd:Yb _{cn}	1.38	1.73	1.60	1.37	1.61	1.35
Eu:Eu*	1.35	1.17	1.02	1.14	1.34	1.53
Tb:Yb	0.15	0.20	0.48	0.25	0.19	0.15
Tb:Ce	0.057	0.038	0.079	0.060	0.044	0.048
Ce:Yb	3	5	6	4	4	3
Zr:Nb	58	54	39	58	31	62
Ti:Zr	343	215	212	136	523	211
Ba:La	107	26	22	18	65	45
V:Ti	0.041	0.027	0.011	0.032	0.037	0.041
Sc:Y	4.21	1.92	1.29	1.80	2.82	4.09
Latitude (N)	24° 46' 16.79"	24° 46' 19.13"	24° 46' 03.50"	24° 46' 02.75"	24° 46' 16.1"	24° 46' 17"
Longitude (E)	34° 53' 49.24"	34° 53' 45.71"	34° 53' 45.92"	34° 53' 34.87"	34° 53' 50.6"	34° 53' 43"

Table 2.3. (continued)

	Porphyrific pillow	Amygdaloidal pillow	Dikes D1	Dikes D2	Dikes 3	Dikes 4	Gabbros
SiO ₂ (wt%)	54.3-57.9	51.3-58.2	48.1-55.4	56.1-59.6	48.5-50.3	52.5-56.97	46.1-50.6
Al ₂ O ₃	16.1-17.3	11.5-14.6	13.5-18.9	16.1-17.0	13.9-18.0	15.4-19.34	14.5-18.7
Fe ₂ O ₃ ^t	7.7-11.0	8.6-14.2	8.3-14.7	6.8-7.9	8.23-15.79	6.7-9.7	9.4-14.3
MgO	2.4	1.9-3.6	3.4-9.1	2.9-5.0	4.4-10.1	4.7-5.7	5.4-11.6
CaO	5.7-7.3	7.0-12.7	6.6-10.0	4.5-8.3	7.7-11.3	6.5-10.0	8.4-11.7
TiO ₂	2.29-2.65	2.98-3.64	1.20-3.15	1.02-1.38	1.05-3.38	0.73-1.92	0.63-4.53
Mg - number	29.4-37.6	29.2-30.6	31.6-63.4	42.8-58.7	35.5-70.5	49.9-60.6	42.6-71.1
Cr (ppm)	25-33	14-59	56-557	21-126	25-328	28-140	n.d.-133
Sc	21-26	33-42	26-35	19-24	27-42	15-26	25-45
V	137-164	337-459	155-327	123-161	184-470	116-199	157-824
Co	25-27	30-41	34-49	18-27	27-44	23-30	32-44
Ni	50-125	47-112	37-197	20-63	83-267	44-79	66-215
Th	6.77-7.48	1.42-2.02	0.87-2.66	2.32-4.19	0.13-1.33	2.55-3.41	0.12-1.48
Y	54.8-55.3	30.2-38.7	20.1-52.4	18.1-29.7	17.7-54.2	14.9-24.6	8.3-31.1
Zr	349-411	153-190	98-269	90-160	43-385	122-204	18-128
Nb	8.6-10.32	3.44-5.01	3.31-5.34	2.52-5.73	0.64-4.41	4.44-8.91	0.29-3.26
La	29.17-31.21	9.19-11.93	5.92-14.36	8.23-12.60	1.59-10.23	12.84-23.45	0.88-7.20
Nd	41.35-43.82	17.72-22.78	10.80-25.99	10.97-15.99	5.55-24.75	15.07-32.29	2.51-14.65
Sm	10.30-10.84	5.00-6.67	2.90-7.72	3.01-4.26	2.09-7.61	3.51-6.72	0.95-5.91
Gd	10.97-11.84	5.88-7.73	3.65-9.45	3.49-4.99	2.92-9.58	3.70-6.03	1.37-5.91
Yb	4.14-5.31	2.72-3.37	1.95-4.87	1.79-3.04	1.61-5.15	1.12-2.28	0.84-3.05
La/Yb _{cn}	4.08-5.40	2.21-2.66	1.90-2.62	2.97-3.36	0.67-1.54	5.48-13.15	0.63-1.69
La/Sm _{cn}	1.83-1.88	1.15-1.25	1.17-1.65	1.77-1.97	0.48-0.9	2.25-2.83	0.49-1.03
Gd/Yb _{cn}	1.76-2.36	1.67-1.99	1.42-1.71	1.35-1.62	1.42-1.73	1.82-3.71	1.35-1.75
Eu/Eu*	0.61-0.65	0.89-1.00	0.89-1.06	0.73-0.96	0.87-1.10	0.81-1.05	1.02-1.53

Table 2.4. Summary of major (wt.%) and trace (ppm) element concentrations and significant element ratios for the Wadi Ghadir ophiolitic complex and associated dikes.

Ghadir Mélange				
	<i>EGY-06-62</i>	<i>EGY-06-63</i>	<i>EGY-06-64</i>	<i>EGY-06-65</i>
SiO ₂ (wt%)	55.84	57.58	50.21	52.02
Al ₂ O ₃	18.36	15.81	14.38	15.48
Fe ₂ O ₃ ¹	5.58	8.28	14.23	11.06
MnO	0.09	0.09	0.23	0.16
MgO	6.07	3.92	4.67	5.62
CaO	6.91	6.14	8.86	8.68
Na ₂ O	4.88	5.08	3.67	4.20
K ₂ O	0.42	0.69	0.47	0.38
TiO ₂	1.52	1.78	2.94	2.31
P ₂ O ₅	0.34	0.62	0.33	0.09
LOI	1.61	2.15	0.52	1.07
Mg-number	68.3	48.4	39.4	50.2
Cr (ppm)	28	47	27	49
Sc	17	13	39	43
V	116	171	422	343
Co	22	25	42	41
Ni	90	101	141	126
Rb	8.8	11.8	7.5	8.4
Cs	0.2	0.6	0.1	0.3
Ba	200	281	80	97
Sr	545	1269	214	249
Pb	6.0	8.8	2.4	5.0
U	2.10	0.89	0.42	0.85
Th	4.31	3.22	1.29	2.62
Y	21.6	14.4	52.8	38.7
Zr	271	191	202	297
Ta	0.53	0.24	0.26	0.32
Nb	6.95	5.47	3.56	3.80
La	18.15	29.13	9.04	10.61
Ce	44.60	68.32	25.16	28.56
Pr	5.59	8.92	4.05	4.03
Nd	23.34	37.83	20.96	18.22
Sm	5.19	7.25	6.72	5.13
Eu	1.55	2.15	2.32	1.63
Gd	4.93	5.40	8.76	6.04
Tb	0.73	0.66	1.48	1.07
Dy	4.32	3.25	9.59	6.98
Ho	0.84	0.55	1.99	1.46
Er	2.42	1.45	5.82	4.42
Tm	0.33	0.16	0.81	0.63
Yb	2.11	0.90	5.24	4.23
Lu	0.31	0.12	0.76	0.62
Mo	0.3	0.2	1.2	0.2
Cu	13.85	34.66	38.61	44.08
Zn	58.8	112.2	544.8	100.9
Ga	67.2	79.7	55.2	56.0
Al ₂ O ₃ /TiO ₂	12.1	8.9	4.9	6.7
Nb/Y	0.32	0.38	0.07	0.10
La/Yb _{cn}	6.17	23.23	1.24	1.80
La/Sm _{cn}	2.26	2.59	0.87	1.33
Gd/Yb _{cn}	1.94	4.97	1.38	1.18
Eu/Eu*	0.94	1.05	0.93	0.89
Th/Yb	2.05	3.58	0.25	0.62
Th/Ce	0.097	0.047	0.051	0.092
Ce/Yb	21	76	5	7
Zr/Nb	39	35	57	78
Ti/Zr	34	56	87	47
Ba/La	11	10	9	9
V/Ti	0.013	0.016	0.024	0.025
Sc/Y	0.79	0.90	0.74	1.11
Latitude (N)	24° 44' 22.7"	24° 44' 22.7"	24° 44' 22.7"	24° 44' 23.7"
Longitude (E)	34° 52' 46.6"	34° 52' 46.6"	34° 52' 46.6"	34° 52' 47.3"

Table 2.5. Major (wt%) and trace element (ppm) concentrations and significant element ratios for ophiolitic mélange fragments and associated fragmented dikes.

Fragmented Dikes in Ghadir Mélange

	EGY-06-85	EGY-06-75	EGY-06-90	EGY-06-91	EGY-06-66	EGY-06-67	EGY-06-68	EGY-06-69	EGY-06-70	EGY-06-71	EGY-06-72
SiO ₂	49.80	50.92	50.09	57.21	50.96	50.07	53.25	49.61	47.69	53.60	52.71
Al ₂ O ₃	18.39	14.10	18.28	15.22	18.10	16.17	13.33	17.00	15.54	14.21	16.02
Fe ₂ O ₃	9.07	14.44	9.36	12.09	8.78	9.00	14.95	9.34	13.25	13.23	10.43
MnO	0.15	0.22	0.15	0.22	0.13	0.14	0.23	0.15	0.21	0.20	0.17
MgO	7.76	4.13	7.93	1.99	5.65	9.46	3.36	8.64	6.86	3.60	5.56
CaO	9.35	8.16	8.97	5.95	10.69	9.70	6.63	10.59	9.94	7.46	9.11
Na ₂ O	2.52	4.36	2.63	4.25	3.10	2.81	3.35	2.76	2.95	3.15	3.44
K ₂ O	1.40	0.39	1.04	0.70	0.64	0.86	1.49	0.35	0.71	1.23	0.60
TiO ₂	1.40	2.89	1.39	1.55	1.67	1.44	2.91	1.41	2.53	2.85	1.75
P ₂ O ₅	0.17	0.38	0.18	0.81	0.30	0.35	0.49	0.15	0.31	0.48	0.23
LOI	3.88	1.43	3.77	0.62	1.23	1.82	0.77	2.16	2	1.24	1.81
Mg-number	62.9	36.2	62.7	24.6	56.1	67.5	30.9	64.7	50.7	35.0	51.4
Cr	64	12	64	n.d.	69	136	17	98	50	16	27
Sc	28	37	29	20	28	30	38	35	41	34	35
V	170	393	175	36	192	202	321	212	314	320	249
Co	37	39	41	17	36	43	36	47	49	33	38
Ni	94	130	101	72	133	236	120	133	149	118	76
Rb	39.8	7.5	25.9	20.0	17.1	19.9	54.6	9.5	16.2	40.7	12.0
Cs	0.6	0.5	0.2	3.6	0.6	0.8	1.9	0.6	0.6	1.8	0.3
Ba	280	53	85	200	158	269	257	163	91	179	131
Sr	480	196	407	371	403	511	292	367	325	265	298
Pb	18.6	3.2	5.3	7.2	3.1	4.2	3.9	2.9	3.1	4.0	3.2
U	0.16	0.63	0.14	0.73	0.69	0.65	0.73	0.26	0.17	0.75	0.54
Th	0.38	1.85	0.37	2.08	2.22	2.47	2.38	0.91	0.65	2.06	1.93
Y	21.1	53.5	21.9	59.3	28.1	21.2	54.4	24.9	36.5	46.4	28.5
Zr	100	203	109	275	178	153	236	131	188	214	135
Ta	0.12	0.32	0.12	0.53	0.31	0.42	0.37	0.16	0.21	0.41	0.22
Nb	1.70	4.12	1.71	7.59	4.32	6.49	4.99	2.45	2.74	5.19	3.22
La	4.57	11.10	4.89	14.50	10.59	15.91	14.15	5.95	7.70	13.39	8.48
Ce	13.10	29.70	13.75	43.98	29.04	36.88	35.96	16.74	23.36	33.52	21.40
Pr	2.03	4.54	2.13	6.34	4.09	4.76	5.21	2.56	3.72	4.87	3.05
Nd	10.29	22.90	10.79	31.90	19.19	20.06	25.79	12.70	18.89	23.64	14.58
Sm	3.07	7.14	3.21	9.30	5.06	4.47	7.69	3.74	5.63	6.90	4.19
Eu	1.18	2.43	1.18	3.36	1.58	1.45	2.55	1.35	2.00	2.24	1.44
Gd	3.83	8.99	4.00	11.13	5.57	4.48	9.64	4.54	6.81	8.43	5.05
Tb	0.63	1.53	0.66	1.79	0.88	0.68	1.59	0.75	1.12	1.37	0.84
Dy	4.03	9.80	4.21	11.12	5.39	4.10	10.05	4.70	6.99	8.68	5.37
Ho	0.82	2.00	0.85	2.25	1.07	0.81	2.04	0.95	1.40	1.76	1.09
Er	2.32	5.85	2.40	6.37	3.08	2.35	5.93	2.75	4.01	5.10	3.20
Tm	0.31	0.80	0.32	0.86	0.42	0.31	0.81	0.38	0.54	0.69	0.44
Yb	1.93	5.11	1.97	5.43	2.68	2.01	5.22	2.40	3.39	4.35	2.83
Lu	0.26	0.71	0.26	0.79	0.39	0.29	0.75	0.34	0.48	0.63	0.41
Mo	0.2	0.6	0.3	0.8	0.2	0.1	0.5	0.2	0.4	0.6	0.2
Cu	35.63	34.98	38.74	27.97	20.70	23.23	28.08	53.60	55.32	39.95	32.65
Zn	103.1	145.9	88.7	167.7	73.4	81.9	134.2	68.8	101.6	120.1	82.1
Ga	85.5	54.4	54.1	92.0	59.5	69.2	81.0	54.5	52.7	66.8	55.4
Al ₂ O ₃ TiO ₂	13.1	4.9	13.2	9.8	10.8	11.3	4.6	12.0	6.1	5.0	9.2
Nb:Y	0.08	0.08	0.08	0.13	0.15	0.31	0.09	0.10	0.07	0.11	0.11
La:Yb _{cn}	1.70	1.56	1.78	1.91	2.83	5.67	1.94	1.78	1.63	2.21	2.15
La:Sm _{cn}	0.96	1.00	0.98	1.01	1.35	2.30	1.19	1.03	0.88	1.25	1.31
Gd:Yb _{cn}	1.64	1.45	1.68	1.69	1.72	1.84	1.53	1.56	1.66	1.60	1.48
Eu:Eu*	1.06	0.93	1.01	1.01	0.91	0.99	0.91	1.00	0.99	0.90	0.96
Th:Yb	0.20	0.36	0.19	0.38	0.83	1.23	0.46	0.38	0.19	0.47	0.68
Th:Ce	0.029	0.062	0.027	0.047	0.077	0.067	0.066	0.054	0.028	0.061	0.090
Ce:Yb	7	6	7	8	11	18	7	7	8	8	8
Zr:Nb	59	49	64	36	41	24	47	53	69	41	42
Ti:Zr	84	85	76	34	56	56	74	65	81	80	78
Ba:La	61	5	17	14	15	17	18	27	12	13	15
V:Ti	0.020	0.023	0.021	0.004	0.019	0.023	0.018	0.025	0.021	0.019	0.024
Sc:Y	1.33	0.69	1.33	0.34	1.00	1.42	0.70	1.41	1.12	0.73	1.23
Latitude (N)	24° 46'	24° 45'	24° 46'	24° 48'	24° 44'	24° 44'	24° 44'	24° 44'	24° 44'	24° 45'	24° 45'
Longitude (E)	16.8°	40.1°	16.6°	42.8°	27.7°	36.4°	42.3°	42.3°	55.5°	24.2°	31°
Longitude (E)	34° 53'	34° 53'	34° 53'	34° 50'	34° 52'	34° 52'	34° 52'	34° 52'	34° 53'	34° 53'	34° 53'
Longitude (E)	14 1°	30.2°	8.6°	51.5°	49.7°	54.2°	58.3°	58.3°	51.1°	9.5°	8.8°

Table 2.5. (continued)

Hafafit Mélange

	<i>EGY-04-34</i>	<i>EGY-04-35</i>	<i>EGY-04-36</i>	<i>EGY-04-37</i>	<i>EGY-04-38</i>	<i>EGY-04-39</i>	<i>EGY-04-40</i>
SiO ₂	56.73	75.63	56.47	52.06	69.60	60.81	50.87
Al ₂ O ₃	15.53	13.67	19.19	20.30	14.06	14.55	17.90
Fe ₂ O ₃	7.55	1.69	7.53	9.01	4.55	7.98	12.64
MnO	0.10	0.03	0.12	0.14	0.06	0.14	0.19
MgO	6.55	0.29	3.24	5.14	2.27	3.77	4.73
CaO	4.77	1.51	6.97	7.21	2.09	7.85	4.52
Na ₂ O	5.86	5.60	3.86	4.59	3.49	2.77	2.59
K ₂ O	1.22	1.31	1.51	0.23	2.99	1.23	3.59
TiO ₂	1.26	0.20	0.88	1.08	0.56	0.62	2.67
P ₂ O ₅	0.44	0.08	0.21	0.23	0.34	0.26	0.31
LOI	3.5	2.4	9.9	5.49	3.94	6.8	5.33
Mg-number	63.2	25.3	46.1	53.1	49.8	48.3	42.6
Cr	512	405	356	377	422	31	n.d.
Sc	18	2	14	20	10	29	31
V	134	8	89	134	110	230	169
Co	29	2	24	28	11	19	32
Ni	193	31	82	85	42	31	74
Rb	20.2	51.6	36.2	3.1	60.6	21.7	52.6
Cs	0.4	1.1	0.9	0.8	0.5	0.3	0.5
Ba	417	201	376	111	434	283	502
Sr	392	175	369	576	193	486	284
Pb	43.4	74.2	28.1	113.5	215.9	3.3	2.1
U	6.23	6.80	0.55	0.48	1.78	0.76	0.55
Th	4.82	19.71	1.37	1.21	6.72	3.58	1.48
Y	22.1	22.3	18.9	18.0	14.2	12.1	33.7
Zr	234	171	105	113	186	108	201
Ta	0.46	2.71	0.22	0.19	0.36	0.22	0.42
Nb	6.46	20.49	2.49	2.35	5.45	4.71	5.12
La	24.85	34.42	9.06	9.10	40.94	20.85	10.23
Ce	55.35	68.42	21.27	21.34	85.03	46.28	26.01
Pr	6.93	7.62	2.95	2.86	10.39	6.00	3.91
Nd	28.78	27.97	12.91	12.51	41.05	25.23	19.15
Sm	5.91	5.53	3.34	3.35	7.41	5.03	5.40
Eu	1.45	0.80	1.15	1.34	1.53	1.30	1.66
Gd	5.77	4.87	3.72	3.35	5.39	4.11	6.49
Tb	0.76	0.71	0.59	0.52	0.57	0.47	1.04
Dy	4.26	4.07	3.50	3.47	2.80	2.48	6.48
Ho	0.88	0.77	0.71	0.70	0.51	0.47	1.33
Er	2.54	2.34	2.18	2.01	1.50	1.33	3.88
Tm	0.33	0.31	0.32	0.29	0.20	0.18	0.53
Yb	2.14	2.14	2.10	1.79	1.29	1.14	3.45
Lu	0.32	0.31	0.32	0.30	0.49	0.18	0.51
Mo	0.9	0.8	1.7	1.2	1.4	0.6	0.5
Cu	71.52	5.51	42.08	41.63	116.59	90.65	24.68
Zn	133.3	103.1	105.5	118.2	210.4	67.5	104.1
Ga	66.5	59.3	70.6	49.2	57.0	50.3	77.1
Al ₂ O ₃ TiO ₂	12.3	69.4	21.8	18.7	25.1	23.3	6.7
Nb/Y	0.29	0.92	0.13	0.13	0.38	0.39	0.15
La/Yb _n	8.33	11.52	3.10	3.65	22.78	13.10	2.13
La/Sm _n	2.71	4.01	1.75	1.76	3.57	2.68	1.22
Gd/Yb _n	2.23	1.88	1.47	1.55	3.46	2.98	1.56
Eu/Eu*	0.76	0.47	1.00	1.23	0.74	0.87	0.86
Th/Yb	2.25	9.20	0.65	0.67	5.21	3.14	0.43
Th/Ce	0.087	0.288	0.064	0.057	0.079	0.077	0.057
Ce/Yb	26	32	10	12	66	41	8
Zr/Nb	36	8	42	48	34	23	39
Ti/Zr	32	7	50	58	18	35	80
Ba/La	17	6	42	12	11	14	49
V/Ti	0.018	0.007	0.017	0.021	0.033	0.062	0.011
Sc/Y	0.81	0.09	0.74	1.11	0.70	2.39	0.92
Latitude (N)	24° 57' 27"	24° 56'	24° 57'	24° 57'	25° 03'	25° 03' 38.7"	25° 03'
		58.81"	33.75"	34.85"	20.56"		38.41"
Longitude (E)	34° 31'	34° 33'	34° 33'	34° 33'	34° 49' 12.5"	34° 48'	34° 48'
	50.63"	34.81"	20.34"	19.58"		42.41"	34.85"

Table 2.5. (continued)

Chapter 3

Formation of Neoproterozoic proto-arc oceanic crust in the Nubian Shield: Geochemical evidence from the Fawakhir Ophiolite, Eastern Desert, Egypt

3.1. Introduction

Since ophiolites were recognized as fragments of oceanic lithosphere preserved within orogenic belts, it has been debated whether they formed at mid-ocean ridges (MOR) or above subduction zones (Nicolas and Boudier, 2003; Pearce, 2003). Although many ophiolites have the structure of oceanic crust formed at MOR, they have typical supra-subduction zone geochemical signatures (Miyashiro, 1973; Pearce et al., 1984; Metcalf and Shervais, 2008). At subduction zones, new oceanic crust may be formed in forearc, volcanic arc and backarc basins (Hawkins, 2003; Stern, 2004). Ophiolites mark the closure sites of ancient oceans within the suture zones of orogens (Şengör, 1990; Brown and Spadea, 1999; Dilek, 2003; Kusky, 2004). The nature of suture zones is obscured by syn-tectonic to post-tectonic intrusions and by deformation and metamorphism. That is why the geochemistry of the least altered ophiolitic rocks provides major insight into understanding the geodynamic evolution of ancient orogens.

The Neoproterozoic Era is characterized by the widespread formation of ophiolitic complexes (Stern, 2005, 2008). These complexes are common in the Arabian-Nubian Shield and range in age from 870 to 690 Ma (Stern et al., 2004). Neoproterozoic crust-forming events of the Arabian-Nubian Shield formed through accretion of island arcs to continental margins, as the Mozambique Ocean was closed (Furnes et al., 1996; El-Shafei and Kusky, 2003; Jöns and Schenk, 2007 and references therein). The closure of the

Mozambique Ocean was marked by the formation of several suture zones (Stern et al., 1990). The final collision between west and east Gondwana resulted in the Pan-African orogeny (Kröner, 1985; Kröner et al., 1987). Subduction, accretion, and crustal thickening processes took place between about 870 and 570 Ma (Stern and Hedge, 1985; Kröner et al., 1992; Stern, 1994). The crustal evolution of the Eastern Desert culminated in the eruption of Dokhan Volcanics, the deposition of molasse-type Hammamat sediments, and emplacement of the Younger Granites (Eliwa et al., 2006).

The Eastern Desert of Egypt constitutes the northwestern end of the Nubian segment of the Arabia-Nubian Shield (Fig. 3.1a). Despite recent progress in understanding the evolution of the Arabian-Nubian Shield, the tectonic setting of the ophiolitic rocks in the Eastern Desert still remains controversial. As with many other ophiolites, the ophiolitic rocks of the Arabian-Nubian Shield have supra-subduction signatures (Stern et al., 2004), but Zimmer et al. (1995) reported the occurrence of MOR-ophiolites at the Gerf area in the southern Eastern Desert (Fig. 3.1b). As with the rest of the ophiolitic rocks of the Arabian-Nubian Shield, the supra-subduction signatures of the ophiolitic rocks in the Eastern Desert led to further debate on whether they were formed in a backarc setting (Furnes et al., 1996; El-Bayoumi, 1983; El-Sayed et al., 1999; Farahat et al., 2004) or as forearc oceanic crust during a subduction initiation (Azer and Stern, 2007; Khalil and Azer, 2007).

Azer and Stern (2007) and Khalil and Azer (2007) proposed that the Neoproterozoic ophiolites of the Eastern Desert formed in a forearc setting based on the depleted nature of the serpentinized mantle section. Although their conclusion is consistent with other Arabian-Nubian Shield ophiolitic mantle rocks (Stern, et al., 2004).

other settings have been proposed for the ophiolitic mantle rocks of the Central Eastern Desert. For example, Ahmed et al. (2001) and Farahat (2008) mentioned that the ophiolitic harzburgite can be fragments of backarc basin lithosphere. Khalil (2007) inferred a mid-ocean ridge (MOR) tectonic setting for the mantle rocks of Wadi Ghadir ophiolite in the Eastern Desert. Given that most ophiolitic ultramafic rocks in the Central Eastern Desert have been extensively serpentinized, their magmatic textures and primary geochemical compositions might have been significantly modified (Yumul, 2004). The composition of the crustal ophiolitic rocks can be used to assess the nature of their mantle source. The widespread serpentinization of the ultramafic rocks in the Eastern Desert and lack of high precision geochemical data on the ophiolitic crustal rocks have generated debate over the nature of the Neoproterozoic mantle in the Central Eastern Desert.

Another problem associated with the evolution of the Nubian segment of the Arabian-Nubian Shield is determining the subduction polarity. El-Ramly et al. (1984) and El Bayoumi and Grieling (1984) inferred the evolution of the Eastern Desert through a west-dipping subduction process, which resulted in the formation and the accretion of the Neoproterozoic island arcs and oceanic crust onto the East Gondwana continental margin before final collision with West Gondwana. Kröner (1985) and Kröner et al. (1987) adopted the west-dipping subduction model for the Nubian segment of the Arabian-Nubian Shield. The accretion of island arcs and oceanic crust to the passive margin through east-dipping subduction was proposed for the Eastern Desert by Ries et al. (1983). Shackleton (1994) attributed the ambiguity of the subduction direction in the Eastern Desert to the lack of geochemical evidence required to establish the arc-magmatic polarity.

In this study, we report new major element (40 samples) and trace element (58 samples) data obtained from different crustal units of the Fawakhir ophiolitic rocks along with some samples from the mélangé along Qift-Qusier Road and the dikes cutting the ophiolitic rocks. These geochemical data are used to: (1) assess the tectonic setting of the Fawakhir ophiolite; (2) evaluate the mantle source of the crustal rocks; (3) define the subduction polarity; and (4) revisit the existing geodynamic models.

3.2. Regional geology and field characteristics

The Qift-Qusier Road traverses the Neoproterozoic basement rocks of the Central Eastern Desert (CED). Precambrian rocks along the road trend NW-SE and are unconformably overlain by Cretaceous Nubian sandstone to the west and by Miocene siliciclastics to the east. Excluding granitic rocks, Precambrian rocks can be grouped into three units: (1) the Meatiq quartzofeldspathic gneisses; (2) the ophiolitic mélangé; and (3) the Hamammat molasse-type elastics to the west end of the road (El-Gaby et al., 1984) (Fig. 3.2). All the units are tectonically juxtaposed. The mélangé is composed of dismembered ophiolitic fragments (serpentinized peridotite, pyroxenite, gabbros, and volcanic rocks), island arc-related volcanic rocks and volcanoclastics of andesitic composition, and amphibolite dispersed in a sheared sedimentary matrix (Ries et al., 1983; El-Gaby et al., 1984; Fowler and Osman, 2001).

The ophiolitic rocks of the CED occur as dismembered blocks in the tectonic mélangé or as olistostromal debris (Shackleton et al., 1980; Ries et al., 1983; El-Gaby et al., 1988) (Fig. 3.1b). The best exposure of the ophiolitic rocks along the Qift-Qusier Road occurs in the Fawakhir area, which is located between the Meatiq gneissic dome to the east and Hamammat sedimentary rocks to the west (Nasseef et al., 1980). All

ophiolitic rocks are recognized in the Fawakhir area near to Bir El-Sid. Andresen et al. (2009) reported crystallization age of 736.5 ± 1.2 Ma for zircons from the ophiolitic gabbro of the Fawakhir area. The Fawakhir ophiolitic sequence starts from the base, to the west, with ultramafic rocks followed by gabbros and volcanic rocks, mainly basalt and basaltic andesite at the top of the sequence towards the east (El-Sayed et al., 1999) (Fig. 3.3). The basal ultramafic rocks are intruded by the Fawakhir monzodiorite which has an emplacement age of 597.8 ± 2.9 Ma (Andresen et al., 2009). Ultramafic rocks have been severely serpentinized. The serpentinite is characterized by mesh texture and contains many shear zones. Along these shear zones the serpentinite is altered to talc and carbonates (Fig. 3.4a). Some pyroxenite bodies form irregular coarse-grained masses, with crystal size up to 5 cm (Fig. 3.4b), within serpentinite close to the ophiolitic gabbros. The serpentinite is sheared along the contacts with the pyroxenite bodies.

Gabbros are the most common unit in the Fawakhir ophiolitic assemblage and are best exposed at Bir El-Sid. Gabbros are isotropic (Fig. 3.4c) and vary systematically in grain size, from coarse-grained to fine-grained from west to east. Pegmatitic gabbros and doleritic varieties occur as pockets within the isotropic gabbros. Gabbros are dissected by many quartz, epidote and carbonate veinlets and are intruded locally by trondhjemite veins (Fig. 3.4d). Gabbros are cut by a major shear zone, up to 5 m wide, trending northwest and dipping southwest and are dissected by smaller faults. Gabbros grade into a dolerite-rich zone with local preservation of sheeted dike features. It is difficult to follow the sheeted dikes to the volcanic rocks due to deformation. The dikes have a northwest-southeast trend and dip mostly towards the northeast and rarely towards the southwest with about 2 m average thickness. Although it is difficult to distinguish

systematic single chilled margins of the dikes, the northern margins of some dikes contain finer crystal sizes. The sheeted dikes and to a lesser extent the gabbros are dissected by brittle fault zones. Some of these zones are parallel to the margins of the dikes facilitating the identification of the margins through the development of hydrothermal mineralization, mainly calcite, along the fault zones. Some of these zones show jigsaw texture formed by hydraulic fracturing. The other brittle fault zones have northeast-southwest trends, normal to the sheeted dikes trend. Their thickness reaches up to 30 cm. The Fawakhir ophiolite is intruded by less deformed dikes which are andesitic in composition.

Further to the east, the volcanic rocks are mostly fine-grained basalts with a greenish gray color. These volcanic rocks display pillow structures and texturally are slightly porphyritic and amygdaloidal (Fig. 3.5a). The pillow lavas are overlain by hyaloclastites (Fig. 3.5b) and very fine-grained red pelites (Fig. 3.5c). Another occurrence of the pillow lavas in the mélangé along the Qift-Qusier Road (Fig. 3.5d) is to the eastern end of the basement along the road close to Qusier City. The pillow lavas in the eastern mélangé young towards the southeast. The eastern pillow basalts are highly jointed and are unconformably overlain by Miocene sedimentary rocks to the west; and they are intruded by granites to the east.

3.3. Petrography

The mineralogical characteristics of the Fawakhir ophiolite and Qift-Qusier mélangé are summarized in Table 3.1. Pyroxene is strongly altered to talc, serpentine and tremolite with some clinopyroxene relicts. The outlines of completely altered pyroxene crystals can be determined through the alignment of iron oxides along the cleavage

planes mimicking bastite texture (Fig. 3.6a). Large talc flakes retain the original outlines of the pyroxene crystals, exhibiting mosaic seriate texture. Small talc crystals aggregate with serpentine and tremolite. Some of the pyroxenite bodies contain less altered plagioclase crystals. Gabbro in the Fawakhir area is medium to coarse-grained comprising plagioclase, amphibole (mostly actinolite), and subordinate augite relics, mainly in the core of hornblende, with accessory apatite and opaque minerals (Fig. 3.6b). In addition to actinolite, chlorite, epidote, sericite, calcite, and titanite are the main secondary minerals in order of decreasing abundance.

Volcanic rocks include medium to fine-grained basaltic flows and pillow lavas. Medium-grained basaltic flows are locally porphyritic. These flows are spatially associated with sheeted dikes. Plagioclase and chloritized pyroxene phenocrysts are set in a groundmass of fine-grained plagioclase, actinolite, chlorite, epidote, and titanite. Chlorite, actinolite, and epidote are alteration products of the pyroxene interstitial to plagioclase laths forming intersertal texture. Pillow basalts have the same mineralogical composition as the volcanic rocks associated with the sheeted dike complex. Dikes show doleritic texture (Fig. 3.6c) but pillow basalts are aphanitic. In addition to the intersertal texture, the plagioclase laths locally develop variolitic texture and epidote forms aggregates of pseudo-phenocrysts (Fig. 3.6d). Pillow basalt in the eastern mélange is weakly porphyritic. The phenocrysts are long thin turbid plagioclase due to quenching (Fig. 3.6e). Closer to the Meatiq gneissic dome the igneous textures start to be obscured and the mélange volcanic rocks change into actinolite schist.

The Fawakhir ophiolite is intruded by basaltic andesite to andesitic dikes. These rocks are locally porphyritic where amphibole and plagioclase are the main phenocrysts

(Fig. 3.6f). Hornblende is euhedral and brown similar to the amphiboles of the Dokhan Volanics of the ED (Basta et al., 1980). These dikes are variably altered to chlorite, sericite, epidote, and calcite in order of decreasing abundance. Iron oxides and apatite are the main accessory minerals

3.4. Analytical methods

Whole-rock samples were crushed by hydraulic press and then pulverized using an agate mill in the Department of Earth and Environmental Sciences, University of Windsor, Canada. Samples were analyzed for both major and trace elements. Major elements were analyzed by Thermo Jarrell-Ash Enviro II ICP at ACTLABS in Ancaster, Canada. Samples were fused with a flux of lithium metaborate and lithium tetraborate in an induction furnace. The melt was immediately mixed with 5% nitric acid containing an internal standard until completely dissolved. Totals of major element oxides are 100 ± 1 wt.% and the analytical precisions for major elements are 1-2%. Standards, DNC-1 and BIR-1, were used as international references to estimate accuracy of the major elements (Table 3.2).

Samples were analyzed for rare earth elements (REE), high field strength elements (HFSE), large ion lithophile elements (LILE) and transition metals (Ni, Co, Cr and V) by a high-sensitivity Thermo Elemental X7 ICP-MS at the Great Lakes Institute for Environmental Research (GLIER), University of Windsor, Canada, using the protocol of Jenner et al. (1990). For sample dissolution, 100-130 mg of powder was dissolved in concentrated HF-HNO₃ mixture in screw-top Teflon (Savillex®) bombs at a temperature of ~120°C for three days until no residue was visible. The sample was further attacked with concentrated HNO₃-H₃BO₃-H₂C₂O₄ and then twice with 50% HNO₃. Standards,

BHVO-1 and BHVO-2, were used as international reference materials to estimate accuracy of the measured trace elements (Table 3.3). Analytical precisions are estimated as follows: 1-10 % for REE, Rb, Sr, Ba, Y, Nb, Co, Cu, Zr, and U; 10-20% for V, Ni, Zn, Cs, Mo, and Ga; and 20-30% for Ta, Th, Cr, and Pb.

Major element analyses are recalculated to 100 wt% anhydrous basis. Mg-numbers (%) were calculated as the molar ratio of $100 \times \text{Mg}/(\text{Mg}+\text{Fe}^{2+})$ after Ragland (1989). Chondrite (cn) and primitive mantle (pm) compositions derived from Sun and McDonough (1989) and Hofmann (1988), respectively. Europium (Eu/Eu*) and cerium (Ce/Ce*) anomalies were calculated with respect to neighboring REE (Rollinson, 1993).

3.5. Geochemical results

Geochemical data for the Fawakhir pyroxenite, gabbro, volcanic rocks, dikes and samples from the mélange along Qift-Qusier Road are presented in Tables 3.4, 3.5, 3.6, and 3.7. All rock units follow the sub-alkaline trend (low Zr/TiO₂) where the gabbros and volcanic rocks plot mostly in the basalt and andesite-basaltic andesite field (Fig. 3.7a). On the Zr versus Y diagram, all the ophiolitic rocks and the mélange fragments plot in the tholeiitic field but the younger andesitic dikes plot in the calc-alkaline field (Fig. 3.7b).

3.5.1. Pyroxenites and gabbros

Pyroxenites are characterized by 51-56 wt% SiO₂, MgO=18-22 wt% and Al₂O₃=3-9 wt% (Fig. 3.8; Table 3.4). Gabbros are less siliceous (SiO₂= 42-52 wt%) and have lower magnesium contents (MgO=7-14 wt%) and higher Al₂O₃ (15-19 wt%) than pyroxenite. Pyroxenites also have lower TiO₂ (0.07-0.1 wt%) than gabbros (0.15-0.73 wt%). In terms of Al₂O₃/TiO₂, both pyroxenites (35-91) and gabbros (21-113) show wide

ranges and overlapping ratios. Pyroxenites have higher concentrations of transition elements (Cr= 411-558, Co= 54-69, Sc=61-72 ppm) than gabbros (Cr= 83-314, Co= 33-49, Sc= 37-47 ppm) but Ni concentrations overlap between the two groups (Fig. 3.9). On the other hand, gabbros have higher concentrations of the incompatible elements (LILE, HFSE, REE) than pyroxenites.

Pyroxenites display LREE-depleted patterns ($La/Sm_{cn}=0.30-0.61$; $La/Yb_{cn}=0.15-0.38$) accompanied by low REE abundances. Their HREE are fractionated ($Gd/Yb_{cn}=0.67-0.79$; Fig. 3.9). Gabbros have similar REE patterns to pyroxenites but are less depleted in LREE ($La/Sm_{cn}=0.40-0.96$; $La/Yb_{cn}=0.33-0.86$), their HREE segments are flat ($Gd/Yb_{cn}=0.88-1.14$) and their REE abundances are higher. Europium anomalies are variable from slightly positive to slightly negative in both rock types. Primitive mantle-normalized patterns for both rock types are characterized by enrichment of LILE (Ba) and Th over HFSE (Zr, Ti, Y) and HREE. Both rock types have negative Nb anomalies (Fig. 3.11a).

3.5.2. Ophiolitic volcanic rocks

The volcanic rocks of the Fawakhir area are characterized by MgO=3-9 wt%, Ni=32-140 ppm and Cr=20-205 ppm (Table 3.5). Mg-numbers (38-66) are generally lower than the values of gabbros (Table 3.7). Similarly, concentrations of TiO₂ (0.40-1.12 wt%), Zr (24-72 ppm), and Y (9.11-23.8 ppm) of volcanic rocks are lower than those of gabbros (Fig. 3.8). In addition, Al₂O₃/TiO₂ ratios in volcanic rocks (13-34) are lower than those in gabbros.

Volcanic rocks display REE patterns characterized by slightly depleted to flat LREE ($La/Sm_{cn}=0.65-1.22$, $La/Yb_{cn}=0.56-1.16$). The HREE are moderately fractionated

(Gd/Yb_{cn}=0.88-1.23) (Fig. 3.10b). The primitive mantle-normalized trace element patterns of the ophiolitic volcanic rocks are characterized by negative Nb anomalies and variable enrichment of Ba and Th (LILE) over HFSE (Fig. 3.11b).

3.5.3. *Mélange blocks*

The major and trace element contents of the volcanic rocks from the mélange blocks to the west of Qift-Qusier Road overlap with the volcanic rocks of the Fawakhir ophiolite. The volcanic fragments from the mélange are characterized by MgO=5-10 wt%, Ni=99-151 ppm, Cr=137-473 ppm and Mg-number=50-66 which are slightly higher than the ophiolitic volcanic rocks (Table 3.6). In contrast, Al₂O₃/TiO₂ ratios of the ophiolitic volcanic rocks (13-34) are higher than the mélange volcanic rocks (8-14). Despite overlap in composition between the ophiolitic volcanic rocks and the volcanic blocks of the mélange, the TiO₂ (0.83-1.86 wt%), Zr (64-303 ppm), and Y (20.7-43.5 ppm) concentrations of the latter group are higher (Table 3.3, Fig. 3.8).

REE patterns (La/Sm_{cn}=0.54-0.66, La/Yb_{cn}=0.72-0.81) of the volcanic blocks in the mélange are similar to those of the ophiolitic counterparts (Fig. 3.10). All volcanic blocks in the mélange have positively fractionated HREE patterns (Gd/Yb_{cn}=1.23-1.41). Volcanic rocks both in the ophiolite and in the mélange are characterized by negative Nb anomalies and slight enrichment of Ba and Th (LILE) over HFSE (Fig. 3.11c).

3.5.4. *Calc-alkaline dikes*

Calc-alkaline dikes are characterized by MgO (4-8 wt%), Cr (34-94 ppm), and Ni (58-159 ppm) concentrations similar to those of the ophiolitic volcanic rocks (Table 3.6). The calc-alkaline dikes are enriched in TiO₂ (0.87-1.82 wt%), Zr (131-262 ppm) and most of the LILE over the ophiolitic volcanic rocks. Their REE patterns are distinguish

by pronounced positive fractionation where $\text{La/Yb}_{\text{cn}}=7.17-18.56$, $\text{La/Sm}_{\text{cn}}=2.13-2.46$, and $\text{Gd/Yb}_{\text{cn}}=2.04-4.25$. The primitive mantle-normalized trace element patterns are characterized by negative Nb anomalies, small negative Ti anomalies, and enrichment of LILE over HFSE.

3.6. Discussion

3.6.1. Alteration

Ophiolites are variably altered and metamorphosed through seafloor hydrothermal circulation systems and during obduction/accretion-related processes (see Gillis and Banerjee, 2000; Furnes et al., 2000). Ophiolitic rocks of the Fawakhir area have suffered various degrees of post-magmatic alteration. Although the original igneous textures are well preserved in gabbros and volcanic rocks of the Fawakhir area, the mineralogical compositions have been largely changed. The primary pyroxene and plagioclase were altered to actinolite, chlorite, epidote, albite and titanite.

Given that the Fawakhir ophiolite suffered greenschist facies metamorphism, the geochemical components may have been changed. Alteration criteria proposed by Polat and Hoffman (2003) are used to assess the element mobility during post-magmatic alteration. Different major and trace elements are plotted against Zr (Fig. 3.8, 3.9), which is one of the least mobile elements under different alteration processes (Winchester and Floyd, 1977). Among the major elements, MgO, Al_2O_3 , and CaO show a moderate correlation with Zr abundances and TiO_2 , P_2O_5 , Ni, Cr, Sc, Co, Th, REE (La, Sm, Yb) and HFSE (Y, Nb, Th) correlate well with Zr abundances (Fig. 3.9). The strong correlation with Zr indicates the relative immobility of these elements during alteration

processes. In contrast to these immobile elements, K₂O and LILE (Rb, Ba) are not correlated with Zr which indicates their mobility during alteration processes (Fig. 3.9).

The relative immobility of REE and HFSE is confirmed by the coherent chondrite-normalized REE patterns and primitive mantle-normalized trace element patterns for different groups of samples. Only one gabbroic sample, EGY-06-19, is severely altered and deformed, but shows a coherent HREE pattern with the other gabbroic samples indicating that LREE are more susceptible to mobility during intense alteration than HREE, in accordance with Humphries (1984). However, the rest of the gabbroic samples are less altered than the ophiolitic volcanic rocks. Geochemically, the LILE (Ba) of the gabbros show more coherent plot on the primitive mantle-normalized diagrams (Fig. 3.10). This may indicate the relative immobile behavior of LILE in the gabbroic rocks. The samples with negative or positive Ce anomalies ($0.9 > \text{Ce}/\text{Ce}^*$ or $\text{Ce}/\text{Ce}^* > 1.1$) are considered as variably altered and should be screened out and not used for petrogenetic interpretation (Polat and Hoffman, 2003). No sample shows any Ce anomaly, except sample EGY-04-01 has small positive Ce anomaly ($\text{Ce}/\text{Ce}^* = 1.22$) but its chondrite-normalized REE pattern and primitive mantle-normalized trace element patterns are consistent with the same rock type from the same exposure.

In summary, most Fawakhir ophiolitic magmatic abundances were not significantly perturbed by alteration except the LILE. The mobility of LILE under most alteration conditions and the relative immobility of the REE and HFSE agree with the results of other studies on variably altered rocks (Winchester and Floyd, 1977; Humphries, 1984; Ordóñez-Calderón et al., 2008; Gardien et al., 2008).

3.6.2. *Fractional crystallization*

Plots of Zr, which is an immobile differentiation index, versus selected major and trace elements are used to assess the role of fractional crystallization on the Fawakhir ophiolitic rocks. The regular variation of abundances of these elements against Zr might indicate a cogenetic origin of the Fawakhir ophiolitic rocks where fractionation can affect their chemistry. The negative relationship of MgO and CaO against Zr indicates the fractionation of olivine and pyroxene from the parent melt of the volcanic rocks. In addition, the negative correlation between Ni and Cr against Zr are also consistent with olivine and pyroxene fractionation. Olivine is reported as a cumulus phase in the peridotite from the Fawakhir area by Nasseef et al. (1980). A sharp increase in Al₂O₃ from pyroxenite to gabbro is attributed to the crystallization of plagioclase. Then, Al₂O₃ decreases systematically from the gabbro to the volcanic rocks, which can be attributed to the fractionation of plagioclase.

Positive correlations between Zr and most of the incompatible trace elements such as, TiO₂, REE, and Y highlight the co-magmatic nature of the ophiolitic rocks. The minor effect of fractional crystallization on trace element chemistry of the ophiolitic rocks can be detected through REE patterns. The patterns show that the absolute REE abundances increase from the pyroxenite to the volcanic rocks without variation in the pattern shape. Collectively, these geochemical characteristics are consistent with the derivation of the Fawakhir ophiolitic rocks from the same parental magma through fractional crystallization.

3.6.3. Mantle source characteristics

The geochemical characteristics of the Fawakhir ophiolite, mélangé blocks along Qift-Qusier Road and dissecting dikes are generally similar. Their primitive mantle-normalized patterns have consistent enrichment of Th, and LILE of the gabbroic rocks, over the rest of the HFSE and pronounced negative Nb anomalies. These geochemical characteristics are similar to those of magmatic rocks formed at convergent plate margins (Pearce, 1982; Saunders et al., 1991; Hawkesworth et al., 1993). Compositions of magmatic rocks in this setting are controlled by both fluid-derived components from the subducted slab and the mantle wedge composition (Tatsumi and Kogiso, 2003). Enrichment of the Th, and LILE of the gabbros, results from the mobility of these elements during slab dehydration (Pearce and Peate, 1995). On the other hand, HFSE (Nb,Zr,Y) and HREE tend to be less mobile than LILE during dehydration processes (John et al., 2008). Thus, ratios of HFSE (Nb,Zr,Y) and HREE in the rocks reflect their values in the mantle wedge (Pearce, 2008).

The relative contribution of both the mantle wedge and the slab-derived fluids can be determined using M/Yb versus Nb(Ta)/Yb plots of Pearce (1983) and Pearce and Peate (1995), where M is the incompatible element of interest (Fig. 3.12). On such a plot any contribution from the slab-derived fluid of the element (M) results in displacement from the mantle array which is defined by mantle-derived oceanic basalts (Mid-ocean ridge basalts, MORB, and Oceanic island basalts, OIB). For HFSE, Zr and Y, all the rock types plot within the mantle array which indicates that HFSE and HREE were not important components in the subduction-related flux. The ophiolitic samples and the mélangé blocks extend close to the MORB end, but the calc-alkaline dikes extend slightly

towards OIB. For the ophiolitic samples and mélangé blocks, both LREE (La) and MREE (Sm) values are confined to the mantle array although the LREE plot closer to the upper boundary, which may reflect some contribution from subduction-related fluids. The calc-alkaline dikes plot above the mantle array reflecting contributions from a source other than the mantle wedge. In contrast, LILE (U, Th) values are displaced above the mantle array towards higher ratios of Th/Yb and U/Yb which indicates a significant LILE and Th contribution from the subducted slab to the mantle wedge.

The nature of the transporting medium from the slab to the mantle wedge, either fluid or melt, influences the behavior of some elements (e.g., Zr) in a conservative or non-conservative way. Zirconium tends to behave in a non-conservative way with melting of the subducted sediment (Pearce and Peate, 1995). The restriction of Zr values of the Fawakhir ophiolitic rocks and mélangé blocks to the mantle array indicate the limited role of subducted sediment melting in the evolution of these rocks. The dominant role of slab-derived fluids over the role of sediments in the genesis of the Fawakhir ophiolitic rocks and mélangé blocks can be detected through the high Ba/La (cf. Woodhead et al., 2001) and Sr/Nd (cf. Schuth et al., 2004) over Th/Yb (Fig. 3.13). As sediment input to the mantle wedge is indiscernible, all of ophiolitic and mélangé samples follow the low Ce/Yb trend (Hawkesworth et al., 1993). Both the ophiolitic and mélangé samples follow the low Ce/Yb trend (Hawkesworth et al., 1993). However, the calc-alkaline dikes show higher Th/Ce values relative to the Fawakhir ophiolite and mélangé blocks. (Fig. 3.14).

As HFSE are less affected by subduction-derived fluxes, they can be used to address the nature of the mantle wedge. Using HFSE ratios to assess the composition of

the mantle wedge revokes the variation in the absolute concentration of HFSE that may result from pooled and fractional partial melting or from fractional crystallization (Pearce and Peate, 1995). As HFSE elements are conservative, they plot within the mantle array which extends from N-MORB source (lower Nb/Yb) to enriched OIB source (higher Nb/Yb). The Fawakhir ophiolitic rocks and the mélange blocks cluster around MORB values and extend towards lower Nb/Yb values, which reflects the variably depleted nature of the mantle source. Melting of such a depleted source is consistent with high Zr/Nb (19-87) ratios of the ophiolitic rocks and resembles other variably depleted mantle sources for many arc-related rocks (Davidson, 1996; Macdonald et al., 2000). Variation in the Zr/Nb ratios between the different types can be attributed to mantle heterogeneity and/or to selective tapping of the mantle column in a dynamic melting model (Pearce et al., 1995). Although the calc-alkaline dikes extend slightly towards an enriched mantle source (OIB-like), their Zr/Nb ratios (21-42) are comparable to N-MORB (N-MORB ratios =11-39, after Sun and McDonough, 1989).

The ratios of Gd/Yb_{cn} are variable for the rock units of Qift-Qusier Road. The Fawakhir ophiolitic rocks have almost flat HREE patterns ($Gd/Yb_{cn} = 0.88$ to 1.23) which indicate a relatively shallow mantle source within the spinel stability zone. On the other hand the mélange blocks from the eastern part of the road show slightly higher Gd/Yb_{cn} ratios (1.23 - 1.41) reflecting either a variable contribution from a deeper garnet-bearing mantle source (>80 km) or subduction-related melt in equilibrium with eclogite (cf. Kessel et al., 2005). Another possibility to obtain a garnet signature is to melt spinel peridotite veined with garnet pyroxenite (cf. Hirschmann and Stolper, 1996). The higher abundance of HREE in the mélange rocks suggests that the mantle source was spinel-

bearing rather than garnet-bearing which may support the possibility of melting spinel peridotite veined with garnet pyroxenite for the origin of the eastern *mélange* blocks. The younger calc-alkaline dikes are different from the ophiolitic and *mélange* rocks in that they have higher concentrations of Nb over Zr and Zr over Y, which indicate a contribution from a source enriched in incompatible elements such as sub-continental lithosphere (Pearce, 1983).

3.6.4. Pyroxenite genesis

Occurrence of pyroxenite is a common feature in most ophiolites. Pyroxenites occur as cumulate rocks in the transitional zone between the petrologic Moho and seismic Moho of the ophiolitic sequence (Stern et al., 2004). The Onib ophiolite provides an example of cumulate pyroxenite formation in the Neoproterozoic Arabian-Nubian Shield (Hussein et al., 2004). Pyroxenites occur also as veins and dikes crosscutting ophiolitic upper-mantle peridotites (Varfalvy et al., 1997). The formation of pyroxenite dikes and veins can be attributed to metasomatism of the mantle peridotite by melt or fluid migration that could be related to the subduction process (Berly et al., 2006). The other formation possibility for the pyroxenite dikes and veins is through intrusion of discrete magma derived from a highly-depleted mantle source representing a youth stage of the life cycle of a supra-subduction ophiolite (Shervais, 2001).

In accordance with field description of Nasseef et al. (1980), pyroxenites of the Fawakhir ophiolite occur as bodies with no clear relationship with the surrounding serpentinitized mantle rocks close to the contact with the ophiolitic gabbros. However, Nasseef et al. (1980) mentioned the presence of pyroxenite veins cutting the serpentinite and some gradational contacts between them. The cumulate transitional zone of the

Fawakhir ophiolite is not recorded (El-Sayed et al., 1999). The absence of cumulative textures and the different degree of alteration between the pyroxenite and the surrounding serpentinite may support the originally intrusive nature of the pyroxenite. The pyroxenites of the Fawakhir ophiolite have geochemical characteristics of a supra-subduction zone magma represented by enrichment of LILE and relative depletion of HFSE and REE combined with negative Nb anomalies (Hawkins, 2003). The subduction zone signature of the pyroxenite could be derived from metasomatising the peridotite of the mantle wedge by a subduction-related flux (Varfalvy et al., 1997) or later melting of refractory mantle in a supra-subduction setting to create a magma with a subduction signature (cf. Kuth-Velz et al., 2004). The high SiO₂ and low Cr and Ni contents of the pyroxenite of the Fawakhir ophiolite indicates the evolved nature of the pyroxenite melt which may support a separate melting event of the depleted mantle source rather than metasomatised peridotite mantle.

3.6.5. Geodynamic setting

The identification of the lithological assemblages of the Fawakhir area along Qift-Qusier Road as an ophiolite, a remnant of Neoproterozoic oceanic crust and mantle rocks, dates back to the early 1980s (Nasseef et al., 1980; Shackleton et al., 1980; Ries et al., 1983; El Gaby et al., 1984). The geochemical characteristics of the Fawakhir ophiolite, the enrichment of LILE over HFSE and the negative Nb anomalies on primitive mantle-normalized diagrams, are consistent with evolution in a supra-subduction zone geodynamic setting (cf. Pearce, 2003). In accordance with Ries et al. (1983) and El-Gaby et al. (1984), El-Sayed et al. (1999) also concluded that the Fawakhir ophiolitic assemblage is a supra-subduction ophiolite which formed in a back-arc tectonic setting.

Supra-subduction zone ophiolites have geochemical affinities of island arcs, but the structure of oceanic crust and were form by sea-floor spreading above subducted oceanic crust (Pearce et al., 1984; Metcalf and Shervais, 2008). These ophiolites can be formed during the initial stages of subduction, ridge-trench intersection and back-arc rifting and spreading (Pearce, 2003). Subduction initiation is considered as the most important process for ophiolite formation within the life cycle of a supra-subduction ophiolite (Casey and Dewey, 1984; Shervais, 2001). With subduction initiation, the early infant arc (or pre-arc as mentioned by Pearce et al., 1984) magmatism is characterized by depleted arc tholeiitic and boninitic magmas that occur in extensional environments similar to slow-spreading centers (Stern and Bloomer, 1992; Bloomer et al., 1995). The formation of many Phanerozoic ophiolites can be attributed to subduction initiation (Casey and Dewey, 1984; Shervais, 2001) and modern tectonic systems stimulate infant-arc formation such as the Izu-Bonin-Mariana (IBM) forearc system in the Western Pacific (Stern and Bloomer, 1992; Bloomer et al., 1995).

The Fawakhir ophiolite is composed mainly of low-Ti tholeiitic rocks and has a poorly developed sheeted dike complex. Although rocks of boninitic affinity were not found in this study, they were recorded for the Fawakhir ophiolite by El-Sayed et al. (1999), and the intrusive(?) pyroxenite within the Fawakhir ophiolitic serpentinite may indicate the presence of a highly depleted mantle source (cf. Kuth-Velz et al., 2004). The presence of the poorly developed sheeted dikes as an extension structure and the chemical affinity of the ophiolitic rocks are characteristics for an oceanic crust formed during subduction initiation (cf. Stern and Bloomer, 1992). With the above criteria, the Fawakhir ophiolite shows similarity with other Phanerozoic ophiolites, such as Troodos

(Cyprus), Semail (Oman), Vourinos (Greece), and Betts Cove (Newfoundland), which depict the birth and youth stages of Shervais (2001) during the life cycle of an ophiolite.

On the Cr versus Y plot of Pearce et al. (1984), the Fawakhir ophiolite plot within the island-arc field (Fig. 3.15). On this diagram, the Fawakhir ophiolitic samples overlap with the field defining Mariana forearc rocks that were formed through early sea-floor spreading during subduction initiation (Bloomer et al., 1995). The infant-arc signature and structure of the Fawakhir ophiolite is consistent with the appearance of depleted harzburgite mantle rocks in the Eastern Desert similar to ultramafic rocks from modern forearc tectonic settings (Azer and Stern, 2007; Khalil and Azer, 2007). A forearc tectonic setting (Fig. 3.16a) is also consistent with the speculation of Andresen et al. (2007) that the Fawakhir ophiolite represents a forearc oceanic crust.

The volcanic blocks within the mélangé, to the east of the Fawakhir ophiolite (Fig. 3.2), also have a supra-subduction signature, as they are enriched in Th relative to the rest of the HFSE and have primitive mantle-normalized patterns with negative Nb anomalies. Although both rock assemblages have overlapping Mg-numbers, the eastern mélangé blocks have higher TiO_2 (0.83-1.86) than the Fawakhir ophiolite (0.15-1.18). The association of high TiO_2 and a supra-subduction signature can be ascribed to formation in a back-arc tectonic setting (Serri, 1981). On the Cr versus Y tectonic discrimination diagram of Pearce et al. (1984), the eastern mélangé blocks plot in the MORB field along with other samples from different back-arc basins (Fig. 3.15). The pillow basalts of the eastern mélangé may be part of the Wadi Ambagi belt, which is inferred to have formed in a mid-ocean ridge setting (El-Mahallawi, 1994). With the mobility of LILE and the

lack of Nb data in his analyses, back-arc basin basalts could be easily interpreted as MORB.

As the Fawakhir ophiolite and the eastern *mélange* blocks overlap on the Cr versus Y plot with Izu-Bonin-Mariana forearc and Mariana Trough rocks, respectively, they can be considered as fragments of a Neoproterozoic forearc-back-arc association analogous to the Mariana system (Fig. 3.16b). Considering the spatial relation of the geochemically different eastern *mélange* blocks and the Fawakhir ophiolite to the west, the subduction direction can be inferred to be east-dipping. The same technique was used by Khan et al. (1997) to predict the subduction polarity of the Kohistan intra-oceanic arc. Near Marsa Alam, the same east-dipping subduction polarity was speculated for the formation of the Ghadir ophiolitic complex, but in a back-arc tectonic setting and the accretion of the Wadi Ghadir complex can be attributed to later west-dipping subduction-accretion (Abd El-Rahman et al., 2009).

The calc-alkaline dikes intruding the Fawakhir ophiolite have a subduction signature represented by Th enrichment over the rest of HFSE. They are different from the ophiolitic and *mélange* rocks in that they have higher concentrations of Nb over Zr and Zr over Y, which indicates a contribution from a source enriched in incompatible elements such as sub-continental lithosphere (Pearce, 1983). Both the petrography and geochemistry of the calc-alkaline dikes are similar to the Dokhan Volcanic unit of the Eastern Desert (cf. Basta et al., 1980; Eliwa et al., 2006). Calc-alkaline dikes and the Dokhan volcanic rocks are Andean-type rocks that might have formed at an active continental margin environment (El-Gaby et al., 1988; Abdel Rahman, 1996; Eliwa et al., 2006).

The calc-alkaline dikes dissecting the Fawakhir ophiolites may mark the transformation of the passive continental margin into an active continental margin with the accretion of island arc and fragments of oceanic crust. The transformation into an active continental margin resulted in calc-alkaline magmatism that occurred at ca. 620-710 Ma (Stern and Hedge, 1985; Loizenbauer et al., 2001; Eliwa et al., 2006, Moussa et al., 2008). In the transformation of the continental margin, east-dipping subducted oceanic crust which was attached to the continental crust may have broken off with the accretion of the ophiolitic and arc rocks. Subsequently, the subduction polarity could be reversed and continental magmatic arc magmatism produced (Fig. 3.16c). The west-dipping subduction associated with the transformation of passive continental margin into active margin is consistent with Kröner et al. (1987), but they proposed a marginal basin origin for the ophiolitic rocks in the Eastern Desert formed above a west-dipping subduction zone, which is not supported by this study. The slab break-off and subsequent subduction polarity reversal might have allowed melting of sub-continental lithospheric mantle to produce calc-alkaline magma. Reversal in subduction polarity after the collision of the Luzon arc and the South China margin may be a modern analogy for subduction polarity reversal in the Arabian-Nubian Shield where the birth of active margins is preferential (Clift et al., 2003). Reversal of the subduction polarity to create continental arc magmatism after the accretion of arc-related rocks is recorded as a crustal growth style in different orogens at different ages, such as the Mesoproterozoic Grenville orogen (Martin and Dickens, 2004), the Paleozoic Appalachian-Caledonian orogen (Van Staal et al., 1998) and the Mesozoic collision between the Kohistan arc and Karakorum (Khan et al., 1997).

3.7. Conclusion and implications

In this study, we used high-precision geochemical data from the Fawakhir ophiolite and mélange fragments from Qift-Qusier Road to assess the geodynamic evolution of this part of the Arabian-Nubian Shield. Previously proposed models for the evolution of the Arabian-Nubian Shield assigned a back-arc tectonic setting for the Neoproterozoic oceanic crust in the Eastern Desert (El-Bayoumi, 1983; El-Sayed et al., 1999; Farahat et al., 2004). The conflict regarding the tectonic setting of the ophiolitic rocks of the Eastern Desert occurs with the appearance of a forearc geochemical signature in the ophiolitic mantle rocks (Azer and Stern, 2007; Khalil and Azer, 2007). The forearc geochemical signature is recorded in many ophiolites, mostly mantle units, in the Arabian-Nubian shield (Stern et al., 2004). Unfortunately, Neoproterozoic oceanic crust with forearc geochemical signatures created during subduction initiation is not commonly identified in the Eastern Desert. The Fawakhir ophiolitic rocks represent a near-complete ophiolite sequence, starting from the west with the ultramafic rocks followed by gabbro, sheeted dikes and pillow basalts towards the east. The extensional structure and the geochemical signature of the ophiolitic crustal rocks ($La/Sm_{cn}=2.13-2.48$, $Gd/Yb_{cn}=2.04-4.25$, $Th/Nb_{pm}=3.2-5.8$, $La/Nb_{pm}=2.5-4.9$) indicate formation in a supra-subduction zone during the initial stage of subduction analogous to forearc rocks in the Izu-Bonin-Mariana system. The magmas derived from melting of a variably depleted N-MORB source within the spinel stability field.

The polarity of the subduction zone, above which the Neoproterozoic ophiolites formed, is another matter of controversy in the Eastern Desert. West-dipping subduction polarity is the common model to account for the subduction zone geochemical signature

of the ophiolitic rocks in the Eastern Desert (El Bayoumi and Grieling, 1984; Kröner, 1985; Kröner et al., 1987). Ries et al. (1983) proposed an east-dipping subduction zone but their model could not account for supra-subduction signatures (see Kröner et al., 1987). In this study, we propose the subduction polarity on the basis of the change of the geochemistry of the volcanic rocks through the mélangé along Qift-Qusier Road. The mélangé blocks to the east of the Fawakhir ophiolite are more enriched in HFSE than the ophiolitic rocks similar to present-day back-arc basin tectonic settings. The chemical difference and the spatial relationship between the western Fawakhir ophiolite and eastern mélangé blocks suggest an east-dipping subduction direction during the formation of these rocks in an intra-oceanic arc system.

After the accretion of the arc-related rocks onto the western Gondwana margin, the Fawakhir ophiolitic rocks were intruded by basaltic to andesitic calc-alkaline dikes which are similar to the Dokhan-type volcanic rocks (Eliwa et al., 2006). The geochemical data from the calc-alkaline dikes ($Ce/Yb=23-63$, $Zr/Yb=101-160$) are consistent with formation at an active continental margin after the accretion of the arc rocks in accordance with a lower degree of metamorphism and deformation of the dikes. The systematic enrichment of the calc-alkaline dikes in highly immobile incompatible elements, similar to other calc-alkaline rocks formed in active continental margins, indicates a contribution of an enriched source in their genesis such as sub-continental lithospheric mantle (Pearce, 1983). One of the reasons mentioned by Kröner et al. (1987) to refute the east-dipping subduction model of Ries et al. (1983) is the difficulty in generating calc-alkaline magmatism from a mantle below a passive continental margin. In partial agreement with the Ries et al. (1983) evolution model, the geochemical data of

the Fawakhir ophiolite and mélangé blocks indicate an east-dipping subduction direction during evolution of the supra-subduction zone magmatism of the Eastern Desert. The intrusion of weakly metamorphosed and weakly deformed calc-alkaline dikes with active continental margin geochemical signatures may suggest flipping in the polarity of the subduction direction. Reversal of the subduction polarity would result in the availability of a sub-continental lithospheric mantle contribution in the evolution of active continental margin magmatism in the Eastern Desert.

The Neoproterozoic Fawakhir ophiolite and the mélangé rocks of the Eastern desert are analogous to the Izu-Bonin-Mariana arc system. The reversal of the subduction polarity proposed for the evolution of the Eastern desert is also similar those recorded in Western Pacific ocean systems in the Luzon arc (Clift et al., 2003) and Papua New Guinea (Harris, 2003) following arc-continental collision. The accretion of complex tectonic and magmatic systems analogous to those in the southwest Pacific Ocean prior to the final continental collision between East and West Gondwana led to the formation of the Arabian-Nubian Shield suture between the two continental margins.

Acknowledgements

We thank J.C. Barrette, J.C. Ordóñez-Calderón and Zhaoping Yang for their help during geochemical analyses. This is a contribution of PREA and NSERC grants (250926) to A. Polat and NSERC grant (83117) to B. Fryer.

References

Abd El-Rahman, Y., Polat, A., Dilek, Y., Fryer, B.J., El-Sharkawy, M., Sakran, S., 2009. Geochemistry and tectonic evolution of the Neoproterozoic Wadi Ghadir ophiolite, Eastern Desert, Egypt. *Lithos*. doi:10.1016/j.lithos.2008.12.014.

- Abdel Rahman, A.M., 1996. Pan-African volcanism: petrology and geochemistry of the Dokhan Volcanic suite in the northern Nubian Shield. *Geological Magazine* **133**, 17–31.
- Ahmed, A.H., Arai, S., Ataia, A.K., 2001. Petrological characteristics of the Pan African podiform chromitite and associated peridotites of the Proterozoic ophiolite complexes, Egypt. *Mineralium Deposita* **36**, 72-84.
- Andresen, A., Abu El-Rus, M.A., Myhre, P.L., Boghdady, G.Y., Corfu, F., 2009. U-Pb TIMS age constraints on the evolution of the Neoproterozoic Meatiq Gneiss Dome, Eastern Desert, Egypt. *International Journal of Earth Sciences*, **98**, 481-497.
- Azer, M.K., Stern, R.J., 2007. Neoproterozoic (835-720 Ma) serpentinites in the Eastern Desert, Egypt: Fragments of forearc mantle. *The Journal of Geology* **115**, 457-472.
- Barrett, T.J., MacLean, W.H., 1994. Chemostratigraphy and hydrothermal alteration in exploration for VHMS deposits in greenstone and younger volcanic rocks. In: Lentz, D.R. (Ed.), *Alteration and Alteration Processes Associated with Ore-Forming Systems*. Geological Association of Canada, Short Course Notes **11**, 433-467.
- Basta, E.Z., Kotb, H., Awadalla, M.F., 1980. Petrochemical and chemical characteristics of the Dokhan formation at the type locality, Gebel Dokhan, Eastern Desert, Egypt. *Bulletin of King Abdelaziz University* **3**, 121-140.
- Berly, T.J., Hermann, J., Arculus, R.J., Lapierre, H., 2006. Supra-subduction zone pyroxenites from San Jore and Santa Isabel (Solomon Islands). *Journal of Petrology* **47**, 1531-1555.
- Bloomer, S.H., Taylor, B., MacLeod, C.J., Stern, R.J., Fryer, P., Hawkins, J.W., Johnson, L., 1995. Early Arc Volcanism and the Ophiolite Problem: A Perspective from Drilling in the Western Pacific. In B. Taylor and J. Natland (eds.) *Active Margins and Marginal Basins of the Western Pacific*. AGU Geophysical Monograph **88**, 1-30.
- Brown, D., Spadea, P., 1999. Processes of forearc and accretionary complex formation during arc-continental collision in the southern Ural Mountains. *Geology* **27**, 649-652.
- Casey, J.F., Dewey, J.F., 1984. Initiation of subduction zone along transform and accreting plate boundaries, triple-junction evolution, and forearc spreading centers: implications for ophiolitic geology and obduction. In: Gass, I.G., Lippard, S.J., Shelton, A.W., (eds.) *Ophiolites and oceanic lithosphere*. Geological Society, London, Special Publication **13**, 269-290.
- Clift, P.D., Schouten, H., Draut, A.E., 2003. A general model of arc-continent collision and subduction polarity reversal from Taiwan and Irish Caledonides. In: Larter, R.D., and Leat, E.T., (eds.) *Intra-oceanic subduction systems: Tectonic and magmatic processes*. Geological Society, London, Special Publication **219**, 81-98.

- Crocket, J.H., Oshin, I.O., 1987. The geochemistry and petrogenesis of ophiolitic volcanic rocks from Lac de l'Est, Thetford Mine Complex, Quebec, Canada: Reply. *Canadian Journal of Earth Sciences* 24, 1273-1275.
- Davidson, J.P., 1996. Deciphering mantle and crystal signatures in subduction zone magmatism. *Subduction: Top to Bottom. Geophysical Monograph* 96. AGU, Washington, 251-262.
- Dilek, Y., 2003. Ophiolite concept and its evolution. In: Dilek Y., Newcomb, S. (Eds.), *Ophiolite Concept and the Evolution of Geological Thought. Geol. Soc. Am. Spec. Paper* 373, 1-15.
- El Akhal, H., 1993. A transect from a tectonic mélange to an island-arc in the Pan-African of SE Egypt (Wadi Ghadir area). *Scientific Series of the International Bureau* 20, 1-244.
- El-Bayoumi, R.M., 1983. Ophiolites and mélange complex of Wadi Ghadir area, Eastern Desert, Egypt. *Bulletin of King Abdelaziz University* 6, 329-342.
- El-Bayoumi, R.M.A., Greiling, R.O., 1984. Tectonic evolution of a Pan-African plate margin in southeastern Egypt – a suture zone overprinted by low angle thrusting? In: Klerkx, J., Michot, J. (Eds.), *Géologie Africaine-African Geology. Musée royal de l'Afrique Centrale, Tervuren, Belg.* 47-56.
- El-Gaby, S., El-Nady, O., Khudeir, A., 1984. Tectonic evolution of the Basement Complex in the Central Eastern Desert of Egypt. *Geologische Rundschau* 73, 1019-1036.
- El-Gaby, S., List, F.K., Tehrani, R., 1988. Geology, evolution and metallogenesis of the Pan-African belt in Egypt. In: El-Gaby, S., Greiling, R.O. (Eds.), *The Pan-African Belt of Northeast Africa and Adjacent Areas: Tectonic Evolution and Economic Aspects of a Late Proterozoic Orogen.* Friedrich. Vieweg, Sohn Verlagsgesellschaft mbH, 17-68.
- El-Mahallawi, M.M., 1994. Contribution to the geochemistry and petrogenesis of some metabasalts from the Ambagi Area, Central Eastern Desert, Egypt. *Egyptian Journal of Geology* 38, 401-419.
- El-Ramly, M.F., Greiling, R., Kröner, A., Rashwan, A.A., 1984. On the tectonic evolution of the Wadi Hafafit area and environs, Eastern Desert of Egypt. *Bulletin of King Abdelaziz University* 6, 113-126.
- El-Shafei, M.K., Kusky, T.M., 2003. Structural evolution of the Neoproterozoic Feiran-Solaf metamorphic belt, Sinai Peninsula: Implications for the closure of the Mozambique Ocean. *Precambrian Research* 126, 269-293.
- El-Sayed M.M., Furnes H., Mohamed F.H., 1999. Geochemical constraints on the tectonomagmatic evolution of the late Precambrian Fawakhir ophiolite, Central Eastern Desert, Egypt. *Journal of African Earth Science* 29, 515-533.

- Eliwa, H.A., Kimura, J.I., Itaya, T., 2006. Late Neoproterozoic Dokhan volcanic rocks, northern Eastern Desert, Egypt. *Precambrian Research* 151, 31-52.
- Farahat, E.S., 2008. Chrome-spinels in serpentinites and talc carbonates of the El Edeid-El Sodmein District, Central Eastern Desert, Egypt: their metamorphism and petrogenetic implication. *Chemie de Erde Geochemistry* 68, 193-205.
- Farahat, E.S., El Mahalawi M.M., Hoinkes G., Abdel Aal A.Y., 2004. Continental back-arc basin origin of some ophiolites from the Eastern Desert of Egypt. *Mineralogy and Petrology* 82, 81-104.
- Fowler, T.J., and Osman, A.F., 2001. Gneiss-cored interference dome associated with two phases of late Pan-African thrusting in the Central Eastern Desert, Egypt. *Precambrian Research* 108, 17-43.
- Furnes, H., El-Sayed, M.M., Khalil, S.O., Hassanen, M.A., 1996. Pan-African magmatism in the Wadi El-Imra District, central Eastern Desert, Egypt: geochemistry and tectonic environment. *Journal of Geological Society of London* 153, 705-718.
- Furnes, H., Skjerlie, K.P., Dilek, Y., 2000. Petrology, tectonics, and hydrothermal alteration of a back-arc oceanic crust: Solund-Stavfjord ophiolite complex of the western Norwegian Caledonides: A review. In: Dilek, Y., Robinson, P.T. (Eds.), *Ophiolites and oceanic crust: new insights from field studies and the Ocean Drilling Program*. GSA Spec. Paper 349, 443-460.
- Gardien, V., Lecuyer, C., Moyen, J-F, 2008. Dolerites of the Woodlark basin (Papuan Peninsula, New Guinea): A geochemical record on the influence of a neighboring subduction zone. *Journal of Asian Earth Sciences* 33, 139-154.
- Gillis, K.M., Banerjee, N.R., 2000. Hydrothermal alteration patterns in supra-subduction zone ophiolites. In: Dilek, Y., Moores, E.M., Elthon, D., Nicolas, A. (Eds.), *Ophiolites and Oceanic Crust: New Insights from Field Studies and the Ocean Drilling Program*. Geological Society of America Special Paper 349, 283–297.
- Green, N. L., 2006. Influence of slab thermal structure on basalt source regions and melting conditions: REE and HFSE constraints from the Garibaldi volcanic belt, northern Cascadia subduction system. *LITHOS* 87, 23-49.
- Harris, R., 2003. Geodynamic patterns of ophiolites and marginal basins in the Indonesian and New Guinea regions. In: Dilek, Y., Robinson, P.T. (Eds), *Ophiolite in Earth History*. Geological Society, London, Special Publication 218, 481-506.
- Hawkesworth, C. J., Gallagher, K., Hergt, J. M., McDermott, F., 1993. Mantle and slab contributions in arc magmas. *Annual Review of Earth and Planetary Sciences* 21, 175–204.

- Hawkins J.W., 2003. Geology of supra-subduction zones-Implications for the origin of ophiolites. In: Dilek, Y., Newcomb, S., (eds) *Ophiolite concept and the evolution of geological thought*. Boulder, Colorado, Geological Society of America Special Paper 373, 227–268.
- Hirschmann, M.M., Stolper, E.M., 1996. A possible role for garnet pyroxenite in the origin of the “garnet signature” in MORB. *Contributions Mineralogy and Petrology* 124, 185–208.
- Hofmann, A.W., 1988. Chemical differentiation of the Earth: the relationship between mantle continental crust and oceanic crust. *Earth and Planetary Science Letters* 90, 297-414.
- Humphries, S.E., 1984. The mobility of the rare earth elements in the crust. In: Henderson, P., (Ed.) *Rare Earth Element Geochemistry*. Elsevier, Amsterdam, 317-342.
- Hussein, I.M., Kröner, A., Reischmann, T., 2004. The Wadi Onib mafic-ultramafic complex: A Neoproterozoic supra-subduction zone ophiolite in the northern Red Sea Hills of the Sudan. In: Kusky TM, ed. *Precambrian Ophiolites and Related Rocks*. *Developments in Precambrian Geology*, vol. 13, Amsterdam: Elsevier. 163-206.
- Jenner, G.A., Longerich, H.P., Jackson, S.E., Freyer, B.J., 1990. ICP-MS - a powerful tool for high-precision trace-element analysis in earth sciences: evidence from analysis of selected U.S.G.S. reference samples. *Chemical Geology* 83, 133-148.
- John, T., Klemd, R., Gao, J., Garbe-schönberg, C-D., 2008. Trace-elements mobilization in slabs due to nonsteady-state fluid-rock interaction: Constraints from an eclogite-facies transform vein in blueschist (Tianshan, China). *Lithos* 103, 1-24.
- Jons, N., Schenk, V., 2007. Relics of the Mozambique Ocean in the central Eastern African Orogen: evidence from the Vohibory Block of southern Madagascar. *Journal of Metamorphic Geology* 26, 17-28.
- Kessel, R., Schmidt, M.W., Ulmer, P., Pettke, T., 2005. Trace element signature of subduction-zone fluids, melts and supercritical fluids at 120–180 km depths. *Nature* 437/29, 724–727.
- Khalil, A.E.S., Azer, M.K., 2007. Supra-subduction affinity in the Neoproterozoic serpentinites in the Eastern Desert, Egypt: Evidence from mineral composition. *Journal of African Earth Sciences* 49, 136-152.
- Khalil, K.I., 2007. Chromite mineralization in ultramafic rocks of the Wadi Ghadir area, Eastern Desert, Egypt: mineralogical, microchemical and genetic study. *Neues Jahrbuch für Mineralogie - Abhandlungen* 183, 283-296.
- Khan M.A., Stern, R.J., Gribble, R.F., Windley, B.F., 1997. Geochemical and isotopic constraints on subduction polarity, magma sources, and paleogeography of the Kohistan intra-oceanic arc, northern Pakistan Himalaya. *Journal of Geological Society* 154, 935-946.

- Kröner, A., 1985. Ophiolites and the evolution of tectonic boundaries in the late Proterozoic Arabian-Nubian Shield of northeast Africa and Arabia. *Precambrian Research* 27, 277–300.
- Kröner, A., Greiling, R.O., Reischmann, T., Hussein, I.M., Stern, R.J., Durr, S., Kruger, J., Zimmer, M., 1987. Pan-African crustal evolution in the Nubian segment of northeast Africa. In: Kröner, A., (Ed.) *Proterozoic lithospheric evolution*. American Geophysical Union, *Geodynamics Series* 17, 237-257.
- Kröner, A., Todt W., Hussein I.M., Mansour M., Rashwan A.A., 1992. Dating of late Proterozoic ophiolites in Egypt and the Sudan using the single grain zircon evaporation technique. *Precambrian Research* 59, 15–32.
- Kurth-Velz, M., Sassen, A., and Galer, S.J.G., 2004. Geochemical and isotopic heterogeneities along and island arc-spreading ridge intersection: evidence from the Lewis Hills, Bay of Islands ophiolite, Newfoundland. *Journal of Petrology* 45, 635-668.
- Kusky, T.M., 2004. Introduction. In: Kusky, T.M., (Ed.). *Precambrian Ophiolites and Related Rocks*. Elsevier, Amsterdam, pp. 1-34.
- Kusky, T.M., Matsah, M.I., 2003. Neoproterozoic dextral faulting on the Najd Fault System, Saudi Arabia, preceded sinistral faulting and escape tectonics related to closure of the Mozambique Ocean. In: Yoshida, M., Windley, B.F., Dasgupta, S. (Eds.), *Proterozoic East Gondwana: supercontinent assembly and breakup*. Geol. Soc. London Special Publ. 206, 327-361.
- Loizenbauer, J., Wallbrecher, E., Fritz, H., Neumayr, P., Khudier, A.A., Kloetzli, U., 2001. Structural geology, single zircon age and fluid inclusion studies of Meatiq metamorphic core complex: Implication for Neoproterozoic tectonics in the Eastern Desert of Egypt. *Precambrian Research* 110, 357-383.
- Macdonald, R., Hawkesworth, C.J., Heather, E., 2000. The Lesser Antiles volcanic chain: a study in arc magmatism. *Earth Science Review* 49, 1-76.
- Martin, C., Dickins, A.P., 2005. Styles of Proterozoic crustal growth on the southeast margin of Laurentia: evidence from central Granville Province northwest of Lac St. –Jean, Quebec. *Canadian Journal of Earth Science* 42, 1643-1652.
- Metcalf, R.V., Shervais, J.W., 2008. Suprasubduction zone ophiolites: Is there really an ophiolite conundrum? In: Wright, J.E., Shervais, J.W. (Eds.), *Ophiolites, Arcs, and Batholiths: A Tribute to Cliff Hopson*. GSA Special Paper 438, 191-222.
- Miyashiro, A., 1973. The Troodos ophiolitic complex was probably formed in an island arc. *Earth and Planetary Science Letters* 19, 218–224.

- Moussa, E.M.M., Stern, R.J., Manton, W.I., Ali, K.A., 2008. SHRIMP zircon dating and Sm/Nd isotopic investigations of Neoproterozoic granitoids, Eastern Desert, Egypt. *Precambrian Research* 160, 341-356.
- Nasseef, A.O., Bakor, A.R., Hashad, A.H., 1980. Petrography of possible ophiolitic rocks along the Qift-Qusier Road, Eastern Desert, Egypt. *Bulletin of King Abdelaziz University* 3, 157-168.
- Nicolas, A., Boudier, F., 2003. Where ophiolites come from and what they tell us. In: Dilek, Y., Newcomb, S., (Eds) *Ophiolite concept and the evolution of geological thought*. Boulder, Colorado, Geological Society of America Special Paper 373, 137-152.
- Ordóñez-Calderón, J.C., Polat, A., Fryer, B., Gagnon, J.E., Raith, J.G., Appel, P.W.U., 2008. Evidence for HFSE and REE mobility during calc-silicate metasomatism, Mesoarchean (~3075 Ma) Ivisaartoq greenstone belt, Southern west Greenland. *Precambrian Research* 161, 317-340.
- Pearce, J.A., 1982. Trace element characteristics of lavas from destructive plate boundaries. In: Thorpe R.S. (Ed.) *Andesites: Orogenic Andesites and Related Rocks*, Chichester: John Wiley, 525–547.
- Pearce, J.A., 1983. Role of sub-continental lithosphere in magma genesis at active continental margins. In: Hawkesworth, C. J., Norry, M. J., (Eds) *Continental Basalts and Mantle Xenoliths*. Nantwich, UK: Shiva, 230–249.
- Pearce, J.A., 2003. Supra-subduction zone ophiolites: the search for modern analogues. In: Y. Dilek and S. Newcomb, Editors, *Ophiolite Concept and the Evolution of Geological Thought*. Geological Society of America Special Paper 373, 269-295.
- Pearce, J.A., 2008. Geochemical fingerprinting of oceanic basalts with applications to ophiolite classification and the search for Archean oceanic crust. *Lithos* 100, 14-48.
- Pearce, J.A., Baker, P.E., Harvey, P.K.; and Luff, I.W. 1995. Geochemical evidence for subduction fluxes, mantle melting and fractional crystallization beneath the South Sandwich island arc. *Journal of Petrology* 36, 1073–1109.
- Pearce, J.A., Lippard, S.J., Roberts, S., 1984. Characteristics and tectonic significance of supra-subduction zone ophiolites. In: Kokelaar, P.B., Howells, M.F. (Eds), *Marginal Basin Geology*. Geological Society, London, Special Publication 16, 77-94.
- Pearce, J.A., Peate, D.W., 1995. Tectonic implications of the composition of volcanic arc lavas. *Annual Review of Earth and Planetary Sciences* 23, 251–285.
- Polat, A., Hofmann, A.W., 2003. Alteration and geochemical patterns in the 3.7–3.8 Ga Isua greenstone belt, West Greenland. *Precambrian Research* 126, 197–218.

- Ragland, P.C., 1989. Basic analytical petrology. Oxford University Press, New York.
- Ries, A.C., Shackleton R.M., Graham R.H., Fitches W.R., 1983. Pan-African structures, ophiolites and mélanges in the Eastern Desert of Egypt: a traverse at 26° N. *Journal of Geological Society* 140, 75–95.
- Rollinson, H.R., 1993. Using geochemical data: evaluation, presentation and interpretation. Longman/Wyllyie, Harlow/New York.
- Saunders, A.D., Norry, M.J., Tarney, J., 1991. Fluid influence on the trace element compositions of the subduction zone magmas. *Royal Society of London Philosophical Transactions* 335, 377-392.
- Schuth, S., Rohrbach, A., Münker, C., Ballhaus, C., Garbe-schönberg, C-D., Qopoto, C., 2004. Geochemical constraints on the petrogenesis of arc picrites and basalts, New Georgia group, Solomon Island. *Contribution to mineralogy and petrology* 148, 288-304.
- Şengör, A.M.C., 1990. Plate Tectonics and orogenic research after 25 years: A Tethyan perspective. *Earth Science Review* 27, 1-201.
- Serri, G., 1981. The petrochemistry of ophiolite gabbroic complexes: a key for the classification of ophiolites into low-Ti and high-Ti types. *Earth and Planetary Science Letters* 52, 203-212.
- Shackleton, R.M., 1994. Review of late Proterozoic sutures, ophiolitic mélanges and tectonics of eastern Egypt and north-east Sudan. *Geologische Rundschau* 83, 537-546.
- Shackleton, R.M., Ries A.C., Graham R.H., Fitches W.R., 1980. Late Precambrian ophiolite mélange in the eastern desert of Egypt. *Nature* 285, 472–474.
- Shervais, J.W., 2001. Birth, death, and resurrection: The life cycle of supra-subduction zone ophiolites. *Geochemistry, Geophysics, Geosciences* 2, 1010, doi:10.1029/2000GC000080.
- Stern, R.J., 1994. Are assembly and continental collision in the Neoproterozoic East African Orogen: implications for the consolidation of Gondwanaland. *Annual Review of Earth and Planet Sciences* 22, 319–351.
- Stern, R.J., 2004. Subduction initiation: spontaneous and induced. *Earth and Planetary Science Letters* 226, 275-292.
- Stern, R.J., 2005. Evidence from ophiolites, blueschists, and ultrahigh-pressure metamorphic terranes that modern episodes of subduction tectonics began in Neoproterozoic time. *Geology* 33, 557-560.
- Stern, R.J., 2008. Neoproterozoic crustal growth: The solid Earth system during a critical episode of Earth history. *Gondwana Research* 14, 33-50.

- Stern, R.J., Bloomer, S.H., 1992. Subduction zone infancy: Examples from the Eocene Izu-Bonin-Mariana and Jurassic California arcs. *Geological Society of American Bulletin* 104, 1621-1636.
- Stern, R.J., Hedge, C.E., 1985. Geochronologic and isotopic constraints on Late Precambrian crustal evolution in the Eastern Desert of Egypt. *American Journal of Science* 285, 97-127.
- Stern, R.J., Johanson, P.R., Kroner, A., Yibas, B., 2004. Neoproterozoic ophiolites of the Arabian-Nubian Shield. In: Kusky TM, ed. *Precambrian Ophiolites and Related Rocks. Developments in Precambrian Geology*, vol. 13. Amsterdam: Elsevier.95-128.
- Stern, R.J., Nielsen, K.C., Best, E., Sultan, M., Arvidson, E., Kroner, A., 1990. Orientation of late Precambrian sutures in the Arabian-Nubian shield. *Geology* 18, 1103-1106.
- Sun, S.-S., McDonough, W.F., 1989. Chemical and systematic of oceanic basalts: implications for mantle composition and processes. In: Saunders, A.D., Norry, M.J. (eds.) *Magmatism in ocean basins*. Geological Society, London. Special Publication 42, 313-345.
- Tatsumi, Y., Kogiso, T., 2003. The subduction factory: its role in the evolution of the Earth's crust and mantle. In: Larter, R.D., and Leat, E.T., (eds.) *Intra-oceanic subduction systems: Tectonic and magmatic processes*. Geological Society, London. Special Publication 219, 55-80.
- Van Staal, C.R., Dewey, J.F., Mac Niocaill, C., Mckerrow, W.S., 1998. The Cambrian-Silurian tectonic evolution of the northern Appalachians and British Caledonides: history of a complex, west and southwest Pacific-type segment of Iapetus. *In*: Blundell, D. J. & Scott, A. C. (eds) *Lyell: the Past is the Key to the Present*. Geological Society, London, Special Publications 143, 199-242.
- Variálvy, V., Hébert, R., Bédard, J.H., Laflèche, M.R., 1997. Petrology and geochemistry of pyroxenite dykes in upper mantle peridotites of the North Arm Mountain Massif, Bay of Islands ophiolite, Newfoundland: implications for the genesis of boninitic and related magmas. *The Canadian Mineralogist* 35, 543-570.
- Winchester, J.A., Floyd, P.A., 1977. Geochemical discrimination of different magma series and their differentiation products using immobile elements. *Chemical Geology* 20, 325-343.
- Woodhead, J.D., Eggins, S.M., Johnson, R.W., 1998. Magma genesis in the New Britain island arc: further insights into melting and mass transfer processes. *Journal of petrology* 39, 1641-1668.
- Woodhead, J.D., Hergt, J.M., Davidson, J.P., Eggins, S.M., 2001. Hafnium isotope evidence for 'conservative' element mobility during subduction processes. *Earth and Planetary Science Letters* 192,331-346.

Yumul, G.P.Jr., 2004. Zambales Ophiolite Complex (Philippines) transition-zone dunite: restite, cumulate, or replacive product? *International Geology Review* 46, 259-272.

Zimmer, M., Kröner, A., Jochum, K.P., Reischmann, T., Todt, W., 1995. The Gabal Gerf complex: a Precambrian N-MORB ophiolite in the Nubian Shield, NE Africa. *Chemical Geology* 123, 29–51.

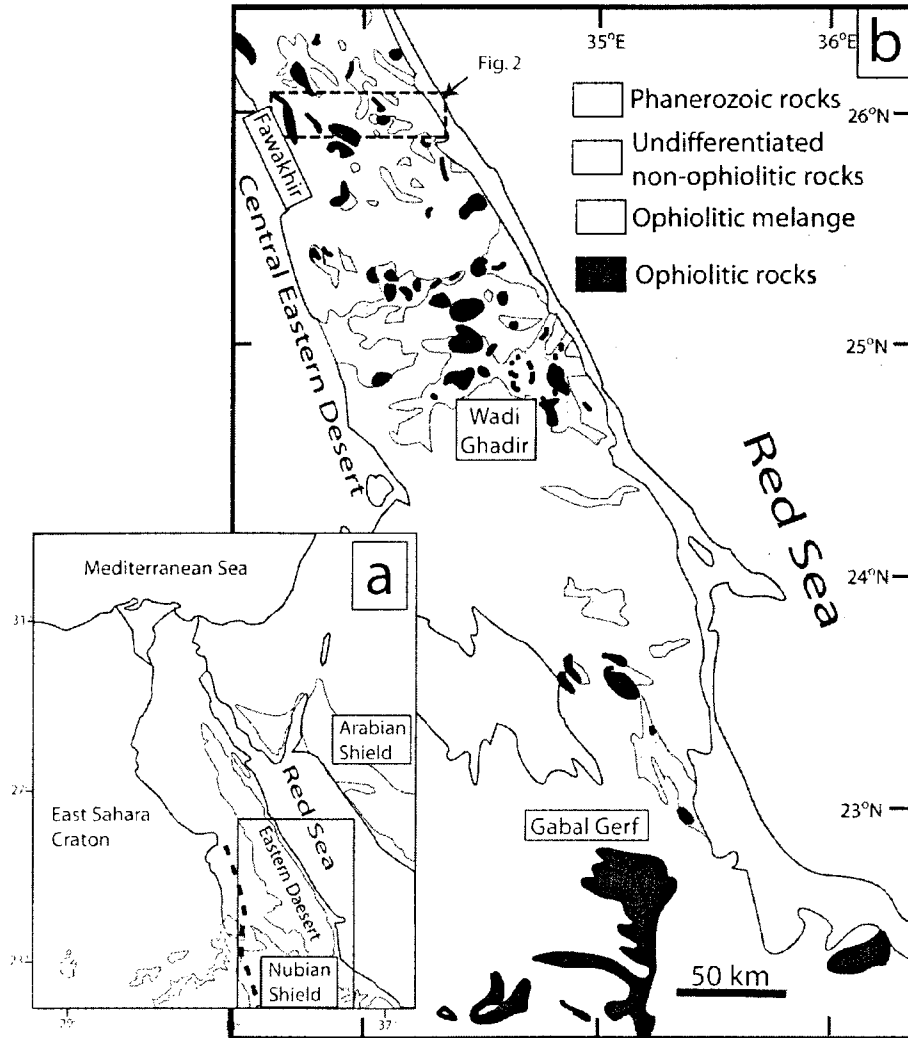


Fig. 3.1. (a) Overview map of the Arabian-Nubian Shield rocks (orange) along the Red Sea. The dashed line is the approximate boundary between the Shield and the Eastern Saharan Craton (After Greiling et al., 1994) (Red strip represents the area in b). (b) Enlargement of the solid rectangle in (a) showing the distribution of ophiolitic fragments in the Eastern Desert of Egypt. (From El-Sayed et al., 1999).

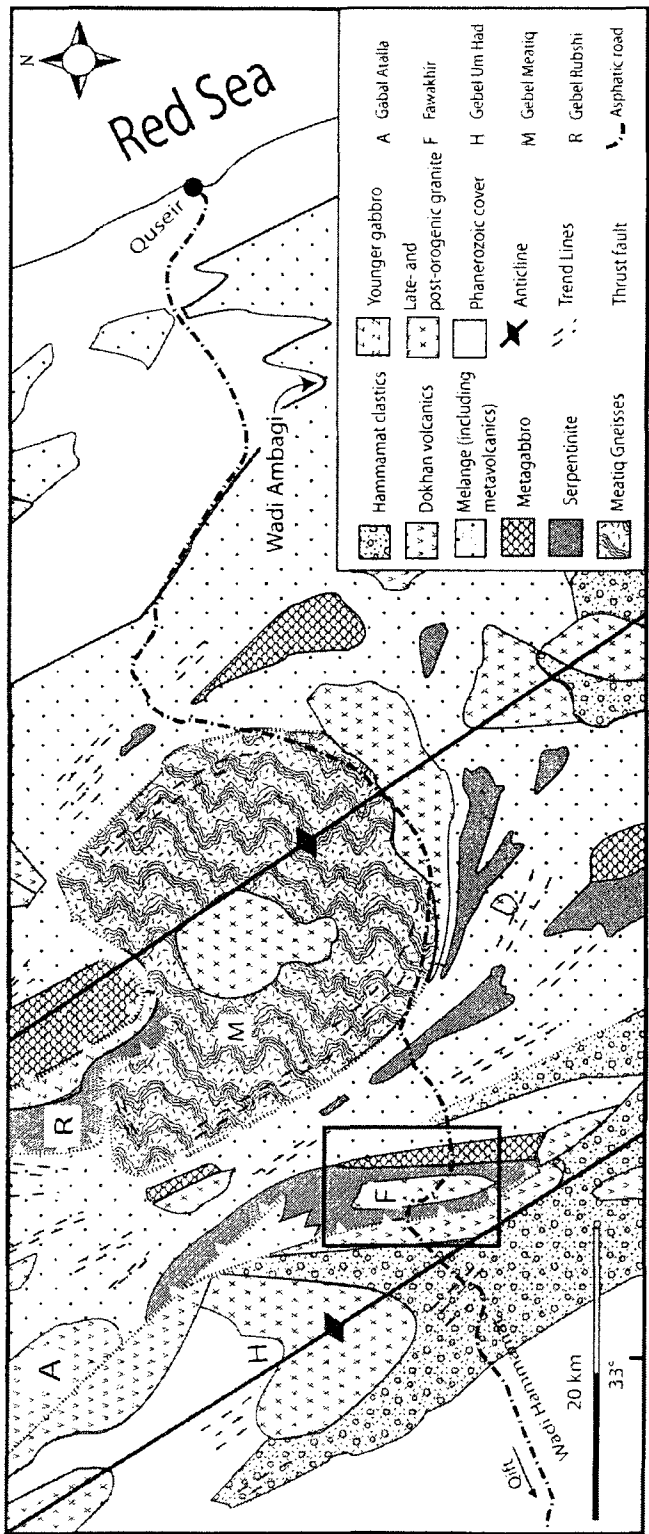


Fig. 3.2. Enlargement of the dashed rectangle in (Fig. 3.1b) showing a simplified geological map of the Qift-Quseir road (From El-Gaby et al., 1984).

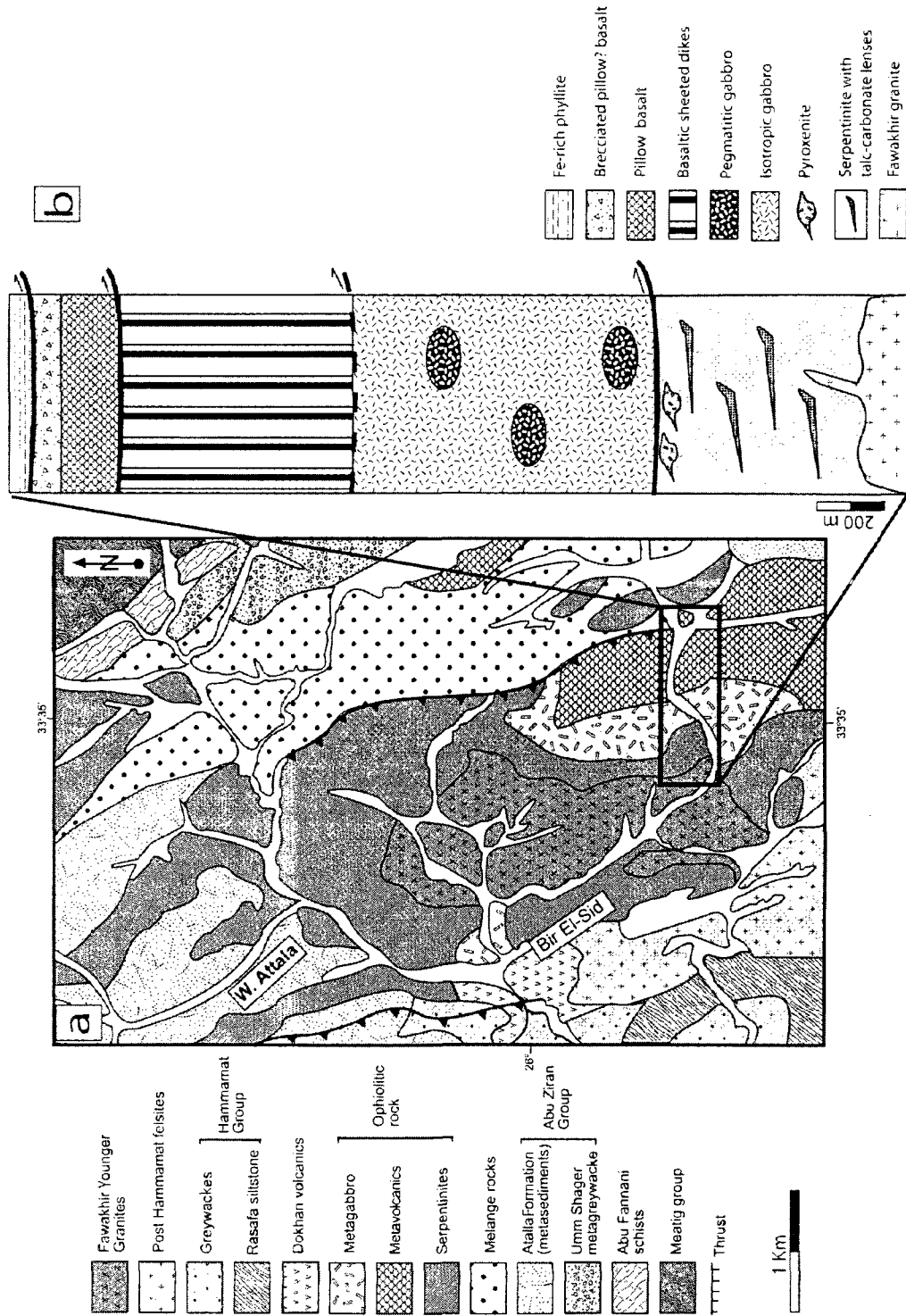


Fig. 3.3. (a) Enlargement of the rectangle in (Fig. 3.2) showing the geological map of the Fawakhir area (modified after, El-Sayed et al., 1999). (b) Schematic stratigraphic section showing the main rocks unit of the Fawakhir ophiolite.

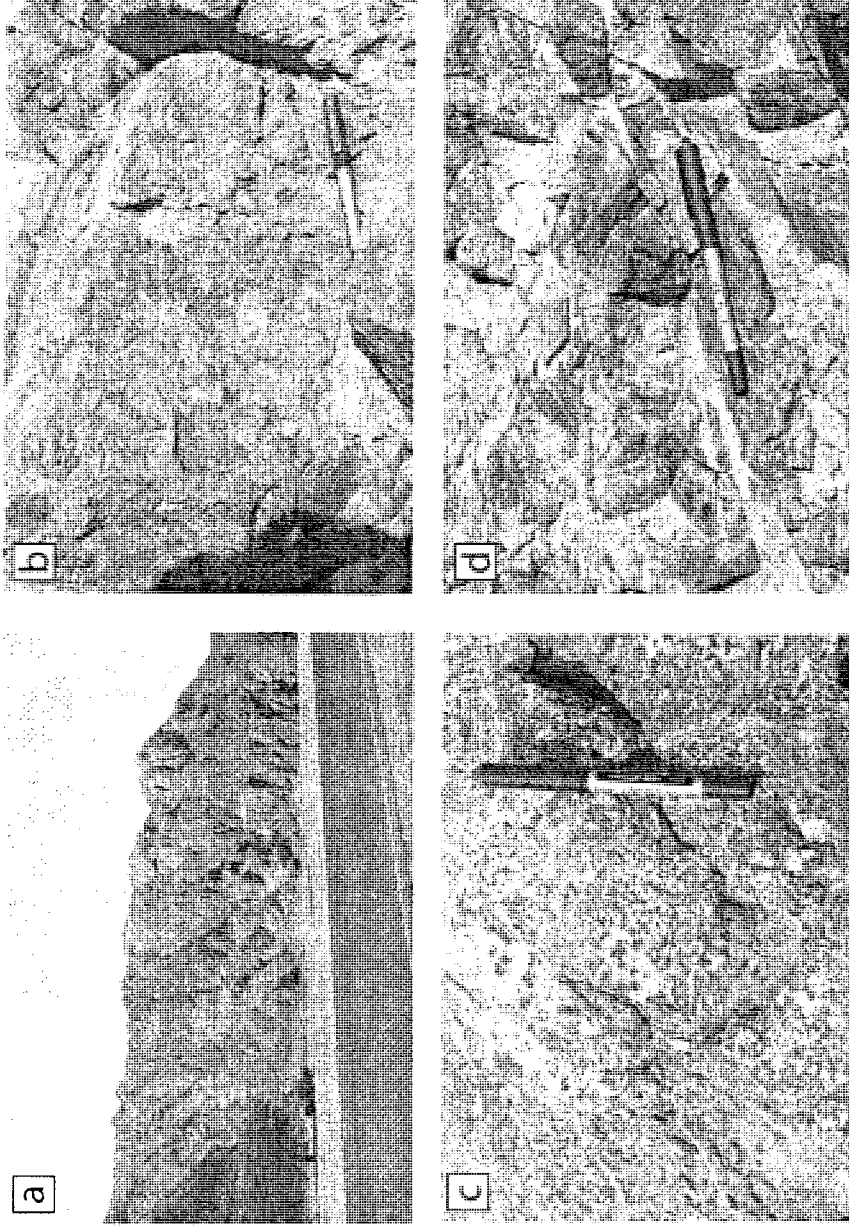


Fig. 3.4. Field photographs of the ophiolitic mantle rocks and plutonic section of Fawakhir area. (a) Massive serpentinite altered to talc-carbonate (buff colour) along localized shear zone. (b) Ophiolitic isotropic gabbro. (c) Coarse-grained pyroxenite body. (d) Epidotization of gabbro along fractures.

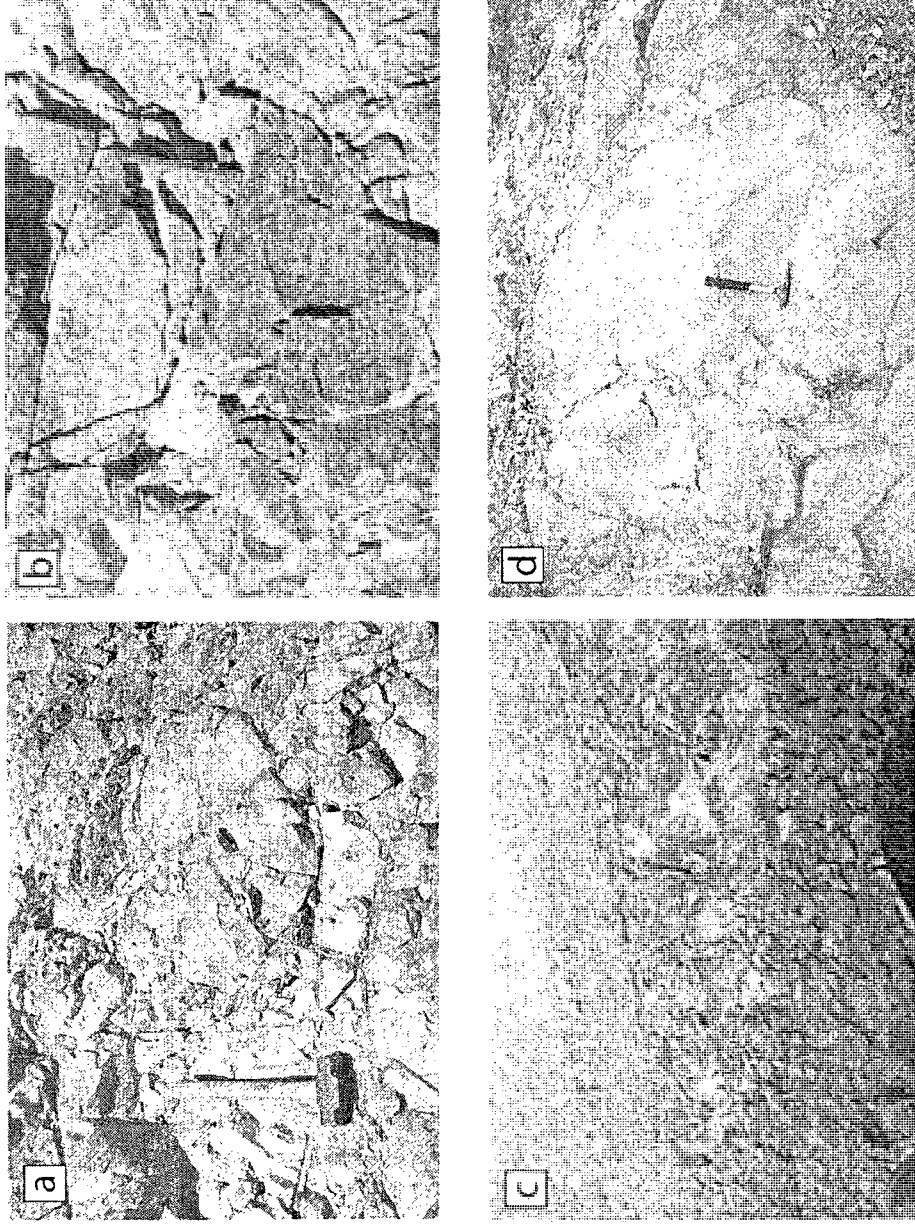


Fig. 3.5. Field photographs of the volcanic rocks and associated metasedimentary rocks. (a) Highly jointed pillow basalt of the Fawakhir ophiolite. (b) Hyaloclastites of the Fawakhir area. (c) Schistose red pelites of the Fawakhir area. (d) Large pillow lava enclosing smaller one of the eastern mélange.

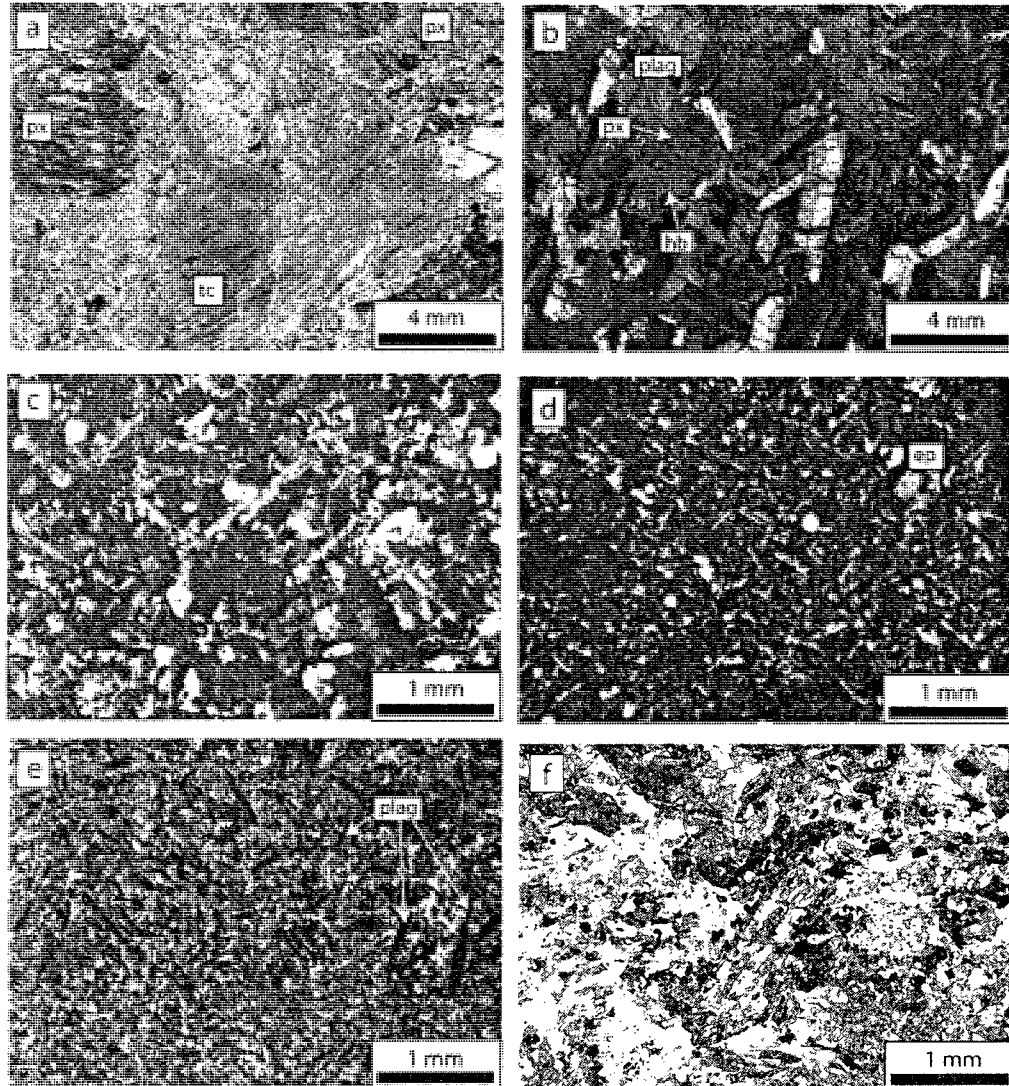


Fig. 3. 6. Photomicrograph of the Fawakhir ophiolite and the mélange fragments. (a) Pyroxene (px) altered to talc (tc) and iron oxide arranged along the cleavage in the pyroxenite of the Fawakhir area. (XPL) (b) Plagioclase (plag) and hornblende (hb) association in the gabbro of the Fawakhir ophiolite with pyroxene (px) relict in the core. (XPL) (c) Doleritic texture of the sheeted dike complex of the Fawakhir ophiolite. (XPL) (d) Intergranular plagioclase laths of the pillow lava, of the Fawakhir ophiolite, enclosing epidote pseudo-phenocryst (ep). (XPL) (e) Long thin turbid plagioclase microphenocrysts (plag) with the finer plagioclase laths of the pillow lava of the eastern mélange blocks. (PPL) (f) Porphyritic andesite with chloritized brown hornblende of the calc-alkaline dike cutting ophiolitic rocks. (PPL). XPL, crossed polarized light. PPL, plane polarized light.

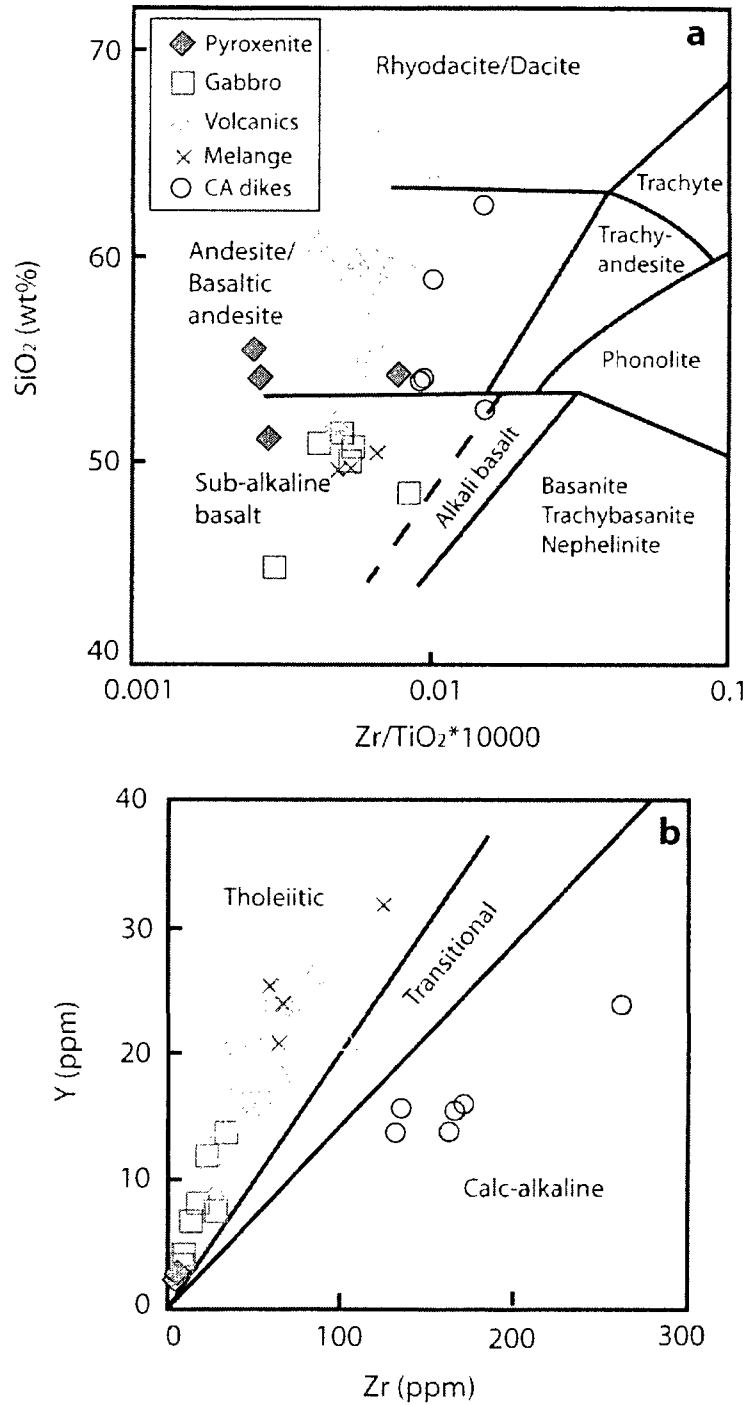


Fig. 3.7. (a) Zr/TiO₂ versus SiO₂ diagram of Winchester and Floyd (1977) for the ophiolitic rocks and cutting dikes and the eastern mélangé rocks. (b) Zr versus Y diagram of Barrett and MacLean (1994) to distinguish the magma series of the different rock types.

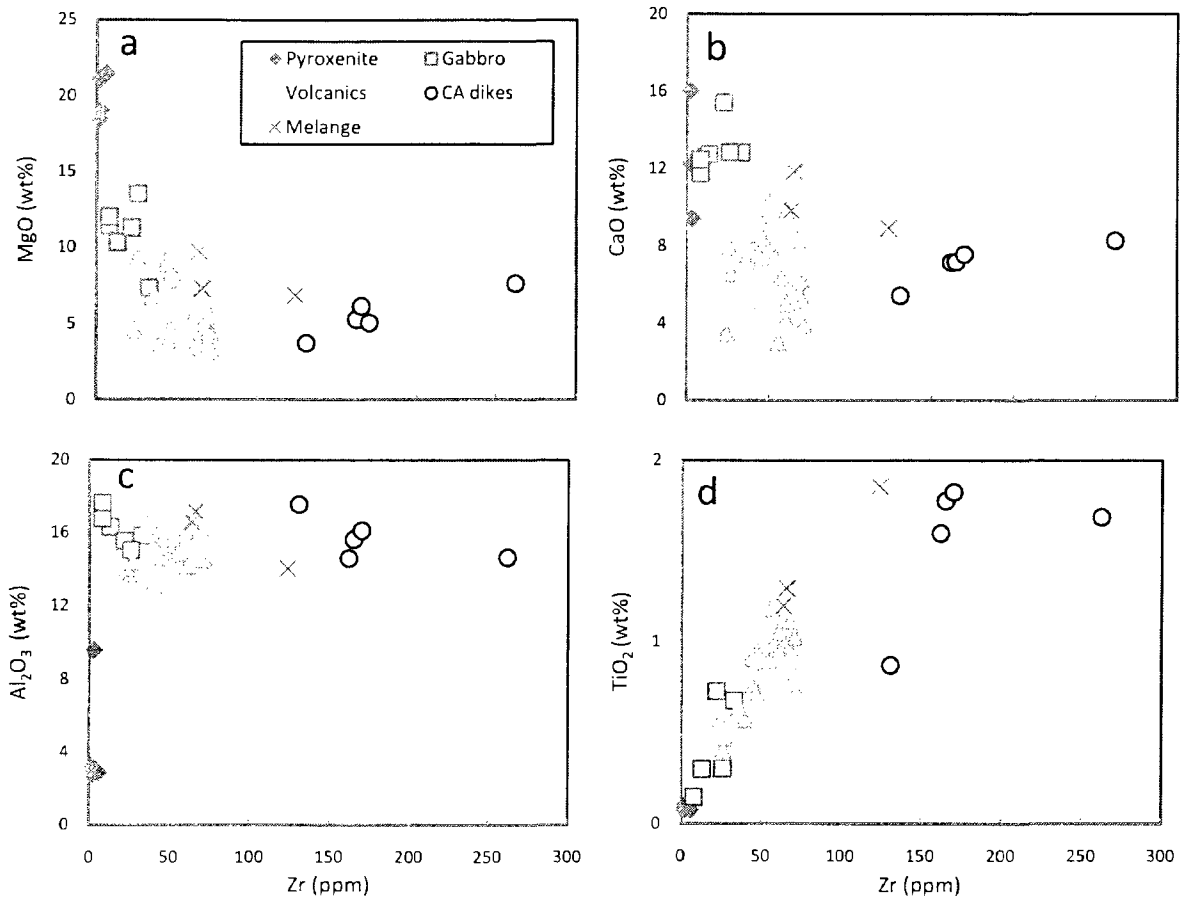


Fig. 3.8. Variation diagrams of Zr versus major and minor elements, (a) MgO, (b) CaO, (c) Al₂O₃, and (d) TiO₂ of the Fawakhir ophiolite and cutting dikes and the eastern mélangé rocks.

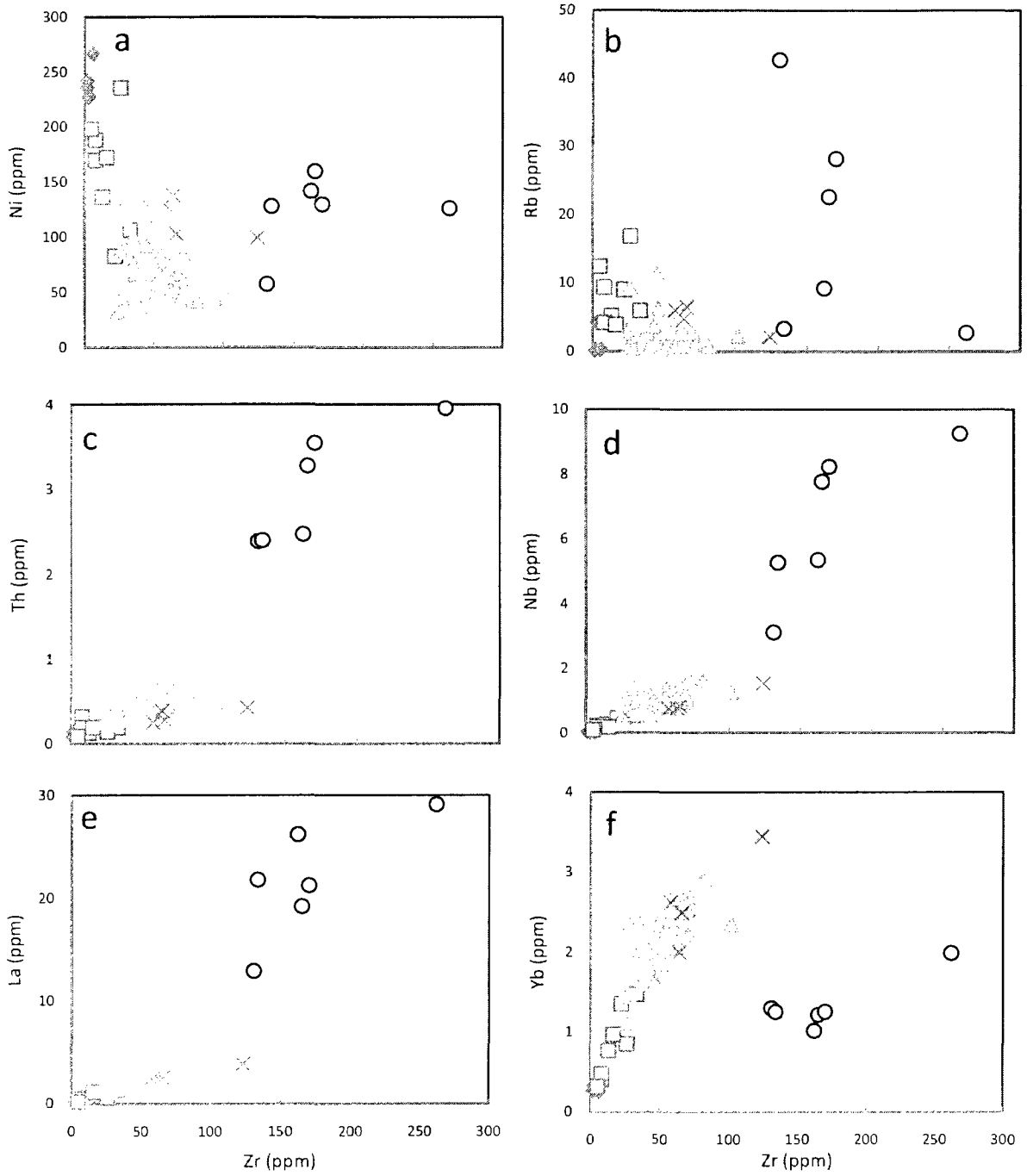


Fig. 3.9. Variation diagrams of Zr versus trace elements, (a) Ni, (b) Rb, (c) Nb, (d) Th, (e) La, and (f) Yb of the Fawakhir ophiolite and cutting dikes and the eastern mélangé rocks (Symbols as Fig. 3.8).

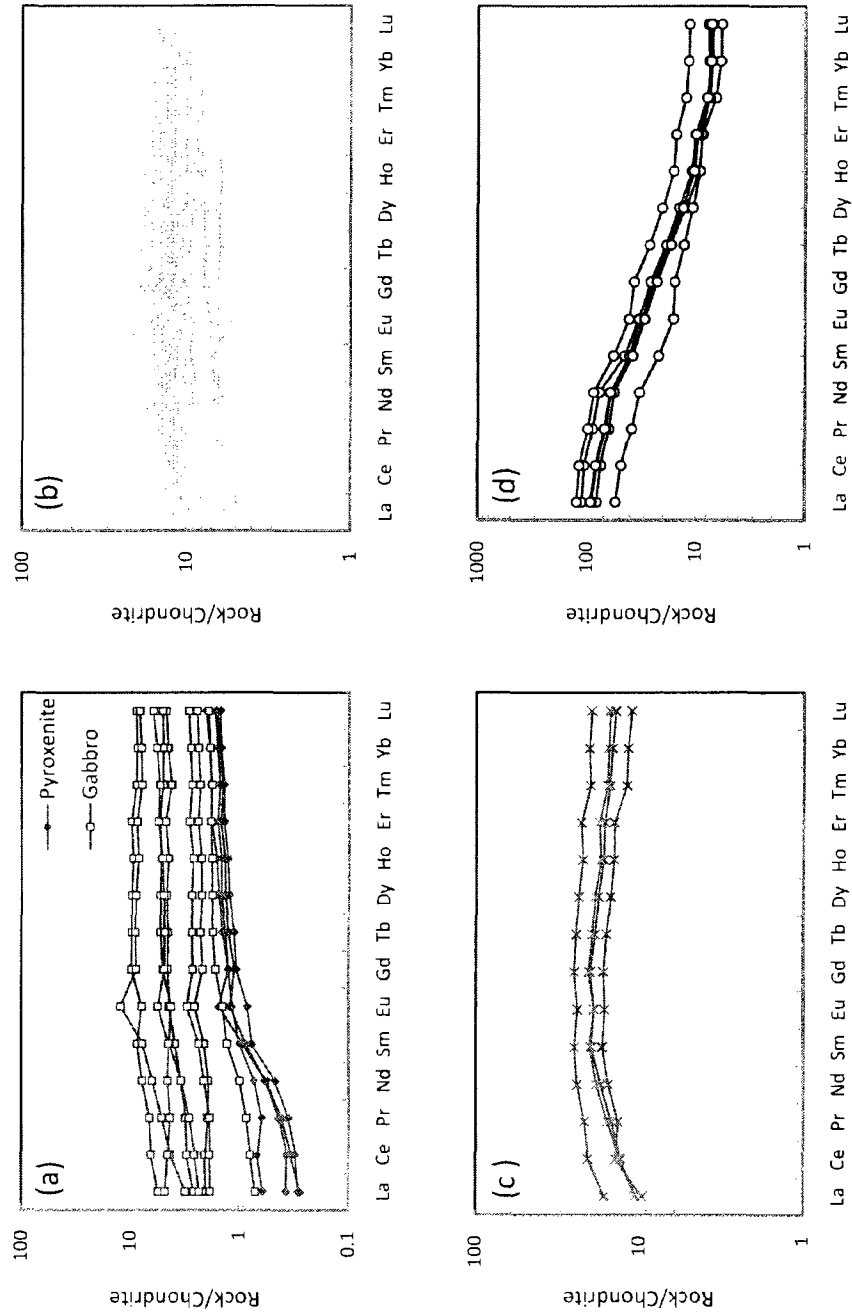


Fig. 3.10. Chondrite-normalized REE patterns for, (a) Ophiolitic pyroxenite and gabbros, (b) Ophiolitic pillow lavas (c) Eastern mélangé volcanic blocks, (d) Calc-alkaline dikes. (Normalizing chondrite values from Sun and McDonough, 1989).

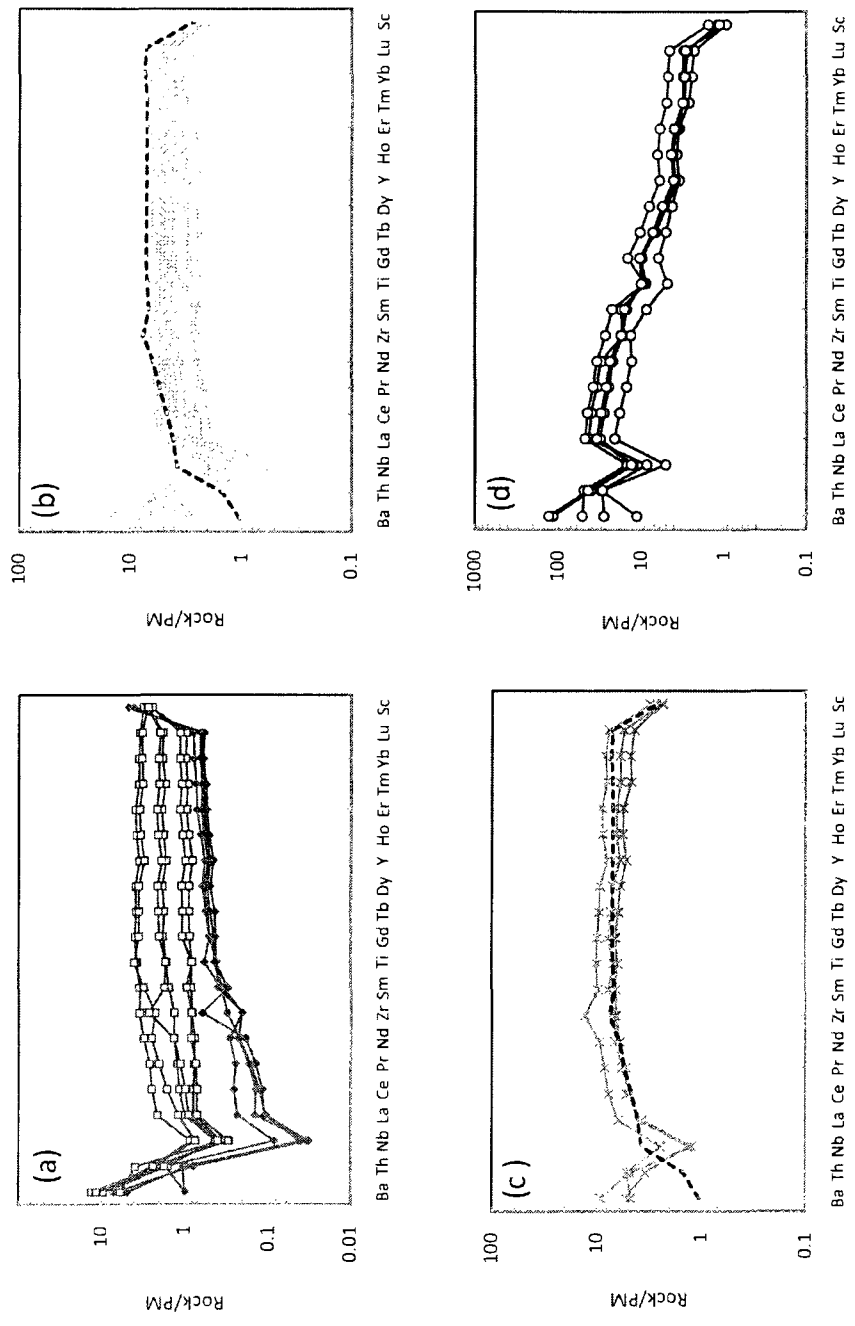


Fig. 3.11. Primitive mantle-normalized trace elements patterns for, (a) Ophiolitic pyroxenite and gabbros, (b) Ophiolitic pillow lavas (c) Eastern mélange volcanic blocks, (d) Calc-alkaline dikes. (Normalizing primitive mantle values after Hofmann, 1988). Dashed line represents N-MORB (N-MORB values after Sun and McDonough, 1989).

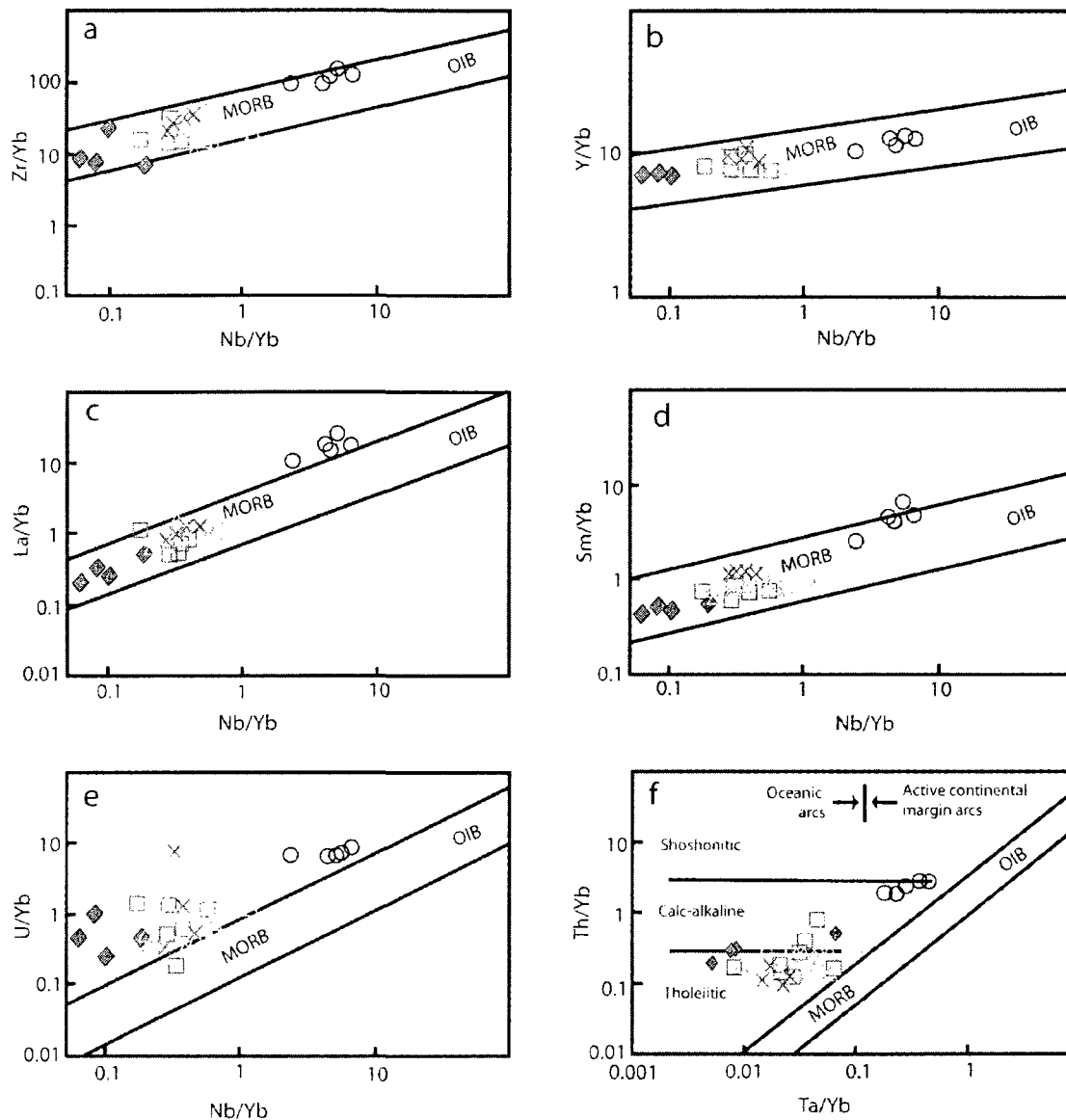


Fig. 3.12. (a-e) Plot of M/Yb versus Nb/Yb for the ophiolitic rocks and associated dikes at the Wadi Ghadir area where M is, (a) Zr, (b) Y, (c) La, (d) Sm, (e) U. MORB and OIB represent the position of the mid-ocean ridge and oceanic island mantle source respectively. The mantle array (MORB-OIB array) after Green (2006). (f) Th/Yb versus Ta/Yb diagrams with mantle array after Pearce (1983) (Symbols as Fig. 3.8).

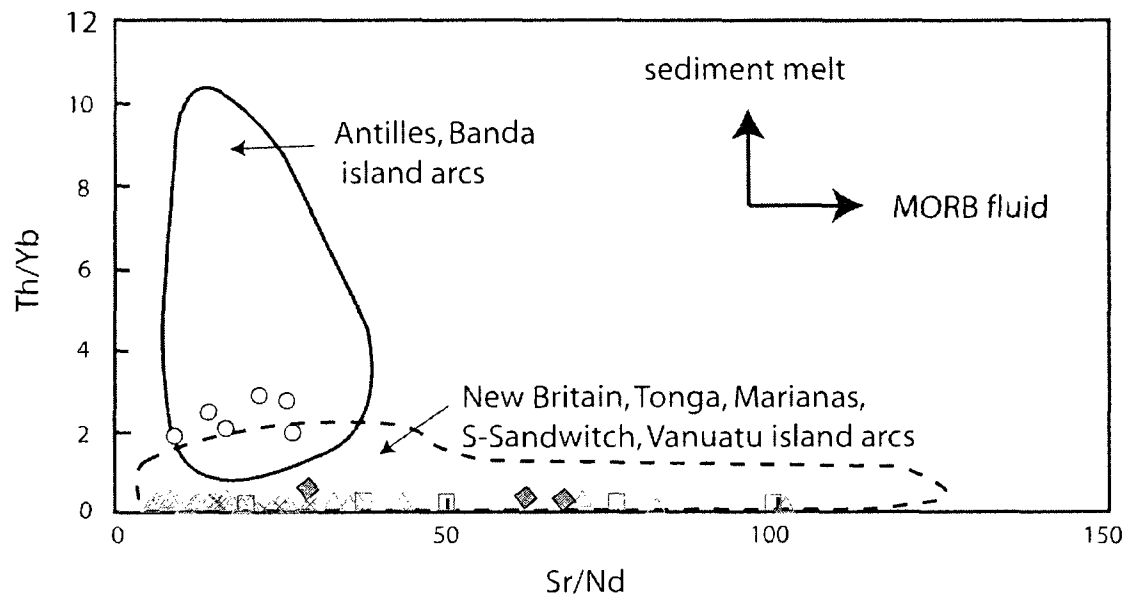


Fig. 3.13. Variation in Th/Yb versus Sr/Nd as an indicator of the nature of contribution for the subducted slab to the mantle wedge after Schuth et al., 2004. (Fields of various island arc settings from Woodhead et al., 1998) (Symbols as Fig. 3.8).

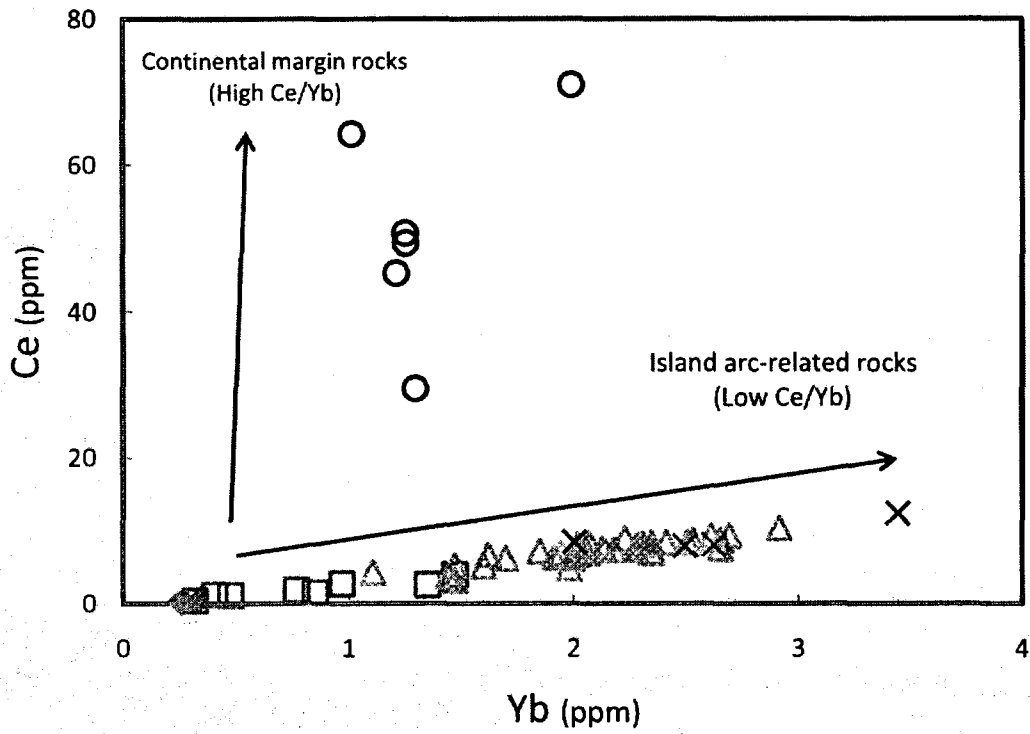


Fig. 3.14. Variation of Ce and Yb contents of the ophiolitic rocks of Wadi Ghadir and associated dikes. Island arc (Low Ce/Yb) and continental margin (High Ce/Yb) trends after Hawkesworth et al. (1993) (Symbols as Fig. 3.8).

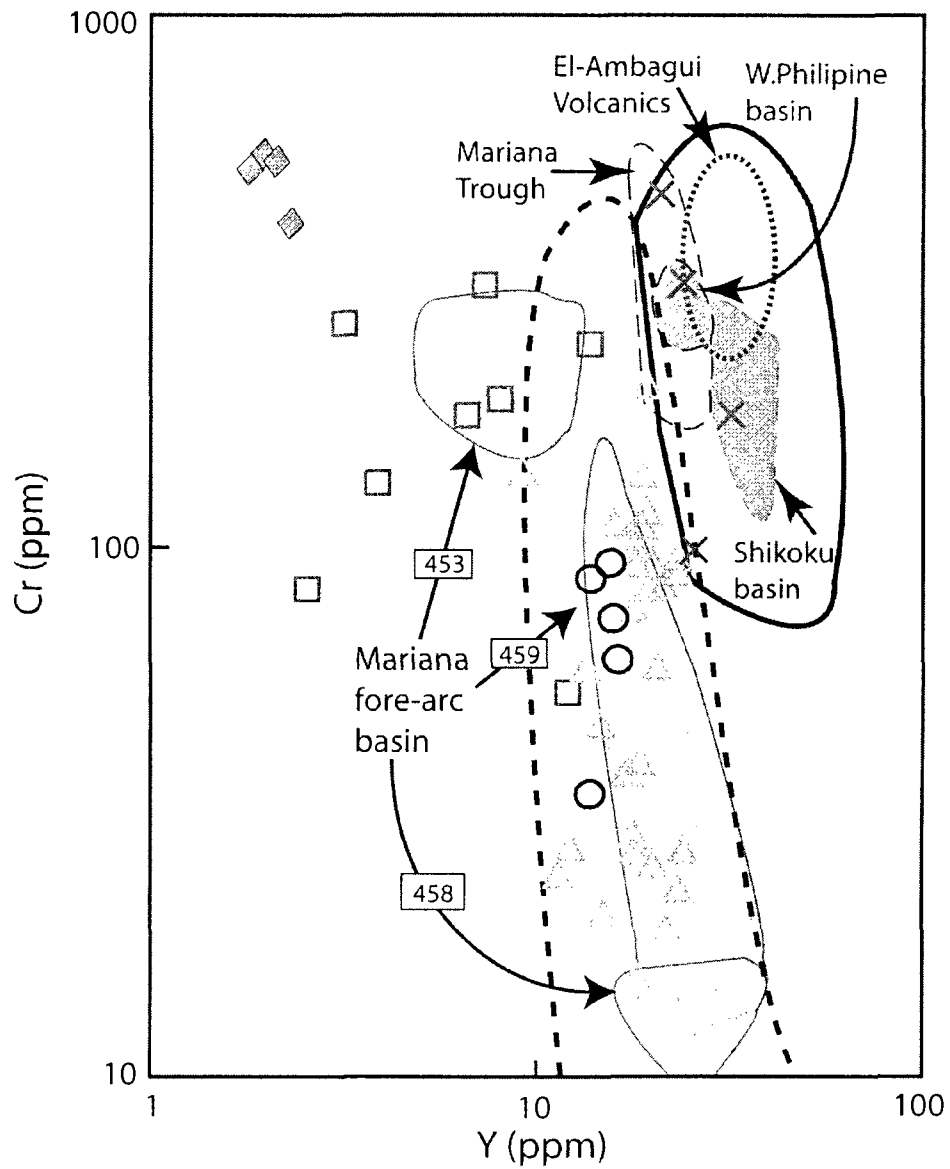


Fig. 3.15. Cr-Y discrimination diagram of Pearce et al. (1984) for the Fawakhir ophiolite, calc-alkaline dikes and eastern mélangé blocks. (The Mariana forearc, Mariana Trough, West Philippine basin, and Shikoku basin fields from Crocket and Oshin, 1987; El-Ambagui field from El-Mahallawi, 1994) (Symbols as Fig. 3.8).

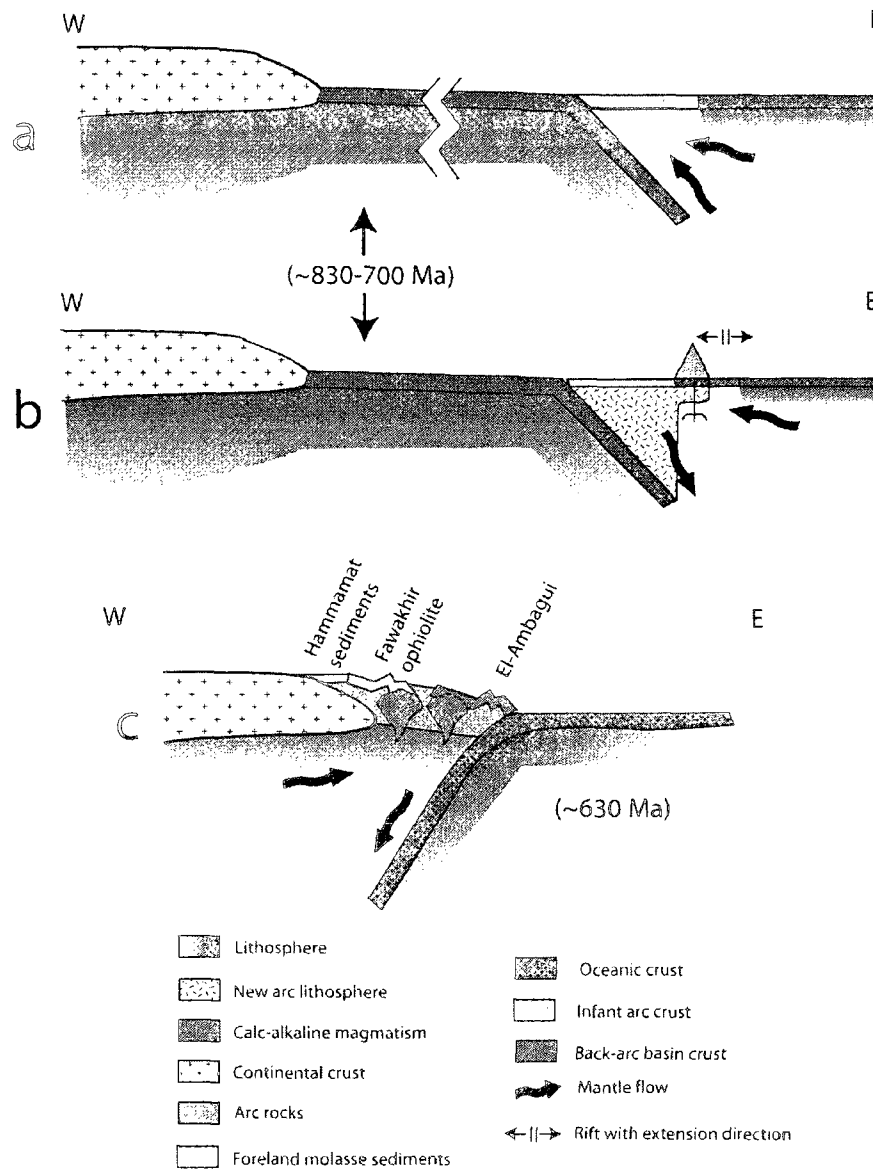


Fig. 3.16. Schematic model for the tectonic evolution of the Fawakhir ophiolite and central Eastern Desert along the Qift-Qusier Road. (a) The formation of nascent arc crust and lithosphere. (b) The formation of arc-back-arc rocks. (c) Obduction-accretion of the oceanic crust-arc association and reversing the subduction polarity from east-dipping to west-dipping and the formation of calc-alkaline magmatism related to Andean-type continental margin and associated foreland sedimentation of Hamammat sediments. (a and b are depicted from Fig. 8 of Stern and Bloomer, 1992). Orientations are in the present coordinate system and ages are approximate after Stern (2007).

Lithology	Mineral assemblage
Pyroxenites	Clinopyroxene + talc ± tremolite ± serpentinite ± plagioclase ± opaques
Gabbros	Plagioclase + augite + hornblende + actinolite + chlorite ± epidote ± calcite ± titanite ± opaques
Sheeted dikes and Pillows	Plagioclase + chlorite + actinolite + epidote ± titanite
Actinolite schists	Actinolite + plagioclase ± quartz ± epidote ± opaques
Andesitic dikes	Plagioclase + hornblende + chlorite ± quartz ± epidote ± apatite ± opaques

Table 3.1. Mineralogical composition of Qit-Qusier ophiolitic rocks

Element	DNC-1		BIR-1	
	Measured	Recommended	Measured	Recommended
SiO ₂	48.1	47	49.0	47.8
Al ₂ O ₃	18.7	18.3	15.8	15.4
Fe ₂ O ₃ ^(T)	9.76	9.93	11.26	11.3
MnO	0.15	0.15	0.18	0.17
MgO	10.2	10.1	9.68	9.68
CaO	11.6	11.3	13.7	13.2
Na ₂ O	1.67	1.87	1.6	1.75
K ₂ O	0.27	0.234	0.09	0.03
TiO ₂	0.49	0.48	0.99	0.96
P ₂ O ₅	0.08	0.09	0.03	0.05

Table 3.2. Measured and recommended major elements values for USGS standards DNC-1 and BIR-1

Element	BHVO-2 (n=21)		BHVO-1 (n=11)	
	Measured	Recommended	Measured	Recommended
Li	4.2	5.0	4.69	
V	313	317	321	
Cr	258	280	247	
Co	44	45	45	
Ni	155	119	150	
Cu	133	127	144	
Zn	110	103		
Rb	8.9	9.8	9.2	
Sr	382	389	390	
Y	22.8	26.0	23.3	28
Zr	156	172	165	179
Nb	14.3	18.0	14.9	19
Cs	0.10		0.11	0.13
Ba	128	130	128	139
La	14.7	15	14.8	16
Ce	36.7	38	37.0	39
Pr	5.18		5.13	5.4
Nd	23.8	25.0	23.4	25
Sm	5.90	6.20	5.83	6.4
Eu	1.98		1.97	2.06
Gd	6.23	6.30	6.20	6.4
Tb	0.89	0.90	0.91	0.96
Dy	5.1		5.10	5.2
Ho	0.94	1.04	0.95	0.99
Er	2.5		2.47	
Tm	0.32		0.31	0.33
Yb	1.92	2.00	1.88	2
Lu	0.26	0.28	0.26	0.29
Hf	4.23	4.10	4.52	4.4
Ta	0.9	1.04	0.86	1.2
Pb	2.58		4.18	2.6
Th	1.6	1.20	1.40	1.1
U	0.43		0.44	

Table 3.3. Measured and recommended values for USGS standards BHVO-1 and BHVO-2.

	Metapyroxenite				Metagabbro							
	EGY6-08	EGY6-09	EGY6-10	EGY6-11	EGY4-10	EGY4-18	EGY4-19	EGY6-15	EGY6-16	EGY6-17	EGY6-20	EGY6-37
SiO ₂ (wt%)	54.3	55.5	51.2	54.2	51.5	50.9	50.7	44.9	50.0	48.5		
Al ₂ O ₃	2.89	2.79	9.56	3.22	15.8	16.3	17.6	15.5	16.8	15.0		
Fe ₂ O ₃ ⁱ	8.20	7.82	9.81	7.79	9.23	7.13	6.68	10.47	6.31	8.09		
MnO	0.14	0.19	0.20	0.17	0.15	0.14	0.12	0.22	0.13	0.15		
MgO	21.5	21.0	19.0	18.4	7.3	10.3	11.5	11.3	12.0	13.5		
CaO	12.7	12.3	9.4	16.0	12.8	12.8	11.8	15.4	12.5	12.8		
Na ₂ O	0.23	0.29	0.66	0.32	2.18	1.79	1.35	0.96	1.66	0.79		
K ₂ O	<0.01	<0.01	0.09	<0.01	0.33	0.28	0.18	0.41	0.51	0.77		
TiO ₂	0.08	0.08	0.10	0.07	0.68	0.30	0.15	0.73	0.15	0.31		
P ₂ O ₅	0.01	0.01	<0.01	<0.01	0.06	0.03	0.02	0.08	0.02	0.02		
LOI	2.86	2.4	4.58	1.88	3.66	3.47	3.29	3.61	3.01	3.99		
Mg-number	84	84	79	82	61	74	77	68	79	77		
Cr (ppm)	526	558	411	541	243	177	266	53	133	314	83	190
Sc	71	72	61	72	47	41	38	42	37	41		
V	193	182	183	175	248	165	135	295	143	171	87	120
Co	69	54	63	54	33	33	35	42	40	49	41	46
Ni	267	236	228	242	106	136	169	83	188	236	198	172
Rb	0.2	0.1	4.2	0.2	5.95	5.18	4.23	9.0	9.4	16.8	12.4	3.9
Cs	0.0	0.0	0.1	0.0	0.45	0.48	0.63	0.4	1.5	0.7	2.6	0.2
Ba	30	6	43	6	61	58	36	80	58	70	97	119
Sr	15	17	36	10	72	121	134	293	155	80	242	79
Pb	0.58	1.53	1.12	0.82	9.70	1.80	1.97	2.21	1.02	0.76	1.31	3.78
U	0.01	0.03	0.02	0.01	0.06	0.04	0.04	0.03	0.02	0.04	0.04	0.13
Th	0.08	0.08	0.06	0.14	0.19	0.13	0.32	0.19	0.19	0.14	0.09	0.19
Y	1.78	1.94	2.28	2.05	13.8	6.54	3.18	12.0	3.88	7.41	2.55	8.05
Zr	6	2	3	2	33	13	8	22	8	26	5	16
Hf	0.07	0.10	0.08	0.35	1.05	0.64	0.34	0.53	0.27	0.43	0.16	0.52
Nb	0.03	0.02	0.02	0.05	0.53	0.27	0.22	0.46	0.19	0.25	0.09	0.17
Ta	0.002	0.002	0.002	0.018	0.04	0.01	0.02	0.03	0.02	0.05	0.01	0.02
La	0.07	0.09	0.07	0.14	1.30	0.61	0.48	0.73	0.44	0.55	0.17	1.12
Ce	0.19	0.22	0.21	0.42	3.94	1.84	1.25	2.60	1.14	1.57	0.48	2.75
Pr	0.03	0.04	0.04	0.06	0.64	0.30	0.19	0.49	0.18	0.27	0.08	0.41
Nd	0.22	0.27	0.27	0.34	3.67	1.59	0.90	2.94	0.99	1.60	0.46	2.12
Sm	0.12	0.13	0.14	0.15	1.34	0.60	0.32	1.19	0.36	0.67	0.20	0.68
Eu	0.05	0.07	0.09	0.07	0.46	0.25	0.15	0.71	0.17	0.25	0.08	0.32
Gd	0.22	0.23	0.26	0.26	2.03	0.93	0.44	1.82	0.55	1.03	0.34	1.00
Tb	0.04	0.05	0.05	0.05	0.36	0.17	0.08	0.33	0.10	0.19	0.06	0.18
Dy	0.32	0.34	0.39	0.37	2.48	1.18	0.56	2.26	0.69	1.34	0.45	1.25
Ho	0.07	0.08	0.09	0.08	0.54	0.26	0.13	0.48	0.15	0.29	0.10	0.29
Er	0.23	0.25	0.30	0.26	1.63	0.78	0.40	1.45	0.47	0.89	0.30	0.92
Tm	0.04	0.04	0.05	0.04	0.23	0.11	0.06	0.20	0.07	0.13	0.05	0.14
Yb	0.25	0.26	0.32	0.27	1.47	0.77	0.40	1.35	0.47	0.85	0.32	0.97
Lu	0.04	0.04	0.05	0.04	0.22	0.12	0.06	0.21	0.07	0.13	0.05	0.15
Mo	0.28	0.09	0.09	0.09	0.49	0.50	0.32	0.10	0.09	0.34	0.12	0.14
Cu	7.5	5.3	2.4	7.5	5.5	74.9	39.4	10.2	32.2	17.1	84.0	76.0
Zn	37.6	41.3	46.4	38.5	77.3	48.2	40.1	62.6	35.1	193.9	35.0	64.0
Ga	9.6	6.3	17.0	8.4	34.3	27.7	21.4	37.5	26.7	28.6	28.0	35.9
Al ₂ O ₃ /TiO ₂	38	35	91	43	23	54	120	21	113	49		
Nb/Y	0.014	0.011	0.009	0.025	0.038	0.041	0.070	0.038	0.048	0.033	0.035	0.021
La/Yb _{cn}	0.20	0.25	0.15	0.38	0.63	0.58	0.86	0.39	0.66	0.46	0.38	0.83
La/Sm _{cn}	0.37	0.42	0.30	0.61	0.63	0.66	0.96	0.40	0.78	0.53	0.54	1.06
Gd/Yb _{cn}	0.73	0.74	0.67	0.79	1.14	1.00	0.91	1.11	0.96	1.01	0.89	0.85
Eu/Eu*	0.93	1.24	1.41	1.04	0.85	1.04	1.21	1.48	1.20	0.90	0.98	1.20
Ce/Ce*	0.95	0.91	0.99	1.10	1.06	1.06	1.03	1.07	1.00	1.00	1.01	1.00
Tu/Zr	77	238	210	224	123	139	110	199	111	71		
Latitude (N)	25° 58'	25° 58'	25° 58'	25° 58'	25° 58'	25° 58'	25° 58'	25° 58'	25° 58'	25° 58'	25° 58'	25° 58'
	2.6"	2.7"	3.4"	3.2"	33.56"	23.3"	25.1"	13.8"	15"	24.8"	25.7"	45"
Longitude (E)	33° 38'	33° 38'	33° 38'	33° 38'	33° 39'	33° 38'	33° 38'	33° 38'	33° 38'	33° 38'	33° 38'	33° 38'
	34.3"	34.3"	34.4"	35.6"	7.92"	53.63"	55.79"	47"	50.3"	52.8"	50.8"	6.4"

Table 3.4. Major (wt%) and trace elements (ppm) concentrations and significant element ratios for ophiolitic gabbro and pyroxenite

Metavolcanics												
	EGY-06-13	EGY-04-08	EGY-04-09	EGY-04-11	EGY-04-12	EGY-04-14	EGY-04-15	EGY-04-17	EGY-06-41	EGY-06-42	EGY-06-43	EGY-06-44
SiO ₂ (wt%)	55.7	59.1	57.6	57.9	56.1	58.6	59.9	60.0	60.8	64.3	66.0	52.3
Al ₂ O ₃	13.7	15.1	15.4	16.3	15.9	15.8	14.2	15.3	14.0	14.5	13.1	15.9
Fe ₂ O ₃ [†]	9.37	8.88	10.08	9.71	11.02	10.38	10.39	11.11	11.42	8.51	6.62	9.76
MnO	0.18	0.13	0.12	0.12	0.14	0.15	0.15	0.16	0.16	0.13	0.15	0.18
MgO	9.36	5.50	4.96	5.52	5.09	4.43	4.17	3.45	4.60	3.19	3.78	9.05
CaO	7.91	6.17	6.37	4.21	8.32	5.20	9.82	5.02	3.48	3.92	5.15	7.58
Na ₂ O	2.82	4.02	4.25	4.99	2.05	4.22	0.20	3.72	4.80	4.47	4.36	4.02
K ₂ O	0.47	0.16	0.13	0.18	0.13	0.09	0.05	0.13	0.16	0.07	0.02	0.19
TiO ₂	0.40	0.82	1.00	0.99	1.12	1.03	1.06	0.94	0.57	0.73	0.58	0.89
P ₂ O ₅	0.05	0.11	0.11	0.10	0.12	0.11	0.12	0.10	0.07	0.17	0.17	0.09
LOI	1.84	6.36	4.62	4.08	5.33	4.55	5.2	2.53	2.95	4.52	2.94	3.32
Mg-number	66	55	49	53	48	46	44	38	44	43	53	65
Cr (ppm)	139	205	117	137	95	90	84	93	24	27	29	110
Sc	39	27	31	33	35	32	29	32	38	28	25	40
V	188	235	312	274	362	249	322	365	320	123	164	295
Co	39	26	28	27	30	27	25	26	33	18	21	41
Ni	123	84	69	75	68	62	56	53	32	37	37	125
Rb	9.3	2.27	0.95	3.45	0.73	0.71	2.58	1.08	3.0	1.3	1.6	3.7
Cs	0.9	0.24	0.15	0.42	0.10	0.08	0.35	0.17	0.5	0.3	0.2	0.2
Ba	80	20	18	69	13	14	15	26	50	41	48	77
Sr	211	65	53	119	41	50	39	56	90	107	220	208
Pb	1.00	123.62	18.43	33.76	1.87	1.70	1.57	6.18	1.98	4.06	2.04	1.98
U	0.14	0.14	0.12	0.11	0.12	0.14	0.11	0.17	0.07	0.21	0.20	0.07
Th	0.38	0.50	0.35	0.38	0.41	0.48	0.42	0.51	0.26	0.64	0.64	0.36
Y	9.1	19.1	19.1	18.6	23.1	22.8	19.2	19.9	11.5	23.8	17.7	18.5
Zr	26	71	58	61	68	71	61	61	24	72	40	43
Hf	0.82	1.97	1.63	1.62	2.32	2.05	1.83	1.79	0.86	2.15	1.29	1.31
Nb	1.34	1.11	0.87	1.00	0.96	1.06	0.91	1.35	0.29	1.72	0.67	0.78
Ta	0.12	0.09	0.08	0.09	0.08	0.04	0.07	0.10	0.01	0.07	0.03	0.06
La	1.83	3.17	2.71	2.66	3.24	3.17	2.66	3.07	1.40	3.53	3.33	2.46
Ce	4.30	8.95	7.37	7.37	8.73	8.68	7.39	8.13	3.73	9.40	8.35	6.75
Pr	0.61	1.30	1.16	1.18	1.41	1.38	1.19	1.26	0.58	1.44	1.22	1.08
Nd	2.98	6.65	6.24	6.17	7.37	7.07	6.09	6.40	3.06	7.47	6.06	5.80
Sm	0.97	2.17	2.08	2.05	2.46	2.39	2.10	2.18	1.07	2.52	1.89	1.97
Eu	0.36	0.74	0.72	0.79	0.92	0.81	0.76	0.73	0.32	0.87	0.79	0.82
Gd	1.33	2.94	2.90	2.88	3.39	3.35	2.86	2.96	1.56	3.47	2.51	2.75
Tb	0.23	0.51	0.52	0.51	0.61	0.59	0.51	0.52	0.28	0.61	0.44	0.48
Dy	1.60	3.40	3.44	3.40	4.09	4.01	3.46	3.51	1.97	4.15	3.03	3.28
Ho	0.35	0.74	0.75	0.73	0.90	0.87	0.76	0.78	0.44	0.89	0.66	0.70
Er	1.08	2.31	2.34	2.25	2.71	2.72	2.29	2.41	1.38	2.74	2.08	2.14
Tm	0.16	0.33	0.33	0.33	0.39	0.38	0.33	0.35	0.21	0.40	0.30	0.30
Yb	1.11	2.23	2.18	2.13	2.65	2.53	2.18	2.30	1.44	2.69	2.07	2.01
Lu	0.17	0.35	0.33	0.32	0.41	0.38	0.33	0.36	0.22	0.41	0.32	0.30
Mo	0.08	0.76	0.46	0.47	0.33	0.42	0.33	0.40	0.20	0.20	0.89	0.11
Cu	4.0	11.6	13.6	54.3	9.9	9.4	8.0	36.2	114.4	20.0	96.3	14.2
Zn	56.3	82.5	48.8	82.0	54.9	56.0	64.4	87.5	62.0	100.9	450.8	77.4
Ga	32.4	35.3	32.1	34.1	37.8	31.1	33.5	30.7	27.1	34.3	28.2	35.7
Al ₂ O ₃ /TiO ₂	34	18	15	17	14	15	13	16	25	20	23	18
Nb/Y	0.147	0.058	0.046	0.054	0.042	0.046	0.047	0.068	0.025	0.072	0.038	0.042
La/Yb _{cn}	1.19	1.02	0.89	0.89	0.88	0.90	0.88	0.96	0.70	0.94	1.16	0.88
La/Sm _{cn}	1.22	0.94	0.84	0.84	0.85	0.86	0.82	0.91	0.85	0.90	1.14	0.81
Gd/Yb _{cn}	0.99	1.09	1.10	1.11	1.05	1.09	1.08	1.06	0.89	1.06	1.00	1.13
Eu/Eu*	0.98	0.90	0.90	0.99	0.96	0.85	0.96	0.89	0.77	0.90	1.12	1.08
Ce/Ce*	1.00	1.08	1.02	1.02	1.00	1.02	1.02	1.02	1.02	1.02	1.01	1.01
Ti/Zr	93	69	103	97	98	87	104	93	143	61	86	124
Latitude (N)	25° 58'	25° 58'	25° 58'	25° 58'	25° 58'	25° 58'	25° 58'	25° 58'	25° 58'	25° 58'	25° 58'	25° 58'
	49°	35 49°	34 79°	35 36°	34 07°	34°	31 4°	24 67°	38 5°	43 8°	36 1°	46 2°
	33 38°	33 39°	33 39°	33 39°	33 39°	33 39°	33 39°	33 38°	33 38°	33 38°	33 38°	33 38°
Longitude (E)	7°	11 66°	10 15°	12 64°	4 07°	8 75°	4 46°	54 28°	8 6°	10 3°	16 4°	17 9°

Table 3.5. Major (wt%) and trace elements (ppm) concentrations and significant element ratios for Metavolcanics

Metavolcanics

	EGY-06-44b	EGY-06-45	EGY-06-49	EGY-06-50	EGY-06-52	EGY-06-53	EGY-06-54	EGY-06-55	EGY-06-56	EGY-06-07	EGY6-25	EGY6-22
SiO ₂	54.8	52.0	54.8	59.6	51.1	59.7	59.4	59.5	58.6	59.3		
Al ₂ O ₃	16.5	16.2	15.3	14.4	15.7	14.8	15.0	15.0	14.6	15.7		
Fe ₂ O ₃ ¹	9.01	10.16	9.09	9.06	10.24	10.29	11.72	9.29	10.34	7.37		
MnO	0.16	0.17	0.21	0.17	0.15	0.13	0.16	0.13	0.15	0.10		
MgO	6.84	8.91	7.82	6.45	8.36	4.67	4.72	4.42	3.92	4.65		
CaO	7.23	8.58	7.39	6.58	10.80	7.43	3.04	6.26	9.28	8.45		
Na ₂ O	4.77	2.91	4.38	2.93	2.66	1.79	4.43	4.09	1.45	3.29		
K ₂ O	0.02	0.06	0.19	0.33	-0.01	0.18	0.27	0.19	0.63	0.33		
TiO ₂	0.64	0.92	0.76	0.48	0.95	0.90	1.18	0.94	0.91	0.73		
P ₂ O ₅	0.07	0.09	0.07	0.06	0.08	0.10	0.12	0.14	0.10	0.11		
LOI	5.8	7.03	3.93	5.95	6.1	4.15	5.89	6.29	7.96	4.82		
Mg-number	60	63	63	59	62	47	44	49	43	56		
Cr	47	93	77	27	105	38	25	23	20	110	59	85
Sc	37	39	36	35	38	34	32	27	30	34		
V	260	293	253	267	278	272	390	250	369	219	112	193
Co	33	42	34	29	43	25	35	26	29	27	32	42
Ni	66	120	92	45	140	65	58	44	56	124	88	119
Rb	0.8	1.7	1.8	1.7	0.7	0.9	1.4	2.8	11.3	6.2	1.0	0.4
Cs	0.1	0.2	0.1	0.2	0.1	0.1	0.1	0.2	0.7	0.3	0.1	0.1
Ba	44	33	84	50	26	13	92	62	106	47	16	26
Sr	76	83	120	47	174	209	171	112	81	232	62	493
Pb	1.40	4.15	0.77	1.86	2.01	5.89	2.02	1.41	1.67	0.83	2.19	3.05
U	0.07	0.10	0.08	0.05	0.23	0.13	0.16	0.15	0.21	0.08	0.11	0.15
Th	0.32	0.40	0.24	0.22	0.53	0.44	0.42	0.48	0.49	0.31	0.29	0.33
Y	14.5	18.0	17.5	12.2	17.3	17.0	19.9	23.0	14.7	15.8	13.2	20.8
Zr	36	44	45	27	47	54	56	69	45	46	26	28
Hf	1.13	1.25	1.22	0.80	1.35	1.63	1.79	2.16	1.32	1.32	0.91	1.02
Nb	0.61	0.90	0.51	0.31	0.89	0.94	1.41	1.18	1.15	0.98	0.87	1.06
Ta	0.05	0.07	0.04	0.07	0.06	0.06	0.12	0.08	0.10	0.07	0.07	0.09
La	1.88	2.53	1.66	1.14	2.35	2.57	3.02	3.42	2.41	2.55	1.89	2.59
Ce	5.11	6.89	4.87	3.25	6.34	7.21	8.10	9.34	6.22	6.70	5.22	7.01
Pr	0.81	1.09	0.82	0.53	0.99	1.13	1.26	1.46	0.93	1.04	0.76	1.12
Nd	4.26	5.80	4.53	2.90	5.28	5.86	6.52	7.56	4.81	5.33	3.98	6.02
Sm	1.46	1.97	1.64	1.07	1.81	1.99	2.16	2.46	1.60	1.77	1.38	2.15
Eu	0.52	0.87	0.56	0.41	0.75	0.74	0.82	0.89	0.76	0.62	0.61	1.38
Gd	2.09	2.69	2.46	1.57	2.60	2.70	2.97	3.43	2.14	2.41	1.92	3.05
Tb	0.37	0.48	0.45	0.29	0.47	0.47	0.53	0.59	0.39	0.42	0.35	0.54
Dy	2.53	3.21	3.07	2.06	3.17	3.13	3.57	4.01	2.60	2.83	2.32	3.69
Ho	0.55	0.69	0.67	0.46	0.69	0.66	0.78	0.87	0.56	0.61	0.51	0.79
Er	1.67	2.08	2.03	1.44	2.06	1.96	2.37	2.67	1.71	1.80	1.53	2.41
Tm	0.24	0.30	0.29	0.21	0.29	0.28	0.34	0.39	0.25	0.25	0.22	0.34
Yb	1.60	1.94	1.98	1.47	1.92	1.85	2.28	2.61	1.70	1.62	1.47	2.34
Lu	0.25	0.29	0.30	0.22	0.28	0.28	0.35	0.40	0.25	0.24	0.22	0.35
Mo	0.10	0.52	0.40	0.38	2.71	0.17	0.36	0.18	1.63	0.15	0.11	0.07
Cu	68.8	212.7	94.6	44.6	48.0	38.5	130.2	58.2	63.5	55.1	28.0	44.3
Zn	68.5	247.9	216.2	138.6	1269.6	74.6	120.5	60.6	683.5	51.8	55.0	77.0
Ga	35.3	33.3	33.9	35.9	35.9	27.7	42.3	37.5	49.4	33.9	39.0	52.0
Al ₂ O ₃ -TiO ₂	26	18	20	30	16	16	13	16	16	22		
Nb Y	0.042	0.050	0.029	0.025	0.051	0.056	0.071	0.051	0.078	0.062	0.066	0.051
La Yb _{cn}	0.84	0.93	0.60	0.56	0.88	1.00	0.95	0.94	1.02	1.13	0.92	0.79
La Sm _{cn}	0.83	0.83	0.65	0.69	0.83	0.83	0.90	0.90	0.97	0.93	0.88	0.78
Gd Yb _{cn}	1.08	1.14	1.02	0.88	1.12	1.20	1.07	1.08	1.04	1.23	1.07	1.08
Eu Eu*	0.92	1.16	0.86	0.96	1.06	0.97	0.99	0.94	1.25	0.92	1.14	1.65
Ce Ce*	1.02	1.02	1.02	1.02	1.02	1.04	1.02	1.03	1.02	1.01	1.06	1.01
Ti Zr	106	125	101	105	121	100	127	82	121	95		
Latitude (N)	25° 58' 46.2"	25° 58' 35.9"	25° 58' 44.1"	25° 58' 35.5"	25° 58' 37.6"	25° 58' 38.6"	25° 58' 35.1"	25° 58' 31.5"	25° 58' 34.8"	25° 58' 22.2"	25° 58' 32.6"	25° 58' 31.9"
Longitude (E)	17.9° 33' 38"	21.5° 33' 38"	27.6° 33' 38"	29.3° 33' 38"	33.3° 33' 38"	33.3° 33' 38"	35.4° 33' 38"	45° 33' 38"	39.4° 33' 38"	0.5° 33' 38"	58.6° 33' 38"	39.2° 33' 38"

Table 3.5. (Continued)

Metavolcanics

	EGY6- 23	EGY6- 27	EGY6- 28	EGY6- 29	EGY6- 30	EGY6- 31	EGY6- 32	EGY6- 33	EGY6- 34	EGY6- 38	EGY6- 39	EGY6- 40
SiO ₂												
Al ₂ O ₃												
Fe ₂ O ₃												
MnO												
MgO												
CaO												
Na ₂ O												
K ₂ O												
TiO ₂												
P ₂ O ₅												
LOI												
Mg-number												
Cr	9	6	15	8	19	13	59	39	13	7	27	15
Sc												
V	222	179	133	87	161	170	101	130	160	179	121	138
Co	57	30	34	23	32	34	27	37	33	28	32	28
Ni	100	51	58	42	79	59	84	77	56	45	61	52
Rb	0.9	0.38	0.83	0.72	0.97	1.49	4.73	1.81	0.67	2.21	0.75	0.89
Cs	0.2	0.07	0.07	0.06	0.18	0.26	0.59	0.17	0.12	0.38	0.06	0.15
Ba	7	11	21	18	16	19	30	19	14	18	41	9
Sr	591	44	47	50	56	47	60	134	74	78	134	72
Pb	2.40	1.48	1.74	3.60	1.63	9.29	2.55	2.96	2.21	2.09	1.35	2.04
U	0.15	0.12	0.18	0.19	0.43	0.17	0.17	0.10	0.12	0.15	0.12	0.13
Th	0.33	0.36	0.44	0.62	0.76	0.50	0.45	0.32	0.33	0.48	0.30	0.40
Y	20.4	20.8	18.0	26.4	21.5	23.0	20.3	18.3	24.0	21.3	17.8	18.4
Zr	35	48	51	82	57	64	55	35	58	102	40	63
Hf	1.28	1.57	1.62	2.21	1.74	1.88	1.69	1.13	1.75	2.73	1.27	1.80
Nb	1.50	0.93	1.01	1.63	1.31	1.07	1.10	0.97	0.82	1.26	0.80	0.95
Ta	0.14	0.08	0.08	0.10	0.11	0.09	0.09	0.07	0.07	0.09	0.07	0.08
La	2.72	2.50	2.74	3.88	3.16	2.95	2.64	3.00	2.59	2.95	2.26	2.58
Ce	6.98	7.10	7.59	10.36	8.37	8.33	7.48	8.04	7.59	8.28	6.26	7.05
Pr	1.09	1.14	1.18	1.58	1.28	1.34	1.19	1.24	1.25	1.26	1.00	1.10
Nd	5.84	6.11	6.11	8.21	6.67	7.05	6.24	6.47	6.78	6.40	5.30	5.70
Sm	2.09	2.16	2.07	2.74	2.26	2.43	2.13	2.14	2.39	2.17	1.84	1.92
Eu	0.84	0.84	0.67	1.00	0.85	0.93	0.78	0.85	0.84	0.72	0.64	0.66
Gd	3.01	3.02	2.71	3.81	3.08	3.35	2.94	2.83	3.37	3.00	2.57	2.63
Tb	0.54	0.54	0.49	0.68	0.55	0.60	0.53	0.50	0.61	0.53	0.45	0.46
Dy	3.66	3.65	3.25	4.54	3.69	4.03	3.57	3.34	4.15	3.66	3.08	3.17
Ho	0.79	0.79	0.71	0.99	0.81	0.87	0.78	0.71	0.90	0.80	0.67	0.69
Er	2.41	2.41	2.16	3.04	2.46	2.64	2.35	2.12	2.73	2.42	2.04	2.12
Tm	0.35	0.35	0.31	0.44	0.36	0.38	0.34	0.30	0.40	0.35	0.29	0.31
Yb	2.35	2.34	2.13	2.92	2.41	2.50	2.27	2.02	2.65	2.34	1.99	2.06
Lu	0.35	0.35	0.32	0.43	0.37	0.38	0.34	0.29	0.40	0.35	0.30	0.31
Mo	0.40	0.09	0.08	0.12	4.09	0.12	0.70	0.11	0.16	1.13	0.07	0.15
Cu	13.9	9.9	32.6	8.5	24.0	8.2	46.3	9.2	19.1	44.7	57.9	28.2
Zn	101.2	47.5	67.2	52.4	2402.5	62.2	422.5	53.2	57.5	70.3	42.4	56.0
Ga	46.2	36.9	30.1	39.3	36.6	40.1	35.5	37.2	32.5	35.6	32.6	30.9
Al ₂ O ₃ /TiO ₂												
Nb/Y	0.073	0.045	0.056	0.062	0.061	0.047	0.054	0.053	0.034	0.059	0.045	0.052
La/Yb _{cn}	0.83	0.77	0.92	0.95	0.94	0.84	0.83	1.06	0.70	0.90	0.81	0.90
La/Sm _{cn}	0.84	0.75	0.86	0.91	0.90	0.79	0.80	0.91	0.70	0.88	0.79	0.87
Gd/Yb _{cn}	1.06	1.06	1.05	1.08	1.05	1.10	1.07	1.16	1.05	1.06	1.06	1.05
Eu/Eu*	1.03	1.01	0.86	0.94	0.99	1.00	0.95	1.06	0.91	0.86	0.91	0.90
Ce/Ce*	1.00	1.03	1.03	1.03	1.02	1.03	1.04	1.02	1.03	1.05	1.02	1.02
Ti/Zr												
Latitude (N)	25° 58'	25° 58'	25° 58'	25° 58'	25° 58'	25° 58'	25° 58'	25° 58'	25° 58'	25° 58'	25° 58'	25° 58'
	35.5"	34.1"	35"	35.4"	36.7"	35"	36.5"	36.5"	37.5"	35.1"	35.1"	35.4"
	33° 38'	33° 38'	33° 38'	33° 38'	33° 38'	33° 38'	33° 38'	33° 38'	33° 38'	33° 38'	33° 38'	33° 38'
Longitude (E)	35.8"	58.7"	58.3"	58.6"	59.5"	7"	6.5"	6.5"	6.7"	7.9"	7.9"	8.1"

Table 3.5. (continued)

	CA dike						Mélange			
	EGY-06-12	EGY-06-14	EGY-06-18	EGY-06-46	EGY-06-47	EGY-06-35	EGY-04-01	EGY-04-02	EGY-04-07	EGY-04-59
SiO ₂ (wt%)	58.9	52.5	62.5	54.2	54.0		49.8	49.8	50.5	
Al ₂ O ₃	14.6	14.7	17.6	15.6	16.1		16.6	17.2	14.0	
Fe ₂ O ₃ ¹	7.51	10.14	5.35	9.56	9.24		9.76	9.45	13.4	
MnO	0.15	0.21	0.08	0.13	0.12		0.15	0.16	0.21	
MgO	5.28	7.65	3.73	6.15	5.06		9.70	7.28	6.87	
CaO	7.14	8.27	5.42	7.17	7.56		9.83	11.84	8.92	
Na ₂ O	3.88	3.66	2.26	3.22	3.72		2.65	2.65	3.87	
K ₂ O	0.45	0.21	1.98	1.63	1.75		0.20	0.30	0.21	
TiO ₂	1.60	1.69	0.87	1.77	1.82		1.20	1.29	1.86	
P ₂ O ₅	0.51	0.94	0.20	0.57	0.62		0.09	0.10	0.16	
LOI	1.98	0.93	4.37	5.68	5.11		3.54	2.33	1.22	
Mg-number	58	60	58	56	52		66	60	50	
Cr (ppm)	87	90	34	94	61	74	473	317	180	99
Sc	14	23	14	18	17		35	36	47	
V	153	208	125	186	189	105	215	226	370	120
Co	41	30	19	35	31	29	40	40	40	45
Ni	142	126	58	159	130	128	138	103	99	129
Rb	9.2	2.7	42.7	22.6	28.1	3.3	4.73	6.47	2.12	6.01
Cs	1.0	0.1	1.3	0.4	1.3	0.0	0.53	0.36	0.14	0.39
Ba	69	308	171	690	778	580	56	32	29	40
Sr	513	687	143	684	608	771	213	202	176	196
Pb	2.25	3.21	4.76	4.40	4.31	6.97	4.28	3.65	99.4	2.12
U	0.74	1.53	0.88	1.10	1.12	0.77	0.27	2.02	0.17	0.09
Th	2.48	3.96	2.39	3.28	3.55	2.40	0.39	0.28	0.42	0.25
Y	13.8	23.9	13.7	15.3	16.1	15.7	20.7	23.9	31.6	25.4
Zr	162	262	131	165	170	134	64	66	124	58
Hf	3.88	5.96	3.38	3.88	4.11	3.44	1.91	1.30	2.23	1.97
Nb	5.35	9.25	3.12	7.77	8.23	5.27	0.76	0.82	1.53	0.75
Ta	0.29	0.48	0.24	0.52	0.47	0.29	0.03	0.04	0.10	0.06
La	26.22	29.12	12.94	19.22	21.29	21.82	2.27	2.51	3.86	2.46
Ce	64.3	71.0	29.6	45.3	49.3	50.7	8.49	7.92	12.5	8.08
Pr	8.42	9.27	3.70	5.99	6.45	6.59	1.28	1.41	2.05	1.49
Nd	36.0	40.4	15.4	26.3	28.2	28.5	7.23	8.04	11.2	8.54
Sm	6.87	8.70	3.37	5.82	6.19	5.83	2.57	3.00	3.79	3.07
Eu	1.95	2.37	0.93	1.78	1.91	1.72	0.97	1.16	1.36	1.09
Gd	5.22	7.36	3.21	5.05	5.37	4.69	3.40	4.10	5.13	4.17
Tb	0.64	0.98	0.47	0.66	0.69	0.62	0.59	0.69	0.89	0.72
Dy	3.14	5.15	2.70	3.38	3.60	3.31	3.83	4.53	5.98	4.74
Ho	0.54	0.92	0.53	0.59	0.62	0.60	0.81	0.94	1.27	0.98
Er	1.45	2.52	1.48	1.59	1.68	1.67	2.36	2.70	3.76	2.91
Tm	0.17	0.32	0.20	0.20	0.21	0.21	0.31	0.39	0.52	0.40
Yb	1.01	1.99	1.30	1.21	1.25	1.25	2.00	2.49	3.44	2.62
Lu	0.15	0.29	0.19	0.18	0.18	0.18	0.28	0.36	0.49	0.38
Mo	14.59	0.24	0.17	0.66	0.46	0.78	0.37	0.37	0.71	0.35
Cu	20.0	23.1	25.3	39.3	39.7	52.6	71.0	42.4	48.9	20.6
Zn	52.6	69.4	81.2	155.7	100.9	99.1	81.6	72.3	122.3	71.5
Ga	43.2	74.8	59.0	121.4	135.0	113.6	28.7	29.9	36.0	40.6
Al ₂ O ₃ /TiO ₂	9	9	20	9	9		14	13	8	
Nb/Y	0.39	0.39	0.23	0.51	0.51	0.34	0.04	0.03	0.05	0.03
La/Yb _{cn}	18.56	10.50	7.17	11.37	12.20	12.53	0.81	0.72	0.80	0.67
La/Sm _{cn}	2.46	2.16	2.48	2.13	2.22	2.42	0.57	0.54	0.66	0.52
Gd/Yb _{cn}	4.25	3.14	2.04	3.43	3.54	3.10	1.41	1.36	1.23	1.32
Eu/Eu*	1.00	0.89	0.86	1.01	1.02	1.01	0.98	0.96	0.96	0.94
Ce/Ce*	1.06	1.06	1.05	1.03	1.03	1.04	1.22	1.03	1.09	1.03
Ti/Zr	59	39	40	64	64		112	118	90	
Latitude (N)	25° 58'	25° 58'	25° 58'	25° 58'	25° 58'	25° 58'	26° 6'	26° 6'	26° 8'	26° 6'
Longitude (E)	37° 3'	7° 4'	25° 4'	35° 7'	37° 4'	40° 2'	33° 52'	24° 7'	1° 32'	16°
Longitude (E)	33° 38'	33° 38'	33° 38'	33° 38'	33° 38'	33° 38'	34° 12'	34° 21'	33° 55'	34° 12'
Longitude (E)	36° 5'	41° 5'	52° 1'	25° 2'	25° 7'	6° 2'	20° 05'	7° 64'	37° 74'	8° 5'

Table 3.6. Major (wt%) and trace elements (ppm) concentrations and significant element ratios for Calc-alkaline dikes and Mélange volcanics.

	Pyroxenite	Gabbros	Metavolcanics	CA dikes	Melange
SiO ₂	51.2-55.5	42.1-51.5	51.1-66.0	52.5-62.5	49.8-56.2
Al ₂ O ₃	2.8-9.6	15.0-18.9	13.1-16.5	14.6-17.6	14.0-17.2
Fe ₂ O ₃ ^l	7.8-9.8	6.3-14.0	6.6-11.7	5.4-10.1	9.5-13.4
MgO	18.4-21.5	7.3-13.5	3.2-9.4	3.7-7.7	4.8-9.7
CaO	9.4-16.0	11.8-15.4	3.0-10.8	5.4-8.3	8.0-11.8
TiO ₂	0.07-0.10	0.15-0.73	0.40-1.18	0.87-1.82	0.83-1.86
Mg - number	79-84	61-77	38-66	52-60	50-66
Cr	411-558	83-314	7-205	34-94	99-473
Sc	61-72	37-47	25-40	14-23	35-47
V	175-193	87-295	87-390	105-208	120-370
Co	54-69	33-49	18-57	19-41	40-45
Ni	228-267	83-198	32-140	58-159	99-138
Th	0.06-0.14	0.09-0.32	0.22-0.76	2.39-3.96	0.25-0.42
Y	1.78-2.28	2.55-13.8	9.1-26.5	13.7-23.9	20.7-31.6
Zr	2-6	5-33	24-102	131-262	58-124
Nb	0.02-0.05	0.09-0.53	0.31-1.72	3.12-9.25	0.75-1.53
La	0.07-0.14	0.17-1.3	1.14-3.88	19.2-29.1	2.27-3.86
Nd	0.22-0.34	0.9-3.67	2.9-7.56	15.4-40.4	7.23-11.2
Sm	0.12-0.15	0.2-1.34	0.97-2.52	3.37-8.7	2.57-3.79
Gd	0.22-0.26	0.34-2.03	1.33-3.81	3.21-7.56	3.4-5.13
Yb	0.25-0.32	0.4-1.47	1.11-2.65	1.01-1.99	2-3.44
La/Yb _{cn}	0.15-0.38	0.38-0.86	0.56-1.19	7.17-18.6	0.67-0.81
La/Sm _{cn}	0.3-0.61	0.4-1.06	0.65-1.22	2.13-2.48	0.52-0.66
Gd/Yb _{cn}	0.67-0.79	0.85-1.14	0.89-1.23	2.04-4.25	1.23-1.41
Eu/Eu*	0.93-1.41	0.85-1.48	0.77-1.65	0.86-1.02	0.94-0.98

Table 3.7. Summary of major (wt.%) and trace (ppm) elements concentrations and significant element ratios for the Wadi Ghadir ophiolitic complex and associated dikes.

Chapter 4

The provenance and tectonic setting of the Neoproterozoic Um Hassa Greywacke Member, Wadi Hammamat area, Egypt: Evidence from petrography and geochemistry

4.1. Introduction

The characteristics of siliclastic sedimentary rocks are controlled mainly by source composition, weathering, transportation and diagenetic processes (McLennan et al., 1993). Petrography of sandstones has been widely used to discriminate the tectonic setting of provenance (Dickinson and Suczek, 1979; Dickinson et al., 1983; Dickinson 1985; Hendrix, 2000). Geochemistry of clastic sedimentary rocks is an important tool for understanding the nature of the source rocks (Roser and Korsch, 1988; 1999; McLennan et al., 1993), weathering and erosion (Nesbitt and Young, 1982; 1996), the tectonic setting of the depositional basins (Bhatia, 1983; Bhatia and Crook, 1986; Roser and Korsch, 1986), and post-depositional modifications (Fedó et al., 1995, 1997).

The Eastern Desert of Egypt constitutes the northern end of the Nubian segment of the Arabian-Nubian Shield (ANS) (Fig. 4.1a). The ANS formed through a series of subduction, accretion and crustal thickening processes during the Neoproterozoic Pan-African Orogeny (Engel et al., 1980; Stern, 1994; Johnson and Woldehaimanot, 2003, Abd El-Rahman et al., 2009). The crustal evolution of the Eastern Desert is marked by the deposition of the molasse-type Hammamat Group (Eliwa et al., 2006). There are some controversies regarding the stratigraphic position, grade of metamorphism,

structure and tectonic significance of the Hammamat Group (Wilde and Youssef, 2002, and references therein).

The Hammamat sedimentary rocks are immature clastic rocks that were deposited through fluvial processes in intramontane basins (Grothaus, 1979). The tectonic setting of such deposits is a matter of debate. Following the intramontane basin hypothesis, Fritz and Messner (1999, and references therein) divided the molasse basins in the Eastern Desert into external foreland basins and Najd strike-slip-related extensional basins. Holail and Moghazi (1998) suggested that the Hammamat sediments were deposited in intra-arc basins. Anderson et al. (2007) proposed that they were deposited in piggy-back basins in the Wadi Hammamat area. However, Wilde and Youssef (2001, 2002) argued for the deposition of the Hammamat sediments in a major fluvial system of continental proportion rather than deposition in isolated intramontane basins. Their argument agrees with Ries et al.'s (1983) suggestion that at least the upper part of the Hammamat Group may have been continuous along the Central Eastern Desert.

The Hammamat Group in the Central Eastern Desert was divided into the lower Iglal Formation and the upper Shihimiya Formation (Akaad and Noweir, 1969; 1980). They divided the Shihimiya Formation lithostratigraphically into a lower Rasafa Siltstone Member followed by the Um Had Conglomerate Member and the upper Um Hassa Greywacke Member. This study reports the petrographical and geochemical characteristics of the uppermost part of the Hammamat Group, the Um Hassa Greywacke Member in the type locality in the Wadi Hammamat area. The objective of the study is to assess the composition and nature of the source rocks, and to determine the tectonic setting of the Um Hassa greywackes. Identifying the provenance and tectonic setting of

these sedimentary rocks will assist in a better understanding of the geodynamic evolution of the Central Eastern Desert proposed from the geochemistry of ophiolites in the previous chapters.

4.2. Field relations and characteristics

The best exposures of the Hammamat Group are located in the west of Qift-Qusier road at their type locality in the Wadi Hammamat area (Fig. 4.1b). The thickness of the Hammamat Group reaches 4000 m where the most complete succession of this group is recorded (Akaad and Noweir, 1969; 1980). To the west of Wadi Hammamat, the Hammamat Group is overlain unconformably by the Phanerozoic Nubian Sandstone (Fig. 4.2a) and is juxtaposed with the ophiolitic and arc-related rocks towards the east. The Hammamat Group is intruded by the Um Had granitic pluton to the north. The emplacement age of the Um Had granites is 596 Ma (Anderson et al., 2009) suggesting that the Hammamat Group was deposited before this age. Ries and Darbyshire (in Ries et al., 1983) suggested that the age of the Hammamat Group should not be younger than 616 Ma, which is the age of the calc-alkaline volcanic rocks (Dokhan Volcanics) from which fragments in the Hammamat Group were derived. Although the Dokhan-type volcanic rocks are thrust westwards over the Hammamat sedimentary rocks in the Wadi Hammamat area, the Hammamat sedimentary rocks originally rested unconformably on the Dokhan Volcanics and older units (Akaad and Noweir, 1980).

The Um Hassa Greywacke Member is the upper unit of the Hammamat Group and it lies conformably on the Um Had Conglomerate Member (Fig. 4.1c). Conglomerates are massive, poorly sorted and either clast- or matrix-supported. The fragments of the Um

Had conglomerate are mostly rounded to sub-angular (Fig. 4.2b). Polymictic conglomerates contain mainly pebbles of Dokhan-type volcanic rocks, granitic rocks, green tuffs, chert, jasper, and epidosite (Ries et al., 1983). The Um Hassa greywackes are mainly greenish-grey to brown, poorly sorted and bedded. Lamination, graded bedding and cross bedding are recorded in the Um Hassa greywackes. The entire Hammamat Group was folded into open NW-SE trending SW-verging folds (Ries et al., 1983; Holail and Moghazi, 1998). Pressure-solution cleavage is recorded in the Um Hassa greywackes especially in the finer grained varieties (Fig. 4.2c).

4.3. Petrography

In order to determine the modal composition of the Um Hassa greywackes, eleven medium to coarse-grained samples were counted to about 300 points using the Gazzi-Dikinson method (Dikinson, 1985). The results are presented (Table 4.1) as monocrystalline quartz (Qm), polycrystalline quartz (Qp), total feldspar (F), plagioclase (P) and K-feldspar (K), and matrix (M). The unstable lithic fragments comprise the volcanic/metavolcanic lithic fragments (Lv) and sedimentary/metasedimentary lithic fragments (Ls). However, total lithic fragments (Lt) stands for unstable lithic fragments and polycrystalline quartz (Lv+Ls+Qp).

The Um Hassa greywackes are poorly to moderately sorted. The detrital components vary from angular to sub-rounded embedded in a mostly silty matrix (> 15%). The matrix probably formed from the breaking down of lithic fragments. Quartz is the most abundant detrital component (Fig. 4.3a). Monocrystalline quartz (an average of

23%), is more abundant than polycrystalline quartz (11%). Most quartz grains exhibit undulatory extinction.

Lithic fragments make up 24% of the greywackes framework. The ratios of the volcanic and sedimentary lithic fragments are variable. Some of the lithic fragments exhibit metamorphism up to greenschist facies. The volcanic lithic fragments are mainly (meta-) andesites and felsites and less abundant mafic volcanic rocks (Fig. 4.3a). They are characterized by the presence of feldspar laths which are associated with quartz, sericite, chlorite, and/or epidote. The coarse-grained greywackes contain some microgranitic fragments with micrographic and myrmekitic quartz-feldspar intergrowth. The sedimentary lithic fragments comprise phyllosilicate-rich rocks such as quartz-sericite rocks (Fig. 4.3b). Sericite-chlorite and quartz-sericite schist fragments are classified as sedimentary lithic fragments.

Feldspar fragments constitute about 11% of the Um Hassa greywackes. Plagioclase (10%) is far more abundant than K-feldspar (1%). Plagioclase fragments are mostly fresh showing albite twinning (Fig. 4.3c). However, altered, mainly sericitized, plagioclase fragments are not uncommon. Other detrital components of the Um Hassa greywackes are epidote, mica, opaque minerals, chlorite, and carbonates (calcite) in order of decreasing abundance. Epidote, opaque minerals, and carbonates are represented by dispersed equant grains (Fig. 4.3d). On the other hand, micas are represented by long, commonly bent, muscovite flakes (Fig. 4.3b). The matrix of the Um Hassa Greywackes consists mainly of silt-size quartz, feldspar, chlorite, and epidote. Holail and Moghazi (1998) reported the presence of illite. Epidote and calcite occur, to a limited extent, as authigenic crystalline patches overprinting the matrix.

4.4. Analytical Methods

The samples were crushed and pulverized using an agate mill in the Department of Earth and Environmental Sciences, University of Windsor, Canada. Major elements and Sc were analyzed by a Thermo Jarrell-Ash Enviro II ICP at ACTLABS in Ancaster, Canada. The samples were fused then dissolved in 5% nitric acid. Totals of major element oxides are 100 ± 1 wt.% and the analytical precisions are 1-2%. International standards, DNC-1 and BIR-1, were used to estimate the accuracy of the major elements (Table 4.2).

Samples were analyzed for rare earth elements (REE), high field strength elements (HFSE), large ion lithophile elements (LILE) and transition metals (Ni, Co, Cr and V) by a high-sensitivity Thermo Elemental X7 ICP-MS in the Great Lakes Institute for Environmental Research (GLIER), University of Windsor, Canada, using the protocol of Jenner et al. (1990). Samples were dissolved in a concentrated HF-HNO₃ mixture in screw-top Teflon (Saville®) bombs and further attacked by HNO₃-H₃BO₃-H₂C₂O₄ and then with 50% HNO₃. Analytical precisions are estimated as follows: 1-10 % for REE, Rb, Sr, Ba, Y, Nb, Co, Cu, Zr, and U; 10-20% for V, Ni, Zn, Cs, Mo, and Ga; and 20-30% for Ta, Th, Cr, and Pb. BHVO-1 and BHVO-2, were used as international reference materials to estimate accuracy of the measured trace elements (Table 4.3)

4.5. Geochemical results

Major and trace element compositions of the Um Hassa greywackes are given in Table 4.4. The Um Hassa sandstones plot mostly in the greywacke field of the log

($\text{SiO}_2/\text{Al}_2\text{O}_3$) versus $\log(\text{Na}_2\text{O}/\text{K}_2\text{O})$ classification diagram of Pettijohn et al. (1972) (Fig. 4.4). In terms of major elements, the Um Hassa greywackes are characterized by 64.2-70.4 wt.% SiO_2 , 1.92-2.77 wt.% MgO , and 4.18-6.48 wt.% Fe_2O_3 . The MgO and Fe_2O_3 are negatively correlated with SiO_2 (Fig. 4.5a,b). The concentrations of MgO and Fe_2O_3 are higher than upper continental crust (UCC) contents of Taylor and McLennan (1985). On the other hand, Al_2O_3 and K_2O of the Um Hassa greywackes show no correlation with SiO_2 and their contents, 11.2-14.58 wt.% and 1.32-2.41 wt.% respectively, are lower than UCC values (Fig. 4.5c,d).

The Um Hassa greywackes have LREE-enriched chondrite-normalized patterns similar to Post-Archean Australian Shale (PAAS) and UCC patterns (Fig. 4.6a). However, the greywacke patterns are slightly less fractionated ($\text{La}/\text{Sm}_n=2.4-3.3$) relative to UCC ($\text{La}/\text{Sm}_n=4.3$). Europium anomalies in the greywackes ($\text{Eu}/\text{Eu}^*=0.61-0.79$) are similar to that of UCC ($\text{Eu}/\text{Eu}^*=0.65$). Upper continental crust-normalized patterns for the Um Hassa greywackes reveal significant enrichment of Cr (234-434 ppm) and Ni (49-72 ppm) but depletions in Nb (4.1-7.7 ppm), Rb (33-63 ppm), and Th (3.64-8.92 ppm) relative to UCC values (35, 20, 25, 112 and 10.7 ppm, respectively) (Fig. 4.6b).

4.6. Discussion

4.6.1. Effects of sedimentary processes on geochemistry

Although siliclastic sedimentary rocks contain a record of their provenance, their reliability as provenance indicators can be affected by sedimentary processes including weathering, transportation, and diagenesis. The effects of sedimentary processes on major and trace element geochemistry of siliclastic sediments are variable. The degree of

compositional changes of siliclastic sediments depends on the extent of the application of weathering erosion and transportation processes on the source rocks and the resulting fragments.

As chemical weathering is the major factor in changing the chemistry of source rocks, siliclastic sediments produced by physical weathering are the most reliable indicators of the provenance (Nesbitt, 2003). Weathering effects can be evaluated using the chemical index of alteration ($CIA = [Al_2O_3 / (Al_2O_3 + CaO^* + Na_2O + K_2O)] * 100$) of Nesbitt and Young (1982). The CIA values of the Um Hassa greywackes are low (48-65). These values are closer to the unweathered upper crust CIA value (50) than to the average shale CIA values (70-75) of Taylor and MacLennan (1985), which indicates limited chemical weathering of the source rocks. On the $Al_2O_3 - (CaO^* + Na_2O) - K_2O$ plot (Fig. 4.7a), the Um Hassa greywackes are clustered on the left side of the feldspar join line with slight extension towards the Al_2O_3 apex which confirms the weakly weathered nature of the source rocks (Nesbitt and Young, 1984).

Erosion of weathered rocks can create chemical differentiation, but not chemical changes, of the transported sediments through hydraulic sorting (Nesbitt and Young, 1996). The Um Hassa greywackes show high angularity of the fragments and poor sorting which suggest high erosion rates of the source rock and rapid sedimentation (Camirè et al., 1993; Nesbitt, 2003). This refutes the possibility of long transportation and sorting that may cause chemical differentiation through clay separation. Due to an increase of quartz at the expense of clay during sediment transport and recycling, the $SiO_2 - Al_2O_3$ ratio can be used to measure the degree of sediment maturity (Roser and Korsch, 1999). The average value of $SiO_2 - Al_2O_3$ ratio for the Um Hassa greywacke is ~5.

which is considered by Zhang (2004) to be low and indicates immature sediments that were deposited close to their source.

The effect of diagenesis on the chemical composition of terrigenous sediments is important but insufficiently addressed (McLennan et al., 2003). Mechanical compaction rather than chemical compaction is noticed in the Um Hassa greywackes. Chemical compaction refers to the compaction processes involving dissolution and precipitation of minerals (Middleton, 2003). It resulted in squeezing of sericite- and chlorite- rich fragments against competent fragments, bending of muscovite flakes, and fracturing of feldspar grains (Fig. 4.3b,c). Matrix formation could have been through the disintegration of labile grains (cf. Whetten and Hawkins, 1970) but the pseudo-matrix represented by deformed fine-grained lithic grains (cf. Zhang et al., 2008). Both compaction and matrix formation decreased porosity and so hindered cementation, which is confirmed microscopically. On the Al_2O_3 -(CaO^*+Na_2O)- K_2O plot (Fig. 4.7a), the samples show small scatter towards the K_2O apex which may suggest minor K-metasomatism (Nesbitt and Young, 1989). This process can occur through the transformation of aluminous clay in the matrix into illite and/or conversion of plagioclase to K-feldspar (Fedo et al., 1995). As the plagioclase grains of the Um Hassa greywackes are fresh and illite is found in the greywacke sediments of Wadi Hammamat (Holail and Moghazi, 1998), transformation of aluminous clays into illite is the reason for the limited K-metasomatism. Chlorite also occurs in the matrix. If it was not detrital in origin, chlorite can be formed at the expense of the kaolinite in case of limited availability of K in the system (Worden and Burley, 2003) or by diagenetic transformation of Fe-rich clays (Aagaard et al., 2000; Grigsby, 2001). Illite and chlorite form during slightly high-temperature burial diagenesis (Worden

and Burley, 2003; Potter et al., 2005) that may indicate limited element mobility into or out of the system. The limited chemical effects of the sedimentary processes during the formation of the Um Hassa greywackes indicate their reliability in determining the provenance of their sediments.

4.6.2. Provenance

The source region of coarse- and medium-grained clastic sedimentary rocks can be inferred from the types and the relative abundances of their grains. The main lithic fragments in the Um Hassa greywackes are andesite and felsites with some metabasalt and metasedimentary rocks. This mixture indicates multiple sources that could be the Dokhan Volcanics and island arc metavolcanics and their associated sediments. The same conclusion was reached by Holail and Mghazi (1998). The contribution of both Dokhan Volcanics and the island arc metavolcanics and associated sediments are recorded generally for the whole Hammamat Group (Akaad and El Ramly, 1969; Akaad and Noweir, 1980). Ries et al. (1983) noticed the same types of fragments in the underlying Um Had Conglomerate Member in addition to granitic rock fragments. The presence of quartz and plagioclase grains may reflect a contribution from a granitic source. In addition to lithic fragments, quartz and plagioclase are dominant. Although the undulatory nature of quartz grains may suggest a metamorphic source (Basu et al., 1975), it does not exclude the possibility for a plutonic source.

Due to limited weathering of the source rocks (low CIA) and the chemical immaturity of the greywackes (low Al_2O_3/SiO_2), the provenance can be addressed chemically. The provenance-discriminant plot of Roser and Korsch (1988) is used to

understand the source rocks based on the major element composition of both the Um Hassa greywackes and possible surrounding sources (Fig. 4.7b). Due to the expected proximity of the source rocks, the discrimination factors of the greywackes are compared to the major element compositions of the Dokhan volcanics and felsites of Wadi Sodmein (Asran et al., 2005), the gneissic granitoids of Qift-Qusier road (Heikal, 2003), and the Fawakhir ophiolites (Abd El-Rahman et al., in review). As the fragments were derived from multiple sources, the data are not constrained to one field, but extend between the Dokhan volcanics and the gneissic granitoids on one side and the Fawakhir ophiolitic rocks on the other side. Limited contribution from recycled sedimentary rocks may be indicated from extension of samples in to the quartzose sedimentary field. On the CN-A-K diagram (Fig. 4.7a), the sample with the least weathered fragments (Lowest CIA) lies on the line connecting the gneissic granitoids-the Dokhan Volcanics-the ophiolitic rocks which suggests the same conclusion.

Provenance terranes have been classified depending on the framework modes (Dickinson and Suezek, 1979; Dickinson et al., 1983) and geochemistry of the sedimentary rocks (McLennan et al., 1993). On the Q-F-L diagram (Fig. 4.8a), the Um Hassa greywackes plot parallel to the quartz-lithic fragments line mainly in the recycled orogen field with an extension towards the arc orogen field. The overlapping area located between the arc orogen and recycled orogen field increases on the Qm-F-L diagram (Fig. 4.8b). According to Dickinson and Suezk (1979), the recycled orogen field indicates that the sediments were derived from a subduction complex; collisional zone and/or foreland uplift. The contribution from a subduction complex and arc terranes to the Um Hassa

greywackes is recognized through the Qp-Lv-Ls ternary diagram where the samples spread between the subduction complex field and the arc orogen field (Fig. 4.8c).

From the geochemical perspective, McLennan et al. (1993) classified source rocks into older upper continental crust, recycled sedimentary rocks, younger, differentiated and undifferentiated arc, and exotic terrane-types. The limited input from an older upper continental crust and recycled sedimentary rocks to the Um Hassa greywackes are inferred from lower Th/Sc (0.33-0.58) and Zr contents (122-260 ppm). The lower content of Nb relative to UCC indicates an arc source for the Um Hassa greywackes (cf. Zhang, 2004) which is supported from modal analyses (Fig. 4.8). In addition to lower Th/Sc ratios, lower LREE ($La/Sm_n = 2.4-3.3$) and Th/U (2.3-3) ratios suggest a significant contribution from arc-derived material (cf. McLennan et al., 1993). The negative Eu anomalies (Fig. 4.6a) in the Um Hassa greywackes indicate a contribution from differentiated felsic volcanics and plutonic rocks of a dissected arc. El-Bouseily (1986) stated that the granitic pebbles from the Um Had Conglomerate Member are mostly low- Al_2O_3 trondhjemite and are similar to some varieties of older granitoids of Egypt. Their chemical characteristics are similar to volcanic arc trondhjemite associated with oceanic island arc-related volcanics in the Central Eastern Desert (Abdel Rahman, 2004). The exposed arc plutonic core can be the main source of the monocrystalline quartz and plagioclase distributed in the Um Hassa greywackes. The Um Hassa greywackes are characterized by high Cr (234-434 ppm) and Ni (49-72 ppm). The high contents of these elements in sediments indicate a proximal ophiolitic source (Hoscitt, 1984; McLennan et al., 1990; 1993; Garver et al., 1996).

4.6.3. Tectonic setting

In terms of the tectonic setting, there is a close relationship between the tectonic setting of depositional basins and the geochemical characteristics of their sandstones (Bhatia, 1983; Bhatia and Crook, 1986). The Um Hassa greywackes show a quartz proportion (24-42 %), a SiO₂ content (67-73 wt.%) and a K₂O/Na₂O ratio (0.4-1.1) similar to those greywackes deposited at an Andean-type continental margin (c.f. Crook, 1974; Schwab, 1975). The same conclusion can be reached using the K₂O/Na₂O versus SiO₂ plot of Roser and Korsch (1986) where the Um Hassa greywackes plot in the active continental margin field (Fig. 4.9a).

Bhatia (1983) and Bhatia and Crook (1986) inferred the tectonic settings of sandstones by using their major and trace element compositions. The applicability of these tectonic discrimination diagrams for the Hammamat Group was criticized by Holail and Moghazi (1997) due to the mixing of mafic and felsic rocks of different tectonic settings. Although our study of the Um Hassa greywackes confirms the mixing source, the greywackes plot consistently on the tectonic discrimination diagrams. Most of the greywackes plot in the continental arc field and extend into the oceanic arc field (Fig. 4.9b,c,d). Irrespective of the depositional process, a continental arc setting for the Um Hassa greywackes is consistent with their data plotting in the active continental margin field of Roser and Korsch (1986).

The tectonic setting of the Um Hassa greywacke Member can be inferred from the context of the geological evolution of the surrounding rocks of the Central Eastern Desert. According to Abd El-Rahman et al. (in review), the Central Eastern Desert, along

Qift-Qusier Road, developed through the accretion of island arc-ophiolitic rocks into a passive continental margin to the west along an east-dipping subduction zone. After the accretion, the polarity of subduction reversed and an Andean-type margin established above a west-dipping subduction zone. The Dokhan Volcanics, which are the surface manifestation of the continental arc magmatism (Eliwa, 2006), were formed on the accreted island arc-ophiolitic substrate. The molasse-type basins of the Eastern Desert can be classified based on their spatial distribution within the orogen and associated structural setting into two main types (Fritz et al., 1996; Fritz and Messner, 1999). The *first type, which is a foreland molasse basin, is associated with thrust faults and is located along the western part of the orogen.* The second type is related to orogen parallel extension and is related to the Najd strike-slip fault system. The Hammamat group in their type locality belongs to the first, the foreland molasse-type basins.

Foreland basins are classified into two types (Dickinson, 1974). The first type is the peripheral foreland basin, which is formed in the front of fold-and-thrust belts, while the second type is the retroarc foreland basin which is formed in the hinterland side of continental arcs (DeCelles and Giles, 1996). It is most likely that the Um Hassa greywackes were deposited in a retroarc, rather than a peripheral, foreland basin where the sediments derived mainly from the continental arcs with a contribution from the basement substrate which is composed of island arc and ophiolitic rocks (Fig. 4.10). The other alternative for the Um Hassa greywackes would have them been deposited in a peripheral foreland basin formed during the accretion of the oceanic island arc and ophiolitic materials into the Saharan Craton to the west, during east-dipping subduction. Such a model is similar to the ones proposed during the evolution of the Taconic orogeny

in northern Appalachians (Garver et al., 1996) and the evolution of the Grenvillian orogeny in South Africa (Basson and Watkeys, 2003). In favor of the peripheral foreland basin model, the plot of the Um Hassa greywackes in the continental island arc and active continental margin fields on the tectonic discrimination diagrams (Fig. 4.9) can be interpreted in terms of mixing sources. These sources would have been the passive continental margin sediments derived from the Saharan Craton to the west and the accreted oceanic island arc-ophiolitic rocks from the west. This model is unlikely because of the scarcity of sedimentary lithic fragments compared to the amount of volcanic lithic fragments (Fig. 4.8c). Thus, the plot of the Um Hassa greywackes in the continental arc field reflects the chemical characteristics of these volcanic lithic fragments. Such chemical affinity of the lithic components suggest the deposition of the Hammamat Group at its type locality in a retroarc foreland basin, similar in its tectonic setting to the cordilleran retroarc foreland basins of North America (DeCelles, 2004).

The tectonic contact between the Dokhan Volcanics and Hammamat Group in the Wadi Hammamat area can be attributed to later reactivation of thrust faults in the accreted island arc and ophiolitic materials. This reactivation might have resulted in the folding and cleavage development recorded in Hammamat sediments. The possibility for the Hammamat Group in the Wadi Hammamat area of being deposited in piggy-back basins as suggested by Anderson et al. (2009) is less likely. In such basins, the sediments are expected to be derived from the accreted arc and ophiolitic thrust sheets rather than being derived from the Dokhan continental arc rocks. In addition, sediments deposited in the piggy-back basins are expected to be severely deformed during thrust reactivation periods. These characteristics match the sediments of Wadi Um Esh, which are located to

the east of the Wadi Hammamat area. The sediments of Wadi Um Esh have restricted pebble types, including trondhjemite, fine-grained basic rocks and epidosite, and are intensely deformed (Ries et al., 1983, and reference therein). Deposition of the Um Esh sediments in a restricted piggy-back basin to the east relative to the less deformed, thick Hammamat sediments to the west supports the probability for the Hammamat Group being deposited in a retroarc foreland basin. Unfortunately, the coverage of the Hammamat Group unconformably by Phanerozoic sandstone prevents following them further west to establish their relation with the Saharan Metacraton.

4.7. Conclusion

The petrographic characteristics of the Um Hassa greywackes are consistent with their derivation from mixed sources similar to the underlying Um Had Conglomerate Member. In addition to petrography, the low CIA and $\text{SiO}_2/\text{Al}_2\text{O}_3$ indicate little weathering of the source rocks and deposition of the fragments close to their source. Limited weathering and transportation of the Um Hassa sediments indicates the reliability of using geochemical characteristics to predict their provenance.

From the geochemistry of the Um Hassa greywackes (low Th/Sc, Zr, Nb, Th/U, and high Cr and Ni), both Dokhan-type continental arc volcanics and accreted ophiolitic-arc materials are the main contributors to the upper part of Hammamat sediments. Similar sources are suggested by using modal analyses of the greywackes. In the context of the evolution of the Central Eastern Desert, the Um Hassa Greywacke Member at Wadi Hammamat area was deposited in a retroarc foreland basin. This basin formed behind the continental arcs established over a west-dipping subduction zone.

Acknowledgements

We thank Dr. Leon Lang for providing us with a copy of the Asran et al. (2005) paper. This is a contribution of the PREA grant to A. Polat. Support from NSERC Grants of Ali Polat (250978) and Brian Fryer (83117) are greatly appreciated.

References

- Aagaard, P., Jahren, J., Harstad, A.O., Nilsen, O., Ramm, M., 2000. Formation of grain-coating chlorite in sandstones: laboratory synthesized vs. natural occurrences. *Clay Minerals* 35, 261-269.
- Abdel Rahman, Y.M.H., 2004. Geology and mineralizations of the Precambrian rocks at Wadi Hamama area, Central Eastern Desert, Egypt. MSc thesis, Cairo University. 189.
- Abd El-Rahman, Y., Polat, A., Dilek, Y., Fryer, B.J., El-Sharkawy, M., Sakran, S, 2009. Geochemistry and tectonic evolution of the Neoproterozoic Wadi Ghadir ophiolite, Eastern Desert, Egypt. *Lithos*. doi:10.1016/j.lithos.2008.12.014.
- Abd El-Rahman, Y., Polat, A., Dilek, Y., Fryer, B.J., El-Sharkawy, M., Sakran, S, in review. Formation of Neoproterozoic proto-arc oceanic crust in the Nubian Shield: Geochemical evidence from the Fawakhir ophiolite, Eastern Desert, Egypt. (Submitted to *Precambrian Research*).
- Akaad, M.K., Noweir, A.M. 1969. Lithostratigraphy of the Hammamat–Um Seleimat District, Eastern Desert, Egypt. *Nature* 223, 284–285.
- Akaad, M.K., Noweir, A.M. 1980. Geology and lithostratigraphy of the Arabian Desert orogenic belt of Egypt between latitudes 25°35' and 26°30'N. *Institute of Applied Geology Bulletin, Jeddah*, 3, 127–136.
- Andreson, A., Abu El-Rus, M.A., Myhre, P.I., Boghdady, G.Y., Corfu, F., 2009. U-Pb TIMS age constraints on the evolution of the Neoproterozoic Meatiq Gneiss Dome, Eastern Desert, Egypt. *International Journal of Earth Sciences* 98, 481-497.
- Asran, A.M.H., Azer, M.K., Aboazom, A.S., 2005. Petrological and geochemical investigation of Dokhan volcanics and felsites in Wadi Sodmein area, Central Eastern Desert, Egypt. *Egyptian Journal of Geology* 49, 1-20.

- Basu, A., Young, S.W., Suttner, L.J., James, W.C., Mack, G.H., 1975. Re-evaluation of the use of undulatory extinction and polycrystallinity in detrital quartz for provenance interpretation. *Journal of Sedimentary Petrology* 45, 873–882.
- Bhatia, M.R., 1983. Plate tectonics and geochemical composition of sandstones *Journal of Geology* 91, 611–627.
- Bhatia, M.R., Crook, K.A.W., 1986. Trace element characteristics of greywackes and tectonic setting discrimination of sedimentary basins. *Contributions to Mineralogy and Petrology* 92, 181–193.
- Bosson, I.J., Watkey, M.K., 2003. Tectonic implications from the geochemistry of Mfongosi Group metasediments, Natal Metamorphic Provenance, South Africa. *South African Journal of Geology* 106, 265-280.
- Camiré, G.E., Laflèche, M.R., Ludden, J.N., 1993. Archaean metasedimentary rocks from the northwestern Pontiac Sub-province of the Canadian Shield: chemical characterization, weathering and modeling of the source areas. *Precambrian Research* 62, 285-305.
- DeCelles, P.G., 2004. Late Jurassic to Eocene evolution of the cordilleran thrust belt and foreland basin system, Western U.S.A. *American Journal of Science* 304, 105-168.
- DeCelles, P.G., Giles, K.A., 1996. Foreland basin systems. *Basin Research* 8, 105-123.
- Dickinson, W.R., 1974. Plate tectonics and sedimentation. *Society of Economic Paleontologists and Mineralogists Special Publication* 22, 1-27.
- Dickinson, W.R., 1985. Interpreting provenance relations from detrital modes of sandstones, in Zuffa, G.G., (ed) *Provenance of arenites*. D. Reidel Publishing Company, Dordrecht, 333–361.
- Dickinson, W.R., Beard, L.S., Brakenridge, G.R., Erjavec, J.L., Ferguson, R.C., Inman, K.F., Knepp, R.A., Lindberg, F.A., Ryberg, P.T., 1983. Provenance of North American Phanerozoic sandstones in relation to tectonic setting. *Geological Society of America Bulletin* 94, 222-235.
- Dickinson, W.R., Suezek, C.A., 1979. Plate tectonics and sandstone compositions. *American Association of Petroleum Geologists Bulletin* 63, 2164-2182.
- El-Bouseily, A.M., 1986. On trondhjemite pebbles from from the late Pan-African Um Had conglomerate, Eastern Desert Egypt. *Journal of African Earth Sciences* 5, 471-480.
- El Gaby, S., Geologic and tectonic framework of the Pan-African orogenic belt in Egypt. 2nd International Conference on the Geology of the Arab World, Cairo University, 3-17.
- El Gaby, S., El-Nady, O., Khudeir, A., 1984. Tectonic evolution of the Basement Complex in the Central Eastern Desert of Egypt. *Geologische Rundschau* 73, 1019-1036.

- Eliwa, H.A., Kimura, J.I., Itaya, T., 2006. Late Neoproterozoic Dokhan volcanic rocks, northern Eastern Desert, Egypt. *Precambrian Research* 151, 31-52.
- Engel, A.E.J., Dixon, T.H., Stern, R.J., 1980. Late Precambrian evolution of Afro-Arabian crust from ocean-arc to craton. *Geological Society of American Bulletin* 91, 385-411.
- Fedo, C.M., Nesbitt, H.M., Young, G.M., 1995. Unraveling the effects of potassium metasomatism in sedimentary rocks and paleosols, with implications for paleoweathering conditions and provenance. *Geology* 23, 921-924.
- Fedo, C.M., Young, G.M., Nesbitt, H.M., Hancher, J.M., 1997. Potassic and sodic metasomatism in the Southern Province of Canadian Shield: Evidence from Paleoproterozoic Serpent Formation, Huronian Supergroup, Canada. *Precambrian Research* 84, 17-36.
- Fritz, H., Messner, M., 1999. Intramontane basin formation during oblique convergence in the Eastern Desert of Egypt: magmatically versus tectonically induced subsidence. *Tectonophysics* 315, 145-162.
- Fritz, H., Wallbrecher, E., Khudeir, A.A., Abu El Ela, F., Dallmeyer, D.R., 1996. Formation of Neoproterozoic metamorphic core complexes during oblique convergence (Eastern Desert, Egypt). *Journal of African Earth Sciences* 23, 311-329.
- Garver, J.I., Royce, P.R., Smick, T.A., 1996. Chromium and nickel in shale of the Taconic Foreland: A case study for the provenance of the fine-grained sediments with an ultramafic source. *Journal of Sedimentary Research* 66, 100-106.
- Greiling, R.O., Abdeen, M.M., Dardir, A.A., El Akhal, H., El Ramly, M.F., Kamal El Din, G.M., Osman, A.F., Rashwan, A.A., Rice, A.H.N., Sadek, M.F., 1994. A structural synthesis of the Proterozoic Arabian-Nubian Shield in Egypt. *Geologie Rundschau* 83, 484-501.
- Grigsby, J.D., 2001. Origin and growth mechanism of authigenic chlorite in sandstones of the Lower Vicksburg Formation, south Texas. *Journal of Sedimentary Research* 71, 27-36.
- Grothaus, B.T., Ehrlich, R., Eppler, D.T., 1979. Facies analysis of the Hammamat sediments, Eastern Desert, Egypt. 5th Conference on African Geology, Cairo. *Annals of the Geological Survey of Egypt* 9, 564-590.
- Hendrix, M.S., 2000. Evolution of Mesozoic sandstone compositions, southern Junggar, northern Tarim, and western Turpan Basin, northwest China: A detrital record of the ancestral Tian Shan. *Journal of Sedimentary Research* 70, 520-532.
- Heikal, M.T.S., 2003. Petrogenesis of gneissic granitoids across Qifi-Qusier road, Central Eastern Desert of Egypt: Petrological and geochemical constraints. 5th International Conference on the Geology of the Middle East, 253-276.

- Hiscott, R.N., 1984. Ophiolitic source rocks for Taconic-age flysch: Trace element evidence. *Geological Society of American Bulletin* 95, 1261-1267.
- Holail, H.M., Moghazi, A.M., 1998. Provenance, tectonic setting and geochemistry of greywackes and siltstones of the Late Precambrian Hammamat Group, Egypt. *Sedimentary Geology* 116, 227-250.
- Jenner, G. A., Longerich, H. P., Jackson, S. E., Fryer, B. J., 1990. ICP-MS - a powerful tool for high-precision trace-element analysis in earth sciences: evidence from analysis of selected U.S.G.S. reference samples. *Chemical Geology* 83, 133-148.
- Johnson, P.R., Woldehaimanot, B., 2003. Development of the Arabian-Nubian Shield: perspectives on accretion and deformation in the northern East African Orogen and the assembly of Gondwana. In: M. Yoshida, B.F. Windley and S. Dasgupta, (Eds), *Proterozoic East Gondwana: Super continent assembly and break-up*. Geological Society of London Special Publications 206, 289-325.
- McLennan, S.M., Bock, B., Hemming, S.R., Hurowitz, J.A., Lev, S.M., McDaniel, D.K., 2003. The role of provenance and sedimentary processes in the geochemistry of sedimentary rocks. In D.R. Lentz (ed.) *Geochemistry of sediments and sedimentary rocks: Evolution considerations to mineral deposit-forming environments*. Geological Association of Canada, *GeoText* 4, 7-38.
- McLennan, S.M., Hemming, S., McDaniel, D.K., Hanson, G.N., 1993. Geochemical approaches to sedimentation, provenance and tectonics, *in* Johnsson, M.J., and Basu, A., (eds) *Processes Controlling the Composition of Clastic Sediments*. Geological Society of America, Special Paper 284, 21-40.
- McLennan, S.M., Taylor, S.R., McCulloch, M.T., Maynard, J.B., 1990. Geochemical and Nd-Sr isotopic composition of deep sea turbidites: Crustal evolution and plate tectonic association. *Geochimica et Cosmochimica Acta* 40, 1537-1551.
- Middleton, G.V., (ed.), 2003. *Encyclopedia of sediments and sedimentary rocks*. Springer-Verlag.
- Nesbitt, H.W., 2003. Petrogenesis of siliclastic sediments and sedimentary rocks. In D.R. Lentz (ed.) *Geochemistry of sediments and sedimentary rocks: Evolution considerations to mineral deposit-forming environments*. Geological Association of Canada, *GeoText* 4, 39-51.
- Nesbitt, H.W., Young, G.M., 1982. Early Proterozoic climates and plate motions inferred from major element chemistry of lutites. *Nature* 299, 715-717.

- Nesbitt, H.W., Young, G.M., 1984. Prediction of some weathering trends of plutonic and volcanic rocks based on thermodynamic and kinetic considerations. *Geochimica et Cosmochimica Acta* 48, 1423-1534.
- Nesbitt, H.W., Young, G.M., 1989. Formation and diagenesis of weathering profiles. *Journal of Geology* 97, 129-147.
- Nesbitt, H.W., Young, G.M., 1996. Petrogenesis of sediments in the absence of chemical weathering: effects of the abrasion and sorting on bulk composition and mineralogy. *Sedimentology* 43, 341-358.
- Pettijohn, F.G., Potter, P.D., Siever, R., 1972. *Sand and sandstone*. Springer-Verlag, New York.
- Potter, P.E., Maynard, J.B., Depetris, P.J., 2005. *Mud and Mudstone: Introduction and Overview*. Springer-Verlag Berlin Heidelberg.
- Ries, A.C., Shackleton R.M., Graham R.H., Fitches W.R., 1983. Pan-African structures, ophiolites and mélanges in the Eastern Desert of Egypt: a traverse at 26° N. *Journal of Geological Society* 140, 75-95.
- Roser, B.P., Korsch, R.J., 1986. Determination of tectonic setting of sandstone–mudstone suites using SiO₂ and K₂O/Na₂O ratio. *Journal of Geology* 94, 635–650.
- Roser, B.P., Korsch, R.J., 1988. Provenance signatures of sandstone–mudstone suites determined using discrimination function analysis of major-element data. *Chemical Geology* 67, 119–139.
- Roser, B.P., Korsch, R.J., 1999. Geochemical characterization, evolution and source of Mesozoic accretionary wedge: the Torlesse terrane, New Zealand. *Geological Magazine* 136, 493-512.
- Stern, R.J., 1994. Arc assembly and continental collision in the Neoproterozoic East African Orogen: implications for the consolidation of Gondwanaland. *Annual Review of Earth and Planet Sciences* 22, 319–351.
- Sun, S.-S., McDonough, W.F., 1989. Chemical and systematic of oceanic basalts: implications for mantle composition and processes. In: Saunders, A.D., Norry, M.J. (eds.) *Magmatism in ocean basins*. Geological Society, London, Special Publication 42, 313-345.
- Taylor, S.T., McLennan, S.M., 1985. *The Continental Crust: its Composition and Evolution*. Blackwell Scientific, Oxford.
- Whetten, J.T., and Hawkins Jr. J.W., 1970. Diagenetic origin of greywacke matrix minerals. *Sedimentology* 15, 347-361.
- Wilde, S.A., Youssef, K., 2001. SHRIMP U-Pb dating of detrital zircons from Hammamat Group at Gebel Um Tawat, Northern-Eastern Desert, Egypt. *Gondwana Research* 4, 202-206.

- Wilde, S.A., Youssef, K., 2002. A re-evaluation of the origin and setting of the late Precambrian Hammamat Group based on SHRIMP-U–Pb dating of detrital zircons from Gebel Umm Tawat, North Eastern Desert, Egypt. *Journal of Geological Society London* 159, 595–604.
- Worden, R.H., Burley, S.D., 2003. Sandstone diagenesis: the evolution of sand to stone. In S.D. Burley, S.D., and R.H. Worden (eds.) *Sandstone Diagenesis: Recent and Ancient*. International Association of Sedimentologists Reprint 4, 3–44.
- Zhang, K-J., 2004. Secular geochemical variations of the Lower Cretaceous siliclastic rocks from central Tibet (China) indicate a tectonic transition from continental collision to back-arc rifting. *Earth and Planetary Science Letters* 229, 73–89.
- Zhang, K-J., Li, B., Wei, Q-G., Gai, J-X., Zhang, Y-X., 2008. Proximal provenance of the western Songpan-Ganzi turbidite complex (Late Triassic, eastern Tibetan plateau): Implication for the tectonic amalgamation of China. *Sedimentary Geology* 208, 36–44.

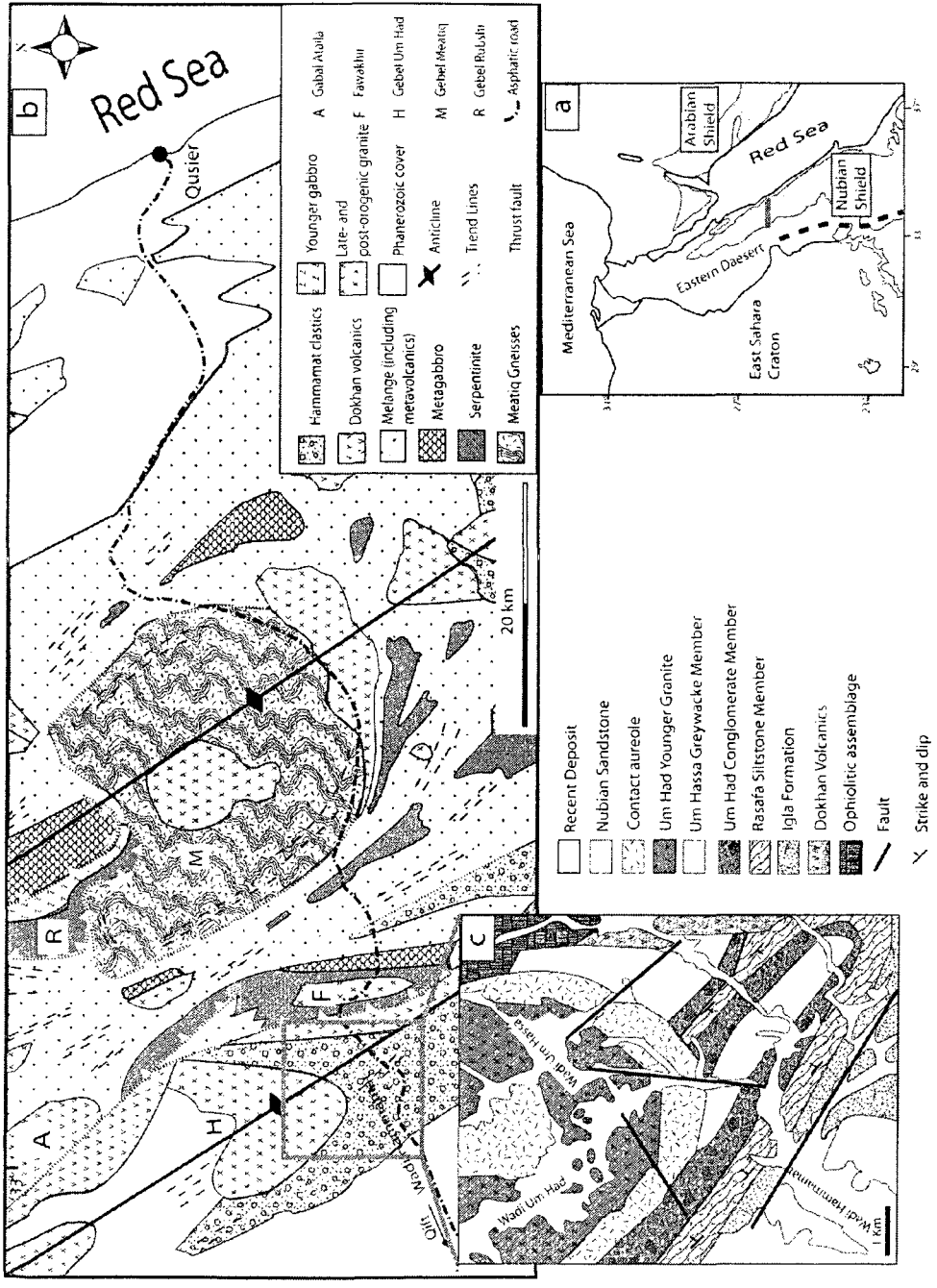


Fig. 4.1. (a) Overview map of the Arabian-Nubian Shield rocks (orange) along the Red Sea. The dashed line is the approximate boundary between the Shield and the Eastern Saharan Craton (After Greiling et al., 1994) (Red strip represents the area in b). (b) Simplified geological map of the Hammamat-Meatig region (after, El Gaby et al., 1984). (c) Geological map of the Hammamat area (after Holail and Moghazi, 1998).

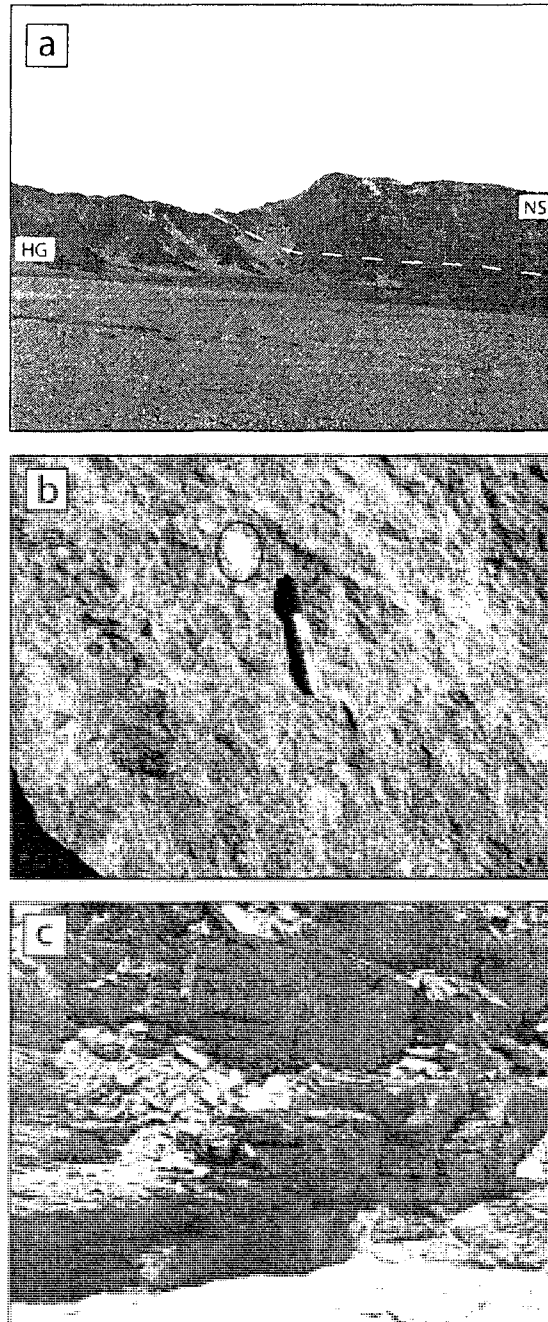


Fig. 4.2. (a) Precambrian Hammamat Group (HG) overlain unconformably by Phanerozoic Nubian Sandstone (NS). (b) Polymictic conglomerate of Um Had Member, notice the purple Dokhan-type volcanic rocks, epidosite (solid ellipse) and plagiogranite (dashed ellipse) fragments. (c) Bedded (upper) and cleaved (lower) greywacke of Um Hassa Member.

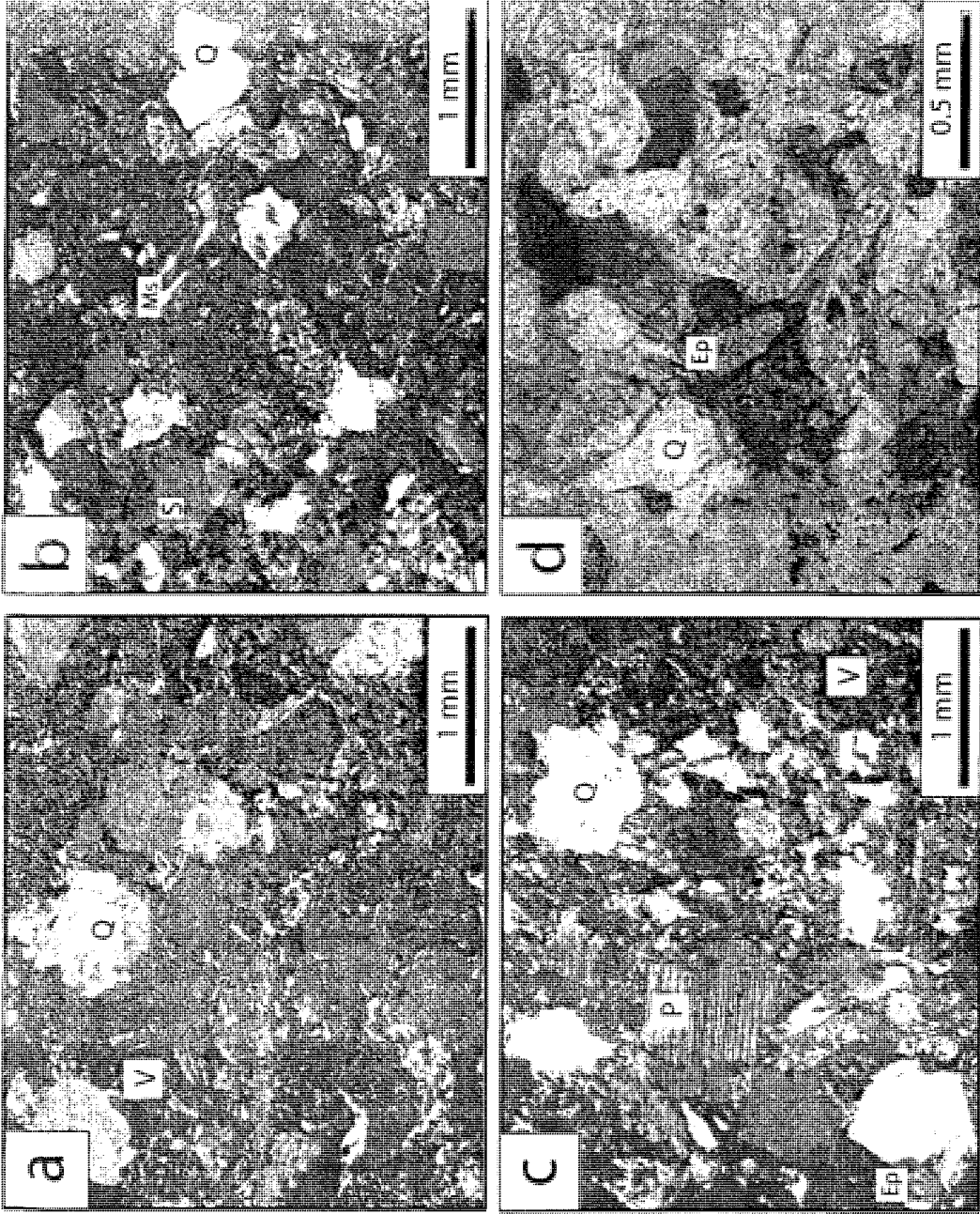


Fig. 4.3. Photomicrographs of Um Hasa greywackes showing different kinds of framework components (a) Monocrystalline quartz (Q) and volcanic fragments (V). (b) Sedimentary fragments (S) and bent muscovite (Ms). (c) Fractured plagioclase with albite twinning (P). (d) Epidote (Ep) and opaque grains.

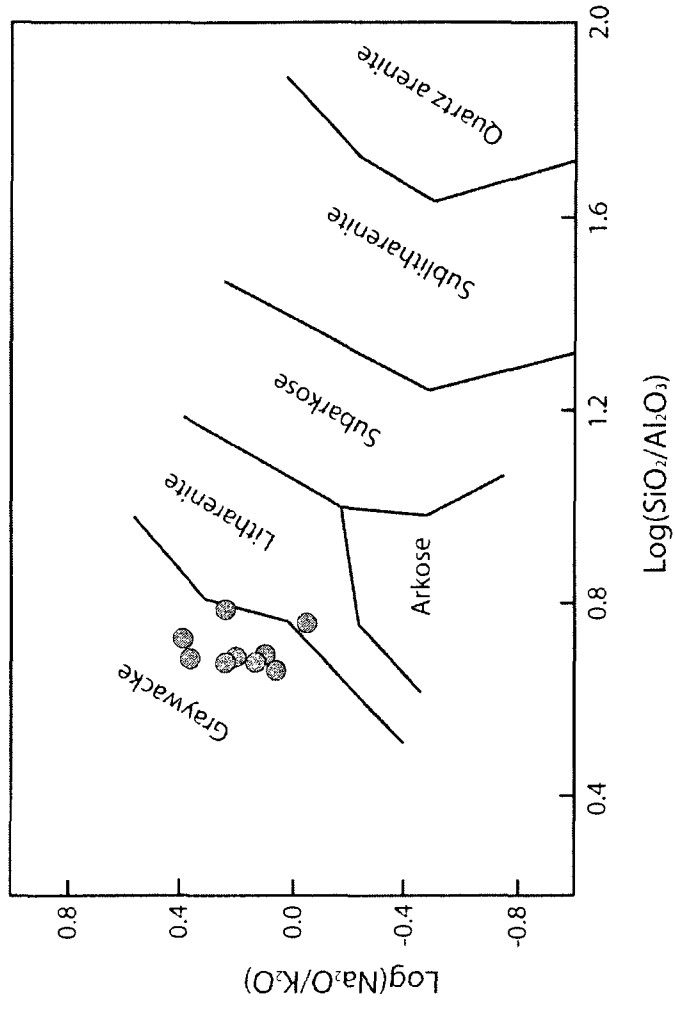


Fig. 4.4. $\text{Log}(\text{Na}_2\text{O}/\text{K}_2\text{O})$ versus $\text{Log}(\text{SiO}_2/\text{Al}_2\text{O}_3)$ of Pettijohn et al. (1972) for chemical classification of sandstones.

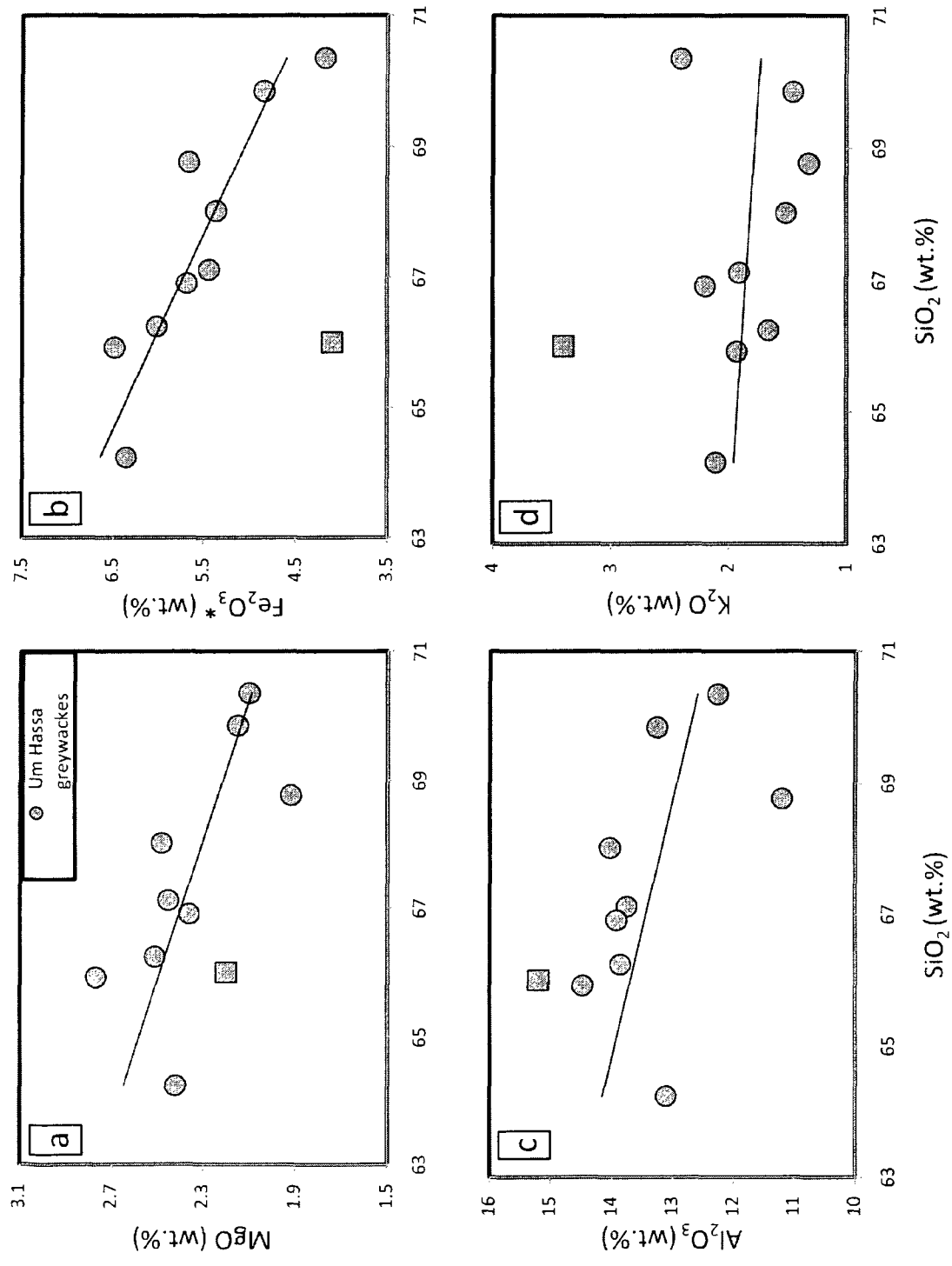


Fig. 4.5. Variation diagrams of SiO_2 against, (a) MgO , (b) Fe_2O_3^* , (c) Al_2O_3 , (d) K_2O . UCC values are from Taylor and McLennan (1985).

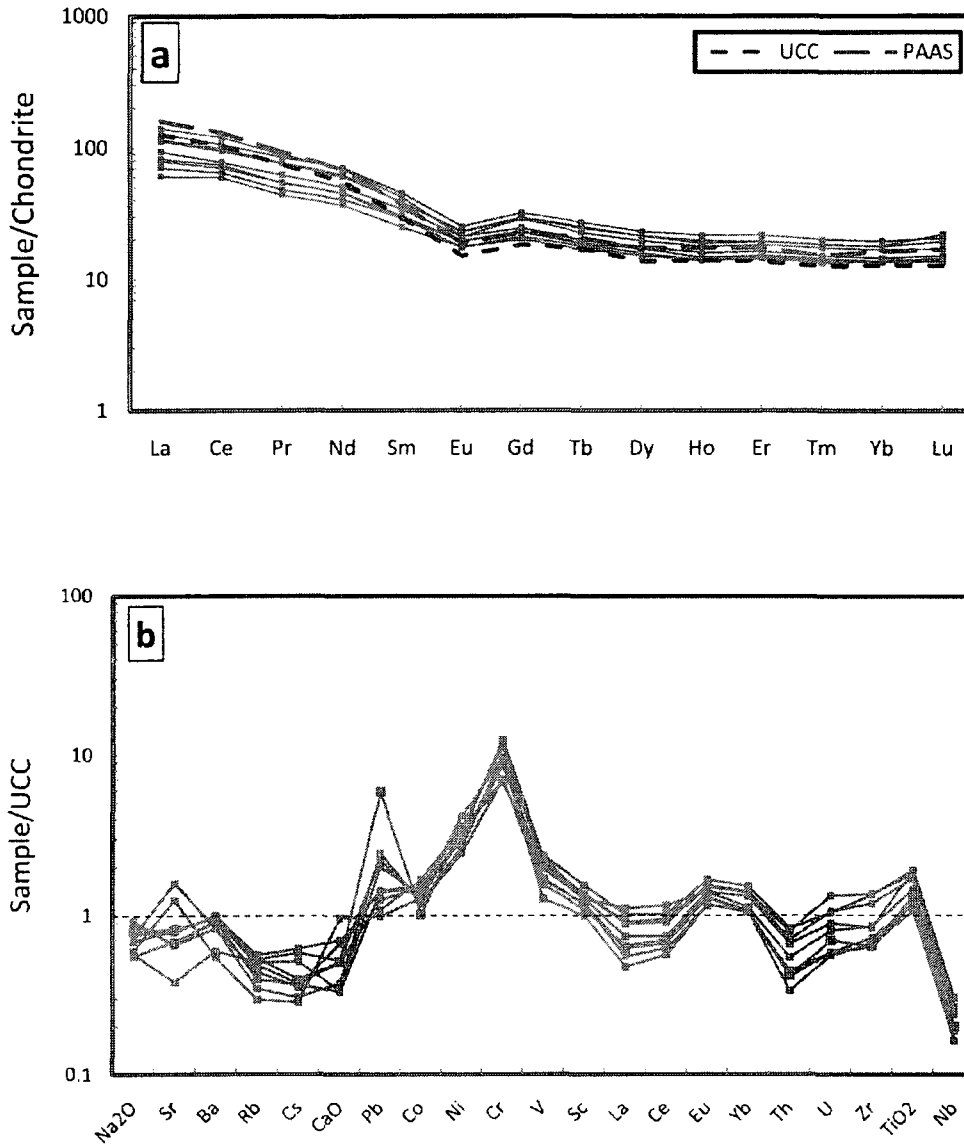


Fig. 4.6. (a) Chondrite-normalized REE patterns for Um Hassa greywackes. Chondrite values from Sun and McDonough (1989), UCC and Post Archean Average Shale (PAAS) values are from Taylor and McLennan (1985). (b) Upper Continental crust-normalized diagram for Um Hassa greywackes. UCC values are from Taylor and McLennan (1985).

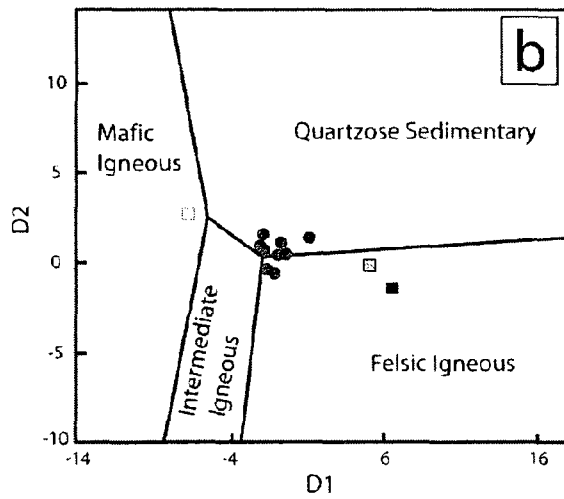
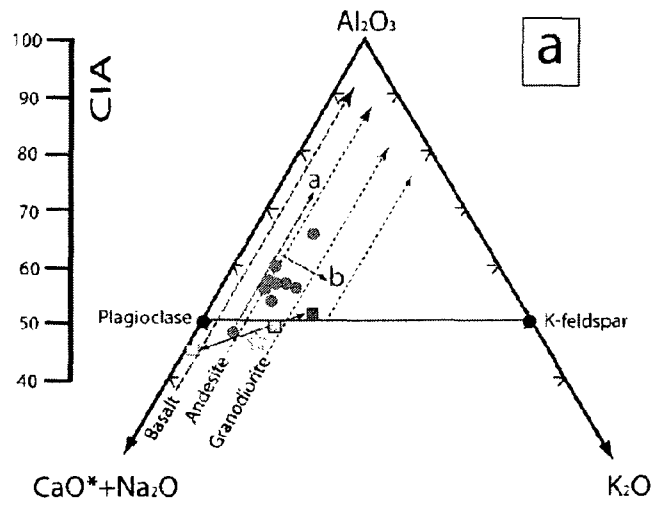


Fig. 4.7. (a) A-CN-K ternary diagram of molecular proportions of Al_2O_3 -($CaO+Na_2O$)- K_2O for Um Hassa greywackes with chemical index of alteration scale (CIA). Dashed black arrows represent weathering trends of different rocks. Dashed blue arrow (a) represents weathering trends of the greywackes and dashed blue line (b) represents K-metasomatism trend. The blue double headed arrow connects the possible source rocks from the Eastern Desert. Green square is the ophiolitic rocks from Abd El-Rahman et al. (in preparation); Brown Square is Dokhan Volcanics from Asran et al. (2005); Red Square is Meatiq gneisses from Heikal (2003); Yellow star is UCC from Taylor and McLennan (1985). (Molecular proportions calculation after Fedo et al., (1995)). (b) Provenance discrimination diagrams of Roser and Korsch (1988). Symbols as in (a).

$$(D1=30..638TiO_2/Al_2O_3-12.541Fe_2O_3/Al_2O_3+7.329MgO/Al_2O_3+12.031Na_2O/Al_2O_3+35.402K_2O/Al_2O_3-6.382)$$

$$(D2=56.5TiO_2/Al_2O_3-10.879Fe_2O_3/Al_2O_3+30.875MgO/Al_2O_3-5.404Na_2O/Al_2O_3+11.112K_2O/Al_2O_3-3.89)$$

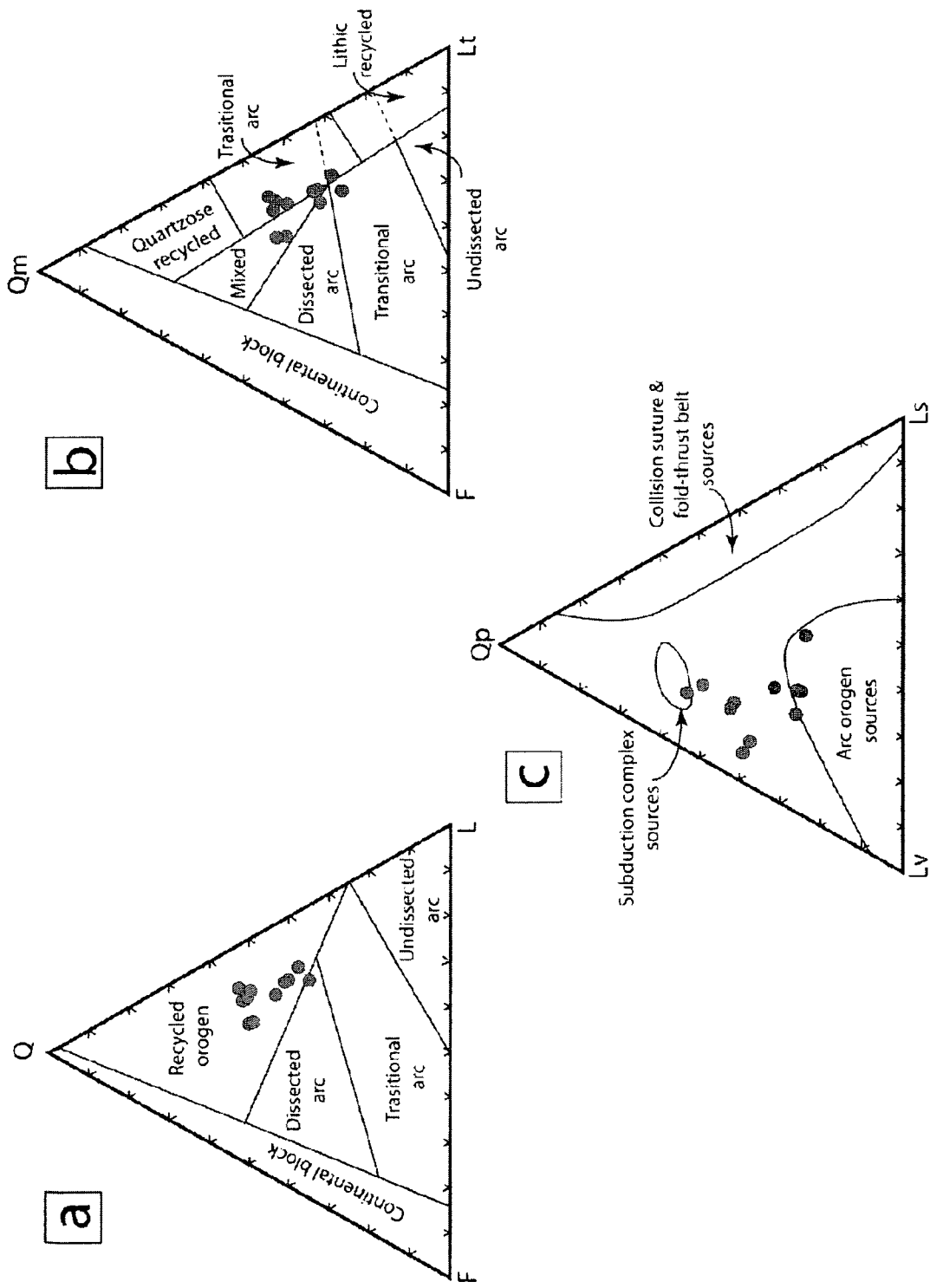


Fig. 4.8. Modal sandstone ternary plots for Um Hasa greywackes (after Dickinson, 1985). (a) Quartz (Q)-Feldspar (F)-Lithic fragments (L). (b) Monocrystalline quartz (Qm)-Feldspar (F)-Total Lithic fragments (Lt). (c) Polycrystalline quartz (Qp)-Volcanic lithic fragments (Lv)-Sedimentary lithic fragments (Ls).

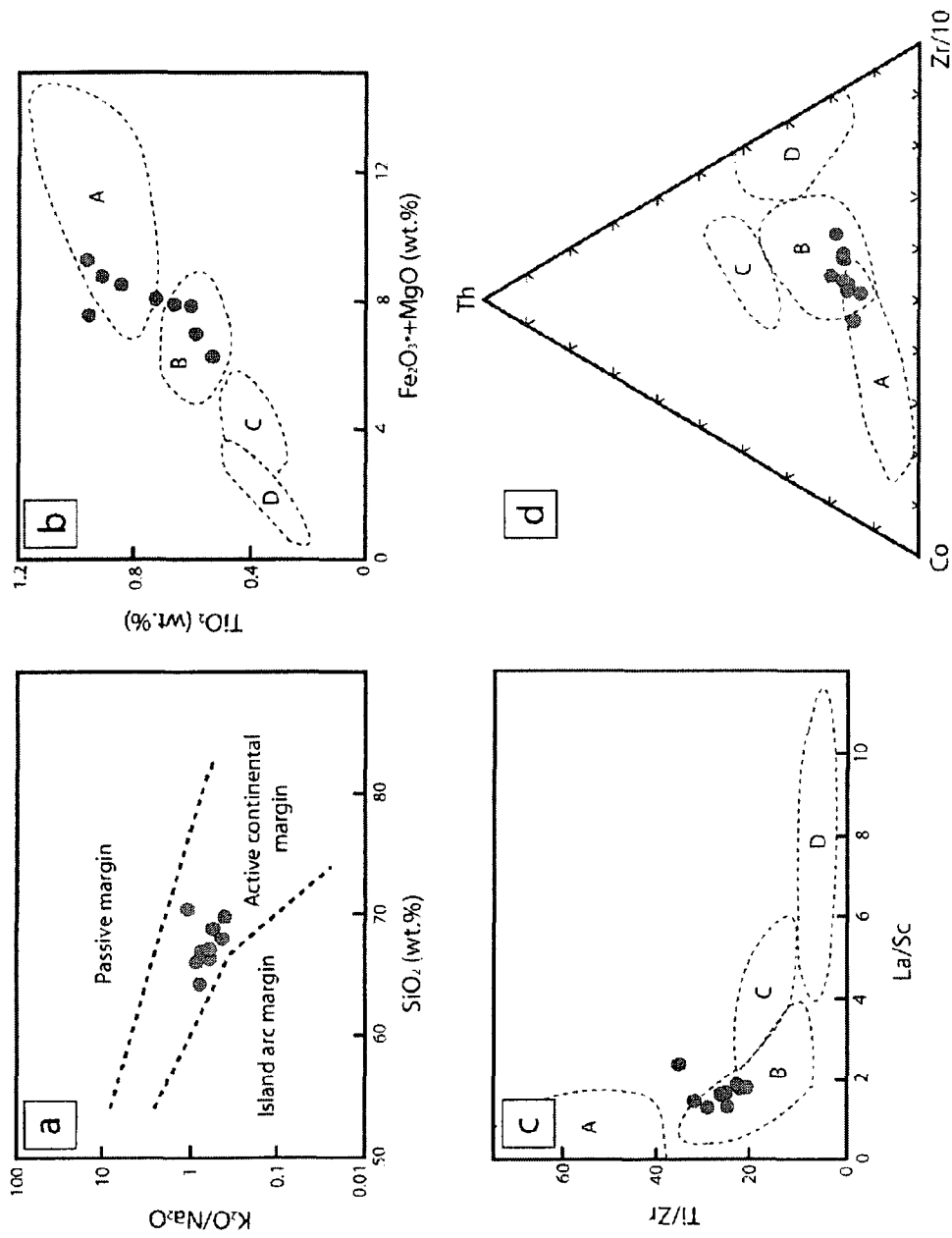


Fig. 4.9. Tectonic setting discrimination diagrams for Um Hassa greywackes, (a) K_2O/Na_2O versus SiO_2 of Roser and Korsch (1986). (b) TiO_2 versus Fe_2O_3+MgO of Bhatia (1983). (c) Ti/Zr versus La/Sc of Bhatia and Crook (1986). (d) Co-Th-Zr ternary diagram of Bhatia and Crook (1986). (Field A is oceanic island arc, field B is continental island arc, field C is active continental margin, and field D is passive continental margin)

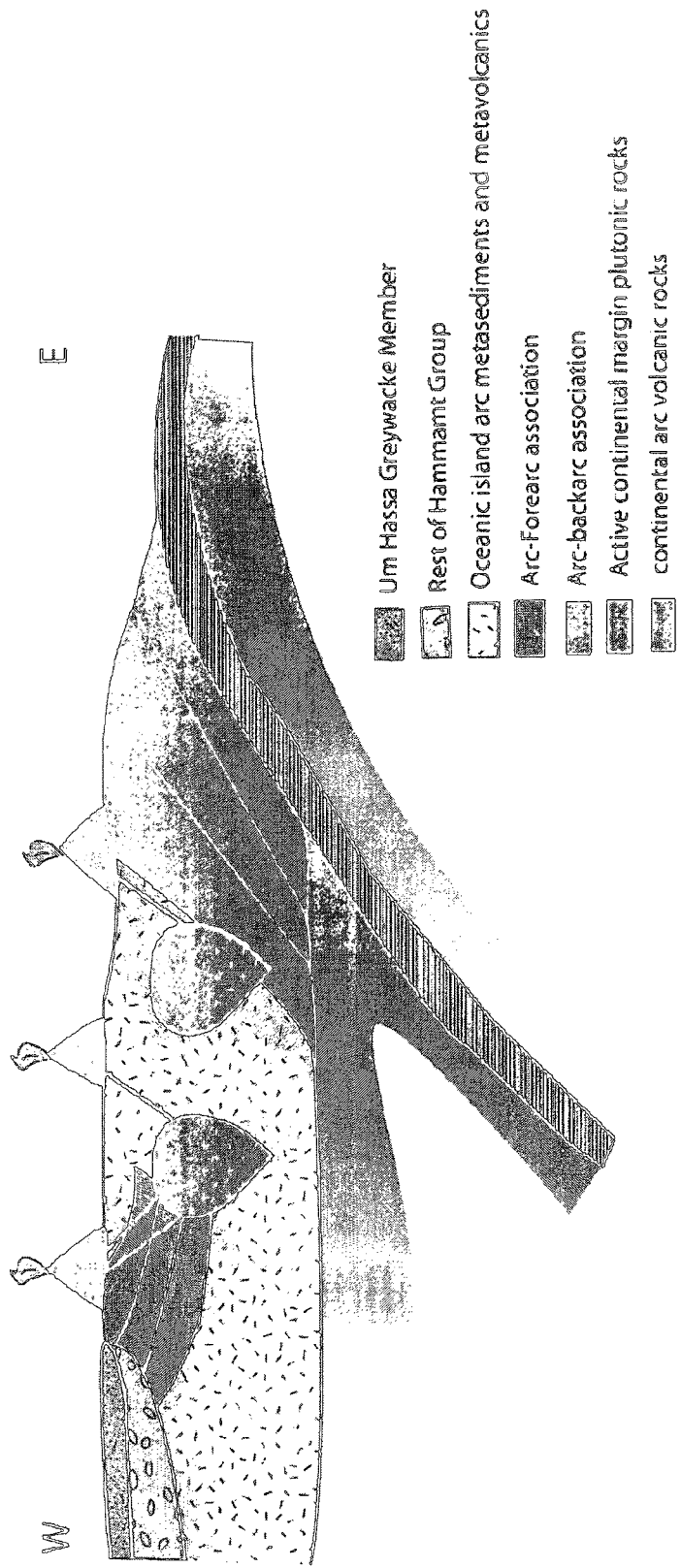


Fig. 4.10. Tectonic model for the formation of Hammamat Group at Wadi Hammamat area inferred from the petrography and geochemistry of the Um Hassa Greywacke Member.

	Q	F	L	Qm	Qp	P	K	Lv	Ls	Lt	Misc	M
EGY04-24	41.6	10.3	16.4	29.4	12.2	8.2	2.1	12.2	4.2	28.6	12	19.7
EGY04-25	41.3	10.2	15.2	26.3	15	8	2.2	10.2	5	30.2	10.6	22.7
EGY04-26	34.3	8	18.5	25.7	8.6	7.5	0.5	11.8	6.7	27.1	15.2	24
EGY04-27	41	15.3	12	27.1	13.9	13.4	1.9	8.7	3.3	25.9	9.3	22.4
EGY04-28	35.6	13	19.6	21.5	14.1	12.9	0.1	14.1	5.5	33.7	7.9	23.9
EGY04-29	32	12.3	13	24.1	7.9	12.3	0	10.9	2.1	20.9	17.3	25.4
EGY04-30	29.2	10	23.7	20.8	8.4	8.9	1.1	15	8.7	32.1	11.8	25.3
EGY04-31	24	11.4	25.1	16	8	9.5	1.9	11.9	13.2	33.1	14.4	25.1
EGY04-32	28.2	9.6	23.4	19.8	8.4	8.7	0.9	16.5	6.9	31.8	10.2	28.6
EGY06-03	27.3	9.1	27	18.2	9.1	8.4	0.7	17.2	9.8	36.1	9.1	27.5
EGY06-05	37.3	6.8	16.3	26.6	10.7	6.8	0	14.5	1.8	27	15.1	24.5
Average	34	11	19	23	11	10	1	13	6	30	12	24

Qm: Monocrystalline quartz; Qp: Polycrystalline quartz; Q: Total quartz (Qm+Qp); P: Plagioclase; K: Potassium feldspar; F: Total feldspar (P+K); Lv: Volcanic and metavolcanic lithic fragments; Ls: Sedimentary and metasedimentary Lithic fragments; L: Lithic fragments (Lv+Ls); Lt: Total lithic fragments (Lv+Ls+Qp); Misc: Other grains (epidote, mica, iron oxides, carbonates); M: Matrix.

Table 4.1. Modal composition of Um Hassa greywackes.

Element	DNC-1		BIR-1	
	Measured	Recommended	Measured	Recommended
SiO ₂ (wt%)	48.1	47.2	49.0	47.7
Al ₂ O ₃	18.7	18.3	15.8	15.4
Fe ₂ O ₃ ^(T)	9.76	9.97	11.26	11.3
MnO	0.15	0.15	0.18	0.18
MgO	10.2	10.1	9.68	9.68
CaO	11.6	11.3	13.7	13.4
Na ₂ O	1.67	1.89	1.6	1.81
K ₂ O	0.27	0.234	0.09	0.03
TiO ₂	0.49	0.48	0.99	0.97
P ₂ O ₅	0.08	0.07	0.03	0.027

Table 4.2. Measured and recommended major elements values for DNC-1 (recommended by USGS) and BIR-1 (recommended by Max-Planck-Institute) standards.

Element	BHVO-2 (n=21)		BHVO-1 (n=11)	
	Measured	Recommended	Measured	Recommended
Li (ppm)	4.2	4.6	4.69	4.6
V	313	317	321	318
Cr	258	280	247	287
Co	44	45	45	45
Ni	155	119	150	118
Cu	133	127	144	137
Zn	110	103		
Rb	8.9	9.11	9.2	9.19
Sr	382	396	390	396
Y	22.8	26.0	23.3	26
Zr	156	172	165	174
Nb	14.3	18.1	14.9	18.6
Cs	0.10	0.1	0.11	0.13
Ba	128	131	128	133
La	14.7	15.2	14.8	15.5
Ce	36.7	37.5	37.0	38.1
Pr	5.18	5.35	5.13	5.42
Nd	23.8	24.5	23.4	24.7
Sm	5.90	6.07	5.83	6.112
Eu	1.98	2.07	1.97	2.09
Gd	6.23	6.24	6.20	6.33
Tb	0.89	0.92	0.91	0.96
Dy	5.1	5.31	5.10	5.13
Ho	0.94	0.98	0.95	0.98
Er	2.5	2.54	2.47	2.55
Tm	0.32	0.33	0.31	0.33
Yb	1.92	2.00	1.88	2
Lu	0.26	0.28	0.26	0.27
Hf	4.23	4.36	4.52	4.46
Ta	0.9	1.14	0.86	1.21
Pb	2.58	1.6	4.18	2.4
Th	1.6	1.20	1.40	1.23
U	0.43	0.403	0.44	0.409

Table 4.3. Measured and recommended values for USGS standards BHVO-1 and BHVO-2 (recommended by Max-Planck-Institute).

	EGY-04- 24	EGY-04- 25	EGY-04- 26	EGY-04- 27	EGY-04- 28	EGY-04- 29	EGY-04- 30	EGY-04- 31	EGY-04- 32
SiO ₂ (wt%)	68.8	70.4	65.9	68.0	69.9	64.2	67.1	66.9	66.2
Al ₂ O ₃	11.2	12.3	14.5	14.0	13.3	13.1	13.8	13.9	13.9
Fe ₂ O ₃ *	5.66	4.18	6.48	5.36	4.84	6.35	5.44	5.68	6.01
MnO	0.13	0.10	0.14	0.19	0.13	0.17	0.14	0.09	0.09
MgO	1.92	2.1	2.77	2.48	2.15	2.42	2.45	2.36	2.51
CaO	4.03	2.2	1.42	1.4	1.59	2.95	2.16	2.15	2.81
Na ₂ O	2.33	2.16	2.22	3.5	3.59	2.67	3.08	2.96	2.87
K ₂ O	1.32	2.41	1.93	1.51	1.45	2.11	1.91	2.2	1.66
TiO ₂	0.96	0.53	0.97	0.60	0.59	0.92	0.67	0.73	0.86
P ₂ O ₅	0.17	0.14	0.24	0.15	0.15	0.21	0.18	0.19	0.22
LOI	2.75	2.72	3.66	3.33	3.37	3.43	3.19	2.9	3.05
Total	99.22	99.15	100.2	100.6	101	98.58	100.1	100.1	100.2
Sc (ppm)	14	11	17	13	12	15	13	14	15
Zr	161	128	257	122	139	260	123	164	227
V	138	76	141	101	93	127	100	117	123
Li	12.5	13.6	28.3	24.2	21.7	21.7	21.3	23.4	20.0
V	227	163	199	183	140	222	138	184	148
Cr	434	335	338	339	247	401	242	301	234
Co	13	12	13	15	12	17	10	15	15
Ni	66	54	84	59	49	72	71	58	69
Cu	49	22	46	41	40	43	44	39	41
Zn	95	114	135	101	98	518	165	248	125
Ga	49	65	59	69	62	69	67	70	65
Rb	33	60	57	45	39	63	55	61	50
Sr	432	240	134	227	228	280	287	273	552
Y	27.3	21.9	32.4	21.7	21.7	29.2	22.8	24.6	29.0
Nb	6.53	4.10	7.70	4.96	4.75	6.57	5.03	6.04	6.73
Mo	0.84	0.70	0.81	0.57	0.72	0.96	0.72	0.61	0.55
Cs	1.15	2.34	2.07	1.48	1.23	2.48	1.50	1.60	1.42
Ba	301	498	330	514	458	535	526	548	453
La	33.2	14.4	30.6	16.8	19.5	26.8	18.8	22.3	27.3
Ce	73.9	36.4	65.5	39.9	45.5	58.0	43.3	47.9	60.8
Pr	8.50	4.17	8.10	4.57	5.16	7.29	5.21	5.94	7.28
Nd	32.4	17.2	33.0	19.0	21.4	28.3	21.2	23.7	29.2
Sm	6.43	3.83	6.95	4.48	4.63	5.91	4.45	5.21	5.88
Eu	1.24	1.03	1.47	1.02	1.14	1.33	1.14	1.23	1.35
Gd	6.00	4.17	6.59	4.36	4.71	6.08	4.82	5.10	6.07
Tb	0.84	0.63	1.01	0.67	0.69	0.91	0.70	0.74	0.93
Dy	5.03	3.91	5.92	3.85	4.05	5.48	4.42	4.52	5.47
Ho	1.03	0.80	1.24	0.82	0.80	1.14	0.84	0.92	1.09
Er	3.07	2.54	3.64	2.47	2.41	3.26	2.57	2.74	3.26
Tm	0.46	0.36	0.53	0.35	0.37	0.48	0.38	0.40	0.48
Yb	2.89	2.32	3.36	2.38	2.31	3.07	2.36	2.49	3.10
Lu	0.43	2.07	0.52	0.36	0.35	0.49	0.37	0.38	0.56
Ta	0.59	0.36	0.71	0.42	0.42	0.59	0.44	0.53	0.61
Pb	20	44	40	28	49	22	118	25	29
Bi	0.19	0.20	0.18	0.25	0.22	0.29	0.21	0.28	0.25
Th	7.14	3.64	8.92	4.47	4.84	8.63	4.53	5.91	7.64
U	2.52	1.59	2.94	1.65	1.66	3.73	1.97	2.27	2.98
SiO ₂ /Al ₂ O ₃	6.1	5.7	4.6	4.8	5.3	4.9	4.9	4.8	4.8
CIA	48	56	65	59	57	53	56	57	56
Eu/Eu*	0.61	0.79	0.67	0.71	0.75	0.68	0.76	0.73	0.69
La/Yb _{cn}	8.2	4.5	6.5	5.1	6.1	6.3	5.7	6.4	6.3
Gd/Yb _{cn}	1.71	1.48	1.62	1.51	1.69	1.64	1.68	1.69	1.62
La/Sm _{cn}	3.3	2.4	2.8	2.4	2.7	2.9	2.7	2.8	3.0
Th/Sc	0.51	0.33	0.52	0.34	0.40	0.58	0.35	0.42	0.51
Th/U	2.8	2.3	3.0	2.7	2.9	2.3	2.3	2.6	2.6

Table 4.4. Chemical composition of Um Hassa greywackes.

Chapter 5

Summary and implications

The geodynamic evolution of the Central Eastern Desert requires a better understanding of the evolution of the Neoproterozoic Egyptian ophiolites and their spatially and temporally associated rocks. To achieve this, ophiolitic rocks from the Wadi Ghadir and Fawakhir areas were analyzed for both major and trace elements and the temporally related ophiolitic blocks from the mélangé. A study of the geochemical characteristics of the younger dikes, intruding the ophiolite complexes, and the associated late orogenic sedimentary rocks improves our understanding of the temporal tectonic evolution of the Central Eastern Desert of Egypt.

5.1. Formation of Neoproterozoic ophiolites in Egypt

In terms of geochemistry, both the Fawakhir and the Wadi Ghadir ophiolitic complexes display subduction zone trace element signatures. They are characterized by enrichment of Th over the rest of high field strength elements and by the presence of negative Nb anomalies (Fig. 2.7, 3.11). Because they are geochemically similar to modern island arcs, both ophiolites are classified as supra-subduction zone (SSZ) ophiolites. Supra-subduction zone ophiolites formed either during subduction initiation and nascent-arc formation or with back-arc rifting and spreading (Pearce et al., 1984; Pearce 2003). The Wadi Ghadir ophiolitic complex has Nb/Yb ratios and HFSE and REE contents similar to MORB and higher than the ratios and values of the Fawakhir ophiolite. Such similarity between the Wadi Ghadir ophiolitic complex and MORB and also to the modern oceanic crusts of the Lau and Manus basins indicates formation at a

back-arc tectonic setting (Fig. 2.13). In contrast, the more depleted mantle source of the Fawakhir ophiolite shows a similarity to the modern forearc of the Mariana-Izu-Bonin arc system, which may indicate formation as a nascent-arc oceanic crust (Stern and Bloomer, 1992) (Fig. 3.15, 3.16).

5.2. Assessing the subduction polarity

In an intra-oceanic arc system, the magma chemistry shows a systematic variation across the arc (Bloomer et al., 1995; Hochstaedter et al., 2001). A transect from the back-arc to the forearc shows that the volcanics become more depleted in incompatible trace elements and more affected by slab-derived fluids (Hochstaedter et al., 2000). Such correlation between the variation of the geochemistry and subduction polarity occurs regardless of the eruption age (Taylor et al., 1992). The lack of highly precise geochemical data on the arc-related rocks of the Central Eastern Desert makes the determination of subduction polarity difficult (Shackleton, 1994).

The Wadi Ghadir ophiolitic complex is a part of a mélangé which is separated from the Hafafit gneissic dome to the west by the Nugrus volcanic arc complex (Fig. 2-15) (Abd El-Naby and Frisch, 2006). Further towards the southwest, the amphibolites of the Hafafit show geochemical characteristics similar to forearc rocks (data was reinterpreted from Abd El-Naby and Frisch, 2006). The systematic spatial variation of the rock affinities from the east back-arc affinity of the Wadi Ghadir ophiolitic complex through Nugrus arc volcanic and volcanoclastic rocks to forearc amphibolite towards the west indicates an arc system formed over a northeast to east-dipping subduction zone (Fig. 2.15).

The same scenario can be proposed along the Qift-Qusier road. The Fawakhir ophiolite shows a forearc geochemical signature whereas the pillow lava blocks in the mélangé to the east have a back-arc geochemical signature. This spatial relation indicates a generally east-dipping subduction zone (Fig. 3.16). The absence of well-exposed arc volcanic and volcanoclastic rocks can be attributed to erosion during exhumation of the Meatic gneiss dome between the Fawakhir ophiolite to the west and the mélangé to the east. The arc volcanic and volcanoclastic rocks were described to the south of Qift-Qusier in the Wadi Hammariya area (Abdel-Karim et al., 2008) and the depleted ophiolitic rocks are exposed to the west of these arc rocks. Formation of an arc system above a southeast-dipping subduction zone was proposed previously for the Central Eastern Desert by Ries et al. (1983). However, their model cannot account for the subduction signature of the ophiolitic rocks.

5.3. From island arc(s) to active continental margin

The closure of a back-arc basin separating an intra-oceanic island arc system from the older continental crust to the west was the common model proposed for the evolution of the Central Eastern Desert during the Neoproterozoic (El Ramly et al., 1984; El Bayoumi and Greiling, 1984; Kröner, 1985). This model was based on the assumption that the ophiolite complexes in the Central Eastern Desert represent only fragments of a back-arc oceanic crust formed above a west-dipping subduction zone (Kröner et al., 1987; El-Sayed et al., 1999; Abd El-Naby and Frisch, 2006). However, this study proposes that the oceanic arc system formed above an east-dipping subduction zone. This arc system accreted or collided with a passive continental margin towards the west. The

stable continental shelf sediments are exposed in parts of the exhumed gneissic domes in the Hafafit area (El Ramly et al., 1984) and in the Meatiq area (Ries et al., 1983).

Both the Wadi Ghadir and Fawakhir ophiolite complexes are intruded by calc-alkaline dikes which are less deformed and less metamorphosed than the accreted arc and ophiolitic rocks. These calc-alkaline dikes have geochemical characteristics similar to the Andean-type suite magmatism (Fig. 2.11, 3.14). These dikes could be a part of the calc-alkaline batholithic phase (650-590 Ma; Benetor, 1985) and its extrusive equivalent represented, at least partly, by Dokhan Volcanics (El-Gaby et al., 1988). This calc-alkaline magmatism formed at an active continental margin (Kröner et al., 1987; El-Gaby et al., 1988; Eliwa et al., 2006). In addition to being a mechanism for lateral continental growth, the arc-passive margin collision is a favorable mechanism for initiating an active continental margin (Casey and Dewey, 1984). The initiation of an active continental margin after arc-passive margin collision was most likely achieved through reversal in the subduction polarity (Clift et al., 2003). Accordingly, the calc-alkaline dikes intruding both the Wadi Ghadir and the Fawakhir ophiolite complexes were formed at an Andean-type margin formed above a west-dipping subducted slab (Fig. 2.15, 3.16, 5.1). The initiation of an active continental margin was induced by subduction polarity reversal from east-dipping, during the formation of the intra-oceanic arc system, to west-dipping following arc-continental collision. Reversal of the subduction polarity resolves the problem over the formation of ophiolites in the Central Eastern Desert above an east-dipping subduction zone which was raised by Kröner et al. (1987). They argued against an east-dipping subduction zone because it was difficult to generate Andean-type

magmatism from the mantle beneath a passive margin of West Gondwanaland. Subduction polarity reversal can make the east-subduction model possible.

5.4. Emplacement of the ophiolite complexes

On the basis of emplacement mechanism, Moores (1982) classified ophiolites into Tethyan-type and Cordilleran-type. Tethyan-type ophiolites are emplaced during the collision of a passive margin with a subduction zone whereas Cordilleran-type ophiolites are incorporated into the accretionary wedge of an active continental margin (Beccaluva et al., 2004). The Fawakhir ophiolite was a part of the forearc that was emplaced during the collision-accretion of a subduction zone into the passive margin to the west and so it can be considered a Tethyan-type ophiolite. In contrast, the Wadi Ghadir ophiolitic complex is a part of an arc complex accreted onto an active continental margin that was initiated above a west-dipping subduction zone and thus it is more appropriately classified as a Cordilleran-type ophiolite.

5.5. Late orogenic sedimentary rocks

The late stage of crustal evolution of the Central Eastern Desert of Egypt is characterized by deposition of the molasse-type Hammamat Group. At their type locality in the Wadi Hammamat area, the Um Hassa Greywacke Member represents the upper unit of the Hammamat Group. Grothaus et al. (1979) proposed that the Hammamat sediments were deposited in intermontane, alluvial to fluvial basins. Spatially, the Hammamat Group at Wadi Hammamat was deposited most likely in a foreland basin beside the orogen. In terms of the evolution of the Central Eastern Desert proposed in this study, the Hammamat sediments could have been deposited in either a peripheral or a retroarc foreland basin. The peripheral foreland basin would have formed during

accretion of the oceanic crust and arc, but the retroarc basin would have formed after the reversal of subduction polarity and behind the continental arc Dokhan Volcanics (Fig. 3.15).

Being intermediate in grain size between conglomerates and siltstones, the study of the Um Hassa greywackes provides an opportunity for both petrographical and geochemical studies. Petrographically, the Um Hassa greywackes are composed mainly of volcanic lithic fragments, quartz and plagioclase. Volcanic arcs and subduction zone complexes are the main sources of these sediments (Fig. 4.8). Such compositions can indicate deposition in either a peripheral or a retroarc foreland basin. However, on the tectonic discrimination diagrams, the Um Hassa greywackes plot in the continental arc field which reflects the geochemical affinity of the major framework component, the volcanic lithic fragments (Fig. 4.9). Plotting of the Um Hassa greywackes in the continental arc fields may indicate the deposition of the Hammamat Group in a retroarc foreland basin formed behind the Dokhan continental arc which formed above a west-dipping subduction zone. The extension of the Um Hassa greywackes to the oceanic island arc fields on the tectonic discrimination diagrams and the ophiolitic geochemical signature (high Cr and Ni; Fig. 4.6b) of the greywackes indicate a contribution from the accreted oceanic crust and island arc materials which constitute a substrate upon which the Dokhan continental arc edifices formed (Fig. 4.10).

5.6. Ophiolite-induced evolutionary model for the Central Eastern Desert

The main goal of this study is to understand the formation and evolution of the Neoproterozoic continental crust in the Central Eastern Desert. This will provide a better understanding of the mechanism of lateral crustal growth proposed for the Arabian-

Nubian Shield. The proposed evolutionary model depends mainly on the spatial geochemical variation of the ophiolitic rocks in the Central Eastern Desert. The following model stems from the above-mentioned summarized conclusions.

The initial stage of the evolution of the Central Eastern Desert during the Neoproterozoic was characterized by the formation of oceanic island arc system(s) above an east- to northeast-dipping subduction zone at ~700-750 Ma (Stern, 2008). Arc formation was associated with creation of oceanic crust either in a back-arc setting, as for the Wadi Ghadir ophiolitic complex, or in a forearc setting, as for the Fawakhir ophiolite. With the consumption of the subducted slab, the island arc system approached a passive continental margin to the west, which is represented by the Saharan Metacraton (Fig. 5.1a). The well-preserved nature of the Fawakhir ophiolite, as a nearly complete sequence, to the north and the highly tectonized nature of the Hafafit forearc amphibolite to the south can be attributed to the nature of the passive continental margin. The passive continental margin could have a promontory to the south at Hafafit area. As the arc system approached from the east, the final arc accretion onto the passive continental margin to the north would have been mild relative to the arc accretion process to the south. Therefore, the preservation is expected to be better for the Fawakhir ophiolite complex than for the Hafafit amphibolite.

The ages of the arc and ophiolitic fragments in the Central Eastern Desert are problematic (Ali et al., 2009). Another hypothesis can be suggested for the better preservation of the Fawakhir ophiolite relative to the Hafafit amphibolite. The Ghadir ophiolitic complex yielded an age of 746 ± 19 Ma (Kröner et al., 1992) and the Fawakhir ophiolite complex yielded 736.5 ± 1.2 Ma (Anderson et al., 2009). According to the above

model, the Fawakhir ophiolite is supposed to have resulted from the subduction initiation and nascent-arc crustal formation. Assuming that the Fawakhir and the Wadi Ghadir ophiolite complexes belong to one extended arc system, the Fawakhir ophiolite should be younger than the back-arc Wadi Ghadir ophiolitic complex. Regarding the uncertainty in ages, the Fawakhir ophiolite could have formed during subduction initiation. If younger than the back-arc crust, the Fawakhir ophiolite could have formed through later forearc extension processes. The collision or accretion of the southern segment of the oceanic island arc chain into the Hafafit promontory might have resulted in a rollback of the subducted plate to the north. The rollback would have induced an extension in the forearc regime of the accreted arc system (Fig. 5.1b). The Fawakhir ophiolite could have been formed during this extensional break and emplaced later on the engraved part of the passive margin with the older accreted arc-back-arc materials.

After the accretion of the arc and ophiolite complexes onto the passive continental margin, reversal of the subduction polarity resulted in the formation of the Andean-type margin (Fig. 5.1c). Both calc-alkaline magmatism and the molasse-type sediments in Wadi Hammamat area are associated with this stage.

5.7. Implication for crust growth

There have been numerous debates over the formation and evolution of the continental crust. One of the debates is related to the degree and the rate of continental growth (Armstrong, 1991; Taylor and McLennan, 1995; Scholl and von Huene, 2007). Another paradox engages the discrepancy between the average andesitic composition of the continent and the basaltic composition of the fluxes from the mantle (Davidson and Areulus, 2006; Rollinson 2008). Another dispute is pertinent to the primary mechanisms

which control continental growth (Rudnick, 1995; Windley, 2003). The first subduction-related model proposed that the continent formed mostly by convergent margin magmatism (Rudnick et al., 1998). The second, plume-related model proposed that the continent formed through the formation of oceanic plateaux which are too thick to be subducted and then become a part of a continent (Stein and Hofmann, 1994; Abbott et al., 2000). In both models, accretionary processes are the main mechanisms of continent growth (Kusky and Polat, 1999, and references therein).

The Neoproterozoic was the most active period of crust formation in Earth history (Rino et al., 2008). During the Neoproterozoic, a single cycle of supercontinent (Rodinia) breakup and assembly (Gondwana) took place (Stern, 2008). Reymer and Schubert (1986) drew the attention to the anomalously rapid generation of the Arabian-Nubian Shield continental crust during the assembly of Gondwana. They found it difficult to explain the high growth rate of the Arabian-Nubian Shield by simple arc accretion. The relation between the mantle plumes and the episodic crustal growth through earth history, including the Arabian-Nubian Shield, was proposed by Stein and Hofmann (1994). To account for the high crust formation rate, Stein and Goldstein (1996) and Stein (2003) related the formation of the Arabian-Nubian Shield to the rise of a large plume head which was responsible for the formation of oceanic plateaux.

The geological and geochemical characteristics of the Egyptian ophiolites and the associated mélangé and dikes presented in this study do not support the presence of an oceanic plateau remnant. The plume-related model proposed for the evolution of the Arabian-Nubian Shield (Stein and Hofmann, 1994; Stein and Goldstein, 1996; Stein,

2003) is not applicable for the Central Eastern Desert. Similar conclusions are stated by Ali et al. (2009).

Reymer and Schubert (1986) in their calculation of the crustal growth rate assumed that juvenile terranes extend into the Moho. Windley (2003) considered the accreted juvenile terranes of the Arabian-Nubian Shield as only crustal flakes with no deep extension to the Moho. Therefore, an anomalously high crustal growth rate during the formation of the Arabian-Nubian Shield in the Neoproterozoic is suspect. The complexity of the deeper crust was deduced from the occurrence of Early Precambrian gneiss terranes intercalated with the juvenile island arc in eastern Yemen (Windley et al., 1996; Whitehouse et al., 1998). The juvenile nature of the volcanics and granitic rocks in the Central Eastern Desert (Moussa et al., 2008) make the predominance of an older continental crust beneath less likely.

Patchett and Chase (2002) interpreted the problem of anomalously high crustal growth in terms of normal plate tectonic processes. They assumed an orogen-parallel strike-slip movement to transport terrane parallel to the continental edge. The oblique subduction and later strike-slip escape tectonics may be able to reconcile between the island arc accretion and the high rate of continental growth during the formation of the Arabian-Nubian Shield during the Neoproterozoic. Hoffmann (1991) proposed a rotational collision between East and West Gondwana with the center of rotation at the base of the East-Africa-Antarctic collisional orogen (Fig. 1.2a). With the closure of East and West Gondwana, the juvenile arcs were transported parallel to the continental edge and finally formed late-orogenic strike-slip fault systems developed (Jacobs and Thomas, 2004).

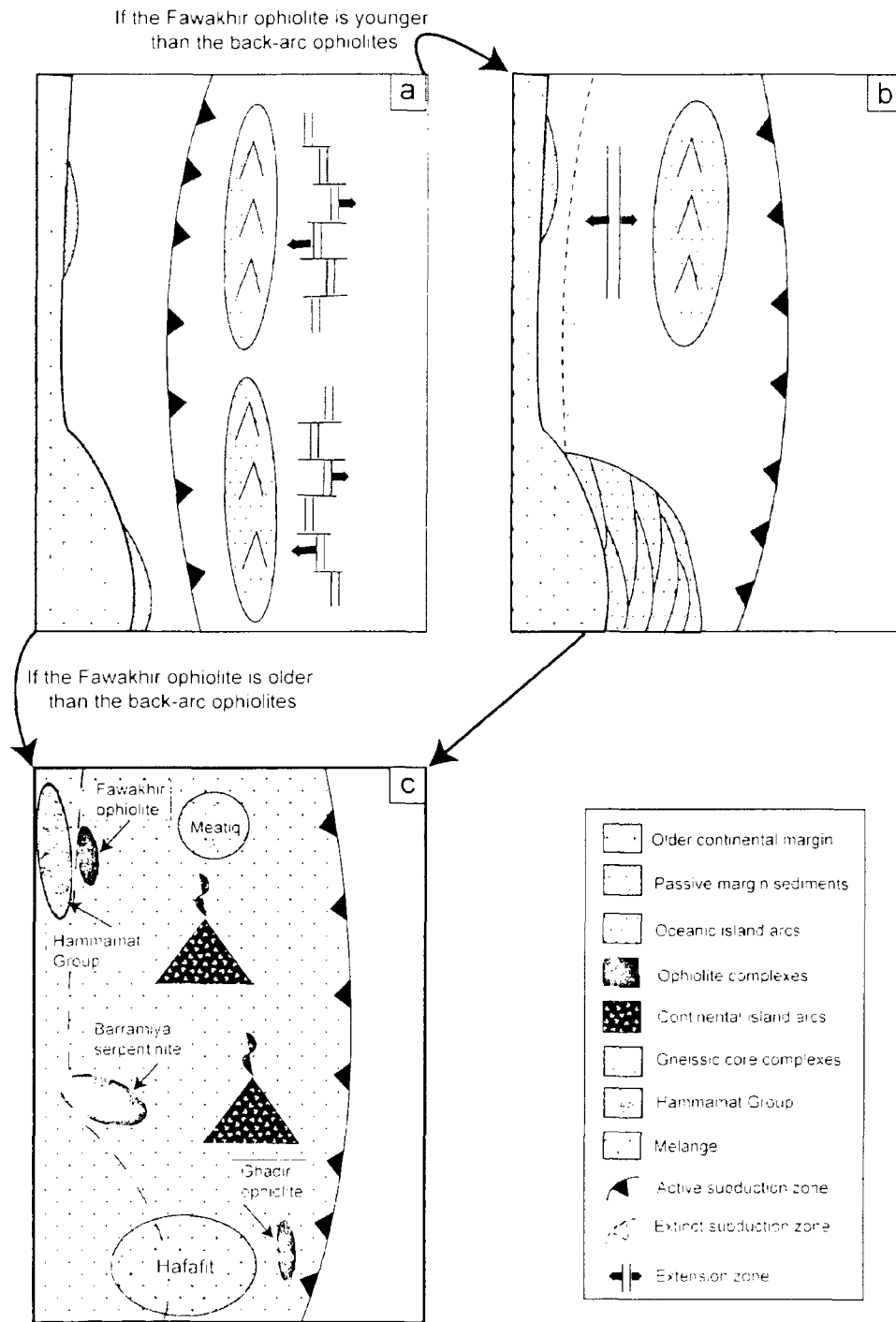


Fig. 5.1. Simplified diagrams showing the geodynamic evolution of the Central Eastern Desert.

References

- Abbott, D., Sparks, D., Herzberg, C., Mooney, W., Nikishin, A., Zhang, Y.S., 2000. Quantifying Precambrian crustal extraction: the root is the answer. *Tectonophysics* 322, 163-190.
- Abdel-Karim, A.M., Azzaz, S.A., Moharem, A.F., El-Alfy, H.M., 2008. Petrological and geochemical studies on the ophiolite and island arc association of Wadi Hammariya, Central Eastern Desert, Egypt. *The Arabian Journal for Science and Engineering* 33, 119-138.
- Abd El-Naby, H., Frisch, W., 2006. Geochemical constraints from the Hafafit Metamorphic Complex (HMC): Evidence of Neoproterozoic back-arc basin development in the Central Eastern Desert of Egypt. *Journal of African Earth Sciences* 45, 173-186.
- Ali, K.A., Stern, R.J., Manton, W.I., Kimura, J-I., Khamees, H.A., 2007. Geochemistry, Nd isotopes and U-Pb SHRIMP zircon dating of Neoproterozoic volcanic rocks from the Central Eastern Desert of Egypt: New insights into the ~750Ma crust-forming event. *Precambrian Research* 171, 1-22.
- Andresen, A., Abu El-Rus, M.A., Myhre, P.I., Boghdady, G.Y., Corfu, F., 2009. U-Pb TIMS age constraints on the evolution of the Neoproterozoic Meatiq Gneiss Dome, Eastern Desert, Egypt. *International Journal of Earth Sciences*, 98, 481-497.
- Armstrong, R.L., 1991. The persistent myth of crustal growth. *Australian Journal of Earth Sciences* 38, 613-630.
- Azer, M.K., Stern, R.J., 2007. Neoproterozoic (835-720 Ma) serpentinites in the Eastern Desert, Egypt: Fragments of forearc mantle. *The Journal of Geology* 115, 457-472.
- Beccaluva, L., Coltorti, M., Giunta, G., Siena, F., 2004. Tethyan vs. Cordilleran ophiolites: a reappraisal of distinctive tectono-magmatic features of supra-subduction complexes in relation to the subduction mode. *Tectonophysics* 393, 163-174.
- Bentor, Y.K., 1984. The crustal evolution of the Arabo-Nubian massif with special reference to the Sinai Peninsula. *Precambrian Research* 28, 1-74.
- Bloomer, S.H., Taylor, B., Macleod, C.J., Stern, R.J., Fryer, P., Hawkins, J.W., Johnson, L., 1995. Early arc volcanism and the ophiolite problem: A perspective from drilling in the Western Pacific. In Taylor, B., and Natland, J., (eds) *Active margins and marginal basins of the western pacific*. Geophysical Monograph, American Geophysical Union 88, 1-30.
- Casey, J.F., Dewey, J.F., 1984. Initiation of subduction zones along transform and accreting plate boundaries, triple-junction evolution, and forearc spreading centres-implications for ophiolitic geology and obduction. In Gass, I.G., Lippard, S.J., Shelton, A.W., (eds)

- Ophiolites and oceanic lithosphere. Geological Society of London Special Publications 13, 269-290.
- Clift, P.D., Schouten, H., Draut, A.E., 2003. A general model of arc-continent collision and subduction polarity reversal from Taiwan and Irish Caledonides. In: Larter, R.D., and Leat, E.T., (eds.) Intra-oceanic subduction systems: Tectonic and magmatic processes. Geological Society, London, Special Publication 219, 81-98.
- Davidson, J.P., Arculus, R.J., 2005. The significance of Phanerozoic arc magmatism in generating continental crust. In Brown, M., Rushmer, T., (eds.) Evolution and differentiation of the continental crust. Cambridge University Press, 135-172.
- El Bayoumi, R.M., 1980. Ophiolites and associated rocks of Wadi Ghadir, east of Gabal Zabara, Eastern Desert, Egypt. Ph.D. Thesis, Cairo University, Egypt. 171 pp.
- El Bayoumi, R.M.A., Greiling, R.O., 1984. Tectonic evolution of a Pan-African plate margin in southeastern Egypt – a suture zone overprinted by low angle thrusting? In: Klerkx, J., Michot, J. (Eds.), Géologie Africaine-African Geology. Musee royal de l'Africaine Centrale, Tervuren, Belg, 47–56.
- El Gaby, S., List, F.K., Tehrani, R., 1988. Geology, evolution and metallogenesis of the Pan-African belt in Egypt. In: El-Gaby, S., Greiling, R.O. (Eds.), The Pan-African Belt of Northeast Africa and Adjacent Areas: Tectonic Evolution and Economic Aspects of a Late Proterozoic Orogen. Friedrich. Vieweg, Sohn Verlagsgesellschaft mbH, 17–68.
- Eliwa, H.A., Kimura, J.I., Itaya, T., 2006. Late Neoproterozoic Dokhan volcanic rocks, northern Eastern Desert, Egypt. Precambrian Research 151, 31-52.
- El Ramly, M.F., Greiling, R., Kröner, A., Rashwan, A.A., 1984. On the tectonic evolution of the Wadi Hafalit area and environs, Eastern Desert of Egypt. Bulletin of King Abdelaziz University 6, 113–126.
- El Sayed M.M., Furnes H., Mohamed F.H., 1999. Geochemical constraints on the tectonomagmatic evolution of the late Precambrian Fawakhir ophiolite, Central Eastern Desert, Egypt. Journal of African Earth Science 29, 515–533.
- Farahat E.S., El Mahalawi M.M., Hoinkes G., Abdel Aal A.Y., 2004. Continental back-arc basin origin of some ophiolites from the Eastern Desert of Egypt. Mineralogy and Petrology 82, 81-104.
- Hochstaedter, A., Gill, J., Peters, R., Broughton, P., Holden, P., 2001. Across-arc geochemical trends in the Izu-Bonin arc: contributions from the subducting slab. Geochemistry, Geophysics, and Geosystem 2, paper number 2000GC000105.

- Hochstaedter, A., Gill, J., Taylor, P., Ishizuka, M., 2000. Across-arc geochemical trends in the Izu-Bonin arc: Constrains on the source composition and mantle melting. *Journal of Geophysical Research* 105, 495- 512.
- Hoffmann, P.F., 1991. Did the breakup of Laurentia turn Gondwanaland inside-out? *Science* 252, 1409-1412.
- Jacobs, J., Thomas, R.J., 2004. Himalayan-type indenter-escape tectonics model for the southern part of the late Neoproterozoic-early Paleozoic East African-Antarctic orogen. *Geology* 32, 721-724.
- Khalil, A.E.S., Azer, M.K., 2007. Supra-subduction affinity in the Neoproterozoic serpentinites in the Eastern Desert, Egypt: Evidence from mineral composition. *Journal of African Earth Sciences* 49, 136-152.
- Kröner, A., 1985. Ophiolites and the evolution of tectonic boundaries in the late Proterozoic Arabian-Nubian Shield of northeast Africa and Arabia. *Precambrian Research* 27, 277–300.
- Kröner, A., Greiling, R.O., Reischmann, T., Hussein, I.M., Stern, R.J., Durr, S., Kruger, J., Zimmer, M., 1987. Pan-African crustal evolution in the Nubian segment of northeast Africa. In: Kröner, A., (Ed.) *Proterozoic lithospheric evolution*. American Geophysical Union, *Geodynamics Series* 17, 237-257.
- Kröner, A., Todt, W., Hussein, I.M., Mansour, M., Rashwan, A.A., 1992. Dating of late Proterozoic ophiolites in Egypt and the Sudan using the single grain zircon evaporation technique. *Precambrian Research* 59, 15–32.
- Kusky, T.M., Polat, A., 1999. Growth of granite-greenstone terranes at convergent margins, and stabilization of Archean cratons. *Tectonophysics* 305, 43-73.
- Moores, E.M., 1982. Origin and emplacement of ophiolites. *Reviews of Geophysics and Space Physics* 20, 735-760.
- Moussa, E.M.M., Stern, R.J., Manton, W.I., Ali, K.A., 2008. SHRIMP zircon dating and Sm/Nd isotopic investigations of Neoproterozoic granitoids, Eastern Desert, Egypt. *Precambrian Research* 160, 341-356.
- Patchett, P.J., Chase, C.G., 2002. Role of transform continental margins in major crustal growth episodes. *Geology* 30, 39-42.
- Pearce, J.A., 2003. Supra-subduction zone ophiolites: The search for modern analogues. In Dilek, Y. and Newcomb, S., (eds.) *Ophiolite Concept and the Evolution of Geological Thoughts*: Boulder, Colorado. Geological Society of America *Special Paper* 373, 269-293.

- Pearce, J.A., Lippard, S.J., Roberts, S., 1984. Characteristics and tectonic significance of supra-subduction zone ophiolites. In Kokelaar, B.P. and Howells, M.F., (eds) *Marginal Basin Geology: Volcanic and Associated Sediments and Tectonic Processes in Modern and Ancient Marginal Basins*. Geological Society of London Special Publications 16, 77-94.
- Reymer A., Schubert, G., 1986. Rapid growth of some major segments of continental crust. *Geology* 14, 299-302.
- Ries, A.C., Shackleton R.M., Graham R.H., Fitches W.R., 1983. Pan-African structures, ophiolites and mélanges in the Eastern Desert of Egypt: a traverse at 26° N. *Journal of Geological Society* 140, 75-95.
- Rino, S., Kon, Y., Sato, W., Maruyama, S., Santosh, M., Zhao, D., 2008. The Grenvillian and Pan-African orogens: World's largest orogenesis through geologic time and their implications on the origin of superplume. *Gondwana Research* 14, 51-72.
- Rollinson, H., 2008. Secular evolution of the continental crust: Implications for crust evolution models. *Geochemistry, Geophysics, and Geosystem* 9, paper number 2008GC002262.
- Rudnick, R., 1995. Making continental crust. *Nature* 378, 571-578.
- Rudnick, R., McDonough, W.P., O'Connell R.J., 1998. Thermal structure, thickness, and composition of continental lithosphere. *Chemical Geology*, 145, 395-411.
- Scholl, D.W., von Huene, R., Crustal recycling at modern subduction zones applied to the past—Issues of growth and preservation of continental basement crust, mantle geochemistry, and supercontinent reconstruction. In Hatcher, R.D.Jr, Carlson, M.P., McBride, J.H., Martinez Catalán, J.R., (eds) *4-D framework of continental crust*. Geological Society of American Memoir 200, 9-32.
- Shackleton, R.M., 1994. Review of late Proterozoic sutures, ophiolitic mélanges and tectonics of eastern Egypt and north-east Sudan. *Geologische Rundschau* 83, 537-546.
- Stein, M., 2003. Tracing the plume material in the Arabian-Nubian Shield. *Precambrian Research* 123, 223-234.
- Stein, M., Goldstein, S.L., 1996. From plume head to continental lithosphere in the Arabian-Nubian Shield. *Nature* 382, 773-778.
- Stein, M., Hofmann, 1994. Mantle plumes and episodic crustal growth. *Nature* 372, 63-68.
- Stern, R.J., 2008. Neoproterozoic crustal growth: The solid Earth system during a critical episode of Earth history. *Gondwana Research* 14, 33-50.
- Stern, R.J., Bloomer, S.H., 1992. Subduction zone infancy: Examples from the Eocene Izu-Bonin-Mariana and Jurassic California arcs. *Geological Society of American Bulletin* 104, 1621-1636.

- Stern, R.J., Johanson, P.R., Kröner, A., Yibas, B., 2004. Neoproterozoic ophiolites of the Arabian-Nubian Shield. In: Kusky TM, ed. *Precambrian Ophiolites and Related Rocks. Developments in Precambrian Geology*, vol. 13, Amsterdam: Elsevier:95-128.
- Taylor, R.N., Murton, B.J., Nesbitt, R.W., 1992. Chemical transects across intra-oceanic-ares: implications for the tectonic setting of ophiolites. In Parson, L.M., Murton, B.J., Browning, P., (eds) *Ophiolites and their modern oceanic analogues*. Geological Society, London, Special Publication 60, 117-132.
- Taylor, S.R., McLennan, S.M., 1995. The geochemical evolution of the continental crust. *Reviews of Geophysics* 33, 241-265.
- Whitehouse, M.J., Windley, B.F., Ba-Bttat, M.A.O., Fanning, C.M., Rex, D.C., 1998. Crustal evolution and terrane correlation in the eastern Arabian Shield, Yemen: geochronologic constraints. *Journal of the Geological Society, London*, 155, 281-295.
- Windley, B.F., 2003. Continental growth in Proterozoic: a global perspective. In: M. Yoshida, B.F. Windley and S. Dasgupta, (Eds), *Proterozoic East Gondwana: Super continent assembly and break-up*. Geological Society of London Special Publications 206, 23-33.
- Windley, B.F., Whitehouse, M.J., Ba-Bttat, M.A.O., 1996. Early Precambrian gneiss terranes and Pan-African island ares in Yemen: crustal accretion of the eastern Arabian Shield. *Geology* 24, 131-134.
- Zimmer, M., Kröner, A., Jochum, K.P., Reischmann, T., Todt, W., 1995. The Gabal Gerf complex: a Precambrian N-MORB ophiolite in the Nubian Shield, NE Africa. *Chemical Geology* 123, 29–51.

Vita Auctoris

Yasser Abd El-Rahman was born in 1976 in Giza, Egypt. He graduated from Ibrahimiya High School in 1994. From there he went on to the Cairo University in Egypt where he obtained B.Sc. in Geology in 1998. He obtained his M.Sc. in Geology (Mineralogy and Petrology) from Cairo University in 2005. He is currently a Ph.D. candidate in Earth Sciences at University of Windsor and he hopes to graduate in summer 2009.